

# **Enhancement of Thermal Performance of Buildings using Cementitious Composites containing Phase Change Material**

*By*

**Sayanthan Ramakrishnan**

A thesis submitted in total fulfilment of the requirements for the  
degree of  
*Doctor of Philosophy*



Faculty of Science, Engineering and Technology  
Swinburne University of Technology  
Melbourne, Australia

2017



# Abstract

---

The incorporation of phase change materials (PCMs) into building fabrics is intended to managing heats by increasing the capacity of thermal energy storage (TES) and reducing interior temperature fluctuations, leading to the enhancement of indoor thermal comfort and building energy efficiency. For the building fabrics, cementitious materials are the most widely used construction materials and incorporation of PCM into these materials would have the greatest potential to improve the overall building thermal performance. However, despite the beneficial outcomes that PCM integrated cementitious materials have on thermal performance, undesired adverse effects have been observed when PCMs are integrated into these materials. This is particularly due to the instability or leakage of PCM during the integration into cementitious materials and its subsequent interaction with the cement matrix. Furthermore, the poor heat transfer rate associated with the low thermal conductivity of PCM also presents a barrier against the effective utilization of its large TES capacity advantages.

This research aims to overcome the issues and barriers in maximising TES capacity of cementitious composites by innovative development of a novel form-stable PCM composite. It is based on paraffin and hydrophobic expanded perlite (EPO), fabricated specifically suit to the integration into cementitious materials. It has been shown that this form-stable PCM composite eliminated the issues of PCM leakage and remained integrated into cement matrix for the significant enhancement of building thermal performances. Experimental investigations were then conducted to develop thermal energy storage cement mortars (TESCMs) by substituting fine aggregates with varying amounts of PCM composite. The physical, mechanical and thermal properties, as well as the thermal performance of TESCMs, were studied and compared with ordinary cement mortars. The results showed that TESCMs had significantly improved TES capacity and thermal performance. Although the compressive strength of TESCMs was relatively reduced due to low strength and stiffness of PCM composite, a substantial level of PCM replacement of up to 60% can be considered for structural cement mortar applications. Furthermore, TESCMs showed good mechanical and thermal reliability when subjected to 3000 accelerated thermal cycles.

On the other hand, to mitigate the poor heat transfer performance of PCM, its thermal conductivity was enhanced by integrating high conductive additives into form-stable PCM. Various carbon-based additives such as graphite, carbon nanotubes (CNT) and graphene nanoplatelets (GNP) were investigated and the feasibility of their performance enhancements for the form-stable PCM composites were studied and compared. The tests for heat storage/release rates as well as heat transfer performance revealed that the dispersion of GNP particles into PCM composite resulted in the greatest performance enhancement, whereas graphite integration showed the least due to their larger particle size and the formation of ineffective heat transfer network into composite PCMs.

Furthermore, the thermal performance of TESCM for the application in building envelopes was evaluated with experimental and numerical studies. The experimental study conducted on prototype test cells and test huts demonstrated that the TESCM could reduce the peak indoor temperature and diurnal temperature fluctuations by up to 2.2°C and 5°C respectively. The numerical simulations revealed that, although TESCM effectively improves the indoor thermal comfort, the interior surface application of PCM caused incomplete solidification at night due to high indoor temperatures. The use of night ventilation was proposed to improve the solidification of PCM and promising results were achieved. The combined application of TESCM and night ventilation reduced the peak indoor operative temperature by up to 3.4°C, whereas only 2.5°C was achieved during the absence of night ventilation. A design optimization study on PCM application in buildings was then conducted by an analytical assessment. Two performance indicators, termed as the efficiency coefficient and the effectiveness coefficient, were developed to measure the performance of PCM in terms of latent heat storage efficiency and indoor thermal comfort respectively. Many parametric factors including, phase transition temperature of PCM, quantity of PCM and night ventilation rate were studied. It was found that the developed performance indicators enabled the effective selection of optimum PCM configurations such that the resultant PCM storage efficiency and indoor thermal comfort remained optimized.

Overall, the novel form-stable PCM composite developed in this study can be successfully integrated into cementitious composites without associated PCM leakages issues and the application of such PCM integrated cementitious composites showed significant enhancement in building thermal performances.

# Declaration

---

I hereby declare that this thesis contains no material which has been accepted for the award to the candidate of any other degree or diploma, except where due reference is made in the text of the examinable outcome. I affirm that to the best of my knowledge, the thesis contains no material previously published or written by another person except where due reference is made in the text of the thesis.



---

Sayanthan Ramakrishnan

July 2017

# List of Publications

---

## Published and Submitted Journal papers

1. **Sayanthan Ramakrishnan**, Jay Sanjayan, Xiaoming Wang, Morshed Alam, John Wilson (2015). "A novel paraffin/expanded perlite composite phase change material for prevention of PCM leakage in cementitious composites" *Applied Energy* 157: 85-94.
2. **Sayanthan Ramakrishnan**, Xiaoming Wang, Morshed Alam, Jay Sanjayan, John Wilson (2016). "Parametric analysis for performance enhancement of phase change materials in naturally ventilated buildings" *Energy and Buildings* 124: 35-45.
3. **Sayanthan Ramakrishnan**, Xiaoming Wang, Jay Sanjayan, John Wilson (2017). "Assessing the feasibility of integrating form-stable phase change material composites with cementitious composites and prevention of PCM leakage" *Materials Letters* 192: 88-91.
4. **Sayanthan Ramakrishnan**, Xiaoming Wang, Jay Sanjayan, John Wilson (2016) "Application of Phase Change Materials to Reduce Heat Related Risks During Extreme Heat Waves in Australian Dwellings" *Energy Procedia* 88: 725-731.
5. **Sayanthan Ramakrishnan**, Xiaoming Wang, Jay Sanjayan, John Wilson (2017). "Thermal performance of buildings integrated with phase change materials to reduce heat stress risks during extreme heatwave events" *Applied Energy* 194: 410-421.
6. **Sayanthan Ramakrishnan**, Xiaoming Wang, Jay Sanjayan, John Wilson. "Development of thermal energy storage cementitious composites (TESC) containing a novel paraffin/hydrophobic expanded perlite composite phase change material" Under review in *Solar Energy*.
7. **Sayanthan Ramakrishnan**, Xiaoming Wang, Jay Sanjayan, John Wilson. "Thermal performance assessment of phase change material integrated cementitious composites in buildings: Experimental and numerical approach" *Applied Energy* (Article in Press).

## Journal papers under preparation

1. **Sayanthan Ramakrishnan**, Xiaoming Wang, Jay Sanjayan, John Wilson. *“A comparative study on heat transfer performance enhancement of paraffin/hydrophobic expanded perlite composite PCM with carbon additives.”*
2. **Sayanthan Ramakrishnan**, Xiaoming Wang, Jay Sanjayan, John Wilson. *“The performance evaluation of form-stable PCM integrated cementitious composites using modular test huts.”*

## Conference proceedings

1. **Sayanthan Ramakrishnan**, Xiaoming Wang, Jay Sanjayan, John Wilson (2014). *“Application of phase change materials to improve indoor comfort during extreme heat waves in Australian cities”* NCCARF 2014, 30 Sep - 2 Oct 2014, Brisbane Australia
2. **Sayanthan Ramakrishnan**, Xiaoming Wang, Jay Sanjayan, John Wilson *“Application of Phase Change Materials to reduce heat related risks during extreme heat waves in Australian dwellings.”* Conference Proceedings: CUE2015-Applied Energy Symposium and Summit 2015: Low carbon cities and urban energy systems
3. **Sayanthan Ramakrishnan**, Xiaoming Wang, Jay Sanjayan, John Wilson. *“Experimental and Numerical study on Energy Performance of Buildings Integrated with Phase change materials”* 8th International Conference on Applied Energy (ICAE2016), 8-11 October 2016, Beijing, China
4. **Sayanthan Ramakrishnan**, Xiaoming Wang, Jay Sanjayan, John Wilson. *“Heat transfer performance enhancement of paraffin/expanded perlite phase change composites with graphene nano-platelets”* 8th International Conference on Applied Energy (ICAE2016), 8-11 October 2016, Beijing, China
5. **Sayanthan Ramakrishnan**, Xiaoming Wang, Jay Sanjayan, John Wilson. *“Development of an energy efficient granular phase change composite containing graphene nanoplatelets”* International Workshop on Mechanics of Energy Materials (IWMEM 2016), 14-15 November 2016, Sydney, Australia.
6. **Sayanthan Ramakrishnan**, Xiaoming Wang, Jay Sanjayan, John Wilson. *“Thermal energy storage enhancement of lightweight cement mortars with the application of phase change materials”* International High-Performance Built Environments Conference (SBE16), 17-18 November 2016, Sydney, Australia.

# Acknowledgement

---

I would like to express my sincere appreciation and gratitude to my supervisors, Adj. Prof. Xiaoming Wang and Prof. Jay Sanjayan, for providing invaluable guidance and research support throughout my way to the completion of this research work. It was a great opportunity for me to work in CSIRO under the supervision of Senior Principal Research Scientist Xiaoming Wang. I have also enthused by Jay's knowledge, patience, generosity and leadership, which provided a strong support to successfully complete my PhD. My sincere thanks also goes to Prof. John Wilson and Dr. Morshed Alam for their valuable guidance and support throughout this research work.

I gratefully acknowledge the financial support granted by Swinburne University of Technology and CSIRO via a SUPRA scholarship and a top-up scholarship for my study in Australia.

I wish to thank the staffs in the smart structures, material characterization, chemistry engineering and wet chemistry laboratories at Swinburne University. In particular, my special thanks go to Mr. Michael Culton, Mr. Firas, Dr. James Wang, Mrs. Savithri and Mr. Xiaohan Yang for their technical assistance to complete the experimental works in a successful way. Further, I owe many thanks to Dr. Eusthousius Petinakis and Dr. Russel Lee for their support and feedback on DSC test and Goniometer test.

I would also be grateful to all staff, PhD students and friends at Swinburne University and CSIRO for their friendship, encouragement, and support during my PhD journey. Special thanks go to Sri, Bara and Hasnat for their time and encouragement in the successful completion of my thesis.

Finally, I wish to thank my lovely family for their ongoing support and encouragement to complete my PhD study. I am also greatly indebted to my beloved partner for her support and patience during this journey. I would never have been able to finish my PhD thesis without her support and help during the experimental works and thesis writing.

# Abbreviations and acronyms

---

TES	Thermal Energy Storage
LHTES	Latent Heat Thermal Energy Storage
PCM	Phase change material
EP	Expanded Perlite
TESC	Thermal Energy Storage Cementitious composite
TESCM	Thermal Energy Storage Cement Mortar
CNT	Carbon Nanotubes
GNP	Graphene Nanoplatelets
NV	Night Ventilation
ACH	Air Circulation per Hour
ASTM	American Society for Testing and Materials
ASHRAE	American Society of Heating, Refrigerating, and Air-Conditioning Engineers
ISO	International Standards Organization
CondFD	Conduction Finite Difference

# Table of Contents

Abstract.....	iii
Declaration .....	v
List of Publications .....	vi
Acknowledgement.....	viii
Abbreviations and acronyms .....	ix
Table of Contents .....	x
List of Tables .....	xv
List of Figures.....	xvii
Chapter 1 Introduction.....	1
1.1 Background.....	1
1.2 Problem statement.....	3
1.3 Aim and objectives .....	5
1.4 Significance of the research.....	6
1.5 Thesis outline .....	6
Chapter 2 Literature review.....	9
2.1 Overview .....	9
2.2 Thermal energy storage (TES) .....	11
2.3 PCMs and its desired characteristics.....	12
2.4 Types of PCMs.....	14
2.5 Methods of PCM incorporation into construction materials.....	17
2.5.1. Direct incorporation methods.....	17
2.5.2. Indirect incorporation methods .....	18
2.6 Building components containing PCM.....	26
2.6.1. PCM incorporated wallboards.....	26
2.6.2. PCM incorporated cement mortar and concrete .....	27
2.7 Potential applications of PCM in buildings.....	41
2.7.1. PCM application methods: passive, active and free cooling .....	41

2.7.2.	Passive application of PCM in buildings.....	42
2.8	Heat transfer performance enhancement of PCMs .....	44
2.8.1.	Overview.....	44
2.8.2.	Metallic materials as thermal conductivity promoters.....	45
2.8.3.	Carbon-based additives as thermal conductivity promoter .....	46
2.9	Thermal performance assessment of PCM incorporated buildings.....	51
2.9.1.	Overview.....	51
2.9.2.	Experimental thermal performance assessments .....	51
2.9.3.	Numerical assessments of thermal performance.....	53
2.9.4.	Building simulations with PCM.....	55
2.9.5.	Thermal performance assessment criteria.....	62
2.10	Thermal performance enhancement of PCM incorporated buildings .....	64
2.10.1.	Thermal performance of PCM integrated wallboards.....	64
2.10.2.	PCM integrated cement mortar and concrete .....	67
2.11	Motivation for the study and research gaps .....	71
Chapter 3	Assessing the feasibility of integrating form-stable PCM into cement-based composites	74
3.1	Introduction.....	74
3.2	Materials and Methods.....	76
3.2.1.	Materials .....	76
3.2.2.	Fabrication of form-stable PCM and PCM integrated cementitious composites.....	76
3.2.3.	Testing methods .....	78
3.3	Results and discussions.....	83
3.3.1.	Particle size distribution of expanded perlites.....	83
3.3.2.	Absorption characteristics of the composites.....	84
3.3.3.	Thermophysical properties of PCM composites.....	89
3.3.4.	Stability of form-stable PCMs in cementitious composites.....	91

3.3.5.	Surface characteristics of PCM composites and PCM leakage.....	94
3.4	Concluding remarks.....	96
Chapter 4	Preparation, characterization, and properties of paraffin/ hydrophobic EP integrated cementitious composites.....	97
4.1.	Introduction.....	97
4.2.	Materials and Methods.....	99
4.2.1.	Materials.....	99
4.2.2.	Fabrication of form-stable PCM and TESC.....	99
4.2.3.	Testing methods.....	101
4.3.	Results and discussions.....	109
4.3.1.	Chemical compatibility analysis.....	109
4.3.2.	Thermal stability of form-stable PCM.....	110
4.3.3.	Specific gravity and density of granular materials.....	111
4.3.4.	Mechanical properties and microstructural analysis of TESC.....	111
4.3.5.	Pozzolanic reactivity of EPO granules.....	114
4.3.6.	Thermal energy storage performance of TESC.....	115
4.4.	Concluding remarks.....	120
Chapter 5	Development of thermal energy storage cement mortars containing form- stable PCM composite.....	121
5.1	Introduction.....	121
5.2	Materials and Methods.....	123
5.2.1.	Materials.....	123
5.2.2.	Fabrication of TESCMs.....	123
5.2.3.	Testing methods.....	124
5.3	Results and Discussions.....	131
5.3.1.	Physical properties of TESCMs.....	131
5.3.2.	Drying shrinkage of TESCMs.....	132
5.3.3.	Mechanical properties and microstructural analysis of TESCMs.....	134

5.3.4.	Thermal conductivity of TESCMs.....	136
5.3.5.	Thermal energy storage performance of TESCMs.....	137
5.3.6.	Mechanical and thermal reliability of TESCMs .....	139
5.4	Concluding remarks .....	143
Chapter 6	Heat transfer enhancement of form-stable PCM with the integration of carbon based additives .....	144
6.1	Introduction.....	144
6.2	Materials and Methods.....	145
6.2.1.	Materials .....	145
6.2.2.	Fabrication of paraffin/EPO/additives.....	146
6.2.3.	Preparation of TESCMs containing high conductive additives.....	147
6.2.4.	Testing methods .....	148
6.3	Results and discussions.....	156
6.3.1.	Morphology characterization of paraffin/EPO/additives .....	156
6.3.2.	Chemical compatibility of PCM composite/additive .....	160
6.3.3.	Thermophysical properties of PCM composite/additive .....	161
6.3.4.	Thermal conductivity of PCM composite/additive .....	163
6.3.5.	Heat storage/release performance .....	164
6.3.6.	Heat transfer performance using IR thermography .....	166
6.3.7.	Thermal energy storage performance of prototypes .....	168
6.4	Concluding remarks .....	171
Chapter 7	Thermal performance assessment of form-stable PCM integrated cement mortars in buildings.....	173
7.1	Introduction.....	173
7.2	Materials and Methods.....	175
7.2.1.	Materials and mix design .....	175
7.2.2.	Prototype experiments under controlled climate conditions.....	176
7.2.3.	Test huts exposed to outdoor climatic conditions .....	178

7.2.4.	Thermal performance of PCMCB in buildings.....	183
7.3	Results and discussions.....	190
7.3.1.	Thermal performance assessment of prototypes.....	190
7.3.2.	Thermal performance assessment of test huts.....	192
7.3.3.	Thermal performance assessment of PCMCB in buildings .....	200
7.4	Concluding remarks.....	207
Chapter 8	Parametric analysis for performance optimization of buildings incorporated with phase change materials.....	209
8.1	Introduction .....	209
8.2	Methodology.....	211
8.2.1.	Building description .....	211
8.2.2.	Development of performance indicators .....	215
8.2.3.	Simulation procedure .....	217
8.2.4.	Derivation of performance indicators .....	218
8.3	Results and discussions.....	221
8.3.1.	Efficiency and effectiveness of PCM .....	221
8.3.2.	Optimized phase transition temperature for local climatic conditions ..	223
8.3.3.	Effect of PCM quantity on the thermal performance enhancement .....	228
8.3.4.	Impact of night ventilation on PCM performance .....	231
8.3.5.	Discussion of optimization process .....	233
8.4	Concluding remarks.....	235
Chapter 9	Conclusions and Recommendations .....	237
9.1	Summary .....	237
9.2	Conclusions.....	240
9.3	Recommendations for future works .....	241
References.....		243

# List of Tables

Table 2-1 Key characteristics of PCMs for thermal energy storage .....	13
Table 2-2 Comparison of different PCM types.....	16
Table 2-3 Fabrication and thermo-physical properties of various form-stable PCM composites.	24
Table 2-4 Mechanical and thermal properties of microencapsulated PCM integrated cement mortar/concrete.....	30
Table 2-5 Mechanical and thermophysical properties of form-stable PCM integrated cement mortar/concrete.....	35
Table 2-6 Heat transfer performance of PCM with the dispersion of high conductive carbon additives .....	49
Table 3-1 Mix proportion of materials.....	77
Table 3-2 Mean diameter and equivalent diameters of EP particles .....	83
Table 3-3 Paraffin absorption capacity for different impregnation methods.....	85
Table 3-4 Phase change temperature and enthalpy of paraffin and form-stable PCMs.....	90
Table 3-5 Leakage of form-stable PCMs in cementitious composites.....	93
Table 3-6 Contact angle and wetting tension of PCM composites .....	95
Table 4-1 Chemical composition of EPO and OPC.....	99
Table 4-2 Mix proportion of materials.....	100
Table 4-3 FT-IR absorption bands and relevant assignments for EPO, paraffin, and EPOP.....	110
Table 4-4 Specific gravity and density of fine aggregates .....	111
Table 4-5 Compressive strength of TESC at 7 and 28 days .....	113
Table 5-1 Mix design of materials.....	124
Table 5-2 Temperature program for accelerated thermal cycles.....	129
Table 5-3 Bulk density and apparent porosity of TESCMs .....	132
Table 5-4 Variation in thermophysical properties of TESCMs after 1000 and 3000 thermal cycles .....	141
Table 6-1 Mix design of materials.....	148
Table 6-2 Thermophysical properties of EPOP with different heat transfer additives .....	163
Table 6-3 Heat charge/discharge durations of EPOP containing heat transfer additives .....	166
Table 7-1 Mix proportion of materials.....	175
Table 7-2 Construction materials/elements of test huts.....	180
Table 7-3 The measurement system and accuracy of Vantage Pro 2 weather station .....	182
Table 7-4 Construction materials/elements of multi-storey office building.....	184
Table 7-5 Thermophysical properties of building materials .....	185
Table 7-6 Test room properties .....	188

Table 7-7 Diurnal temperature amplitudes in GPB and PCMCB test huts.....	196
Table 7-8 Diurnal temperature amplitudes in OCB and PCMCB test huts .....	199
Table 8-1 Construction materials/elements of residential house.....	212
Table 8-2 Thermophysical properties of building materials.....	213
Table 8-3 Test room properties.....	214
Table 8-4 Factors influencing the performance indicators.....	215
Table 8-5 Efficiency and effectiveness of PCM on two consecutive days (1-2 December) .....	222
Table 8-6 Summary of results for highest efficiency and effectiveness.....	225
Table 8-7 Optimized results of PCM refurbishment for various climate zones .....	234

# List of Figures

Fig. 2-1. Building as a thermodynamic system and potential of PCM to improve thermal comfort .....	10
Fig. 2-2. TES behavior of sensible and latent heat storage materials .....	12
Fig.2-3. Various macro-encapsulation configurations (a) metal ball, (b) polypropylene flat panel, (c) spherical PCM balls and (d) PCM in tubes .....	20
Fig.2-4. Microencapsulated PCM (a) description of a microcapsule (b) SEM image of micro-encapsulated PCM particles .....	21
Fig. 2-5. Shape stabilized PCM (a) paraffin/HDPE shape stabilized PCM with graphite additives (b) SEM image of paraffin/HDPE shape stabilized PCM .....	21
Fig. 2-6. Typical vacuum impregnation setup .....	22
Fig. 2-7. Granulate PCM integrated gypsum plasterboard (a) Granular PCM composite (b) PCM integrated wallboard .....	27
Fig. 2-8. Comparison of TES capacity of PCM wallboard with conventional wallboard .....	27
Fig. 2-9. SEM images of (a) an open pore covered with solidified wax (b) part of the cement matrix containing broken capsules and pure leaked wax .....	29
Fig. 2-10. Leakage of paraffin in cement mortar mixture .....	38
Fig. 2-11. Fabrication process of epoxy coated PCM composites.....	39
Fig. 2-12. Interfacial properties of surface coated PCM composites in cement matrix (a) epoxy coated composites (b) modified cement paste coated composites.....	41
Fig. 2-13. Macro encapsulated Bio-PCM™ in mat form.....	43
Fig. 2-14. Paraffin/diatomite/MWCNT composite PCM (a) MWCNT-porous diatomite network (b) PCM composite .....	48
Fig. 2-15. Paraffin/expanded perlite composite PCM before and after GO deposition process ..	48
Fig. 2-16. Enthalpy-temperature function of Bio-PCM™-27 .....	55
Fig. 2-17. CondFD space discretization in EnergyPlus .....	59
Fig. 2-18. Validation of a full-scale residential house with and without PCM (a) thermal zone with PCM (b) thermal zone without PCM.....	61
Fig. 2-19. Concrete cubicles integrated with MOPCON concrete.....	67
Fig. 2-20. Test room with concrete floor containing microencapsulated PCM (a) schematic diagram (b) physical set up.....	68
Fig. 3-1. Particle size distribution test conducted in dry mode.....	78
Fig. 3-2. Diffusion-oozing circle test (a) filter paper (b) specimen prepared on the filter paper...79	79
Fig. 3-3. SEM test (a) SEM equipment (b) gold coated specimens .....	79

Fig. 3-4. DSC test (a) DSC equipment (b) encapsulating press.....	80
Fig. 3-5. Cementitious composite mixture poured in transparent cylindrical cup .....	81
Fig. 3-6. FTA32 contact angle goniometer.....	82
Fig. 3-7. Particle size distribution of the EP particles (a) volume percentage passing (b) cumulative volume passing.....	83
Fig. 3-8. Diffusion-oozing circle test for EPWP samples, (a) & (b) 35 wt% & 40 wt% of paraffin, natural immersion (c) & (d) 40 wt% & 50 wt% of paraffin, vacuum impregnation.....	86
Fig. 3-9. Diffusion-oozing circle test for EPOP samples, (a) & (b) 35 wt% & 40 wt% of paraffin, natural immersion (c) & (d) 40 wt% & 50 wt% of paraffin, vacuum impregnation.....	87
Fig. 3-10. SEM morphology of EPW.....	87
Fig. 3-11. SEM morphology of EPO (a) EPO granules (b) single spherical frustule.....	88
Fig. 3-12. SEM morphology of composite PCMs (a) EPWP (b) EPOP .....	88
Fig. 3-13. Chemical composition of PCM composites .....	88
Fig. 3-14. DSC curves of paraffin and PCM composites .....	90
Fig. 3-15. Leakage of paraffin in cementitious mixtures.....	93
Fig. 3-16. DSC curve for exuded liquid and PCM integrated cementitious composites.....	93
Fig. 3-17. Behavior of water droplet on the surface of composite PCMs (a) EPWP (b) EPOP.....	95
Fig. 4-1. TESC panels for thermal performance test (a) timber molds (b) compaction of TESC using mechanical vibration.....	101
Fig. 4-2. Nicolet™ iS5 Spectrometer for FT-IR test.....	102
Fig. 4-3. Thermo-gravimetric analysis (a) TGA apparatus (b) ceramic pan .....	103
Fig. 4-4. Density bottle test (a) water pycnometer (b) sand slurry filled with water .....	104
Fig. 4-5. Technotest C030/2T compressive strength testing machine.....	105
Fig. 4-6. Preparation of thin TESC specimen slice using precision diamond saw.....	105
Fig. 4-7. Schematic diagram of pozzolanic reactivity test.....	106
Fig. 4-8. Self-designed heat storage set up (a) schematic diagram of test setup (b) physical arrangement.....	108
Fig. 4-9. FT-IR spectra of paraffin, EPO and EPOP .....	109
Fig. 4-10. TGA curves of paraffin and EPOP .....	111
Fig. 4-11. SEM images of TESC (a) distribution of EPOP in cement matrix (b) a single EPOP composite.....	113
Fig. 4-12. SEM image of the fracture surface of cement/ EPOP paste .....	114
Fig. 4-13. pH variation trend of EPO-Ca(OH) <sub>2</sub> solution with time .....	115
Fig. 4-14. Thermal inertia variation of NC and TESC .....	118
Fig. 4-15. Thermal energy storage rate of NC and TESC .....	118
Fig. 4-16. Interior surface heat transfer behavior of NC and TESC.....	119
Fig. 5-1. Flow table test (a) flow table apparatus (b) flow measurement of TESCM-60.....	124

Fig. 5-2. Apparent porosity test (a) vacuum pressure vessel (b) digital balance .....	125
Fig. 5-3. Drying shrinkage measurement with length comparator.....	126
Fig. 5-4. Precision diamond cutting saw.....	128
Fig. 5-5. Thermal conductivity test with the specimens kept at 10°C in thermal chamber .....	128
Fig. 5-6. Specimens subjected to accelerated thermal cycles test .....	130
Fig. 5-7. Apparent porosity and density of OCM and TESCMs .....	131
Fig. 5-8. Drying shrinkage development in OCM and various TESCMs .....	133
Fig. 5-9. Empirical relationship between shrinkage strain and PCM substitution level .....	134
Fig. 5-10. Compressive strength of OCM and various TESCMs at 7 and 28 days.....	135
Fig. 5-11. SEM morphology of TESCM-60.....	135
Fig. 5-12. SEM of interfacial contact zone of EPOP and cement matrix .....	136
Fig. 5-13. Thermal conductivity of OCM and various TESCMs.....	137
Fig. 5-14. Thermal inertia of OCM and various TESCMs.....	138
Fig. 5-15. TES capacity of OCM and various TESCMs .....	138
Fig. 5-16. Compressive strength of TESCMs after accelerated thermal cycles.....	140
Fig. 5-17. DSC curves of TESCMs before and after accelerated thermal cycles (a) TESCM-60 (b) TESCM-80.....	142
Fig. 6-1. Dispersion of CNT in acetone using ultrasonic bath (a) before dispersion (b) after dispersion.....	147
Fig. 6-2. Pelletizing of PCM composite discs containing carbon additives.....	150
Fig. 6-3. Schematic diagram of heat storage/release performance test.....	152
Fig. 6-4. Thermal imaging test (a) Testo thermal imaging camera (b) schematic diagram of specimen arrangement .....	153
Fig. 6-5. Prototype experiment set up (a) schematic diagram of test cell (b) physical set up .....	154
Fig. 6-6. SEM images of EPOP-G (a) graphite (b) EPO/graphite (c) & (d) EPOP-G.....	157
Fig. 6-7. SEM images of EPOP-CNT (a) & (b) MWCNTs, (c) & (d) EPO-CNT, (e) & (f) EPOP-CNT .....	158
Fig. 6-8. SEM images of EPOP-GNP (a) & (b) GNP, (c) & (d) EPO-GNP, (e) & (f) EPOP-GNP..	159
Fig. 6-9. FT-IR spectra of EPOP, EPOP-G, EPOP-CNT and EPOP-GNP .....	160
Fig. 6-10. DSC curves of paraffin and EPOP-G.....	161
Fig. 6-11. DSC curves of paraffin and EPOP-CNT.....	162
Fig. 6-12. DSC curves of paraffin and EPOP-GNP.....	162
Fig. 6-13. Thermal conductivity of composite PCMs containing heat transfer additives.....	164
Fig. 6-14. Heat storage behavior of EPOP containing heat transfer additives .....	165
Fig. 6-15. Heat discharge behavior of EPOP containing heat transfer additives .....	165
Fig. 6-16. IR thermography of EPOP integrated with carbon additives, (a) EPOP, (b) EPOP-GNP, (c) EPOP-CNT and (d) EPOP-G.....	167

Fig. 6-17. Comparison of inner surface heat gain rate of TESCM-80 with additives .....	169
Fig. 6-18. Convective heat gain energy variation of TESCM-80 with additives.....	170
Fig. 7-1. Summer daily temperature variation during seven consecutive days (22-26, January) in Melbourne, Australia .....	177
Fig. 7-2. Summer design day outdoor air temperature variation in the climate chamber.....	178
Fig. 7-3. Test hut set up (a) installation of insulation to the interior walls (b) PCM CB installed to the interior surfaces.....	179
Fig. 7-4. View of the test huts at site.....	180
Fig. 7-5. Meteorological station at the test site (a) weather station (b) console unit.....	182
Fig. 7-6. Simulated building model (a) thermal zones of the house (b) test room details .....	184
Fig. 7-7. Enthalpy temperature curve of PCM CB.....	187
Fig. 7-8. Indoor temperature variation during typical summer days .....	191
Fig. 7-9. Indoor temperature variation during summer design days.....	192
Fig. 7-10. West-wall surface temperature in GPB and PCM CB test huts.....	195
Fig. 7-11. Floor surface temperature in GPB and PCM CB test huts.....	195
Fig. 7-12. Indoor air temperature in GPB and PCM CB test huts.....	196
Fig. 7-13. West-wall surface temperature variation in OCB and PCM CB test huts .....	198
Fig. 7-14. Floor surface temperature variation in OCB and PCM CB test huts .....	198
Fig. 7-15. Indoor air temperature variation in OCB and PCM CB test huts .....	199
Fig. 7-16. Indoor operative temperature variation in the test room.....	203
Fig. 7-17. Variation of inner surface convective heat gain rates .....	203
Fig. 7-18. Inner surface temperature variation of the exterior wall (west wall) .....	204
Fig. 7-19. Effect of night ventilation on indoor operative temperature variation .....	206
Fig. 7-20. Effect of night ventilation on inner surface temperature of exterior wall (west wall) .....	206
Fig. 8-1. (a) Residential house for case study (b) living zone taken for analysis .....	211
Fig. 8-2. Floor plan of the residential house.....	212
Fig. 8-3. Airflow network for night ventilation in living zone .....	218
Fig. 8-4. Enthalpy temperature relationship for Bio-PCM <sup>TM</sup> -25.....	220
Fig. 8-5. Effective latent energy storage variation for a typical daily cycle .....	220
Fig. 8-6. Effect of PCM application on two consecutive days (1-2 December) .....	222
Fig. 8-7. Effect of phase transition temperature on PCM performance.....	226
Fig. 8-8. Variation of efficiency factors for different phase transition temperatures.....	227
Fig. 8-9. Effect of PCM layer thickness on efficiency.....	230
Fig. 8-10. Variation of efficiency factors for different PCM layer thicknesses.....	230
Fig. 8-11. Effect of night ventilation on PCM performance .....	233

# Chapter 1 Introduction

---

## 1.1 Background

The importance of reducing global fossil fuel consumption has long been identified as a major issue. However, it was only during the last few decades that much attention was given along with adequate economic incentives to take this into practice. More recently, atmospheric contamination of harmful gasses due to the combustion of fossil fuels for power generation has pressurized governments and institutions to seek alternative solutions. Moreover, climate change due to the anthropogenic activities leading to global temperature rise has also become a catalyst for the acceleration of research in the fields of energy conservation and management as well as the widespread implementation of renewable energy systems.

The building sector is responsible for approximately 30-40% of the primary energy consumption and 25% of greenhouse gas (GHG) emissions globally, of which more than 50% accounts for space-conditioning demands in developed countries [1]. Yet, a large amount of this energy is lost through the building envelope due to poor thermal characteristics such as thermal resistance and thermal energy storage (TES) capacity. In particular, modern developments in construction techniques and methods have urged buildings to become more structurally lightweight with very little thermal mass. This inadequacy of thermal mass hinders the ability of buildings to mitigate the effects of external thermal solicitations on its indoor, leading to large diurnal indoor temperature variations and increased space conditioning energy demands. Therefore, in recent years, much effort has been dedicated to developing more energy efficient building designs through the improvement in thermal resistance and TES capacity of building fabrics. Amongst the various energy efficient design techniques investigated, the use of dynamic thermal masses such as phase change materials (PCMs) is regarded as a potential method to achieve large TES capacity in buildings, which would lead to improved energy efficiency, GHG reduction as well as indoor thermal comfort. The key benefit of using PCMs is that it can significantly improve TES capacity without adding much to a

building's mass. This is due to the inherent merits of PCMs, which are high volumetric heat capacity as well as small temperature and volume variation during the phase transition process [2-4].

Meanwhile, cementitious materials such as cement mortar and concrete are among the most widely used construction materials worldwide and, integrating PCMs into these materials would have the greatest potential for its application in buildings. Thermal energy storage cementitious composites (TESCs) fabricated by integrating PCM into cement-based materials increases the TES capacity of cementitious materials and hence, facilitates energy conservation and energy savings in buildings. However, despite the beneficial outcomes shown by TESCs on thermal properties and thermal performance, undesired adverse effects have been reported on mechanical and durability properties [5-8]. This is mainly due to the instability or leakage of PCM and its subsequent interaction with cement matrix, thereby adversely affecting the physical and mechanical properties of developed TESCs. Hence, it is necessary to integrate PCM into cementitious materials without any associated leakage issues.

On the other hand, the heat transfer performance of a TES system can be very important to enable high heat storage and discharge rates in buildings so that the TES can be effectively operated. However, most of the PCMs have low thermal conductivity and heat storage/release rates are very limited [9-11]. Therefore, it is essential to improve the heat transfer performance of PCM in TES materials through efficient and economic enhancement methods such as, preferably, integrating high conductive additives into PCMs. Furthermore, experimental investigations on the enhancement of thermal performance in buildings incorporated with TESC would also be highly useful to demonstrate the actual effects of PCM in buildings, which are seldom detailed in the literature. Thus, a systematic experimental approach is crucial to overcome the above-mentioned issues so that the resultant PCM integrated cementitious composites can be successfully used in buildings.

Dynamic thermal simulations would be very helpful in understanding the effects of PCM and its thermophysical properties on the buildings' thermal performance under various boundary conditions. Although several criteria exist for evaluating the thermal performance of PCM in buildings, proper guidelines to optimize thermal performance of building incorporated with PCM are still deficient [12, 13]. Moreover, past research

has focused primarily on the performance enhancement of PCM on indoor thermal comfort or energy savings in buildings, while the latent heat storage efficiency of PCM has not been adequately addressed. Therefore, a combined optimization of latent heat storage efficiency and improvement in indoor thermal comfort would lead to an optimized TES system design.

The above-mentioned issues including the highlighted research gaps have been addressed through the development of a new kind of TESC that comprises a novel form-stable PCM integrated into cementitious composites. The present research uses experimental and numerical investigations on the novel form-stable PCM composite and the so-called TESCs. The following subsections provide detailed descriptions on the research problem statement, the significance of this research and the structure of this thesis.

## **1.2 Problem statement**

Two major issues among those identified in the previous section must be overcome for the successful application of TESCs in buildings. The first is the instability or PCM leakage associated with the direct integration of PCM into cementitious composites that must be prevented. The indirect incorporation methods such as microencapsulation and shape stabilization techniques as well as form-stable PCM have been reported as capable of preventing PCM leakage when integrated into cementitious composites. However, studies show that these methods not only have PCM instability issues but are also detrimental to the cement matrix, thus leading to significant effects on the mechanical and durability performance of the produced TESCs. The second major issue is the poor heat transfer performance associated with PCMs due to their low thermal conductivity. This poor heat transfer performance, particularly with organic PCMs such as paraffin, prevents the efficient use of the large LHTES capacity of TESCs in buildings.

Therefore, this research will primarily focus on addressing these two major problems along with the main objective to develop and characterize new form-stable PCM composites for integration into cementitious composites. Recent research has indicated that form-stable PCMs can be a good candidate for integration into cementitious materials, provided that the aforementioned issues are eliminated. Furthermore, form-

stable PCMs have several advantages over other PCM types such as ease in availability and fabrication, low cost and ability to be tailor-made for specific applications.

The physical, mechanical and thermal performance are key aspects that need to be studied when new form-stable PCMs are introduced into cementitious composites. It appears that the TESC developed by integrating form-stable PCM into cementitious composites resulted in reduced mechanical performance, even though they have significantly improved the thermal properties and thermal performance. This reduction in mechanical performance or loss of strength can be due to the instability of form-stable PCMs in cementitious composites and its interaction with the cement matrix. Furthermore, the low strength and stiffness of PCM composites also affect the strength development in TESCs. Hence, a detailed study of the mechanical, physical and thermal performances of TESCs is crucial.

To address the second major issue of PCM application in buildings, the thermal conductivity of composite PCMs must be improved. As far as different thermal conductivity enhancement methods are concerned, the integration of high conductive additives such as carbon-based additives can be considered as an effective technique. However, most of published research describes the use of a unique additive, and there is a lack of comparison between various additive components and their ability to enhance thermal performance. Carbon nanotubes (CNTs) and graphene nanoplatelets (GNPs) are advanced heat transfer promoters with surface area and thermal conductivity values exceeding  $750 \text{ m}^2/\text{g}$  and  $2000 \text{ W}/(\text{m}\cdot\text{K})$  respectively. Incorporating these materials into organic PCMs can yield significant improvements in heat transfer performance. Therefore, this research details the integration of different carbon-based additives into form-stable PCM as well as the evaluation of their respective performance enhancements. The carbon-based additives used in this study are graphite, CNTs, and GNPs.

While the thermal performance of PCM incorporated building components has been extensively studied with experimental and numerical approaches, these studies were mainly focused on PCM incorporated wallboards and concrete. The thermal performance assessment of form-stable PCM integrated cement mortars as an interior surface plastering mortars in buildings has been scarcely reported in the literature. Additionally, since this research undertakes the development of a new kind of TESC, its

thermal performance enhancement must be evaluated with respect to its application in buildings. Thus, the current research utilizes laboratory scale prototype test cells and modular sized test huts for the application of Thermal Energy Storage Cement Mortar (TESCM) as interior surface plastering mortars. The thermal performance of TESCM was evaluated and compared with ordinary cement mortar boards (OCB) and gypsum plasterboards (GPB).

Apart from the thermal performance enhancement of PCMs in buildings, one should also identify techniques to improve the efficiency of LHTES in buildings by utilizing maximum exploitation of PCM. The suitable phase transition temperature, the amount of PCM and PCM placement methods are some of the key factors used for determining the efficiency of PCM. Furthermore, the optimization studies should be conducted for the entire summer period to operate the PCM application effectively. However, the lack of any appropriate methodology to conduct such optimization studies and the limitations of existing methodologies are challenges to be overcome. It is, therefore, necessary to develop new thermal performance indicators to measure and optimize the thermal performance of PCM incorporated buildings. The building thermal simulations can be more appropriate to conduct such case studies.

Therefore, a comprehensive research program has been undertaken with the intention of conducting an extensive experimental and numerical study. The aims and objectives defined by the above-established research questions are further discussed in the following subsections along with the significance of this study.

### **1.3 Aim and objectives**

Based on the established research questions, the main aim of this research is to assess the feasibility of integrating form-stable PCM into cementitious composites for the application in buildings to enhance TES capacity and improve thermal performance. The specific research objectives can be outlined as follows:

1. Assess the feasibility of integrating form-stable PCM composites into cementitious materials and to prevent the leakage of PCM by developing new composites that are more stable.

2. Investigate the physical, mechanical and thermal properties of TESCs and TESCMs developed by integrating newly developed PCM composite into cement-based materials.
3. Enhance the energy storage performance of TESCMs by integrating high conductive heat transfer additives into PCM composites.
4. Evaluate the potential applications of TESCM in buildings through a comprehensive experimental and numerical study.
5. Optimize thermal performance and TES efficiency of PCM application in buildings by conducting a parametric case study.

## **1.4 Significance of the research**

Although the integration of PCM into cementitious composites can be a good technique to increase TES capacity in buildings, undesired adverse effects have been reported during the integration process into cement-based materials. A detailed analysis on the instability or PCM leakage in cementitious composites was carried out with the intention of developing new PCM composites that are less susceptible to such effects. The prevention of PCM leakage in cementitious composites and the enhancement of heat transfer performance with acceptable mechanical properties along with the identification of potential applications for TESCs in buildings, are major outcomes of this research.

Thermal simulations were conducted on buildings incorporated with PCM for the evaluation and optimization of thermal performance as well as for the assessment of TES efficiency by considering various parameters. The thermal performance indicators developed for conducting such parametric studies are another significant outcome of this research.

## **1.5 Thesis outline**

The research work consists of nine different studies, organized and presented in this thesis. All these studies were devised to address the defined objectives for enhancing the performance of TESCs and promoting its application in buildings. The current chapter presents the introduction to this research, the research problems, its scope, and objectives as well as the outline of this thesis. This is followed by an extensive literature

review on experimental and numerical studies related to this research in Chapter 2. Critical reviews on relevant studies, outlining the problems associated with the instability of PCM in cementitious composites and low heat transfer rates, will also be discussed. The incorporation of PCMs into building components will be reviewed, highlighting the potential benefits of PCM such as improvement in indoor thermal comfort and energy efficiency. Chapter 2 also summarizes the available literature, identifying existing research gaps and discussing the motivation behind this study.

Both Chapter 3 and Chapter 4 investigate the feasibility of integrating different form-stable PCM composites into cementitious composites. Particularly in Chapter 3, two different composite PCMs were considered; one with conventional expanded perlite (representing the most common practice of integrating form-stable PCM into cementitious composites) and the other with hydrophobic expanded perlite (which is introduced as a novel form-stable PCM composite). Both composite PCMs were fabricated, characterized and tested for their feasibility for integration into cementitious composites. The leakage of composite PCMs was observed and measured using various techniques as well as correlated to the surface characteristics of composite PCMs such as its contact angle and wetting tension properties.

Chapter 4 presents the material characterization, mechanical properties and thermal performance of PCM integrated cementitious composites based on the hydrophobic expanded perlite variant. Material characterization techniques including chemical compatibility (with Fourier transform infrared spectroscopy - FT-IR), thermal stability (with thermo-gravimetric analysis - TGA) and microscopic analysis (Scanning Electron Microscopy - SEM) are carried out. Mechanical properties and thermal energy storage performances are also assessed by compressive strength tests and self-designed heat storage experiments, respectively.

As an extended study of Chapter 4, a detailed study is performed in Chapter 5 to investigate the physical, mechanical and thermal properties along with the mechanical and thermal reliability of cement mortars integrated with varying amounts of form-stable PCM. The experimental program was conducted to develop TESCMs by replacing fine aggregates in conventional cement mortars with PCM composites. Volume replacement levels starting from 20% till 80% were studied for their impact on physical, mechanical and thermal properties.

Chapter 6 describes the study of adding various carbon-based heat transfer additives such as graphite, CNTs, and GNPs into form-stable PCMs. The fabricated PCM composites were characterized for their micro-morphology, thermophysical properties and chemical compatibility using SEM, DSC, and FT-IR respectively. The enhancement of thermal conductivity and thermal performance are also studied and included within this chapter.

Chapter 7 is dedicated to experimental and numerical studies conducted to evaluate thermal performance enhancement in buildings with TESCMs. The experimental study utilizes laboratory scale prototype test cells subjected to controlled climate conditions and test huts exposed to the outdoor environment. While the prototype test cell experiments enable thermal performance evaluation under controlled climate conditions, the test hut experiments assess the thermal performance under realistic climate conditions. In addition, numerical studies were used to assess the thermal performance of full-scale buildings with TESCMs. A multi-storey office building without any active air-conditioning systems was considered with its conventional interior surface plastering mortar replaced by TESCMs for application onto brick walls. Dynamic thermal simulations were performed using the building energy and thermal load simulation software, EnergyPlus, for the climate zone of Melbourne, Australia. Furthermore, studies were also conducted to enhance the thermal performance of TESCM by improving the solidification process of PCM with the activation of night ventilation.

Chapter 8 contains details of the parametric study conducted for the optimization of thermal performance in buildings incorporated with PCM. As opposed to traditional methods, this study optimizes the performance of PCM by increasing the latent heat storage efficiency of PCM and improving the indoor thermal comfort. New performance indicators were developed and utilized to measure the thermal performance of a residential building incorporated with PCM. This is followed by the identification of the optimum phase transition temperature, quantity of PCM and effective night ventilation through a case study for four major climate zones in Australia: Melbourne, Sydney, Brisbane, and Perth.

Finally, Chapter 9 summarizes the major conclusions of this thesis. Recommendations for future work will also be discussed.

# Chapter 2 Literature review

---

## 2.1 Overview

A building can be considered as a complex thermodynamic system, subjected to internal and external thermal solicitations, with the building's envelope as the boundary of the system. The thermal balance of this system is affected by the internal and external thermal loads, the thermal resistance of the envelope and energy storage capacity. The incorporation of appropriate thermal energy storage (TES) system into building fabrics enhances the energy storage capacity, helping to store excess thermal energy and hence lowering the required energy production to attain the energy balance. Thermal energy storage in buildings can be achieved by sensible heat storage and latent heat storage. Compared with sensible heat storage, latent heat storage methods provide much higher energy storage density within a narrow temperature range [4, 14, 15]. Latent heat storage are operated by the absorption/release of energy during a phase change process.

It has been reported that the TES enhancement of buildings with latent heat storage methods, by incorporating PCM into building fabrics, can significantly increase the energy utilization rate. Lightweight buildings in particular, due to their low thermal mass, tend to have high indoor temperature fluctuations and hence, result in high energy demands. Incorporating PCM into such buildings can reduce indoor temperature fluctuations and energy demands without significantly adding to its building mass. In this regard, the incorporation of PCM into building components is the very first step that needs to be considered. The cementitious materials are the most widely used construction materials in buildings and therefore, they have great potential to incorporate PCM. However, it must be noted that the incorporation of PCM into cementitious composites should not be detrimental to the mechanical and durability performance of produced thermal energy storage cementitious composites (TESCs). An encapsulation method involving the absorption of PCM into porous granular materials, known as form-stable PCM composites, can be considered as the preferred method of incorporation of PCM into cementitious composites. This is due to the inherent merits of

form-stable PCMs such as ease of availability and fabrication, low cost and compatible with construction materials. However, there are several limitations and issues present for the integration of form-stable PCM into cementitious composites, which present as barriers for the successful development of form-stable PCM integrated TESCs. This chapter presents an extensive literature review related to the application of PCM for TES enhancement in buildings. The literature review has been systematically carried out to report the studies that are relevant to the main objectives of this research. Fig. 2-1 illustrates the thermal balance of a building with the consideration of internal and external thermal solicitations as well as the thermal properties of building envelope influencing the indoor thermal comfort. Furthermore, the research framework with the critical areas of literature review to address the specific objectives of this research are also provided in Fig. 2-1.

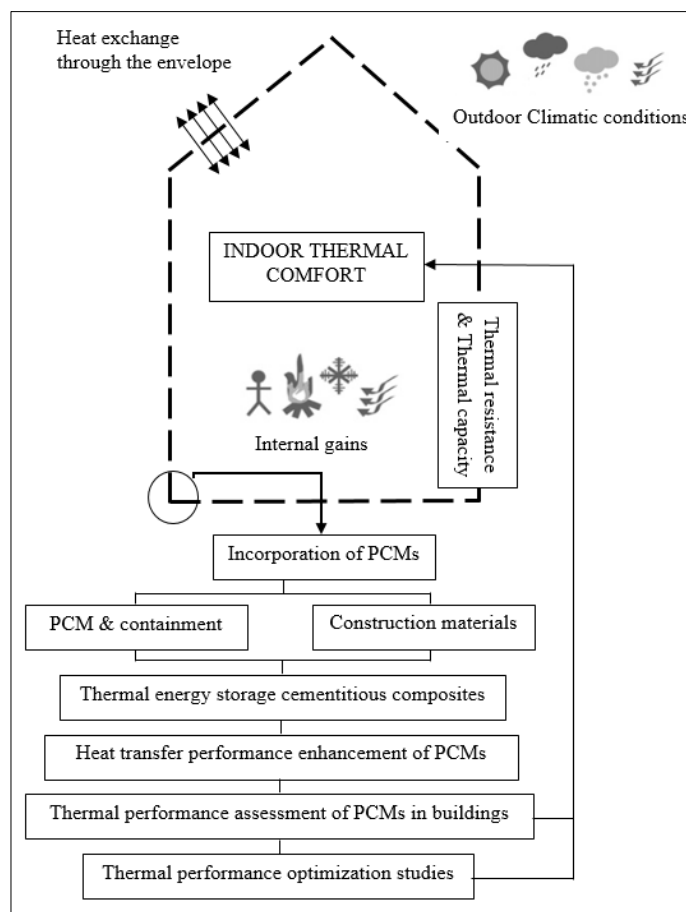


Fig. 2-1. Building as a thermodynamic system and potential of PCM to improve thermal comfort [2, 9, 16]

## 2.2 Thermal energy storage (TES)

The buildings incorporated with TES systems have the ability to store the daytime surplus solar thermal energy and subsequently released back to the indoor during cooler nights. TES can be in the form of sensible storage and latent heat storage. Sensible storage methods are based on the heat storage by raising the temperature of the material and the amount of energy storage ( $Q$ ) is directly proportional to the mass ( $m$ ) and temperature raise of the material ( $dT$ ) as shown in Eq (2-1).

$$Q = \int_{T_i}^{T_f} m C_p dT \quad (2-1)$$

where  $m$  and  $C_p$  are the mass and the specific heat capacity of the material respectively.  $T_i$  and  $T_f$  are initial temperature ( $^{\circ}\text{C}$ ) and final temperature ( $^{\circ}\text{C}$ ) of the TES system respectively.

The traditional materials used for sensible storage in buildings are bricks, concrete, water, etc. Although this form of TES can be easily achieved in buildings, provision of adequate thermal storage with sensible heat capacity requires large building mass. Moreover, it has several drawbacks such as large temperature variation during the heat storage/release process; large building mass incurs high cost and the payback period of such high building mass is too long, and accumulated heat in such large mass could make the building very uncomfortable until it cooled down [17].

Latent heat thermal energy storage (LHTES) is based on the heat energy absorbed or released when a material undergoes a phase change process. These materials when changing from one phase to another (e.g. solid to liquid, liquid to gas, or vice versa), they absorb or release thermal energy according to the latent enthalpy of the material. The Eq. (2-2) shows the formula for stored heat energy ( $Q$ ) when the material subjected to the temperature variation from  $T_i$  to  $T_f$ . The specific characteristics of latent heat storage are very high energy storage density and the energy storage occurs within a narrow temperature range. The materials used for latent heat storage are generally referred as phase change materials (PCMs). Fig. 2-2 shows the typical energy storage behaviour of sensible and latent heat storage materials with the temperature.

$$Q = \int_{T_i}^{T_m} m.C_p.dT + m.a_m.\Delta H_m + \int_{T_m}^{T_f} m.C_p.dT \quad (2-2)$$

where  $T_m$  is the phase transition temperature ( $^{\circ}\text{C}$ ),  $a_m$  and  $\Delta H_m$  are melted fraction of PCM and latent heat capacity per unit mass ( $\text{J}/\text{kg}$ ) respectively.

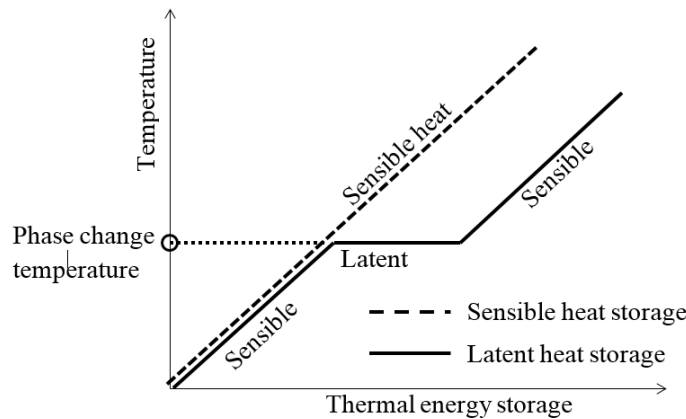


Fig. 2-2. TES behavior of sensible and latent heat storage materials

### 2.3 PCMs and its desired characteristics

The PCMs used for LHTES applications in buildings mostly have their phase transformation from solid to liquid as other phase change processes have specific limitations. For example, phase change vaporization process (i.e. solid to gas and liquid to gas processes) has the highest latent enthalpy, however, it cannot be used for TES purposes due to large volume change during phase transition process. The singular storage capacity within a narrow temperature variation and negligible volume changes are the key advantages of solid-liquid PCMs, thus enabling them to implement large energy savings in buildings. Moreover, some PCMs can be operated within the human comfort temperature range so that the uncomfortable temperature variations associated with sensible heat storage  $Q$  can be avoided.

The PCMs used for building applications should possess certain desired properties to suit for TES application. These desired properties can be classified into thermophysical, kinetic, chemical and economic properties and the relevant key characteristics are summarized in Table 2-1. It is worth mentioning here that the real PCMs cannot have all these desired properties. Therefore, the choice of appropriate PCM for particular TES application should be made on certain level of compromise.

Table 2-1 Key characteristics of PCMs for thermal energy storage [3, 4, 18]

Thermophysical properties	Suitable phase change temperature for building application
	High latent heat of fusion and high thermal conductivity to assure high heat transfer rate
	High specific heat capacity to accommodate further storage as sensible energy
	Small volume change during phase transition
	Congruent melting and freezing to ensure homogeneous phase during transition
	Physically and thermally reliable under thermal loading and unloading conditions so that it can be used in the long run
Kinetic properties	Minimum supercooling effect
	Little or no decomposition during crystallization
Chemical properties	Chemical compatibility with encapsulated materials and building materials
	Non-corrosiveness to encapsulated materials and building materials
	Non-toxic, non-flammable, non-explosive and little or no decomposition
	Chemical non-degradation in the long run
Economic feasibility	Cost effective
	Available in abundant quantity
Environmental feasibility	Minimum impact to the environmental during the service life
	Environmentally sustainable material
	renewable sources of supply

## 2.4 Types of PCMs

PCMs are divided into three categories according to its chemical composition, which are

- Inorganic PCM
- Organic PCM
- Eutectic PCM

Among those different PCM types, inorganic PCMs were the very first investigated as LHTES materials, which are broadly classified into metallic PCMs and hydrated salts. Of the inorganic PCM, metallic PCM have not received much attention due to high weight concerns, corrosion and very high phase change temperatures [14]. However, hydrated salts have been widely investigated for low and medium temperature TES applications. The phase transition processes in hydrated salts occur by hydration and dehydration processes for solid to liquid and liquid to solid processes, respectively. When the temperature increases, the hydrated salt crystals dissolve in its water and absorb heat. Similarly, when the temperature drops, the anhydrate salts become hydrated and crystallizes with the evolution of heat [19]. Some of the advantages of hydrated salts compared with organic PCMs are that they are non-flammable, inexpensive and they have relatively high latent heat capacity per unit volume. However, these materials are corrosive and require special containers to use in building applications. Although special containment can be achieved by incurring additional cost, the major limitations of inorganic PCM in building applications are their tendency to supercool and melt incongruently [16]. More precisely, when melted phase of dehydrated salts reaches the solidification temperature, partial solid phase settles out and resulting in incomplete conversion to the hydrated product below the melting temperature. As a consequence, the latent heat is decreased and unless prevented, this process is irreversible. Therefore, inorganic PCMs were not considered as suitable for the incorporation into building materials and components [17].

Organic PCMs including paraffin and non-paraffin or fatty acids have been widely studied for the incorporation into building materials and components. They have several advantages over inorganic PCMs as summarized below:

The advantages of organic PCMs [18]:

- Wide temperature range to choose
- They are chemically inert and thermally stable (can withstand for large number of melt/freeze cycles)
- Congruent melting process, no supercooling effect and do not undergo phase segregation
- Most of the organic PCMs are nontoxic and non-corrosive (although fatty acids are mild corrosive)
- low vapor pressure in melted state
- They are compatible with construction materials
- Recyclable

The limitations of organic PCMs

- Low thermal conductivity
- Moderately flammable
- Quite expensive compared to inorganic PCMs

On the other hand, Eutectic PCMs are a mixture of two or more different PCMs to reduce the incompatibility issues such as supercooling effect and large phase transition temperature range. Eutectic PCMs have many advantages over singular PCM including, sharp melting temperature and high volumetric heat storage density. However, a limited test data is available on their thermophysical properties. A comparative analysis of the advantages and disadvantages of different PCM types is given in Table 2-2 [2, 18, 20, 21].

Table 2-2 Comparison of different PCM types

Features	Organic PCM		Inorganic PCM		Eutectic PCM		
	Paraffin	Non-paraffin	Hydrated salts	Metallic	Organic-inorganic mixture		
General formula	$C_nH_{2n+2}$	-COOH	$AB.nH_2O$	-	-	-	-
General features	Most widely used and commercially available PCMs		Oldest and most studied	Much attention has not been paid	Mixture of two or more PCMs		
Thermo-physical properties	Do not have sharp melting temperature	Sharp melting point	Sharp melting point	-	Desired phase change temperature can be achieved with very sharp melting point		
	120- 260 J/ g	130- 250 J/ g	100- 200 J/ g	25- 90 J/ g	100- 230 J/ g		
	High volume change		Low volume change	Slats settle down at bottom and reduce capacity	Low volume change		
	No tendency to phase segregation		supercooling	-	Melts and freeze without segregation		
	Low thermal conductivity		High thermal conductivity		Moderately high conductivity		
Chemical properties	Chemically inert	Mild corrosive	Corrosion on metal containers		No data available		
	Flammable	Flammable	non flammable				
Economic feasibility	expensive	2 to 3 times than paraffin	Low cost	Expensive	Very expensive		

## 2.5 Methods of PCM incorporation into construction materials

Thermal energy storage of a building can be increased by incorporating PCM into construction materials such as cement mortar, gypsum boards and concrete for the application in building components of walls, floor, ceiling, etc. The successful utilization of PCM and resultant TES capacity largely depends on the method of incorporation into construction materials. Some of the considerations when choosing an incorporation method include problems associated with PCM leakage, heat transfer performance, volume changes during the phase change process and adverse effects on the physical and mechanical properties of the building materials/components [22-24]. PCM incorporation methods can be broadly classified as direct incorporation and indirect incorporation methods.

### 2.5.1. Direct incorporation methods

#### 2.5.1.1. *Immersion*

PCM can be directly incorporated into construction materials/elements by using immersion method, where construction elements such as concrete blocks, bricks, and wallboards are dipped into the liquid PCM for the absorption into construction elements. Immersion process is simple and easy to use, where impregnation process can be carried out at the end of the production line of building elements or at a later time [25]. Additionally, it enables the conversion of conventional building elements to PCM-enhanced building elements when required. However, the problems associated with immersion method are leakage of liquid PCM, especially when it is exposed to multiple thermal cycles, leading to decreased TES capacity, mechanical properties and durability of construction materials [2, 3, 16].

Feldman et al. [25] successfully incorporated a mixture of fatty acids into gypsum wallboard by immersion technique. The resultant PCM wallboard retained 25% of fatty acids without showing any leakage. Thermal properties of PCM wallboard was reported as the melting temperature and thermal storage capacity of 17 - 18°C and 350 J/m<sup>2</sup> respectively.

### 2.5.1.2. *Direct impregnation method*

This method introduces PCM at the point of production of building elements where PCM is mixed with other construction materials during the production line. Direct impregnation method has many advantages over immersion technique as stated below [26]:

1. Production cost lowers as additional labors are not required.
2. Require little additional equipment.
3. Conventional production facilities can be easily modified to produce PCM-enhanced building materials.
4. Economic benefits can be achieved by continuous processing.

A commercial mixture of fatty acid esters was used as PCM to directly impregnate into gypsum wallboard [25]. The maximum amount of fatty acid ester retained was 21-22 wt% with the melting temperature and latent heat was being as 17.6°C and 29.1 J/g respectively. Furthermore, authors claimed that the PCM-enhanced wallboard has tenfold thermal energy storage capacity compared to conventional gypsum wallboard.

Direct incorporation methods such as immersion and direct impregnation are simple and easy to use; however, the amount of PCM absorption and hence TES capacity are very low. Furthermore, they are more vulnerable to PCM leakage and can adversely affect the mechanical and durability performance of construction elements. Therefore, direct incorporation methods are currently rarely practiced [18].

## 2.5.2. Indirect incorporation methods

### 2.5.2.1. *Overview*

Indirect incorporation methods include encapsulating or supporting PCM by solid surface materials before incorporating into building materials/elements. Indirect incorporation of phase change materials has several advantages over direct incorporation. Especially, it can hold liquid PCM effectively and reduce the reactivity with the outer environment. However, containment materials should have specific physical, thermal and chemical properties as listed below [10, 18]:

- It should meet the strength, durability, thermal stability and thermal reliability requirements
- Protect the PCM from destruction and interaction with the outer environment by acting as a physical and chemical barrier
- Provide adequate surface area for efficient heat transfer
- Structurally stable to provide rigidity to the structure
- Environmentally sustainable material

Indirect incorporation methods can be further classified into -macro and -micro encapsulations, shape stabilization and form stable PCMs based on the method of incorporation and supporting materials. The following sections explain different indirect incorporation methods.

#### **2.5.2.2. *Macro-encapsulation***

In the macro-encapsulation method, PCMs are enclosed in macroscopic containers (encapsulation size from few millimeters to up to several liters) such as tubes, poaches, spheres and panels for subsequent use in construction elements [27]. Macro-encapsulation improves the compatibility of PCM with the outer environment by acting as a barrier and preventing the liquid PCM leakage. It also reduces the external volume changes as containers are capable of accommodating internal volume change of PCM. A major drawback of this application is, however, the poor thermal conductivity of PCM and hence, heat transfer performance of PCM is largely reduced. It also needs to be protected against destruction while embedding into building construction such as drilling holes and nails [28, 29]. Fig.2-3 shows different types of macro encapsulation techniques such as metal ball encapsulation, flat panel encapsulation, spherical PCM balls and PCM encapsulated in tubes.

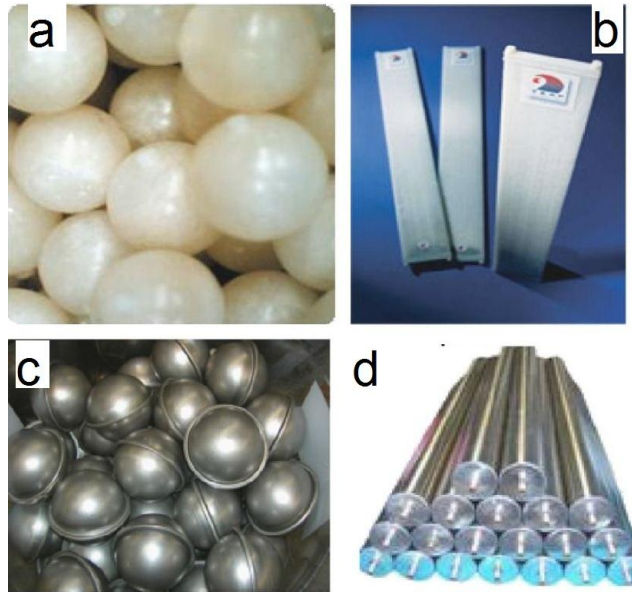


Fig.2-3. Various macro-encapsulation configurations (a) metal ball, (b) polypropylene flat panel, (c) spherical PCM balls and (d) PCM in tubes [21]

### 2.5.2.3. *Microencapsulation*

In this technique, a thin solid shell, usually made from natural or synthetic polymers, is used to encapsulate with the particle size ranging from 1  $\mu\text{m}$  to 1000  $\mu\text{m}$ . Fig.2-4 shows the microencapsulation technique in terms of a schematic diagram of microcapsule and scanning electron microscopy (SEM) image of the capsules. The microcapsule essentially contains a composite of core and shell elements, where core consists of PCM and the outer shell made of polymers. This method has several advantages over other incorporation methods, such as prevention of PCM leakage and reactivity with surrounding environment as the polymer shell acts as a barrier for physical and chemical interaction. It also possesses high heat transfer rate compared to macro encapsulation due to the micronized size of the particles and increased surface area. Furthermore, the phase segregation and volume changes during the phase change process are significantly reduced within the microscopic scale of the materials [30, 31]. However, a major drawback of microencapsulation technique is the low strength and stiffness of polymer microcapsules and hence, they are prone to be destructed and destroyed during mixing with other materials. Microencapsulated PCMs can be fabricated by physical or chemical processes. Some of the commonly used physical methods are pan coating, air-suspension coating, spray drying, etc., while the chemical methods include interfacial polymerization, in-situ polymerization, and coacervation methods [32-34].

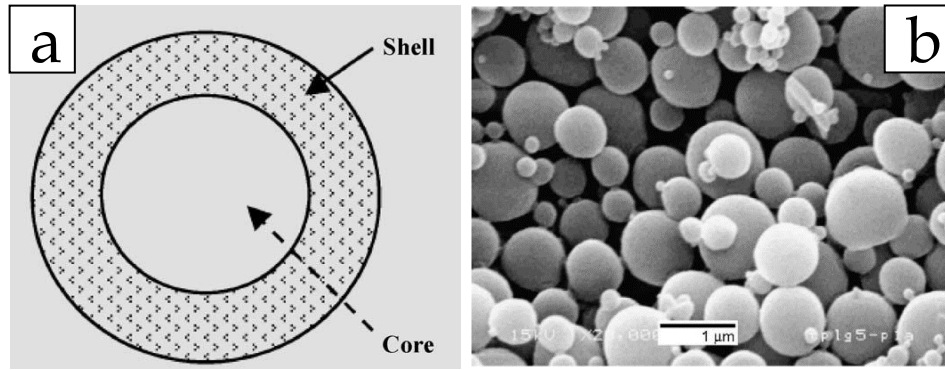


Fig.2-4. Microencapsulated PCM (a) description of a microcapsule (b) SEM image of micro-encapsulated PCM particles [31, 32]

#### 2.5.2.4. *Shape-stabilized PCMs*

In this technique, PCMs are packed into a supporting material which has higher melting temperature than PCM and typically used supporting materials include high-density polyethylene (HDPE), styrene and butadiene. The fabrication process of shape stabilized PCMs are conducted by blending the PCM and supporting material above the melting temperature of the supporting material and then cooling down below the glass transition temperature until the composition becomes solid [35]. The compound material remains its shape during the operative temperature of PCM and this reduces the susceptibility of liquid PCM leakage. Although this kind of PCMs can well keep its shape during the melting process of PCMs, they have low thermal conductivity, and hence the heat transfer rate of PCMs are limited [36, 37]. Some studies attempted to increase the heat transfer rate of shape stabilized PCMs with the addition of high conductive filler materials such as graphite [38-40].

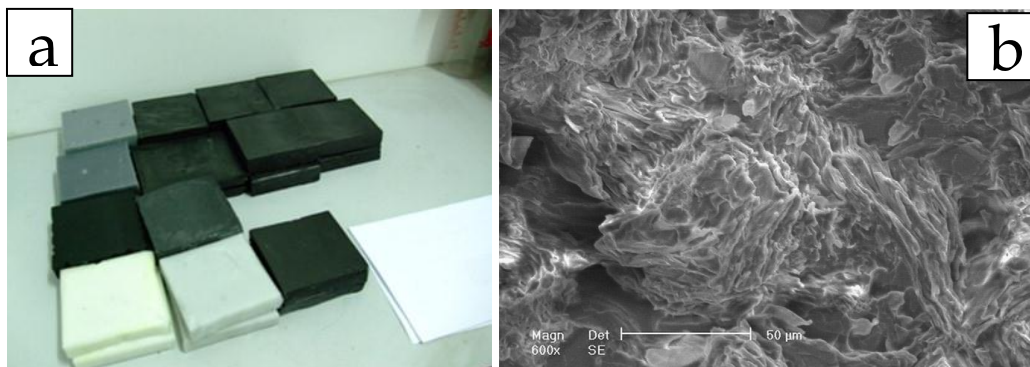


Fig. 2-5. Shape stabilized PCM (a) paraffin/HDPE shape stabilized PCM with graphite additives (b) SEM image of paraffin/HDPE shape stabilized PCM [38]

### 2.5.2.5. *Form-stable PCMs*

Form-stable PCMs are a composition of PCM and porous supporting material, where the PCM is absorbed and retained into the open pores of supporting materials due to capillary forces and surface tension forces. Unlike shape stabilized PCMs, form-stable PCMs do not require high temperature treatment to melt the supporting materials.

Form-stable PCM composites are fabricated by impregnating PCM into porous supporting materials and the impregnation method can either be natural immersion or vacuum impregnation. Natural immersion is conducted by directly mixing melted PCM and porous supporting material at atmospheric pressure conditions to absorb PCM into the pores of supporting materials naturally. Although this method is simple, easy to implement and do not require special equipment, the retention capacity of supporting material and resultant TES capacity was significantly low compared to the porosity of supporting materials [18, 41-44]. Therefore, vacuum impregnation method is adopted to increase the PCM absorption ratio into supporting materials. Vacuum impregnation mechanism can be described as impregnating liquid PCM into the porous granules under very low-pressure conditions. This process evacuates the air and moisture filled in the pores and enables the porous materials to absorb a large amount of PCM. Thus, high absorption amounts and large TES capacity can be achieved. Fig. 2-6 shows a typical vacuum impregnation apparatus used to fabricate form-stable PCMs.

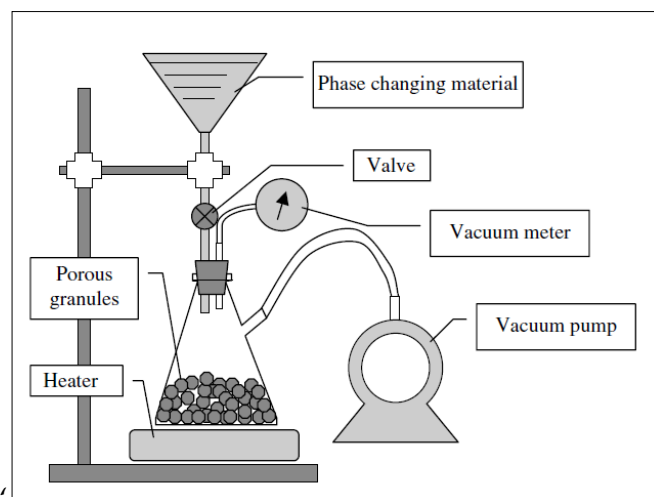


Fig. 2-6. Typical vacuum impregnation setup [41]

Many researchers have studied the effect of impregnation method on the absorption capacity of form-stable PCMs. For instance, Zhang et al. [44] stated that large amount of PCM could be impregnated into the pores of supporting materials with pore diameter starting from 1 to 100  $\mu\text{m}$  by vacuum impregnation, which enables the granular composite has large TES capacity. In another study, Zhang et al. [42] observed that, although porosity of porous aggregates was very high (up to 75%), it absorbed a small amount of PCM when following natural immersion method. They explained the main reason as pores blocked by air, which prevented the migration of liquid. Furthermore, by vacuum evacuation of air, 72.5% of pores are filled with liquid compared to just 11% for natural immersion method. Also, Ling et al. [45] compared natural immersion and vacuum impregnation technique and concluded that the absorption capacity of granular composites prepared by vacuum impregnation method increased by 30% and leakage after 100 thermal cycles were reduced.

As far as the performance of form-stable PCMs is concerned, several studies reported that composite material comprising working substance (PCM) and a supporting material (porous granules) enables the PCM to store and release heat energy, while supporting material retain the melted phase from leakage and keep the whole system in solid state [46-48]. An additional advantage of granular supporting materials is that the improved heat transfer rate as supporting materials have higher thermal conductivity than most of the PCMs [49-51]. Moreover, they are non-corrosive, have high specific surface area, and with the provision of high porosity, a large heat storage density can be achieved [52].

In the last two decades, a large number of form-stable PCMs have been fabricated by incorporating PCMs such as paraffin, fatty acids and eutectic mixtures of binary PCM into porous supporting materials such as diatomite, expanded perlite, expanded graphite and clay minerals. A summary of literature related to the fabrication and thermophysical properties of form-stable PCMs are presented in Table 2-3, and relevant findings are also discussed.

Table 2-3 Fabrication and thermo-physical properties of various form-stable PCM composites

Supporting material	PCM	Relevant findings	Ref
Diatomite	Polyethylene glycol (PEG)	<ul style="list-style-type: none"> <li>The form-stable PCM fabricated by vacuum impregnation method retained 50wt% of PEG in diatomite.</li> <li>The composite PCM had melting temperature and latent heat of 27.70°C and 87.09 J/g respectively.</li> </ul>	[53]
	decanoic-dodecanoic acids	<ul style="list-style-type: none"> <li>Composite PCM retained 57 wt% of binary fatty acids</li> <li>The melting temperature and latent heat derived as 16.74°C and 66.81 J/g respectively.</li> </ul>	[54]
	Paraffin	<ul style="list-style-type: none"> <li>Paraffin/calcined diatomite prepared by natural immersion method retained 61wt% of paraffin in the composite.</li> <li>The phase transition temperatures and latent heats were 33.04°C and 89.54J/g for melting and 52.43°C and 89.80J/g for freezing respectively.</li> </ul>	[55]
Expanded perlite	Lauric acid	<ul style="list-style-type: none"> <li>60 wt% of lauric acid can be retained by vacuum impregnation method.</li> <li>The phase transition temperatures and latent heats were 44.13°C and 93.36 J/g for melting and 40.97°C and 94.87 J/g for freezing respectively.</li> </ul>	[56]
	Capric acid	<ul style="list-style-type: none"> <li>55 wt% of capric acid can be achieved by vacuum impregnation method.</li> <li>The phase transition temperatures and latent heats were 31.80°C and 98.12 J/g for melting and 31.61°C and 90.06 J/g for freezing respectively.</li> </ul>	[57]
	Paraffin	<ul style="list-style-type: none"> <li>Direct impregnation method resulted in the retention capacity of 60 wt% of paraffin in expanded perlite.</li> <li>The melting temperature and latent heat were determined as 27.56°C and 80.9 J/g respectively.</li> </ul>	[58]

Vermiculite	Capric-myristic eutectic acid	<ul style="list-style-type: none"> <li>• 20 wt% of eutectic acid can be retained using vacuum impregnation method.</li> <li>• The phase transition temperatures and latent heats were 23.35°C and 27.46 J/g for melting and 14.54°C and 31.42 J/g for freezing respectively.</li> </ul>	[59]
	Paraffin	<ul style="list-style-type: none"> <li>• 60 wt% of paraffin can be retained into the open pores of vermiculite for direct impregnation method.</li> <li>• Composite PCM had onset melting temperature and latent capacity of 27°C and 77.6 ± 4.3 J/g respectively.</li> </ul>	[60]
Expanded graphite (EG)	Polyethylene glycol (PEG)	<ul style="list-style-type: none"> <li>• 90% of PEG can be achieved for natural immersion method.</li> <li>• The melting temperature and latent heat of 61.46°C and 161.2 J/g respectively.</li> </ul>	[61]
	Sebacic acid (SA)	<ul style="list-style-type: none"> <li>• The SA/EG composite contains 85wt% of SA in the composite.</li> <li>• The composite PCM has melting temperature and latent heat of 128°C and 187 J/g respectively.</li> </ul>	[62]
	Paraffin	<ul style="list-style-type: none"> <li>• 85.6wt% of paraffin can be achieved for natural immersion method.</li> <li>• Two melting peaks were observed with the melting temperatures of 31.85°C and 48.93°C and latent heats of 46.55 J/g and 114.9 J/g respectively.</li> </ul>	[63]

## 2.6 Building components containing PCM

### 2.6.1. PCM incorporated wallboards

The application of PCM into plasterboards such as PCM-enhanced wallboards and plasterboards are widely studied for improving the building energy efficiency. PCM incorporated wallboard prepared by immersion and direct impregnation method showed a significant increase in energy storage capacity. Wallboards can be considered as a successful candidate to incorporate PCM due to the following reasons [64]:

1. They are widely used in lightweight construction practices and are economical
2. Wallboards have large heat exchange surface to depth ratio
3. Surface tension and capillary forces can effectively hold liquid PCM from leakage
4. PCM wallboards can be used in new construction or can be applied as a refurbishment

Some of the previous works mainly focusing on the fabrication of PCM impregnated wallboards are explained herein. Ahmad et al. [65] prepared a PCM integrated gypsum wallboard by mixing a commercially available PCM granulates (GR25) having a particle size range of 1-3 mm and containing 35 wt% of paraffin in the granules. The fabricated PCM wallboard (Fig. 2-7) contained 15 wt% of granulate PCM with the melting temperature of 26°C. Authors reported that the PCM granulate integrated wallboard did not bring any significant improvement in the attenuation of temperature oscillations since the amount of PCM in the wallboard is insufficient. Furthermore, increasing the amount of PCM will result in thicker wallboards which will eventually lose the function of lightweight envelopes. The effusion of paraffin from granulates was also observed, which could substantially affect the durability and TES capacity of such wallboards.

Shilei *et al.* [66] prepared a PCM wallboard by impregnating eutectic mixture of binary fatty acids (capric acid and lauric acid) into conventional gypsum wallboard by immersion technique. The team successfully impregnated 26 wt% of PCM into the wallboard and the PCM wallboard showed higher heat storage ability than conventional wallboard as shown in Fig. 2-8. In another study [67], a novel form-stable phase change wallboard was prepared by impregnating a eutectic mixture of binary fatty acids into gypsum granules followed by the fabrication of PCM wallboard. The form-stable PCM wallboard containing 25 % of binary fatty acids showed good thermal stability with high

TES capacity. Oliver [68] also prepared a gypsum wallboard by mixing gypsum with a commercially available microencapsulated PCM (Micronal DS 5001X) and other reinforcing additives in a weight ratio of 37.5 – 47.5% of microencapsulated PCM. Authors claimed that a PCM wallboard containing 45% of microencapsulated PCM stores three times more energy than conventional wallboard, five times more than a thermal brick and 9.5 times more than a brick wall.

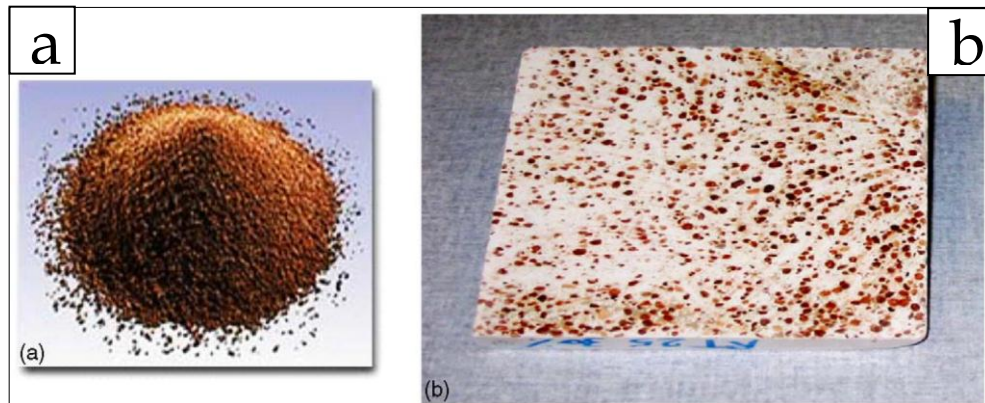


Fig. 2-7. Granulate PCM integrated gypsum plasterboard (a) Granular PCM composite (b) PCM integrated wallboard [65]

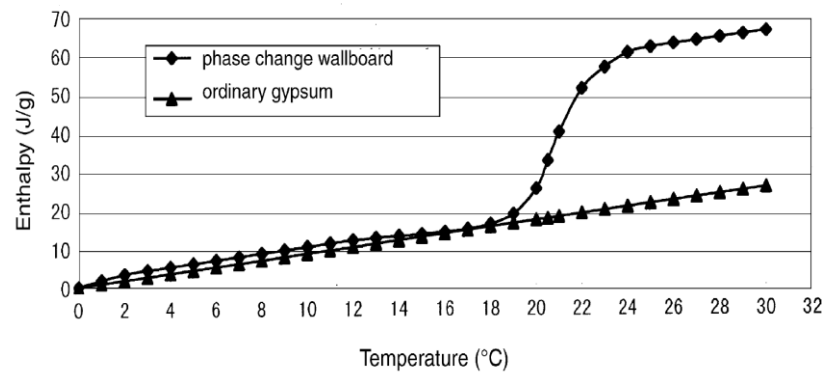


Fig. 2-8. Comparison of TES capacity of PCM wallboard with conventional wallboard [66]

### 2.6.2. PCM incorporated cement mortar and concrete

Cementitious materials such as cement mortar and concrete are most widely used construction material and incorporation of PCM into cementitious materials not only enhance the TES capacity of this popular building material but also facilitates energy conservation and savings in buildings. Among the different cementitious materials, concrete is one of the well-known construction material and its large thermal mass can

be advantageous to reduce the heating and cooling energy demands in buildings [69]. TES capacity of concrete can be further increased with the incorporation of PCM into concrete. A concrete mixture produced with appropriate PCM and having acceptable structural and thermostatic properties is called thermocrete [20].

A wide variety of application methods has been employed to enhance the TES capacity of cement-based materials with PCM. A direct impregnation method that involved directly mixing the cementitious composite with PCMs was initially adopted to develop TESCs. However, this method suffered from leakage of liquid PCM and subsequent adverse effects on cement matrix due to the interaction between leaked PCM and cementitious composites in construction system [18, 70]. Therefore, this method is currently rarely used. To overcome these issues, encapsulation techniques such as polymer microencapsulation and form-stable PCMs are introduced into cementitious composites. In this technique, the PCM encapsulated by polymer shells or porous supporting materials are either replaced for aggregates or added as cement admixture in cementitious composites. An extensive review of existing literature related to different PCM incorporation methods into cementitious composites is presented in the following sections.

#### ***2.6.2.1. Direct impregnation of PCM into cementitious composites***

This is very old method adopted to increase the thermal capacity of cement-based materials with the incorporation of PCM. In this approach, a direct impregnation or immersion method was used to integrate PCM into cement-based materials. Hawes and Feldman [71] studied the PCM absorption and stability into concrete with the consideration of different PCM types such as paraffin, polyethylene glycol, and butyl stearate into different concrete types such as regular concrete block, pumice concrete and lightweight concrete by immersion technique. The effect of main parameters including PCM temperature, viscosity and void ratio of concrete on PCM absorption capacity was investigated. It was found that most concrete specimens were absorbing in the range of 7-17% of the voids with the allowance of sufficient immersion time. However, their stability in the long term was significantly affected by the alkaline attack in the concrete environment [72]. This is due to the presence of  $\text{Ca}(\text{OH})_2$  in concrete, which are not compatible with PCMs. Authors recommended to improve the compatibility of PCM and concrete by introducing pozzolanic additives into concrete.

### 2.6.2.2. *Microencapsulated PCM integrated cementitious composites*

In this technique, finely dispersed polymer modified PCMs are integrated into cementitious composites either as an additive to cement or replacement to aggregates. The polymer encapsulation prevents the contact of PCM with the alkaline concrete environment and eliminates the unpleasant effects associated with PCM leakage and interaction with cement matrix. A summary of mechanical and physical properties of microencapsulated PCM integrated cementitious composites are given in Table 2-4.

Although this method is more versatile compared to direct impregnation techniques, there are some incompatibility issues present when microencapsulated PCMs are integrated into cementitious composites. This is due to the thin and low stiff polymer shell of the microcapsules and therefore, they are more prone to break during the mixing procedure of cementitious composites. For instance, Hunger et al. [73] visually observed a white color liquid accumulating on the top surface of fresh concrete mixture containing microencapsulated PCM. This was further verified by the microscopic analysis of concrete containing PCM capsules where partially destroyed polymer shells with damaged PCM capsules were observed as shown in Fig. 2-9. Authors described the reason for the destruction as collision and abrasion of microcapsules with other aggregates and the high pH environment of the concrete system. Similar observations were also reported by Gschwander et al. [74] and Li et al. [7]. Furthermore, the complex polymerization process of microencapsulation and high cost hinders the application of microencapsulated PCM in construction industry.

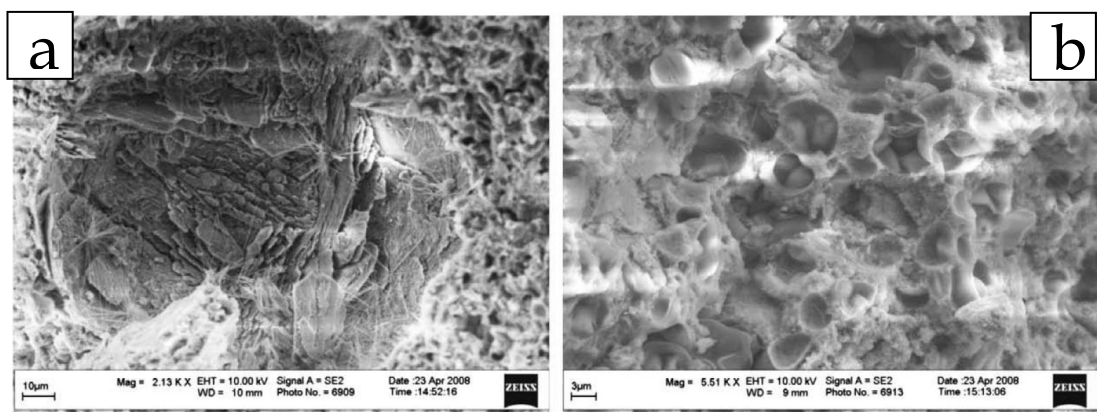


Fig. 2-9. SEM images of (a) an open pore covered with solidified wax (b) part of the cement matrix containing broken capsules and pure leaked wax [73]

Table 2-4 Mechanical and thermal properties of microencapsulated PCM integrated cement mortar/concrete

PCM type	Application method	Results	Ref
Micronal® PCM $T_m=26^\circ\text{C}$	The mix proportions and mixing methods were not discussed	The MOPCON concrete reached a compressive strength and tensile strength of 25 MPa and 6 MPa respectively.	[75]
Micronal DS 5008X, $T_m$ at $23^\circ\text{C}$	Self-compacting concrete containing PCM of 0-5wt%.  Physical, mechanical, microstructural and thermal properties were assessed.	The compressive strength was reduced from 74.1 MPa to 21.4 MPa for 5 wt% of PCM  Open porosity was increased from 15% to 27%  Thermal conductivity of concrete reduced from 3.4 to 2.1 W/(m.K)	[73]
MPCM-28 wet cake	PCM replacement method (volume replacement of PCM to fine aggregate) and PCM additive method (PCM is considered as additive to cement) at the volume ratio of 0-20% was considered	Compressive strength reductions of 19.25% and 26.31% for replacement method and 43.4% and 41.67% for additive method were observed at 7 days and 28 days respectively.  Increasing the PCM content from 10% to 20% resulted in the drying shrinkage increase of 25% for replacement method.	[76]
Microencapsu lated paraffin (MPCM)	Cement paste prepared by integrating MPCM into cement slurry at 0-25 wt% of cement	Compressive strength, flexural strength and thermal conductivity were reduced by 66.34%, 46.23% and 13.2% for 25wt% of MPCM.  The density reduced by 23% for 25% of MPCM	[77]

Micro-encapsulated paraffin in the form of dry powder, $T_m=26^\circ\text{C}$	PCM mixes containing 0.5-5 wt% of PCM in concrete.	Compressive strength reduced from 52 MPa to 9.7 MPa for the PCM content of 5wt%.  Flexural strength reductions from 5.5 MPa to 3.0 MPa was observed.	[78]
Micronal DS 5001X, $T_m=23^\circ\text{C}$	PCM concrete was developed by integrating 0-5% of PCM.	Compressive strength was reduced from 25 MPa to 17 MPa for 5wt% of PCM integration.  A slight decrease (3%) in thermal conductivity was observed.	[79]
Micronal® DS 5008X, $T_m=23\pm3^\circ\text{C}$	PCM was added at 10 vol% and 20 vol% into concrete.	The relative compressive strength of concrete containing PCM at 10% and 20% were 78% and 60% of normal concrete.	[80]
Micronal DS 5040X, $T_m=23^\circ\text{C}$	PCM cement mortar and concrete by volume replacement of PCM to fine aggregate.	Compressive strength reduced by up to 69% for 5% of PCM replacement in concrete.  The mortar specimens showed the reduction in compressive strength of 50% for 55% replacement of PCM.  Thermal conductivity reduction of 0.016 W/(m.K) for a unit reduction in compressive strength (1 MPa) was observed.	[81]

### 2.6.2.3. *Macro encapsulated PCM integrated cementitious composites*

This method utilizes comparatively larger size encapsulated PCMs integrated into cementitious composites such as cement mortars and concrete. Macro encapsulated PCM allows a higher PCM content fraction and higher encapsulation ratio compared to other encapsulation techniques. They also have advantages of low production cost and direct use in concrete as aggregates [82-84]. Different macro-encapsulation techniques including polymer encapsulation [85], steel ball encapsulation [82, 86] and impregnation into porous aggregates [83, 84] were widely investigated for the integration into cement-based materials.

Dong et al. [86] developed macro-encapsulated PCM by absorbing paraffin into hollow steel ball (HSB) for the incorporation into concrete. The hollow steel ball PCM retained up to 80.3% of paraffin in the composite and leakage after 1600 thermal cycles were found to be less than 1%. However, the compressive strength of macro-encapsulated concrete was decreased with increasing PCM content in the concrete. In another study [82], the mechanical bonding between hollow steel ball aggregates and cement was improved by attaching metal clamps to the hollow steel balls. It was found that the effect of metal clamps on improving the compressing strength was not significant for 25% of macro-encapsulated PCM content in concrete. However, the addition of metal clamps became significant when the macro-encapsulated PCM content increased to 50% or higher. It was recommended to have macro encapsulated PCM replacement levels of 50% and 75% for producing concrete with the consideration of mechanical, thermal and economic aspects.

On the other hand, the development of macro encapsulated PCM using porous aggregates was also regarded as a potential technology to improve thermal capacity of cement-based materials. Zhang et al. [42] developed thermal energy storage aggregates by impregnating PCM into porous expanded clay and expanded shale aggregates for the development of thermal energy storage concrete. It was reported that the thermal energy storage aggregates are comparable to commercial grade PCM products and can significantly improve the thermal capacity of concrete and hence, assist in building energy conservation. Memon et al. [87] also prepared macro-encapsulated PCM by impregnating technical grade paraffin into synthetic lightweight aggregates manufactured from expanded clay. The PCM impregnated aggregates were integrated

into normal concrete for the development of structural-functional concrete. It was shown that the macro encapsulated PCM integrated concrete resulted in the 28-days compressive strength of 33.29-53.11 MPa, revealing its use for structural purposes.

#### **2.6.2.4. *Form-stable PCM integrated cementitious composites***

This method involves the incorporation of form-stable PCMs into cementitious composites as a partial replacement for cement or aggregates. As opposed to direct impregnation and micro-encapsulation, the form-stable PCMs have hard shell structure (supporting materials) and hence, the destruction effects of PCM composite can be minimized. Moreover, when they are mixed with cementitious composites, composite PCMs will be surrounded by cement matrix which further improves the structural stability of composites. A large number of experimental and numerical studies have been conducted for the incorporation of form-stable PCM into cementitious composites to study the mechanical and thermophysical properties as well as the thermal performance of such PCM integrated cementitious composites in buildings. An extensive literature review for the integration of form-stable PCM into cementitious composites with the identification of relevant research gaps is presented in the following sections.

#### **Mechanical and thermophysical properties of form-stable PCM integrated cementitious composites**

The introduction of new composite materials into cementitious matrices can affect the strength development in many ways including, interfering with the cement matrix and hence affecting the matrix strength development, soft composites can weaken the load transfer path in the produced concrete, etc. Furthermore, thermophysical properties of PCMs may also differ when they are integrated into cementitious composites due to the surrounded cement matrix environment and interaction with the alkaline environment. Therefore, the essential characteristics of mechanical and thermophysical properties of PCM integrated cementitious composites must be reported for building applications. A summary of existing literature in PCM integrated cementitious composites with the findings of mechanical and thermophysical properties are presented in Table 2-5. It should be noted that the mix design and mixing method differ among the referred studies and hence, direct comparison may not be feasible. However, a common trend on mechanical and thermophysical behavior can be studied.

From Table 2-5, it can be seen that the incorporation of form-stable PCM into cementitious composites resulted in significant enhancement of thermophysical properties and TES capacity. Such results reveal that the application of form-stable PCMs in cementitious composites will lead to a significant enhancement in building thermal mass effect and hence, building energy efficiency. Besides, it should also be noted that this method of incorporation suffers from substantial reduction in mechanical properties such as compressive strength and flexural strength properties. Furthermore, this reduction increases with increasing amount of PCM content in the mixture. As cementitious composites, such as cement mortar and concrete, are mainly used as structural elements to carry large load bearing capacity, the reduction in mechanical properties could be detrimental to the application of such PCM-enhanced construction materials.

The main reason behind the strength loss can be identified as low strength and stiffness of composite PCMs compared to other aggregates in cementitious composites as reported by many researchers [70, 88]. Furthermore, a weight based mix design procedure could also lead to strength loss because the cement content per unit volume of concrete mixture reduces as the composite PCMs have very low density compared to other ingredients in concrete. This will result in low binder content in the produced concrete [81]. Therefore, it is necessary to properly choose the mix design of materials for the comparison of mechanical properties in PCM integrated cementitious composites.

Although the strength loss in form-stable PCM integrated cementitious composites can be mitigated by increasing the cement content, the major problem associated with the integration of form-stable PCM are the instability/leakage of PCM and subsequent interaction of leaked PCM with cement matrix. In particular, the form-stable PCM composites with the phase transition temperature lower than ambient temperature resulted in significant amount of PCM leakage when mixed with cementitious materials, mainly due to the instability of the liquid state in water environment. As a consequence, the PCM integrated cementitious composites will have low TES capacity as well as low mechanical and durability properties. A detailed analysis of the stability of form-stable composite PCMs in cementitious composites and relevant impacts on the mechanical and thermophysical properties are presented in the following section.

Table 2-5 Mechanical and thermophysical properties of form-stable PCM integrated cement mortar/concrete

PCM type	Application method	Results	Ref
Paraffin/diatomite $T_m=41.1^\circ\text{C}$	The composite PCM is used as cement admixture with the weight proportion of 0-30%.	The 28-day compressive strength, flexural strength, thermal conductivity and early age shrinkage strain were reduced by up to 48.7%, 47.5%, 33.6% and 80.73% respectively.	[70]
n-octadecane/expanded graphite $T_m$ at $27^\circ\text{C}$	The PCM composite was added at the weight ratio of 0-0.1 to cement. The maximum weight ratio of PCM composite in cement mortar was determined as 2.5%.	The compressive strength was reduced from 23.7 MPa to 10.5 MPa with the inclusion of 2.5% of PCM. The bulk density decreased from 1.89 to 1.71 g.cm <sup>-3</sup> . The thermal conductivity of cement mortar reduced by 15.5% for 2.5% of PCM inclusion.	[88]
Paraffin/expanded vermiculite $T_m$ at $27^\circ\text{C}$	The PCM composite was utilized as volume replacement to fine aggregate at the replacement levels of 0%, 50%, and 100%. Ordinary Portland cement (OPC) and silica fume (SF) were used as binder in the cementitious composites	The 28-days compressive strength and flexural strength were reduced by 56.5% and 21.9% respectively for 100% replacement. The bulk density of produced TESC reduced from 1848 kg.m <sup>-3</sup> to 1392 kg.m <sup>-3</sup> .	[60]
Paraffin/expanded perlite $T_m=28^\circ\text{C}$	Four kinds of slurries were prepared with cement, PCM composite, and water. The weight ratio of PCM were 10%, 20%, 30% and 40%.	Compressive strength increased from 0.35 MPa to 0.57 MPa for the PCM content of 40 wt%. Apparent density increased from 0.32 g.cm <sup>-3</sup> to 0.43 g.cm <sup>-3</sup> .	[89]

		Thermal conductivity increment from 0.11 to 0.149 W/m.K was observed.	
paraffin/expanded clay composite PCM $T_m=20^\circ\text{C}$	The composite PCM added as a dosage of 50, 75 and 100 kg/m <sup>3</sup> .	The compressive strength and flexural strength at 28 days were reduced from 34 MPa and 7.2 MPa to 15 MPa and 3.9 MPa respectively. The dry density of mortars reduced from 2089 to 1266 kg/m <sup>3</sup> .	[90]
Paraffin/expanded graphite $T_m=28^\circ\text{C}$	PCM composite was added as 20wt% of cement	The compressive strength, bending strength and bonding strength were determined as 5.10, 2.01 and 0.30 MPa respectively for PCM integrated cement mortars, compared to 5.50, 2.31 and 0.47 MPa respectively for ordinary cement mortar. The dry density reduced from 1635 to 1406 kg/m <sup>3</sup> Thermal conductivity increased from 0.75 to 0.81 W/(m.K).	[91]
lauric-myristic acid/expanded perlite $T_m=39.88^\circ\text{C}$	The PCM composite was added as a dosage of 100 and 200 kg/m <sup>3</sup> .	The 28-days compressive strength was determined as 2.71 MPa and 2.21 MPa for 100 and 200 kg/m <sup>3</sup> dosage rate respectively, compared to 4.09 MPa in a blank mortar. Dry densities were obtained as 676.7 and 655.5 kg/m <sup>3</sup> for PCM dosage of 100 and 200 kg/m <sup>3</sup> respectively. Thermal conductivity reduced from 0.107 to 0.098 W/(m.K) with 200 kg/m <sup>3</sup> dosage rate.	[92]

**Stability of form-stable PCM in cementitious composites**

Apart from the adverse effects of PCM integrated cementitious composites in mechanical properties, the instability of form-stable PCM composites in cement matrix have recently been reported as a major issue. This is because the PCM is held in the open pores of the porous supporting materials and hence become exuded when mixing with water hardening materials. To prevent the PCM leakage in form-stable PCM composites, two different approaches were used: hydrophobic surface modification of PCM composite and application of surface coatings to the PCM composite. The former method facilitates the deposition of hydrophobic particles on the surface of the composites as a way of preventing the contact of water with the PCM composite. This method can be achieved by mixing the composite PCM with the hydrophobic particles so that the guest particles (hydrophobic particles) deposit on the host material (composite PCM) due to the high surface energy of guest particles. This process is called as dry powder coating and widely used in many industrial applications to change the surface science of host particles [5, 7]. On the other hand, the latter application can be achieved by mixing the PCM composite with the surface coatings such as epoxy coatings and cement coatings [8]. In this method, coating materials form a thin solid protective coatings on the composite PCM and prevent the leakage. A summary of the literature reporting the instability of PCM in form-stable composites and relevant PCM leakage prevention measures are presented here.

Li et al. [5] fabricated a PCM composite based on paraffin/diatomite and reported a significant amount of PCM leakage (up to 67% of total PCM content in the mixture) when it is mixed with concrete. The leaked PCM also found to segregate to the top surface of the mixture as shown in Fig. 2-10. Furthermore, the leakage ratio increased with the increasing water/cement ratio or water content in the mixture. Authors reported the reason behind this phenomenon as the water replacing the paraffin in the PCM composite due to high water affinity of diatomite. The PCM leakage was prevented by applying a hydrophobic surface modification of PCM composite with Aerosil® R202 from Evonik®.

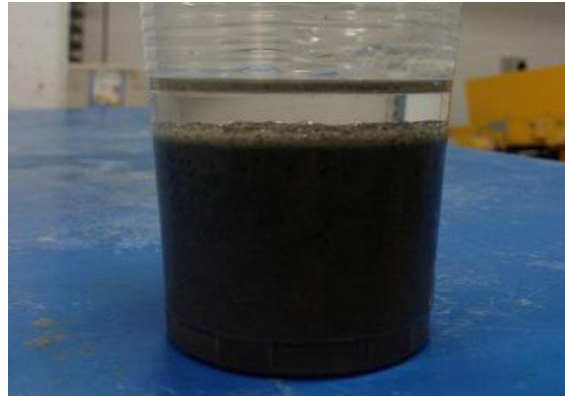


Fig. 2-10. Leakage of paraffin in cement mortar mixture [5]

Li et al. [6] also investigated the feasibility of integrating a commercially available form-stable PCM (PX powder from Rubitherm®) into the cementitious composite as a way of increasing the TES capacity in buildings. However, without prevention, a significant amount of PCM leakage of 57.3% was observed. The authors also reported that the leaked PCM interacts with the cement matrix and significantly affects the mechanical properties of produced concrete. The instability or PCM leakage was prevented by applying hydrophobic nanosilica surface coatings to the PCM composite and promising results were achieved. Here, hydrophobic nanosilica particles deposit on the surface of PCM composite and prevent the contact between composite PCM and water due to hydrophobic or water repellent properties.

More recently, the same team [7] studied the development and stability of granular PCM composites with paraffin/expanded perlite form-stable PCM for the development of TESCs. However, when the form-stable PCM was integrated into cement mortar, a significant amount of PCM leakage of up to 78% was observed. The main reason behind the instability of PCM in such form-stable composite PCMs was regarded as hydrophilic surface properties of supporting material and authors investigated different hydrophobic surface modification methods such as hydrophobic silane and hydrophobic nanosilica modifiers. Authors claimed that hydrophobic silane was most effective than hydrophobic nanosilica in preventing paraffin leakage under high temperature, but the silane modification resulted in compressive strength reduction of 27% compared to that of nanosilica modifiers.

It can be concluded, therefore, that the form-stable PCMs cannot be directly incorporated into cementitious composites and hydrophobic surface modifications are necessary to prevent the PCM leakage and subsequent adverse effects in the cement matrix. Hydrophobic surface modifications with hydrophobic nanosilica and silanes were considered as promising technologies to prevent the PCM leakage in cementitious composites. Nevertheless, the deposition of guest particles on the composite PCMs could also interact with the cement matrix and adversely affects the mechanical and durability properties of produced concrete. However, the mechanical and durability performance of such surface modified composite PCMs in cement-based materials were seldom reported in the literature.

On the other hand, the application of surface coatings to prevent the PCM leakage was also treated as an effective method in the literature. For instance, thermal energy storage aggregates were prepared by absorbing technical grade paraffin into porous expanded clay minerals to develop thermal energy storage concrete [84, 87]. The composite PCMs were coated with epoxy resin, while silica fume was used as the separator of the composites. Fig. 2-11 shows the schematic diagram of the fabrication of epoxy coated composite PCMs. Authors claimed that the epoxy coated composite PCMs significantly enhance the TES properties while maintaining adequate mechanical properties to use as structural-functional concrete.

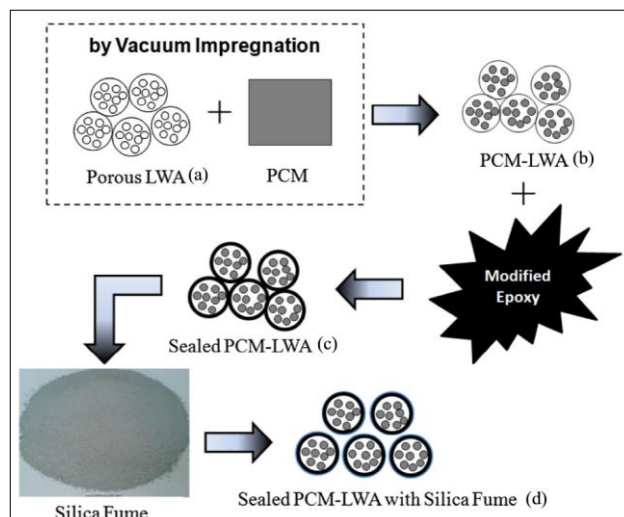


Fig. 2-11. Fabrication process of epoxy coated PCM composites [87]

Cui et al. [83] also developed thermal energy storage aggregates by absorbing Lauryl alcohol into porous expanded clay minerals and investigated the effectiveness of different surface coatings such as epoxy and cement paste coatings for the prevention of PCM leakage. This team claimed that, epoxy coatings were performing better than cement paste coatings. This is due to a good interfacial contact between epoxy-coated composites and cement mortar compared to cement coated composite PCM, as supported by SEM images (Fig. 2-12) and compressive strength properties.

Kheradmand et al. [8] assessed the feasibility of different sealants in PCM impregnated lightweight aggregates to prevent PCM leakage. The porous lightweight aggregates including, expanded clay, expanded vermiculate, expanded perlite and granulated expanded cock were used to impregnate PCM and various waterproofing sealants are applied to prevent PCM leakage in composites. Authors reported that the effectiveness of different waterproofing agents was found different due to varying thickness of waterproofing layer. Nonetheless, the amount of PCM leakage for different encasement methods were found to be lesser than 0.5%, which indicates a very minimal level of PCM leakage in composite PCMs with waterproofing layer encasement.

Therefore, an alternative method to prevent PCM leakage in form-stable PCM was investigated with the application of protective coatings to the surface of composite PCMs. Although this method is favorable in terms of the easy fabrication process and good mechanical properties in the produced concrete, the fabrication at large scale for construction practices would not be feasible as the dispersion of coated granules would be difficult. Furthermore, the thermal stability and thermal reliability of such protective coatings should be investigated for the feasibility of those materials in buildings.

Thus, existing literature shows that the instability or PCM leakage in PCM integrated cementitious composites presents as a barrier for the application of form-stable PCM in construction applications. Furthermore, various methodologies used to prevent the PCM leakage in cementitious composites also lack sufficient information regarding the mechanical and thermal performance of resulting cement based materials. Therefore, development of new form-stable composite PCM that can be directly applied into cementitious composites without any surface modification or protective coatings are essential as it eliminates the PCM leakage and any incompatibility issues arise from the coating materials.

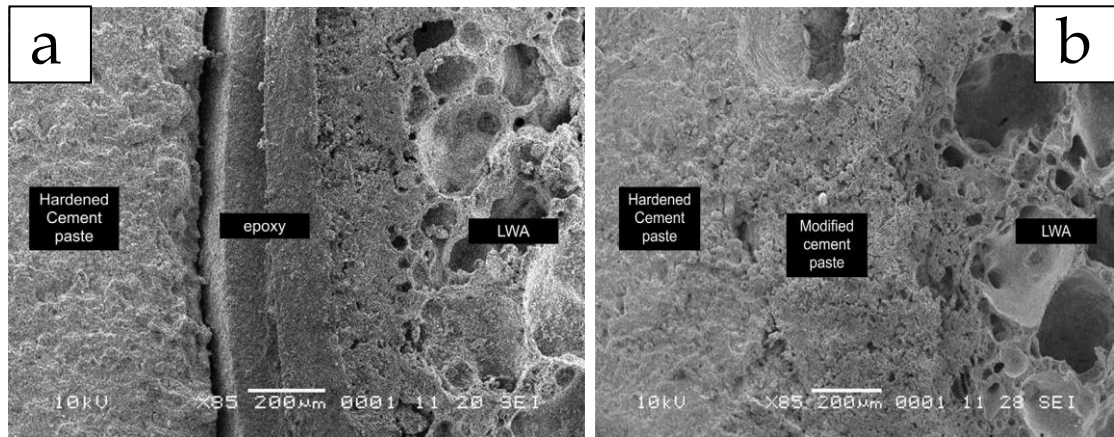


Fig. 2-12. Interfacial properties of surface coated PCM composites in cement matrix (a) epoxy coated composites (b) modified cement paste coated composites [83]

## 2.7 Potential applications of PCM in buildings

### 2.7.1. PCM application methods: passive, active and free cooling

The LHTES with PCMs has been widely investigated as a potential technology to improve the building energy efficiency and indoor thermal comfort. The application of PCMs in buildings can be categorized into three methods which are passive, active and free cooling methods. Passive methods are referred to the technologies where the TES system is operated without the use of external energy supply. Typical applications of passive methods are PCM integrated into building fabrics such as walls, floors, ceiling and roofing materials. In contrast, an active TES system integrates the PCM into an HVAC system such as air-conditioning unit [93, 94], floor heating system [95, 96] and domestic ground heat pumps [97] to reduce the peak energy demands and annual energy consumptions. Free cooling technology, on the other hand, also similar to the active system, where it utilizes the external energy supply to operate the TES systems. However, as opposed to active TES systems, an HVAC unit is not required in this application [98]. The free cooling system stores the coldness of night ambient air and extracts it during day-time by supplying the indoor/outdoor air through PCM storage unit.

Although these three methods have their pros and cons, passive TES systems are more preferred over other two methods due to the availability of large heat transfer surface area and they do not require additional TES systems [2]. More precisely, passive TES

systems can be achieved by incorporating PCM into existing building fabrics and hence do not require special equipment to achieve TES capacity. Furthermore, when PCMs are incorporated into building fabrics, large accessible surface area facilitates better heat transfer performance and eliminates thermal stratification issues associated with active and free cooling applications. Therefore, this research work mainly focuses on the passive TES application with the integration of PCM into building components for the improvement in indoor thermal comfort.

### **2.7.2. Passive application of PCM in buildings**

The passive application of PCM in buildings can be achieved by either using PCM as a prefabricated building component or integrating PCM into building materials and components. The former method enables the incorporation of PCM in the form of flat panels, tubes or macro-encapsulated PCM mats and boxes. The examples of this application include the installation macro-encapsulated PCM mats between insulation and plasterboards in ceilings and PCM panels installed below floor finishes [99, 100]. Bio-PCM™ (Fig. 2-13) is a commercially available macro encapsulated PCM that can be directly incorporated into building fabrics for TES in buildings. Bio-PCM™ consists of refined fatty acids in square pouches and they are produced as mat-form. The compound material contains as much as 90% of PCM and it remains stable during the operative temperature range. This reduces the liquid PCM leakage problems during the operational stage of buildings. Alam et al. [100] investigated the energy saving potential of Bio-PCM™ in Australian residential buildings and reported that the integration of Bio-PCM™ into building fabrics can provide 17-23% of energy savings.

Shi et al. [101] also developed a macro-encapsulated PCM by encasing paraffin into 20 mm thick stainless steel boxes. Their study mainly focused on the position of such macro encapsulated PCM in concrete walls to provide comfortable and healthy indoor environment by controlling indoor temperature and relative humidity respectively. It was found that the macro encapsulated PCM laminated within the concrete walls showed the best performance in reducing the indoor temperature, whereas, the PCM placement at inner surface of the concrete wall resulted in best humidity control.

The use of PCM as a prefabricated component has many advantages such as easy installation, low cost, compatibility with any surrounding environment, and reduced

changes to the external volume. Furthermore, they can be used in existing buildings as an energy refurbishment approach. However, the major limitation of this method can be described as poor heat transfer performance as PCMs are packed in macroscopic containers. Thus, the PCM occupied on the surface of the package contributes to the melting and freezing operations, while the core content does not solidify completely due to poor heat transfer performance or low thermal conductivity.



Fig. 2-13. Macro encapsulated Bio-PCM™ in mat form [102]

On the other hand, the integration of PCM into construction materials has been recently considered as a potential technology due to high heat transfer performance, large heat transfer surface area and a wide variety of application methods can be adopted. Some of the prominent applications of this method can be explained as the integration of microencapsulated and form-stable PCMs into cement mortar, concrete and gypsum plasters. Although this method is more sophisticated than using PCM as a component, it also has few drawbacks. The integration methods of PCM into construction materials incur high cost and can adversely affect the structural integrity of construction materials/elements. Moreover, it would be difficult to incorporate PCM into existing buildings as a retrofitting approach. Yet, with the consideration of heat transfer performance as the prime important in a TES system and the other associated issues can be overcome with appropriate prevention measures, this research focuses on the integration of PCM into construction materials/elements. The following sections explain the summary of literature related to different methods of PCM integration into building materials/elements.

## 2.8 Heat transfer performance enhancement of PCMs

### 2.8.1. Overview

While the mechanical and durability performance of PCM integrated cementitious composites are of primary requirement, their thermal performance should also be assessed. A typical but most significant drawback which affects the thermal performance of LHTES systems is the low thermal conductivity of most PCMs. In fact, the thermal conductivity of most inorganic PCMs are less than  $1.0 \text{ W/(m}\cdot\text{K)}$ , whilst organic PCMs have even lesser thermal conductivity values of  $0.2 \text{ W/(m}\cdot\text{K)}$  [7]. Such low thermal conductivity of PCMs could lead to low heat transfer rate, resulting in slow heat exchange performance during melting and solidification processes. Furthermore, in a LHTES system, the major cost is associated with the heat transfer technology that employs to achieve a large amount of heat charge/discharge rates to achieve high efficiency [103, 104]. Therefore, enhancing the thermal performance of PCM is a key requirement in terms of efficient and economic perspective. There are many different methods that can be adopted to improve the heat transfer performance of PCM and out of those, using extended surfaces, dispersing high conductive additives and fabrication of micro-sized PCM composites are some of the commonly used approaches.

Among these different technologies, increasing the heat transfer surface area or adopting extended surfaces in a TES system is the most straightforward approach. However, this method suffers from reduced PCM content due to large volume contribution of extended surfaces such as metal fins [103, 104]. Another most versatile approach in heat transfer enhancement is to disperse high conductive additives in the PCMs, both in -micro and -nano sized particles. The dispersion of high thermal conductive additives into PCMs improves the effective thermal conductivity and increases the heat transfer performance. A wide variety of high conductive additives including, metallic materials and carbon based conductive additives were studied in the literature to promote heat transfer performance of PCM applications. Yet, a TES system also requires large amounts of latent heat of fusion and the addition of high conductive additives will reduce the latent heat of fusion, because the promoter is not engaged in phase change operation. Therefore, there is a need for compromising between the thermal conductivity and latent heat and hence, filler materials with high conductivity and the larger surface area will be the best choice.

### 2.8.2. Metallic materials as thermal conductivity promoters

Metallic particles including, copper, nickel and aluminum were widely studied for thermal conductivity enhancement of PCMs due to their high thermal conductivity, open porosity, and very high specific strength and stiffness. Wang et al. [105] introduced copper fibers into paraffin to increase heat transfer performance of PCM. Authors reported that the effective thermal conductivity of PCM composite was increased by 27-134 times without large reduction in latent heat capacity. In another study [7], copper nanoparticles with the average particle size of 20 nm were dispersed into paraffin wax to synthesis Cu-PCM nanocomposites. It was found that the addition of up to 2.0wt% of Cu increased the thermal conductivity of paraffin by 46.3%. Furthermore, nano-Cu also acted as nucleation agent to reduce the supercooling effect during the phase change process. Xiao et al. [106] also prepared composite PCMs using copper and nickel forms with 95% porosity. The results showed that the effective thermal conductivity increased from 0.305 to 4.9 W/(m.K) and 1.3 W/(m.K) for paraffin/copper and paraffin/nickel composite PCMs respectively. However, the latent heat capacity and specific heat capacity were reduced by 22-30% and 14-24% respectively.

Nourani et al. [107] developed a new kind of composite PCM by dispersing aluminum oxide ( $\text{Al}_2\text{O}_3$ ) nanoparticles into paraffin with the presence of sodium stearoyl lactylate (SSL) as a dispersing agent/surfactant. The thermal conductivity and melting heat transfer rate enhancement were reported as 31% and 27% respectively. Thermal reliability studies revealed that the PCM composite had good thermal reliability after subjected to 120 thermal cycles. Cabeza et al. [11] also investigated the heat transfer performance enhancement of water as PCM with stainless steel pieces, copper pieces and graphite matrix as the thermal conductivity promoter. The results showed that graphite matrix performed best out of those three options and stainless steel pieces had lowest performance enhancement.

From the above studies, it can be seen that there is a significant improvement in thermal conductivity with the dispersion of high conductive metallic particles. However, the latent heat is reduced because of the involvement of a lot of metal materials. Furthermore, corrosion of metallic materials and deposition of heavy metals to the surface are present as the limitation to the widespread application of metallic fillers in PCM [103].

### 2.8.3. Carbon-based additives as thermal conductivity promoter

Carbon based high conductive additives including expanded graphite, carbon nanotube, and graphene materials are also widely studied and utilized as thermal conductive additive. Carbon based materials have many advantages over metals such as very high thermal conductivity and high stability which makes it suitable for corrosive environments. The application of carbon materials in composite PCMs can be achieved by integrating -micro and -nano sized carbon materials (i.e. carbon nanotubes and graphene) into PCM and their form-stable composites.

In this application method, high conductive carbon additives are dispersed into PCM or form-stable PCM composites to formulate a high conductive interconnecting network to the PCM, as such, the heat transfer -to and -from the PCM is accelerated. Particularly, carbon nanotubes and graphene are promising high conductive additives, which have thermal conductivities exceeding even several thousand in  $W/(m.K)$ . Apparently, such large thermal conductivities are helpful for enhancing the heat transfer performance of composite PCM with even a smaller addition. However, it should also be noted that the significant heat transfer enhancement can only be achieved when an effective heat transfer network is formed [104]. Therefore, fabricating appropriate carbon-porous material network is necessary to guarantee the heat is being transferred quickly from outside to the inside of the pores, where PCM is occupied.

A summary of findings from the literature in the dispersion of carbon materials to improve heat transfer performance of PCM are presented in Table 2-6. It should be noted that many studies here referred to the thermal conductivity enhancement of pure PCMs, which could not be able to use in building applications as they are not encapsulated and will result in instability or PCM leakage. On the other hand, many other studies investigate the incorporation of carbon additives after the fabrication of composite PCMs which could also result in reduced performance enhancement. This is because the carbon additives are not connected with the PCM occupied inside the pores and thus, heat transfer to PCM was not improved. Very few studies integrated the carbon additives with the form-stable PCMs by fabricating an effective carbon-porous material network first and then fabricating form-stable PCM composites. This method will have a potential enhancement in heat transfer performance as carbon additives are forming a high

conductive network inside the pores of supporting materials and hence, increasing the heat transfer to PCM.

For example, form-stable PCM composite fabricated by Xu and Li [108] consist of multi-walled carbon nanotube (MWCNT) as the heat transfer promoter to paraffin/diatomite composite PCM. The micro-morphology characteristics of the carbon-diatomite porous network, as shown in Fig. 2-14(a), illustrates that the MWCNTs are well dispersed and randomly distributed among the diatomite frustules. In addition, Fig. 2-14(b) displays the random arrangement of CNTs, which are connecting the paraffin occupied inside the pores of diatomite to outside. By having an effective high conductive network, the smaller addition of WMCNTs (0.26%) resulted in significant thermal performance enhancement of composite PCMs. Lu et al. [109] fabricated a composite PCM on expanded perlite/paraffin/graphene oxide (EP/PA/GO) with the deposition of GO films on the surface of the EP/PA composite PCM. Fig. 2-15 shows the paraffin/expanded perlite composite PCM before and after the GO deposition process. The authors claimed that the addition of 0.5% of GO resulted in the heat storage/release performance enhancement by 2 times without larger reduction in latent heat capacity. Furthermore, GO films prevent the PCM leakage due to the formation of GO sheets on the exterior surface of PCM composites.

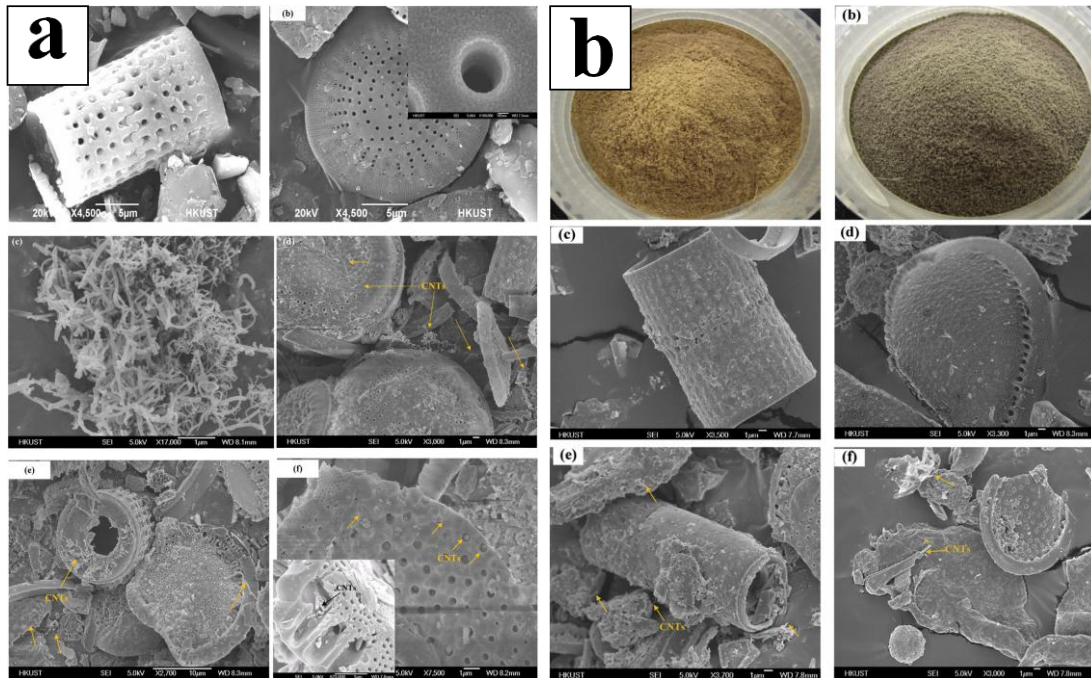


Fig. 2-14. Paraffin/diatomite/MWCNT composite PCM (a) MWCNT-porous diatomite network (b) PCM composite [108]

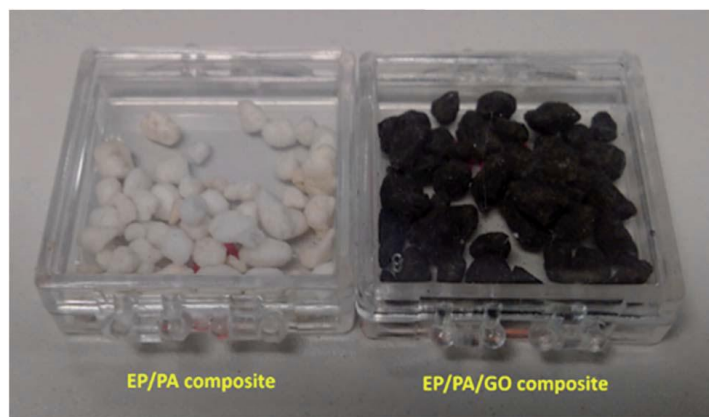


Fig. 2-15. Paraffin/expanded perlite composite PCM before and after GO deposition process [109]

Table 2-6 Heat transfer performance of PCM with the dispersion of high conductive carbon additives

Composite PCM	Mass fraction of additive (wt%)	Heat transfer performance assessment and results	Ref
Graphite/ paraffin	0-20	Thermal conductivity can be increased by up to 319.2% with 20% loading of graphite.	[110]
MWCNT/ paraffin (RT50)	25	Thermal conductivity increased from 0.38 to 0.58 W/(m.K).	[111]
MWCNT/ paraffin (RT60)	25	Thermal conductivity changed from 0.41 to 0.36 W/(m.K).  Poor dispersion of MWCNTs caused low thermal conductivity measurement.	
Carbon nanofibers/ paraffin	4	Thermal diffusivity increased to 0.00268 cm <sup>2</sup> /s compared to pure paraffin of 0.00151 cm <sup>2</sup> /s.	[112]
xGnP/ Paraffin	1-7	Thermal conductivity increased from 0.26 to 0.8 W/(m.K) with 7% loading of xGnP.	[113]
xGnP/Bio- PCM	25	Thermal conductivity increased by 375% (from 0.154 to 0.577 W/(m.K)).	[114]
CNT/ Bio- PCM	1-5	Thermal conductivity increased by up to 248% (an effective increment from 0.154 to 0.536 W/(m.K)).	[114]
Graphene nanofibers (GNF) /Paraffin	2.8-11.4	Thermal conductivity increased from 0.2 to 0.32 W/(m.K) at a loading amount of 8.5% of GNF.  Thermal diffusivity increased from 0.04 to 0.17 mm <sup>2</sup> /s with 11.4% of GNF loading.	[115]
PEG/ Diatomite/ graphite	0-10	Thermal conductivity increased by 103% for the graphite loading of 10%.	[53]

		Thermal performance test showed a reduction in melting duration from 28 to 14 minutes and reduction in the freezing process from 38 to 20 minutes.	
Paraffin/EP/EG	5	Thermal conductivity enhanced by 46%. Thermal performance test showed a reduction in melting duration from 20 to 17 minutes and reduction in freezing process from 23 to 17 minutes	[116]
Capric acid/EP/EG	10	Thermal conductivity enhanced by 64%. Thermal performance test showed a reduction in melting duration from 25 to 15 minutes and reduction in the freezing process from 42 to 37 minutes.	[57]
Paraffin/diatomite/MWCNT	0.26	Thermal conductivity increased by 42.45%. Thermal performance test showed a reduction in melting duration from 783 s to 602 s and reduction in the freezing process from 1084 s to 818 s.	[108]
Paraffin/EP/GO	0.5	Thermal performance tests revealed faster heat storage/release rates of 4.1 and 7.5 minutes for heat storage and release respectively compared to 8.8 and 14.2 minutes for paraffin/EP composites	[109]

## **2.9 Thermal performance assessment of PCM incorporated buildings**

### **2.9.1. Overview**

The incorporation of PCMs into building components are to increase TES capacity of building envelope and hence, enhancing the building energy efficiency and indoor thermal comfort. Many research studies assessed the thermal performance enhancement of PCM integrated buildings in terms of improvement in indoor thermal comfort and energy efficiency. Over the past decades, experimental studies on thermal performance assessment have been conducted from small-scale laboratory test room to large scale buildings. However, with the recent developments in building thermal simulations tools, numerical simulations of thermal performance assessments become more popular and convenient approach. Moreover, rigorous validation and verifications of numerical approaches with experimental data enabled the confident of results derived from numerical simulations. They also provided more flexibility in terms of analyzing the influence of various parameters and hence choosing the optimum solution for PCM applications in buildings. Nevertheless, it should also be noted that the numerical simulations have limitations within their calibrated experimental data and cannot be directly extrapolated beyond the simulation capacity [13, 117, 118]. The following subsections report the existing literature on the thermal performance assessment of PCM incorporated buildings with experimental and numerical approaches.

### **2.9.2. Experimental thermal performance assessments**

The experimental investigations on thermal performance enhancement were carried out based on either improvement in thermal comfort conditions in passive buildings or the energy consumption reduction in air-conditioned buildings. Many experimental research studies focused on assessing the improvement in indoor thermal comfort conditions as the energy assessments with the consideration of air-conditioners would be difficult to achieve. Some studies extended the experimental temperature profiles to analytical models or theoretical assessments to evaluate the energy efficiency [119-121].

In the early days, thermal performance assessment was mainly focused on the indoor air temperature, where a comparison of the peak indoor air temperature reduction in PCM

incorporated test rooms with the control room was performed [12]. Furthermore, increase in minimum indoor air temperature and reduction in diurnal indoor temperature fluctuation were also considered to assess the thermal performance enhancement in buildings. A significant reduction in peak indoor temperature and indoor temperature fluctuations have been reported in the literature, as a way of improvement in indoor thermal comfort. However, with the recent developments in thermal comfort theories and thermal sensation behavior of the human body, more advanced thermal performance assessments come into practice. Particularly, the most recent development in thermal comfort theories such as ASHRAE adaptive comfort models measures the indoor thermal comfort sensations based on the combination of indoor air temperature and mean radiant temperatures. Eqn. (2-3) and (2-4) illustrates the calculation of indoor operative temperature with the optimum comfort temperature ( $T_{comf}$ ) defined by adaptive comfort model on ASHRAE Standard 55-2013 [122]. The comfort region with 90% acceptability limits and 80% acceptability limits are defined as when the  $T_{OPE}$  falls in the range of  $T_{comf} \pm 2.5^\circ\text{C}$  and  $T_{comf} \pm 3.5^\circ\text{C}$  respectively.

$$T_{OPE} = \gamma T_{MRT} + (1 - \gamma) T_{drybulb} \quad (2-3)$$

$$T_{comf} = 0.31 x T_{a,out} + 17.8 \quad (2-4)$$

where  $T_{OPE}$ : Indoor operative temperature ( $^\circ\text{C}$ ),  $T_{drybulb}$ : Indoor air drybulb temperature ( $^\circ\text{C}$ ),  $T_{MRT}$ : Mean radiant temperature ( $^\circ\text{C}$ ),  $T_{comf}$ : Optimum comfort temperature ( $^\circ\text{C}$ ) and  $T_{a,out}$ : Mean monthly outdoor air temperature ( $^\circ\text{C}$ )

Furthermore, ASHRAE adaptive comfort models consider the seasonal variations in the thermal comfort conditions. The optimum thermal comfort temperature is calculated based on the monthly average outdoor air temperature as depicted in Eq. (2-4). For example, the optimum comfort temperature for January (a representation of summer month) in Melbourne is  $22.5^\circ\text{C}$  and for the same climatic region, the optimum comfort temperature in June (a representation of winter month) is  $19.5^\circ\text{C}$ . This considers the adaptive capacity of human body exposed to different temperature for longer periods. However, the experimental evaluation of indoor operative temperature would be difficult and hence, most of the previous studies adopted indoor air temperature for the performance assessment.

### 2.9.3. Numerical assessments of thermal performance

The numerical analysis considers the heat balance of building envelope subjected to external and internal thermal solicitations, where heat transfer through building elements are solved with complex heat transfer algorithms. Generally, heat transfer problems in building elements with constant thermophysical properties are numerically solved by assuming one-dimensional heat transfer process through the building elements. However, the incorporation of PCM into building components causes varying thermophysical properties involving a melting or freezing heat transfer behavior when the temperature overpasses or undergoes the melting temperature. Thus, a moving solid-liquid boundary condition exists between two phases during this transformation and hence, linear heat transfer models cannot be executed. Heat transfer problems in PCM applications are related to non-linear heat transfer processes with a moving solid-liquid interface that is generally known as “moving boundary” problem. Due to the complexity of moving boundary problems, the analytical solutions are limited to simple geometries and constant boundary conditions [123, 124]. Therefore, the building simulations with complex geometry and varying boundary conditions are generally solved through numerical simulations.

The storage and release of thermal energy are primarily governed by latent heat storage of PCM and several methods are used to solve the phase change problems in TES applications. Three most commonly used methods for phase change processes are effective heat capacity method, enthalpy method and heat source method.

#### 2.9.3.1. *Effective heat capacity method*

This method modifies the heat capacity of material by varying the heat capacity value during the phase change process. Eq. (2-5) shows the heat transfer model through the PCM layer as a function of temperature and effective heat capacity, where  $C_p(T)$  is the effective heat capacity (J/kg/K) at the temperature of  $T$  (°C). The effective heat capacity is considered as specific heat capacity of the material beyond the phase transition range. During the phase transition temperature range, it is linearly proportional to the specific heat and latent heat, and inversely proportional to the phase transition temperature range [125].

$$\rho.C_p(T).\frac{\partial T}{\partial t} = \nabla.(k\nabla T) \quad (2-5)$$

$$\text{where, } C_p(T) = \begin{cases} C_{ps} & \text{if } T \leq T_1 \\ C_p + \frac{L}{(T_2 - T_1)} & \text{if } T_1 < T \leq T_2 \\ C_{pl} & \text{if } T \geq T_2 \end{cases}$$

where  $C_{ps}$  and  $C_{pl}$  are solid state and liquid state specific heat capacity respectively. L is the latent heat capacity of PCM.  $T_1$  and  $T_2$  are onset and endset melting temperatures of PCM respectively. The effective heat capacity method is most widely used method as the temperature is the only variable that has to be solved.

### 2.9.3.2. *Enthalpy method*

In the enthalpy method, specific heat and latent heat are combined to form enthalpy term and an enthalpy-temperature function is used for the phase change process. The enthalpy-temperature function can be derived from differential scanning calorimetry (DSC) experiment or heat flow meter apparatus. For conduction dominated heat transfer, the enthalpy method can be written as [125]:

$$\rho \frac{\partial H(T)}{\partial t} = \nabla.(k\nabla T) \quad (2-6)$$

where  $\rho$  is the density of the material ( $\text{kg/m}^3$ ) and k is the thermal conductivity ( $\text{W/(m.K)}$ ).  $H(T)$  and  $T$  are the enthalpy of PCM ( $\text{J/kg}$ ) at the temperature of  $T$  and temperature of the material ( $^{\circ}\text{C}$ ) respectively. The advantage of enthalpy method is that this algorithm can be used for materials having sharp and gradual phase change processes. Fig. 2-16 shows the enthalpy-temperature function of a commercially available Bio-PCM.

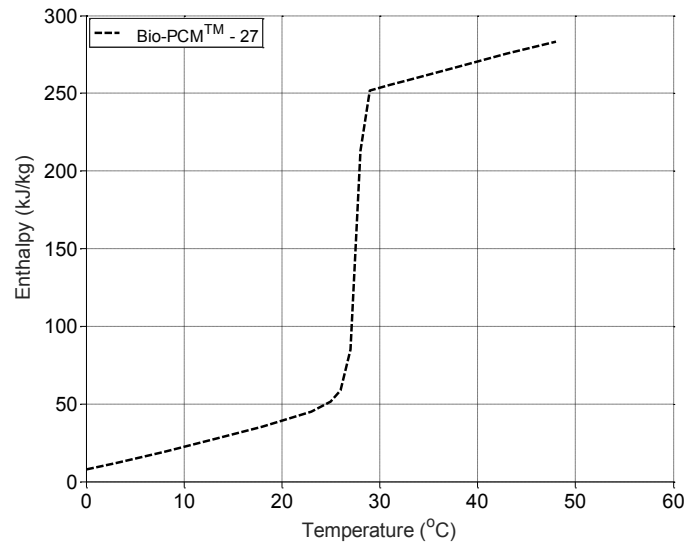


Fig. 2-16. Enthalpy-temperature function of Bio-PCM™-27 [100]

### 2.9.3.3. Heat source method

This method assumes the latent heat as an internal heat source that is operated during the phase transition temperature of PCM and therefore, total enthalpy is updated as the combination of specific heat and latent heat as shown in Eq. (2-7) [126]:

$$\rho C \frac{\partial T}{\partial t} = \nabla \cdot (k \nabla T) - \rho L \frac{\partial f_1}{\partial t} \quad (2-7)$$

$$f_1 = \begin{cases} 0 & \text{if } T \leq T_1 \\ \frac{(T-T_1)}{(T_2-T_1)} & \text{if } T_1 < T \leq T_2 \\ 1 & \text{if } T \geq T_2 \end{cases}$$

where  $\rho$  and  $C$  are the density and specific heat capacity of PCM respectively.  $f_1$  is the liquid fraction.  $T_1$  and  $T_2$  are the onset and endset melting temperatures respectively.  $T$  is the temperature of the PCM layer at the time of  $t$ .

### 2.9.4. Building simulations with PCM

With the advent of more accurate and high-speed computational methods, numerical simulation is becoming increasingly popular for thermal performance assessments in buildings. The numerical simulations enable accurate evaluation of the dynamic thermal behavior of PCM and relevant impact on the indoor thermal comfort and building energy efficiency. Indeed, thermal performance enhancement with the application of

PCM depends on several factors such as thermophysical properties of PCM (mainly phase transition temperature), amount/quantity of PCM, local climatic conditions as well as application method and location. Thus, building thermal simulations is the most appropriate method to determine the influence of different factors and to evaluate the optimum solution based on different alternatives. Development of accurate simulation tools also offers the flexibility, innovation and accurate assessments of energy or thermal performance tailored to local climatic conditions. A wide variety of simulation tools were developed by researchers and commercial developers to carry out the thermal simulation of buildings. However, thermal performance simulations with PCM incorporated building components can only be handled with few simulation programs. The following building simulation programs have the capability to simulate the buildings incorporated with PCMs and out of those, EnergyPlus and TRNSYS have been most widely studied.

1. TRNSYS
2. EnergyPlus
3. ESP-r
4. BSim

#### **2.9.4.1. TRNSYS**

TRNSYS is a modular simulation software, where a series of components are linked together in which, the output of one component will be fed as input to another component in the model. Due to the modularity process of TRNSYS, users can choose in between available modules or develop a new module for serving their purposes. Thermal balance in buildings is defined through TYPE56: multi-zone building module in TRNSYS. This module analyses the building envelopes consisting the constant thermophysical properties of building materials. The building materials with varying thermophysical properties such as PCMs has not been included in this module and several add-on PCM modules were developed and available for research purposes [127]. These modules analyze the phase change behavior of PCM by using different heat transfer methods such as enthalpy method, effective heat capacity method and heat source method, and numerical simulation formulation can be chosen in between one-dimensional, two-dimensional or three-dimensional finite difference solution. Although

TRNSYS is convenient in modeling and simulating PCMs, it has several limitations as reported below [128]:

- Most of the modules have limitations in simulation time and full year thermal simulations cannot be performed due to computational limitations.
- Lack of validation of PCM modules with experimental and analytical data and hence, inaccuracy issues exist.
- Some modules are limited to isothermal melting/freezing temperature and constant specific heat capacity at all other stages, which may not represent real PCMs.

#### 2.9.4.2. *EnergyPlus*

EnergyPlus is a highly-accredited software tool developed by the U.S. Department of Energy (US DoE) and continuously upgraded by several researchers around the world. It is a powerful dynamic thermal simulation software, though not user-friendly, with adequate carefulness and users' experience successful simulation results can be achieved. It has been successfully used for the predictive evaluation of energy and thermal performance for buildings integrated with PCMs [129-131]. However, EnergyPlus is a simulation engine only and it requires a third-party graphical software such as DesignBuilder or Google Sketchup for the definition of building geometry.

EnergyPlus simulates the building materials with varying thermophysical properties, such as PCMs, by using one-dimensional conduction finite difference (CondFD) algorithm. According to EnergyPlus Engineering Reference [132], the CondFD algorithm can be chosen in between two different formulations, which are Crank-Nicholson scheme and fully implicit scheme. The Crank-Nicholson scheme is semi-implicit and it is considered as second-order in time. Eq. (2-8) shows the semi-implicit finite difference scheme function for an internal node.

$$C_p \rho \Delta x \frac{(T_i^{j+1} - T_i^j)}{\Delta t} = \frac{1}{2} \left( k_w \frac{(T_{i+1}^{j+1} - T_i^{j+1})}{\Delta x} + k_E \frac{(T_{i-1}^{j+1} - T_i^{j+1})}{\Delta x} + k_w \frac{(T_{i+1}^j - T_i^j)}{\Delta x} + k_E \frac{(T_{i-1}^j - T_i^j)}{\Delta x} \right) \quad (2-8)$$

On the other hand, the fully-implicit scheme also uses the CondFD method by using enthalpy method. However, it is based on the first order in time. Therefore, a user defined enthalpy-temperature function is adopted to account for phase change energy. The model equation for this scheme is shown in the following equation:

$$C_p \rho \Delta x \frac{T_i^{j+1} - T_i^j}{\Delta t} = \left( k_W \frac{(T_{i+1}^{j+1} - T_i^{j+1})}{\Delta x} + k_E \frac{(T_{i-1}^{j+1} - T_i^{j+1})}{\Delta x} \right) \quad (2-9)$$

EnergyPlus model updates the effective heat capacity value at every iteration, according to Eq.(2-10). The iteration scheme assures that the correct enthalpy and therefore correct  $C_p$  is used in every time step.

$$C_p = \frac{h_i^{j+1} - h_i^j}{T_i^{j+1} - T_i^j} \quad (2-10)$$

With reference to Eq. (2-8), (2-9) and (2-10), “ $\rho$ ” is the density of material. “ $\Delta x$ ” and “ $\Delta t$ ” are the finite difference layer thickness and calculation time step respectively. “ $h$ ” is the user defined specific enthalpy as a function of temperature, “ $T$ ” is the node temperature, “ $i$ ” is the node being modeled, “ $i+1$ ” and “ $i-1$ ” are the adjacent nodes in the directions of inner side and outer side of building structure respectively. “ $j+1$ ” and “ $j$ ” are the simulation time step and previous time step respectively. “ $k_W$ ” and “ $k_E$ ” are thermal conductivities of interfaces between nodes “ $i$ ” and “ $i+1$ ” and between nodes “ $i-1$ ” and “ $i$ ” respectively.

For both schemes, EnergyPlus uses CondFD approach in which each surface layer is divided into a number of nodal points based on the node spacing of each layer ( $\Delta x$ ) as shown in Fig. 2-17, and the node spacing is determined by the following equation:

$$\Delta x = \sqrt{C \times \alpha \times \Delta t} \quad (2-11)$$

Where, C: Space discretization constant

$\alpha$ : Thermal diffusivity of material

$\Delta t$ : Time step

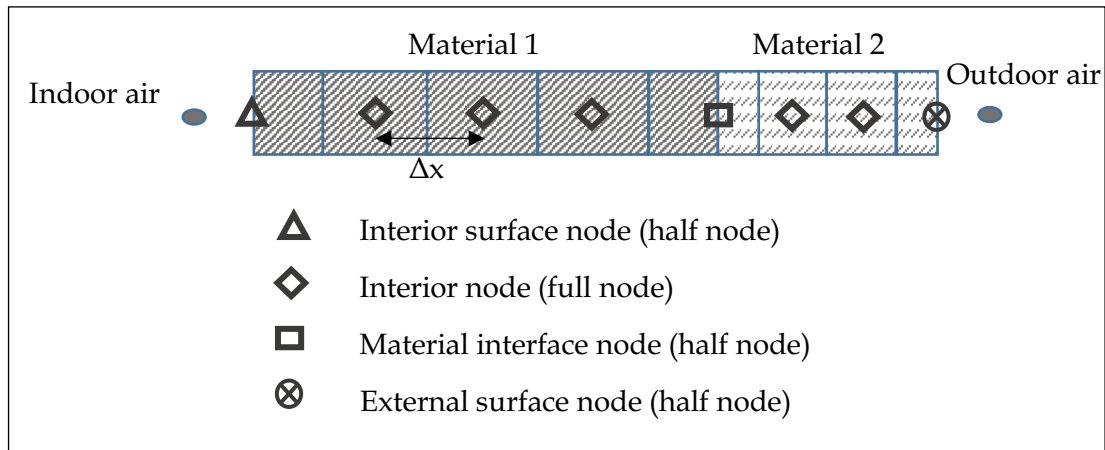


Fig. 2-17. CondFD space discretization in EnergyPlus

The space discretization constant ( $C$ ) is the inverse of the Fourier number and must be greater than 2, based on the stability requirement for the explicit mode. However, CondFD algorithm uses the implicit mode that does not have the same stability requirement. The default value of  $C$  is set as 3 and user can choose a value according to their finite difference refinement requirement. After determining the node spacing of each layer, EnergyPlus determines the number of nodes ( $N$ ) in a layer by simply dividing the layer thickness ( $L$ ) by node spacing ( $\Delta x$ ). The integer value of  $N$  is obtained by rounding off the  $L/\Delta x$  value, after which the  $\Delta x$  is adjusted by dividing the layer thickness by the number of nodes ( $\Delta x = L/N$ ;  $N$  integer).

### Validation of EnergyPlus model for PCMs

It must be highlighted that rigorous verification and validation studies were performed by many researchers [133-136] as well as the EnergyPlus developer team [117, 118], to study the reliability of EnergyPlus for simulating PCMs. For example, Zhuang et al. [137] validated the CondFD solution algorithm for PCM module in EnergyPlus with the consideration of two different envelope systems having one layer of PCM and two layers of PCM respectively. The results showed that the largest deviation in the indoor temperature between experiment and the numerical model was 12.41%, while the least difference was 0.71% during the run period of 36 hours in single layer PCM envelope. On the other hand, double PCM layered envelope showed the largest relative difference of 8.33% and least difference of 0.33% during the run period of 72 hours. This study concluded that the relative discrepancy in the results could be minimized by using actual weather data and accurate thermal characteristics of building materials.

Shrestha et al. [136] developed a PCM-enhanced dynamic insulation system in EnergyPlus and validated the simulation results with the field data. The dynamic insulation system consists of 20 wt% PCM and this system is installed in the exterior stud cavities of walls. Authors claimed this construction as advanced double wall construction. The study reported that the measured indoor temperature distribution has good agreement with the simulated data apart from some delayed response compared to measurement. In addition, recorded daily average heat flux measurements through the walls was within 9% of the simulated data, representing accurate simulation results. Some of the other prominent validation studies were conducted by Adam et al. [100], Campbell [138] and Chan [139] using published experimental data by Kuznik et al. [140]. It is worth mentioning here that the all validations studies had shown good agreement with the experimental results.

More recently, Jamil et al. [141] investigated the feasibility of incorporating macro-encapsulated Bio-PCM mats as an energy retrofitting option in a duplex residential house in Melbourne, Australia. The Bio-PCM mats are installed in the ceiling of a bedroom (BED 2), in between ceiling insulation and plasterboard. The indoor air temperature was monitored for 16 consecutive days and compared with simulation data for the same period. Fig. 2-18 shows the comparison of experimental and simulated data for two thermal zones to validate the numerical model with and without PCM layer. The results showed that the simulated data well agree with measured data with an RMS error of only 1.1°C with less than 1°C temperature difference for 73.5% of the period.

In addition to the above-mentioned validation studies, EnergyPlus developer team has also performed validation studies periodically for general heat transfer algorithms as well as CondFD algorithms [117, 118, 142]. The study conducted by Tabares-Velasco et al. [117] concluded that v6.0.0.037 of EnergyPlus contains two bugs and these bugs need to be fixed to simulate the buildings incorporated with PCMs accurately. Consequently, v7.1 was released with a validated PCM model and the following recommendations are given when modeling PCMs:

- The time step must be equal to or shorter than three minutes.
- The smaller node space (1/3 of the default value is recommended) should be used when accurate hourly performance is required.
- Modeling PCMs with strong hysteresis may lead to inaccuracy issues.

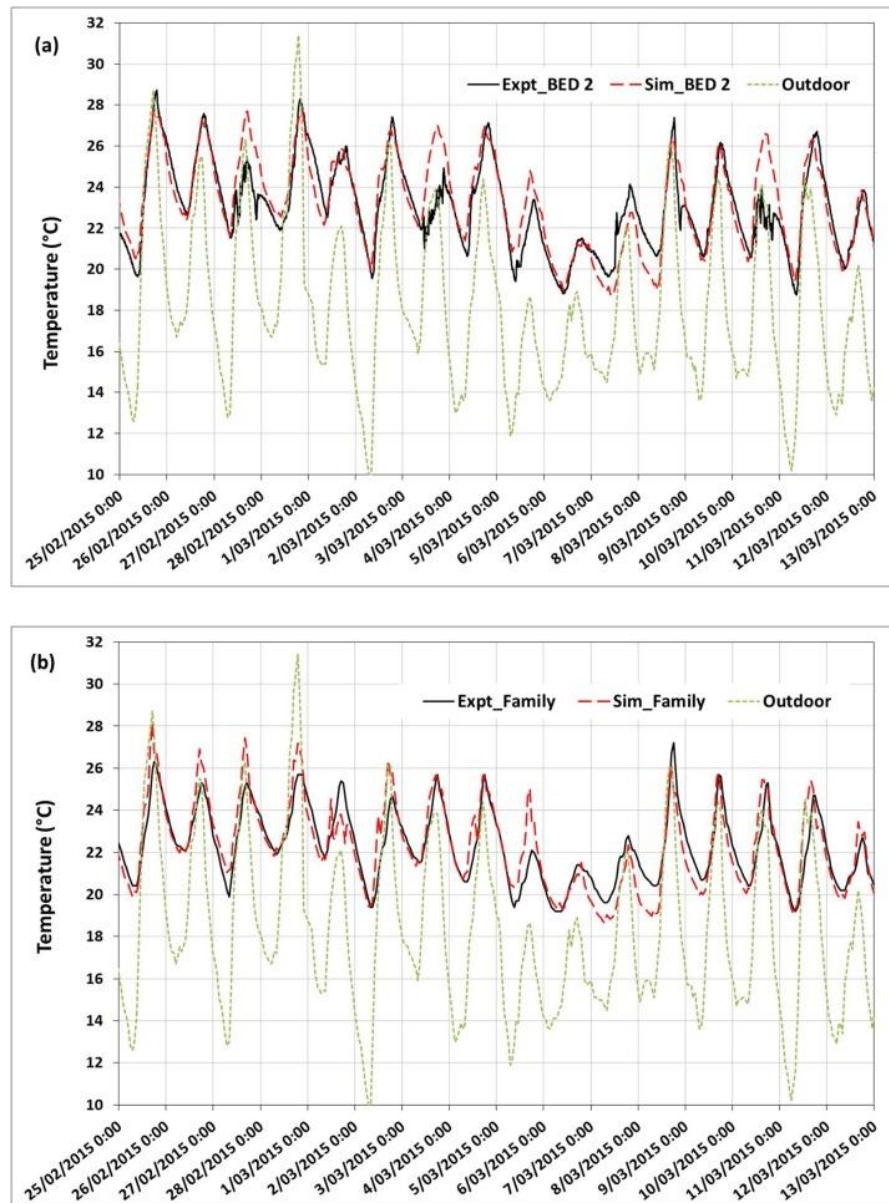


Fig. 2-18. Validation of a full-scale residential house with and without PCM (a) thermal zone with PCM (b) thermal zone without PCM [141]

### 2.9.5. Thermal performance assessment criteria

The numerical simulation provides the versatility of thermal performance assessments with many different assessment criteria, as opposed to experimental assessments where users are limited to measure the indoor temperature and heat flow measurements. Furthermore, numerical simulations enable the use of well-defined thermal comfort theories to evaluate the improvement in indoor thermal comfort, representing the enhancement of thermal performance of a building incorporating PCM compared to ordinary buildings. For example, EnergyPlus adopts many thermal comfort theories including, Fanger model, Pierce model and adaptive comfort models such as EN 15251 [143] and ASHRAE adaptive thermal comfort models [122].

In addition to thermal performance assessment using thermal comfort theories, many researchers developed new indices to evaluate the thermal performance of PCM incorporated buildings. The purpose of the development of new indices is to explore the thermal behavior of PCM incorporated buildings beyond the improvement in indoor thermal comfort and energy efficiency. Such explorations could lead to enhance and optimize the PCM performance in addition to indoor thermal comfort. For example, Ye et al. [144] developed new energy indices such as energy saving equivalent (ESE) and energy saving index (ESI), based on hypothetical energy input required to maintain the indoor temperature of a passive room at a constant comfort level. A case study was also carried out to assess the feasibility of the developed indices in a residential room. It was reported that the PCM application has better performance during summer and worse performance during the winter period, while insulation has better performance throughout the year when performance is assessed in terms of energy standpoint for a passive house.

Pisello et al. [145] proposed new non-dimensional indices termed as “thermal deviation indexes” (TDI) based on the distance between the targeted thermal condition and the existing condition in terms of intensity and frequency, to propose different optimization strategies and sensitivity analysis of PCM application in buildings. The developed TDI indicators were also correlated with adaptive comfort indicator represented by Degree Hours (DH) in CEN EN 15251 [143]. It was shown that the TDI could be an alternative representation of thermal comfort indicator (DH) for both seasons (i.e. summer and winter).

In another study [146], thermal performance indicators such as time lag and decrement factor were used to analyze the thermal performance of shape stabilized PCM (SSPCM) wallboard subjected to sinusoidal outside heat flux waves and to compare the performance with traditional building materials – brick, foam concrete and expanded polystyrene insulation. Here, time lag and decrement factor are defined as the time delayed by the peak inside heat flux with reference to the peak outside heat flux and ratio of the heat flux wave amplitude of inner surface to the outer surface respectively. It was reported that these performance indicators are useful for the selection of appropriate SSPCM and their application in passive solar buildings. Some of the other prominent studies to optimize PCM performance by identifying ideal parameters for thermal conductivity and specific heat capacity can be found in Zhang et al. [147] and Zeng et al. [148].

Although these new performance indicators can be more accurately reflecting the thermal performance of PCM applications, they are targeted at the indoor thermal environment and do not consider the PCM behavior in buildings. However, as PCMs are solely used for TES purposes in buildings, the operation or behavior of PCM in terms of latent heat storage should be evaluated. In order to take advantage of this opportunity, Evola et al. [12] introduced a set of performance indicators based on the PCM energy storage as well as the indoor operative conditions. Their study focused on optimizing the combined benefits of LHTES of PCM and the improvement in indoor thermal comfort. Authors determined the latent energy gain rate based on the difference between positive heat fluxes entering from both sides of the wall. From the latent energy storage behavior, they introduced set of indicators known as *Thermal Discomfort for overheating* ( $ITD_{over}$ ), *Frequency of Thermal Comfort* (FTC), *Frequency of Activation* (FA) and *PCM storage efficiency*, to represent the effect of PCM on its latent heat storage and indoor thermal comfort. These performance indicators can be more accurate and quite useful when representing the latent heat storage efficiency of PCM in buildings. However, this study also lacks in some aspects, where the indicators evaluate the performance enhancement in terms of many parameters and optimizing the PCM properties would be difficult since there is no singular performance indicator. The wallboard they investigated contained only 60% of microencapsulated PCM and the heat flux difference would also include the sensible energy stored in non-PCM materials. Furthermore, in a typical building construction that features multilayers, this approach cannot be used to isolate the energy

stored in the PCM. Therefore, there is still need to develop appropriate performance indicators to measure the thermal performance of PCM applications in buildings with the consideration of latent heat storage efficiency as well as the enhancement in indoor thermal comfort.

## **2.10 Thermal performance enhancement of PCM incorporated buildings**

### **2.10.1. Thermal performance of PCM integrated wallboards**

During the last two decades, the PCM integrated building components such as PCM wallboards, PCM-enhanced cement mortars and concrete have regained interest due to the popularity of these materials in building construction. In the early stage, PCM-enhanced wallboards were prepared by directly impregnating PCM into wallboard (using direct impregnation and immersion methods described in Section 2.5.1) and investigating the thermal performance enhancement using test rooms. Some of the prominent studies of thermal performance enhancement using direct impregnation of PCM into wallboards are presented here. Scalat et al. [149] conducted a full-scale experimental test room setup (2.29 x 2.27 x 2.45 m) with PCM integrated gypsum wallboards. The wallboard impregnated with 25.2 wt% of PCM was built as the interior surface of the test room and compared with identical control test room consisting ordinary wallboards. The operation was carried out by heating the rooms for 24 hours, then the heater is stopped and indoor temperature variation is monitored. This operation is called heating mode performance to assess the heat storage performance on a cold day. On the other hand, cooling mode performance was also assessed by cooling the room at 16°C for 24 hours and then the cold storage of PCM is allowed to cool the room. The results showed that the comfort period could be increased from 15.1 hours to 35.5 hours during the heating mode (135% increment in PCM room compared to ordinary room) and from 24.1 hours to 45.6 hours (89% increment) for cooling mode due to latent heat storage of PCM.

Athienitis et al. [150] experimentally and numerically studied the application of PCM impregnated gypsum wallboard for thermal energy storage in a full-scale outdoor passive solar test room. The wallboard contained 25wt% of butyl stearate with the phase transition temperature of 20.4-20.9°C and latent heat capacity of 25.5-26.6 J/g. It was

demonstrated that the PCM-enhanced wallboard reduced the peak indoor temperature by up to 4°C compared to ordinary gypsum wallboard.

Neeper [151] studied the thermal dynamics of wallboards impregnated with PCMs such as paraffin and fatty acids for the building applications. The PCM wallboard was subjected to diurnal temperature variation without the direct illumination of solar radiation. The thermal dynamics parameters of PCM wallboard such as PCM melting temperature, melting range and latent heat capacity per unit area of wallboard were investigated to propose optimal thermal dynamics properties of PCM wallboards. It was shown that the maximum energy storage occurs when the PCM melting temperature is close to the average comfort room temperature. Diurnal energy storage decreases when the melting occurs in a larger range of temperature. More importantly, the authors found that the diurnal energy storage achieved in practical applications could be limited to 300-400 kJ/m<sup>2</sup>, even if the wallboard has larger latent heat capacity.

Shilei et al. [66] experimentally studied the performance enhancement of PCM wallboard with 26 wt% of fatty acids as PCM. The test rooms constructed with the dimensions of 5 x 3.3 x 2.8 m was monitored for three consecutive days in the climate zone of Shenyang, China. According to the test results, the maximum temperature fluctuation in the PCM-enhanced test room was reduced by 1.15°C compared to the ordinary test room. Furthermore, thermal flow in the PCM room walls was lower than ordinary room walls.

The abovementioned studies have shown a significant enhancement in thermal performance of buildings incorporated with PCM integrated wallboards. However, they also have limitations associated with the thermal stability and reliability. Many studies reported that direct impregnation methods lead to PCM leakage or thermal instability issues when subjected to multiple thermal cycles [2, 3, 16, 18]. Moreover, the application of PCM in buildings are expected to withstand for a substantial period during the life cycle of the building and hence, it is necessary to prevent undesired effects of PCM during the operation. Therefore, direct impregnation of wallboards is rarely investigated in the latter period and encapsulation techniques such as microencapsulated PCM and form-stable PCMs are widely used to enhance the TES capacity of wallboards. Nowadays microencapsulated PCM wallboards are commercially available that can be directly incorporated into buildings as an energy refurbishment. ENERGAIN® is a commercially available PCM wallboard produced by Dupont de Nemours Society,

which can be incorporated into building interior surface elements for TES enhancement in buildings. The wallboard contains 60% of micro-encapsulated PCM with the melting temperature and latent heat capacity of 22°C and 185 J/g. The final form of the board is flexible sheets of 5 mm in thick with the density of 1019 kg/m<sup>3</sup> [140].

Kuznik et al. [140] conducted an experimental and numerical study for the application of ENERGAIN® wallboards to improve the TES capacity of a lightweight building envelope. The full-scale experiment of test cells with the dimensions of 3.10 x 3.10 x 2.50 m was investigated for summer day climatic conditions in Lyon, France. It was reported that the indoor air temperature and surface temperature fluctuations were significantly reduced with PCM wallboard, enhancing the indoor thermal comfort. Moreover, 5 mm thick PCM wallboard had twice higher energy storage and this corresponds to an equivalent concrete layer of approximately 8 cm.

Kuznik and Virgone [152] developed a test cell facility to assess the performance enhancement of a copolymer composite wallboard containing 60% of microencapsulated paraffin. The test program was conducted on three different scenarios including, a summer day, a winter day and a mid-season day. Authors claimed that the test room with PCM wallboard reduced the indoor air temperature by up to 4.2°C, compared to the control room. Furthermore, uncomfortable thermal stratifications were also avoided with the use of PCM. The same team also used this PCM wallboard for the renovation of an office building room and monitored the performance for year-round performance [153]. It was shown that the maximum air temperature and globe temperature were reduced by 2.2°C and 3°C respectively in the test room fitted with PCM wallboard.

Borreguero et al. [154] investigated the feasibility of incorporating microencapsulated PCM into gypsum wallboard as a potential technology to improve indoor thermal comfort in buildings. The thermal behavior of three different gypsum wallboards, one without PCM, and the other two are loaded with 4.7 % and 7.5% of PCM were investigated. The results showed that the indoor temperature increased smoother as the PCM content increases and tend to keep same steady state conditions for a longer time. Besides, the maximum/minimum temperature can be reduced/increased by up to 1.3°C with the PCM incorporation of 7.5%, compared to the wallboard without PCM.

Oliver [68] studied the thermal behavior of gypsum board containing 45 wt% of microencapsulated PCM (Micronal DS 5001X). The results showed that the 1.5 cm thick

PCM gypsum board stores 5 times more energy than a brick wall, and almost 3 times more energy per unit weight than ordinary gypsum board within the comfort temperature range of 20-30°C.

### 2.10.2. PCM integrated cement mortar and concrete

Cementitious composites such as cement mortar and concrete have also been widely investigated for thermal performance enhancement in buildings. However, they are largely limited to the laboratory scale experimental test-room studies as constructing large test room facilities would be time-consuming and require significant energy and cost. Therefore, few studies investigated the thermal performance of PCM integrated cementitious composites in large scale experiment. Cabeza et al. [75] developed thermal energy storage concrete containing microencapsulated PCM (named as MOPCON) with the phase transition temperature and latent heat capacity of 26°C and 110 kJ/kg respectively. The MOPCON concrete was used to construct a real size concrete cubicle (2 x 2 x 3 m with the PCM panel thickness of 0.12 cm) and to study the effect of PCM inclusion in concrete to improve thermal inertia and to reduce peak indoor temperatures. Two identical concrete cubicles, one with MOPCON concrete and the other with ordinary concrete, were constructed in Puigverd of Lleida, Spain as shown in Fig. 2-19. The results showed that maximum indoor temperature was reduced by 1°C and minimum indoor temperature was increased by 2°C. Furthermore, the peak indoor temperature in the PCM test cubicle occurred approximately 2 hours later than the cubicle without PCM.



Fig. 2-19. Concrete cubicles integrated with MOPCON concrete [75]

Entrop et al [155] studied the application of PCM in concrete floors with the use of 5 wt% of microencapsulated paraffin having the melting temperature and latent heat capacity of 23°C and 110 J/g respectively. Moderate sized box cubicles (1130 x 725 x 690 mm) were constructed by fully insulating the box envelope and having a window located on the south wall as shown in Fig. 2-20. Test boxes were placed in the outdoor environment in the climate zone of Twente, Netherlands and continuously monitored for indoor temperature and floor temperature. It was found that the PCM integrated concrete floor reduced the maximum floor temperature by up to  $16 \pm 2\%$  and increased the minimum floor temperature by up to  $7 \pm 3\%$ .

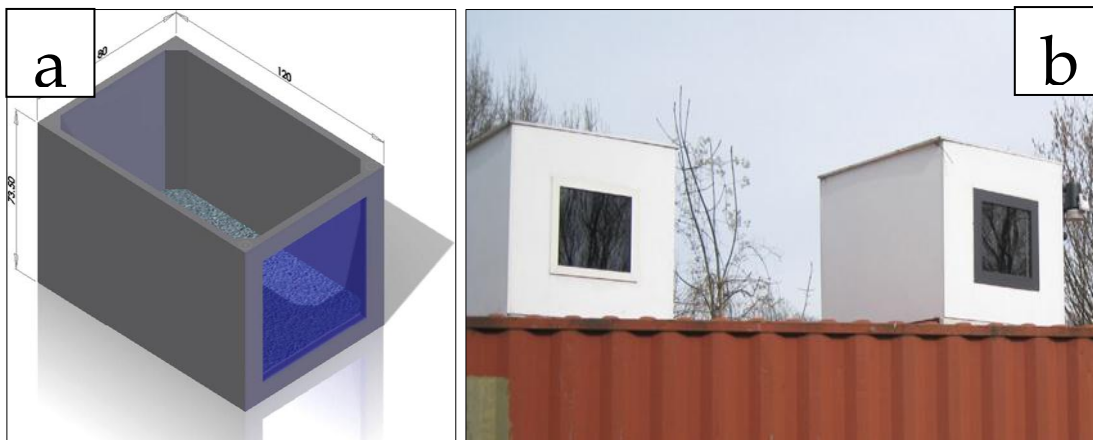


Fig. 2-20. Test room with concrete floor containing microencapsulated PCM (a) schematic diagram (b) physical set up [155]

Zhang et al. [88] investigated the thermal performance of n-octadecane/EG form-stable PCM integrated cement mortar with small sized test room (100 mm x 100 mm x 100mm) facility. The test room contained PCM integrated cement mortar boards on the top surface, while all other surfaces were considered as ordinary cement mortar boards. It was shown that the peak indoor temperature of the PCM test room was reduced by 4°C and 8.7°C for the PCM content of 1.2 and 2.5 wt% respectively. Outdoor thermal performance experiments were also conducted by Cui et al. [83] for lauryl alcohol/lightweight aggregate integrated thermal energy storage concrete in a small sized test cubicle (500 x 500 x 500 mm). The PCM integrated concrete test room showed up to 4.3°C reduction of peak indoor temperature compared to ambient temperature and the minimum indoor temperature was also higher than 1.4°C compared to ambient temperature. Furthermore, numerical analysis was also conducted on similar sized cubicle to study the enhancement in thermal performance and energy efficiency. The

results indicated that the PCM integrated concrete walls can reduce the peak indoor temperature by up to 10°C, while PCM integrated concrete floors and roof showed only a reduction of 2.5°C and 5°C respectively. On the other hand, an energy efficiency rate can be enhanced by up to 65.3% with PCM walls.

Li et al. [91] fabricated a heat storage cement mortar (HSCM) by integrating paraffin/EG composite PCM into cement mortar and compared the thermal performance with ordinary cement mortar board (OCM) in a small test room setup. It was reported that the inner surface temperature and interior temperatures of the PCM test room were reduced by up to 3.4K and 2.2K respectively in PCM-enhanced test room, compared to control room. Furthermore, heat storage coefficient of HSCM board, as measured by the thermal energy storage, was calculated as 1.74 times higher than that of OCM board.

In addition to concrete and cement mortar, PCM-enhanced plastering mortars were also widely studied for the building interior and exterior surface coating applications. PCM integrated plastering mortars including cement plastering mortars and gypsum plasters provide the versatility of a large amount of PCM integration compared to structural concrete applications, as they are non-structural members and require very low mechanical properties (i.e. compressive strength of 2.5 MPa according to EN1015-11). Schossig et al. [30] experimentally investigated the thermal performance of microencapsulated PCMs in gypsum plasters. Two full sized test rooms, one with PCM plasters and the other with the ordinary gypsum plaster, were applied as internal coatings in the test rooms. Wall surface temperature and air temperature were monitored throughout the testing period. Two different PCM types were tested: 6 mm thick dispersion-based plaster with 40% weight PCM and 15 mm thick gypsum plaster with 20% weight of PCM. It was reported that the peak indoor temperature was reduced by up to 4 K for the test room containing 15 mm thick gypsum plaster with 20% of PCM, compared to the ordinary test room. Furthermore, during the three weeks of temperature monitoring period, the period of temperature exceedance above 28°C was recorded as 50 hours and 5 hours for the test room with ordinary gypsum plaster and PCM gypsum plaster respectively. However, few limitations were discussed when PCMs are applied in this manner. The main limitation is that the PCM plaster act as a heat sink during night, thus discharging the stored heat at night would be difficult. Therefore, authors suggested that this kind of passive system require higher air-change

rate at night to discharge the PCM. Active cooling systems such as a cooling tower with capillary tubes embedded into plaster was recommended.

Voelker et al. [156] developed a modified gypsum plaster with the incorporation of microencapsulated paraffin having the capsule diameter and melting temperature of 5  $\mu\text{m}$  and 25-28°C respectively. Full-sized test rooms were constructed to investigate the thermal performance enhancement of PCM modified gypsum plasters. It was shown that the maximum indoor temperature reduction of 4°C could be achieved with the modified gypsum plaster. However, the PCM forfeit its heat storage capacity after few consecutive hot days of operation, as they cannot be discharged during night. Night ventilation techniques were recommended to counteract this issue.

Sá et al. [119] developed and characterized PCM-enhanced plastering mortars by incorporating microencapsulated paraffin into cement plastering mortar. The developed PCM-enhanced plastering mortar was characterized to meet the requirements of EN 1015 for the guidelines of standard plastering mortars. Pilot scale experiments having the plastering mortars as inner surface coatings indicated that the interior temperature of test room could be reduced by up to 2.6°C with the application of PCM in plastering mortars. Furthermore, parametric studies were conducted with numerical simulations to identify the appropriate melting temperature and melting range of PCM. It was reported that the optimum solution to achieve thermal comfort highly depends on environmental thermal cycles and a unique PCM would not provide optimal operation throughout the year. Therefore, a compromise solution should be made to achieve near-optimum performance throughout the year.

Kheradmand et al. [121] also developed PCM-enhanced plastering mortars by incorporating hybrid microencapsulated PCM into ordinary cement mortars. The hybrid PCM mortar, containing three distinct PCMs in ordinary cement mortar with the melting temperatures of 10°C, 26°C, and 28°C, were tested for the thermal energy storage during different climate seasons such as winter and summer [120]. The prototype experiments conducted on a small sized test room revealed that the HPCMM could reduce the daily temperature amplitude from 13°C to 8.9°C on a summer day and 5.6°C to 4°C during a winter design day respectively. However, it is also noted that internal temperatures during the winter scenario were unrealistically low compared to thermal comfort conditions, though PCM helped in reducing the daily amplitude of variation.

## 2.11 Motivation for the study and research gaps

Based on the literature review presented so far, it turns out to be clear that the use of PCM in construction applications are growing, especially showing regained interest in the integration of PCM into cementitious composites such as cement mortar and concrete for the building interior and exterior applications. In this regard, the PCM incorporation method is the very first step that needs to be carefully determined and the first research question comprises of the following:

1. What is the most suitable method of PCM integration into cement-based materials and how to prevent associated PCM instability or leakage issues?

Out of the different PCM integration methods discussed so far, form-stable PCMs can be considered as most suitable form of integration into cementitious composites compared to other techniques such as direct incorporation and microencapsulation. However, in most of the research works, the stability of form-stable PCM composites in cement matrix has not been extensively studied. Also, studies that are investigating the integration of form-stable PCM into cement matrix showed a significant amount of PCM leakage and adverse effects to cement matrix. Therefore, it is of primary important to investigate the stability of form-stable PCM composites with cementitious materials to identify the factors influencing the PCM leakage in the cement matrix. Such investigation can also provide a solution to develop new PCM composites that can prevent the PCM leakage in cementitious composites. In the present study, the stability of form-stable PCM composites in cement matrix along with the development of new PCM composites will be investigated in Chapter 3. Furthermore, the development of new form-stable composite PCM implies various characterizations including, micro-morphology, chemical compatibility and thermal stability. The integration of new composite PCM into cement matrix should also be studied for mechanical and thermal performance evaluation. The relevant experimental research for these characterizations is reported in Chapter 4.

Once the new form-stable PCM has been developed, characterized and investigated for the integration into cementitious composites, its intended application in buildings should be investigated. Therefore, the second research question is presented as follows.

2. What is the intended application of PCM integrated cementitious composites in buildings? What are the properties that must be studied for such PCM application method?

The intended application of form-stable PCM in cementitious composites can be considered as the use of thermal energy storage cement mortars (TESCM) for the structural-functional cement mortars as well as the non-structural surface plastering mortars. In any case, the TESCMs developing in this study must be studied for its physical, mechanical and thermal properties. This thesis will undertake a study on the physical, mechanical and thermal properties of new PCM composite integrated as partial replacement to fine aggregate in ordinary cement mortars. Furthermore, the mechanical and thermal reliability of TESCMs will also be studied with the accelerated thermal cycling tests. A systematic study to this end will be carried out and relevant analyses are presented in Chapter 5.

Apart from that, PCMs have very low thermal conductivity and results in poor heat transfer performance during diurnal charging and discharging operation. Therefore, the performance enhancement in PCM integrated cementitious composites applications are essential for the effective utilization of large latent heat capacity. Hence, the third research question is as follows:

3. How to improve the heat transfer performance of cementitious composites containing form-stable PCM? Which additive is most suited for largest performance enhancement?

The most effective heat transfer enhancement method in form-stable PCM composites was identified as the dispersion of high conductive additives into PCM composites for the effective enhancement of heat transfer rates to PCM occupied in the pores. Therefore, it is vital to focus on the application of different high conductive additives in enhancing the heat transfer performance of form-stable PCM integrated cementitious composites. The Chapter 6 of this thesis will investigate the thermal performance enhancement of form-stable PCM integrated cementitious composites with different high conductive additives such as graphite, carbon nanotubes (CNT) and graphene nanoplatelets (GNP).

It is well known that the integration of form-stable PCM composites into cement mortars is to enhance the TES capacity of building envelopes and to increase the building energy

efficiency and indoor thermal comfort. Therefore, it is necessary to assess the thermal performance of proposed PCM application in buildings and hence, the fourth research question is formulated as follows:

4. What is the effectiveness of the developed PCM integrated cementitious composites in improving the thermal performance of buildings?

The thermal performance studies are required to assess the performance enhancement of TESCM in buildings compared to ordinary cement mortars in terms of improving indoor thermal comfort and/or reduction in peak indoor temperature and temperature fluctuations. This thesis investigates the thermal performance enhancement of TESCMs with comprehensive experimental and numerical analyses. The relevant experimental and numerical studies with corresponding results are presented in chapter 7.

Finally, even if several criteria are used for evaluation of the thermal performance of PCM in buildings, there is still a lack of proper indicators to optimize the thermal performance of PCM. Moreover, previous research has primarily focused on the performance enhancement of PCM in improving indoor thermal comfort and/or energy savings in buildings, whilst the storage efficiency of PCM has not been adequately addressed. Thus, the fifth research question of this study will be as follows:

5. How can the thermal performance of PCM be optimized? What are the parametric factors need to be studied for the optimization of PCM in buildings?

In order to optimize the PCM application in buildings, thermal performance of PCM should be evaluated in terms of the latent heat storage efficiency of PCM and effectiveness in improving the indoor thermal comfort. The current study presents a design optimization method of PCM application in buildings by developing new thermal performance indicators. The parametric analysis will also be carried out to identify the influence of thermophysical properties of PCM and effect of night ventilation on the thermal performance enhancement of PCM applications. Furthermore, the study will be carried out for the entire cooling season (December-February) in four major cities of Australia: Melbourne, Sydney, Perth, and Brisbane. The relevant analysis and results are presented in Chapter 8.

# Chapter 3 Assessing the feasibility of integrating form-stable PCM into cement-based composites

---

## 3.1 Introduction

As discussed in the literature review, the incorporation of PCM into building components lead to increased TES capacity and reduced interior temperature fluctuations, thereby enhancing the building energy efficiency and indoor thermal comfort. A wide range of methods are available to incorporate PCM into building components, and out of those, integration of PCM into cementitious composites has been identified as an effective methodology, as they are widely used in building construction and hence, large amounts of PCM can be incorporated into buildings [18, 70]. Among the studied PCMs, organic solid-liquid PCMs (i.e. paraffin and fatty acids) are considered as promising candidates due to its sharp melting temperature, large volumetric heat capacity, little or no supercooling effects and are chemically inert materials. However, pure PCMs limit its usage in many TES applications due to the leakage issues [2, 60].

To overcome the PCM leakage issues, microencapsulated PCM [30, 155] and form-stable PCMs [22, 157] have been investigated recently, as they are encapsulated with polymeric shells and porous supporting materials respectively. Nevertheless, most recent studies showed that these encapsulation techniques are also resulting in PCM leakage when integrated into cementitious composites. Furthermore, such PCM leakage causes adverse effects on physical, mechanical and durability properties of produced cement mortar or concrete. In particular, form-stable PCM composites with the phase transition temperature lower than ambient temperature showed a significant amount of PCM leakage when integrated into cementitious composites. As a consequence, they require protective surface coatings such as hydrophobic coatings or epoxy coatings for the

prevention of PCM leakage and to overcome associated adverse effects on the cement matrix [5-8].

The main aim of this chapter is to investigate the stability of form-stable PCM composites in cementitious composites and prevention of PCM leakage by developing new PCM composite which do not require any protective surface coatings for the integration into cementitious composites. A commonly studied PCM composite, which is based on paraffin/expanded perlite will be fabricated for the investigation of instability or PCM leakage in cementitious composites. On the other hand, a novel form-stable PCM composite will be fabricated by using hydrophobic coated expanded perlite as supporting material to mitigate the problems associated with PCM leakage or instability. It is believed that the PCM composite fabricated on paraffin/hydrophobic expanded perlite would prevent the PCM leakage due to the counter water affinity properties of this expanded perlite supporting material. To our knowledge, this hydrophobic expanded perlite has never been reported for the development of thermal energy storage composites in the literature. The expanded perlite (EP) based materials are chosen as supporting materials for this study due to the advantages of EP such as abundant availability with very low density, high porosity and relatively low cost [158, 159]. Because of its highly porous structure and very high surface area, EP can absorb a large amount of PCM. The PCM Composites were fabricated by two methods including, natural immersion and vacuum impregnation methods to investigate the effect of fabrication method on the PCM absorption capacity and to achieve maximum absorption capacity. The developed PCM composites were then characterized and assessed for the stability or PCM leakage with cementitious materials. Furthermore, the issues associated with PCM leakage in form-stable PCMs were correlated with its surface characteristics such as contact angle and wetting tension measurements with water.

## **3.2 Materials and Methods**

### **3.2.1. Materials**

The expanded perlite having an average particle size of 40  $\mu\text{m}$  was supplied from Australian Perlite Pty Ltd. Hydrophobic expanded perlite was purchased from Filchem Australia Pty Ltd., which contains ultra-lightweight porous expanded perlite granules chemically coated with alky alkoxy silane compound to make them hydrophobic [160]. A commercial grade paraffin (RT27) with the manufacturer specified melting temperature of 27°C was purchased from Rubitherm®. It consists of saturated hydrocarbons with the molecular formula of  $\text{C}_n\text{H}_{2n+2}$ . In this chapter, normal EP and hydrophobic coated EP are denoted as EPW and EPO respectively based on their water affinity and counter water affinity properties and their relevant form-stable PCM composites are termed as EPWP and EPOP respectively. Ordinary Portland cement (OPC) complying with AS3972 was used to integrate form-stable PCM composites in order for the assessment of PCM leakage in cementitious composites.

### **3.2.2. Fabrication of form-stable PCM and PCM integrated cementitious composites**

Two commonly used fabrication methods of form-stable PCMs were adopted in this research: natural immersion and vacuum impregnation, to evaluate the effect of different impregnation methods and to achieve maximum absorption capacity of PCM into porous supporting materials. A sequence of composites, with the increasing mass fraction of PCM (at an increment rate of 5wt% of PCM in composite), was fabricated to find the optimum PCM absorption capacity. The fabrication process of form-stable PCM composites is as follows.

For both methods, porous granules (EPO and EPW) were initially heated at 105°C for 24 hours to remove the moisture occupied in the pores. The paraffin (RT27) was melted at 60°C until it becomes clear and transparent as this indicates the completely melted state of PCM. It has been reported that increasing the PCM temperature will reduce the viscosity of the fluid and hence, accelerate the absorption rate into the pores [5]. In the natural immersion method, the paraffin and EP granules were mixed at atmospheric pressure until the paraffin was completely absorbed into the pores of EP. This was

ensured by visual observation until a uniformly dispersed and non-agglomerated powder mix is obtained. For the vacuum impregnation method, the paraffin and EP are mixed at atmospheric pressure and immediately transferred to a vacuum chamber to enable the vacuum impregnation process. After the vacuuming process of 30 minutes, the pressure was gradually released to reach the atmospheric pressure. Then the composite was mixed thoroughly to obtain a uniformly dispersed PCM composite. Finally, the form-stable PCMs were obtained after cooling at room temperature. Once a series of PCM composites are fabricated with increasing paraffin content, the optimum amount of paraffin loading in the composite was determined according to the diffusion-oozing circle test described in section 3.2.3.2.

The PCM integrated cementitious composites were fabricated by mixing form-stable PCMs with cement and water. The mix proportion of materials used in developing PCM integrated cementitious composites are given in Table 3-1, where the weight ratio of composite PCM to cement was chosen as 0.43 and the water to cement ratio was chosen according to the workability requirement. To evaluate the liquid PCM leakage, the operational temperature must be kept above the PCM melting temperature. Therefore, to determine maximum leakage, all experiments were carried out at the room temperature of 30°C, which can also be assumed as an approximate construction site temperature [6]. The mixing procedure was as follows. First, cement and PCM composite were dry mixed at low speed (60 RPM) for 1 minute in a Hobart mixer. After the dry materials had been uniformly mixed, water was added and mixed for 3 minutes at low speed (60 RPM), during which time the mixer was stopped at every minute and material adhering to the surface of the mixer was scraped down. Finally, the mixing was completed by following the medium speed (120 RPM) mixing for one minute. The fresh mixes were poured into transparent cylindrical cups to observe the PCM leakage visually and to measure the leakage ratio when integrated into cementitious composites.

Table 3-1 Mix proportion of materials

PCM integrated cementitious composite	Cement (wt%)	PCM composite (wt%)	Water/cement ratio
EPWP - cementitious composite	70	30	0.6
EPOP - cementitious composite	70	30	0.7

### 3.2.3. Testing methods

#### 3.2.3.1. Particle size distribution measurements

The particle size distribution of different expanded perlite materials was determined by a laser particle size analyzer (CILAS 1190 from Scientex Pty Ltd). The measurements have been made in dry dispersion mode. CILAS 1190 can measure the particles ranging from 0.04  $\mu\text{m}$  to 2.5 mm at an accuracy of 0.04  $\mu\text{m}$ . It also enables the specific surface area measurements with the provision of shape factor and particle density.

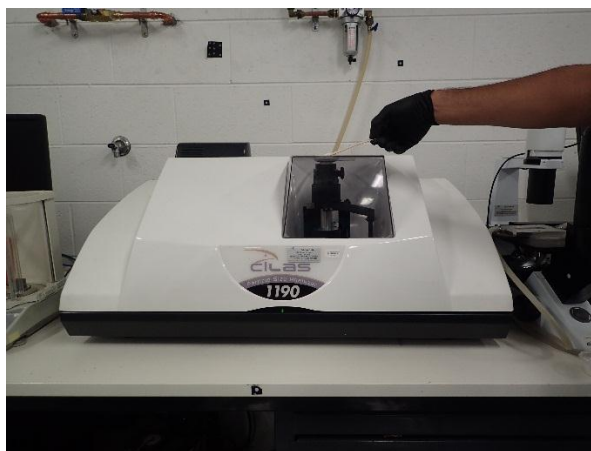


Fig. 3-1. Particle size distribution test conducted in dry mode

#### 3.2.3.2. Absorption characteristics

The optimum absorption capacity of paraffin in the form-stable PCM composites was determined using diffusion-oozing circle test method proposed by Ma et al. [161]. In this method, about 20 g of PCM composite was dispersed on a filter paper as shown in Fig. 3-2 and gently pressed to provide good contact between composite PCM and filter paper. The filter paper with composite PCM was kept at 60°C for one hour to ensure the paraffin had completely melted so that the excess PCM could be exuded on the filter paper. After one hour, the filter paper was removed from the oven and visually observed for any trace of liquid leakage. The maximum PCM absorption capacity was determined as when the leakage diameter retained within the contact area.

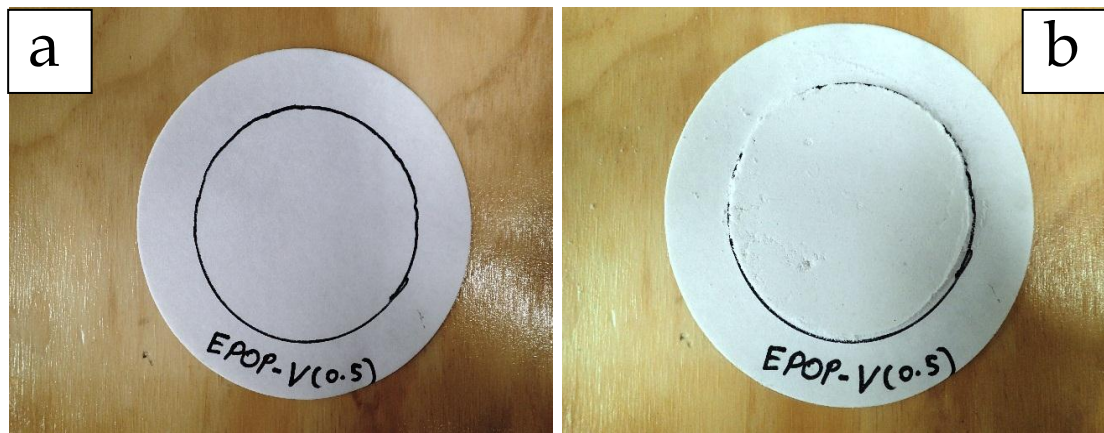


Fig. 3-2. Diffusion-oozing circle test (a) filter paper (b) specimen prepared on the filter paper

The absorption characteristics of PCM composites were investigated by studying the micro-morphology characteristics of porous granules and fabricated composite PCMs with Scanning Electron Microscopy (SEM) and energy dispersive X-ray spectroscopy (EDXS) analysis. The SEM analysis was conducted on ZEISS Supra 40 VP SEM at an accelerating voltage of 3 kV. Since the PCM composites are not electricity conductive themselves, the powder samples were coated with a very thin layer of gold before SEM testing. The testing was conducted in low vacuum conditions at a working distance of 6 mm. EDX analysis was conducted at an accelerating voltage of 20 kV for the same specimens to probe the chemical compositions of the granular materials after PCM absorption.

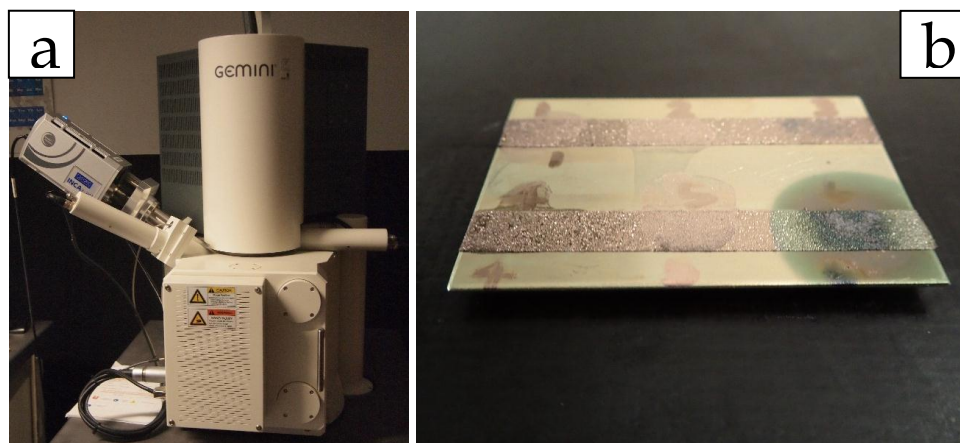


Fig. 3-3. SEM test (a) SEM equipment (b) gold coated specimens

### 3.2.3.3. *Thermal properties of composite PCMs*

The thermal properties of paraffin and form-stable composites, such as phase transition temperatures and latent heat capacity were measured by a differential scanning calorimetry (DSC). DSC test was conducted using a Heat flux DSC (Q1000 from TA Instruments). The temperature and enthalpy accuracy of Q1000 are 0.1°C and 1% respectively. The heat flux DSC measures the thermal properties of materials by measuring the differential heat supplied to sample specimen compared to a reference specimen during an endothermic process. Similarly, it measures the differential heat released from specimen during an exothermic process. Approximately 6 mg of specimens were prepared in aluminum crucibles with 20 µl capacity and sealed with specimen lid by using an encapsulating press. The weight measurements were carried out using a Mettler Toledo MX5 microbalance with an accuracy of 0.01 mg. The DSC test was conducted over the temperature range of -20 to 60°C at a temperature ramping rate of 5°C/min in Nitrogen (N<sub>2</sub>) atmosphere.

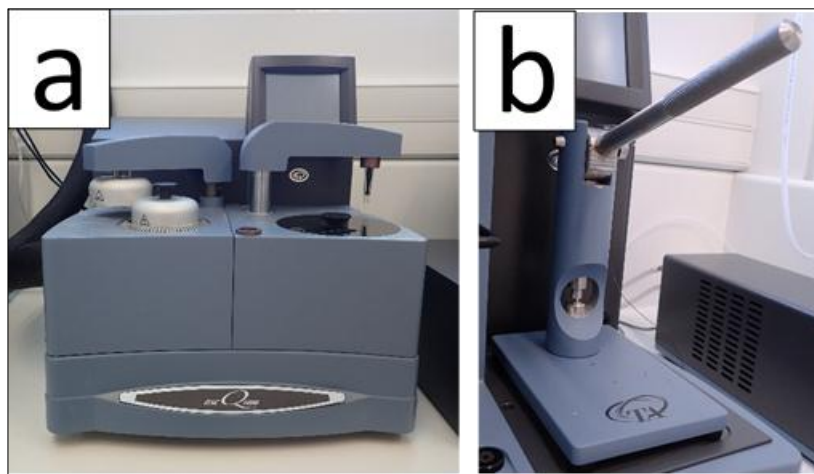


Fig. 3-4. DSC test (a) DSC equipment (b) encapsulating press

### 3.2.3.4. *Stability or PCM leakage of composite PCMs in cementitious composite*

The instability or PCM leakage of form-stable PCM in cementitious composites was initially evaluated by visual observation of paraffin leakage in PCM integrated cementitious composites poured into transparent cylindrical cups. This provided a preliminary qualitative evaluation of PCM leakage for different form-stable PCMs. This was followed by quantitative evaluation of the amount of PCM leakage in the cementitious mixture. The fresh cementitious mixture was poured into transparent

cylindrical cups and kept in a controlled thermal environment having ambient temperature and relative humidity of 30°C and 95% respectively as described in Section 3.2.2. As soon as the mix hardened, the leaked liquid was poured out and the weight was measured. The leakage ratio of PCM was defined as the weight ratio of leaked paraffin to the total paraffin content used in the mixture.



Fig. 3-5. Cementitious composite mixture poured in transparent cylindrical cup

In order to further verify the leakage of PCM in cementitious composites and to accurately determine the PCM leakage ratio, the latent heat capacity of hardened cementitious composites was determined by DSC experiment and compared with the theoretical latent heat capacity calculated from the amount of PCM absorption as shown in Eq. (3-1):

$$H_T = H_{CPCM} \times \frac{W_{CPCM}}{(W_{cement} + W_{CPCM} + W_{Water})} \quad (3-1)$$

In Eqn. (3-1),  $H_T$  and  $H_{CPCM}$  are the theoretical values of the latent heat capacities of PCM integrated cementitious composite and developed PCM composite respectively.  $W_{cement}$ ,  $W_{CPCM}$  and  $W_{Water}$  are the mass fraction of cement, composite PCM, and water in cementitious composite respectively. For this test, hardened cement pastes were crushed into fine powder and approximately 6 mg of powder specimens were prepared for DSC test. Furthermore, DSC test was also conducted to exuded liquid to identify the content and purity of paraffin in this liquid.

**3.2.3.5. *Surface characteristics measurement of composite PCMs and relationship with leakage phenomenon***

The surface characteristics of PCM composites such as contact angle and wetting tension properties were measured by sessile drop method using a contact angle goniometer equipped with a nanodispenser (model FTA32, First Ten Ångstroms, Inc., USA). The composite PCM powders were compressed into solid disc samples with the diameter of 25.4 mm and thickness of around 3 mm by using a hydraulic press. Both form-stable PCM composite samples (i.e. EPOP and EPWP) were prepared with the same amount of specimen as well as same compression force and holding time. Three samples from each composites were used for the contact angle measurement and average of the contact angle and wetting tension measurement were calculated. The disc specimens are placed in the working platform of the goniometer and 1.0 µl water droplet was dispensed on the specimen surface. The high-resolution cameras connected to the goniometer captured the profile of water droplet on the composite PCM substrate and the captured images were then analyzed using the image analysis software provided with goniometer apparatus.



Fig. 3-6. FTA32 contact angle goniometer

### 3.3 Results and discussions

#### 3.3.1. Particle size distribution of expanded perlites

The particle size distribution of granular porous materials (EPW and EPO) measured using the laser diffraction particle size analyzer is presented in Fig. 3-7 in terms of volume passing percentage and cumulative volume passing percentage. Table 3-2 also summarizes the major results of the particle size analysis such as mean particle diameters and particles sizes that are passing at 10%, 50% and 90% of the content. As shown in Fig. 3-7, both expanded perlite materials are very fine powders and have approximately similar particle size distributions. It can also be observed that the particle size distributions of both materials have nearly symmetrical bell shapes, with the central peak at approximately 50  $\mu\text{m}$  and 75  $\mu\text{m}$  for EPW and EPO respectively.

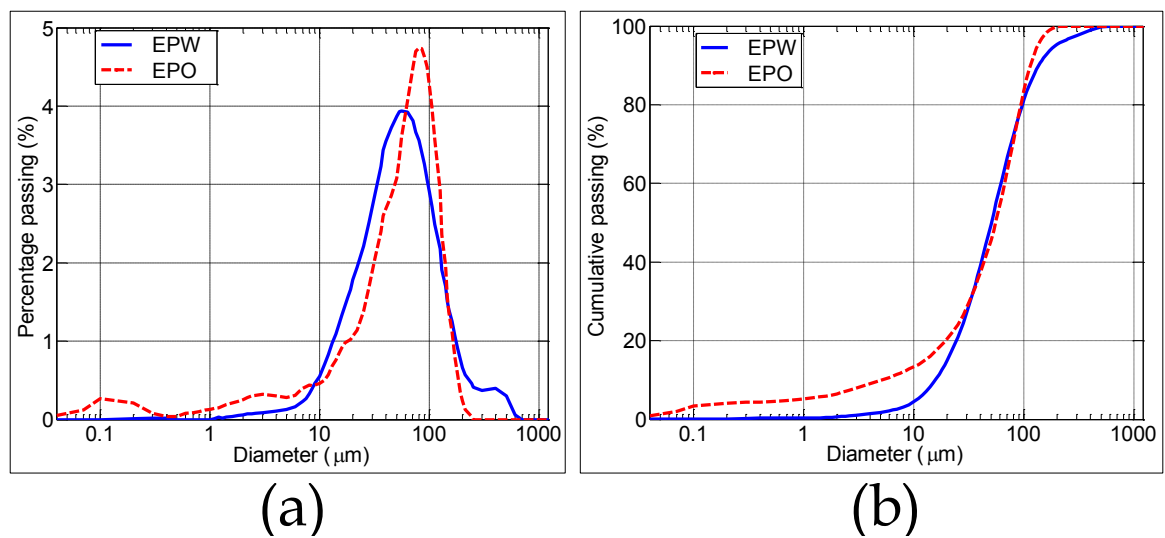


Fig. 3-7. Particle size distribution of the EP particles (a) volume percentage passing (b) cumulative volume passing

Table 3-2 Mean diameter and equivalent diameters of EP particles

	Mean diameter ( $\mu\text{m}$ )	D(0.1) ( $\mu\text{m}$ )	D(0.5) ( $\mu\text{m}$ )	D(0.9) ( $\mu\text{m}$ )
EPO	58.95	5.12	55.31	114.78
EPW	52.38	15.65	50.46	136.23

### 3.3.2. Absorption characteristics of the composites

The maximum absorption capacities determined for the different impregnation methods are shown in Table 3-3. Fig. 3-8 and Fig. 3-9 shows the exudation stability of PCM composites for different PCM proportions measured using diffusion-oozing circle test. Here, the maximum PCM loading capacity in porous granules were considered as when the exudation retains within the contact surface area of PCM composite with filter paper as recommended by Ma et al [161]. As can be seen from Fig. 3-8, for the EPWP composite PCM, both impregnation methods showed maximum PCM loading capacity of 35 wt% as they both have shown the PCM exudation beyond the contact surface area for 40 wt% of paraffin. Thus, vacuum impregnation method had negligible improvement on the PCM absorption capacity of EPW based PCM composite. EPOP composite PCM, however, showed a different behavior for different fabrication methods (see Fig. 3-9). The natural immersion method could lead to a maximum absorption capacity of 35 wt% whereas vacuum impregnation method had retained the PCM exudation within the contact surface area for 50 wt% of paraffin. Further increase of PCM content above 50 wt% lead to agglomeration of composites and thus, they cannot be derived in powder form. Therefore, the optimum absorption capacity of paraffin in the composites was determined as 35 wt% and 50 wt% for EPWP and EPOP respectively using vacuum impregnation method.

The micro-morphology characteristics of granular porous materials studied by using SEM are depicted in Fig. 3-10 and Fig. 3-11 for EPW and EPO respectively. As seen from Fig. 3-10, the EPW has a highly porous tunnel-like structure that makes to have high porosity and large specific surface area. The EPO, however, has individual, spherical and porous frustules (see Fig. 3-11) with an irregular bubble-like shape that could create a strong bond with cement matrix. Fig. 3-11b shows single spherical frustule of EPO. On the other hand, the micro-morphology characteristics of composite PCMs at their optimum absorption level are depicted in Fig. 3-12. The inspection of Fig. 3-12(a) reveals that the pores in the EPW have decreased and the edges of EPW turned to smooth and round, indicating that the open pores of EPW had been completely loaded with liquid paraffin. Besides, Fig. 3-12(b) shows that the open pores of individual porous frustules in EPO are no longer visible and it is likely that they were uniformly filled with liquid paraffin. Furthermore, by comparing the particle sizes of EPO and EPOP granules, it can

be observed that the paraffin is well absorbed into the pores of EPO granules and it is not coated to the surface of EPO.

On the other hand, the chemical composition of composite PCMs determined by EDXS testing is charted in Fig. 3-13. It can be seen that there is a large amount of carbon detected in both composite PCMs. However, as there is no carbon element in EP materials the finding likely reflects the absorbed paraffin, which has the molecular formula of  $C_nH_{2n+2}$ . Moreover, surface characterization of composite PCMs using EDXS analysis showed a greater amounts of Si, Al and O, which are elements of EP granules. This further validates that the paraffin was absorbed into the pores of EP materials and they have not been surface coated to porous granules.

Table 3-3 Paraffin absorption capacity for different impregnation methods

Sample	PCM impregnation method	Maximum absorption capacity (% by weight)
EPOP	Natural immersion	35
	Vacuum impregnation	50
EPWP	Natural immersion	35
	Vacuum impregnation	35

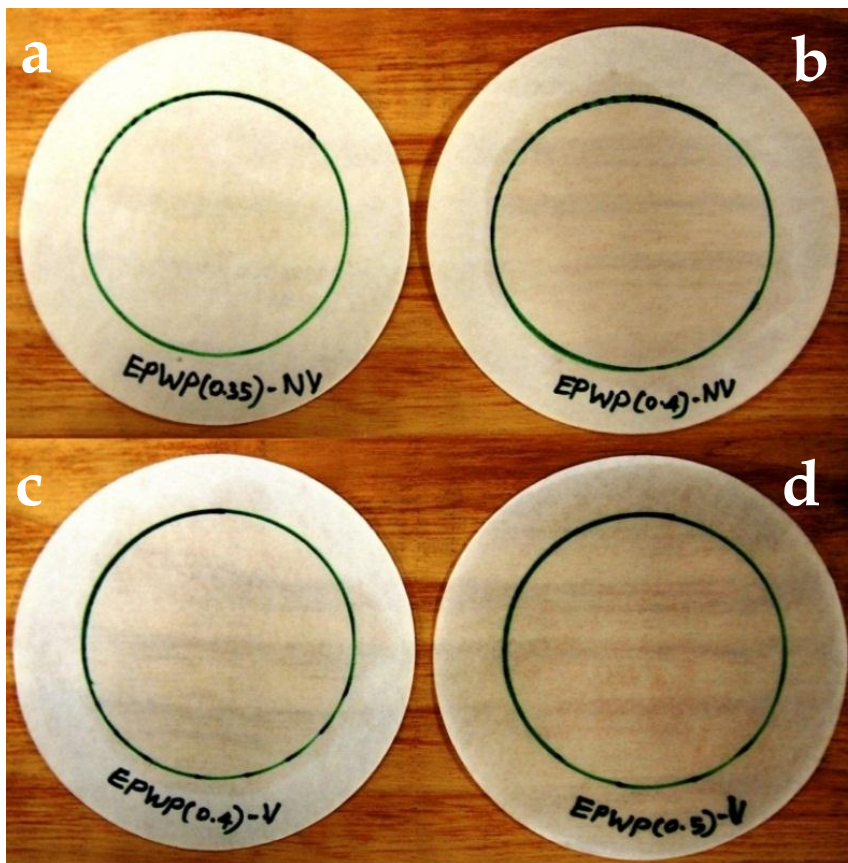


Fig. 3-8. Diffusion-oozing circle test for EPWP samples, (a) & (b) 35 wt% & 40 wt% of paraffin, natural immersion (c) & (d) 40 wt% & 50 wt% of paraffin, vacuum impregnation

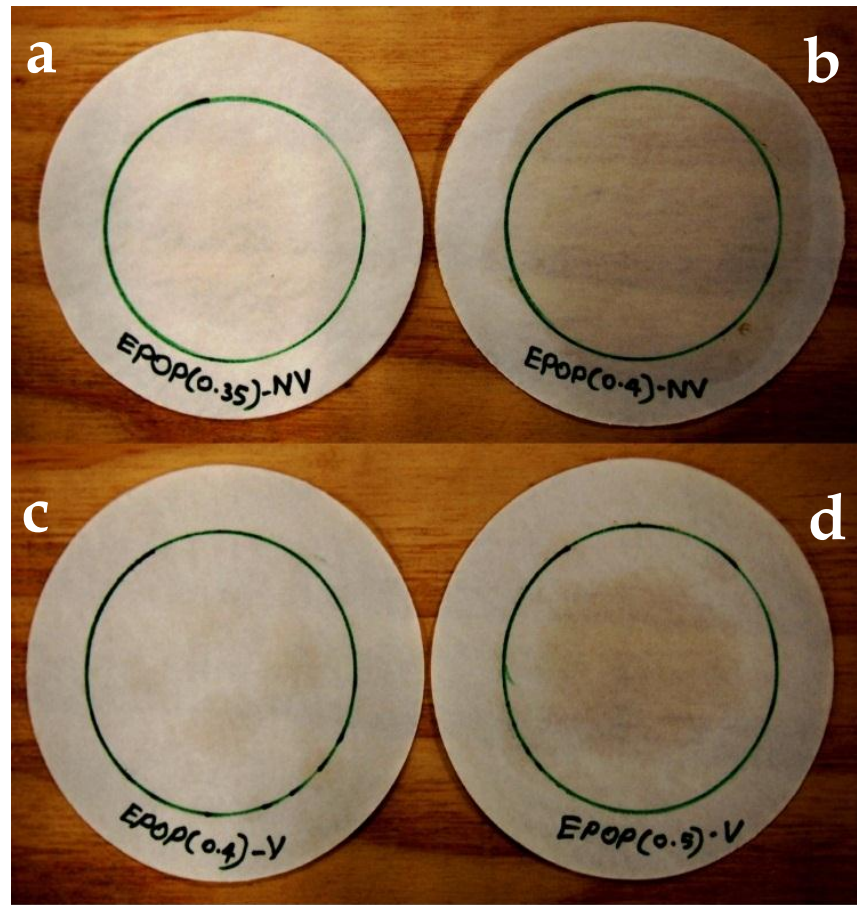


Fig. 3-9. Diffusion-oozing circle test for EPOP samples, (a) & (b) 35 wt% & 40 wt% of paraffin, natural immersion (c) & (d) 40 wt% & 50 wt% of paraffin, vacuum impregnation

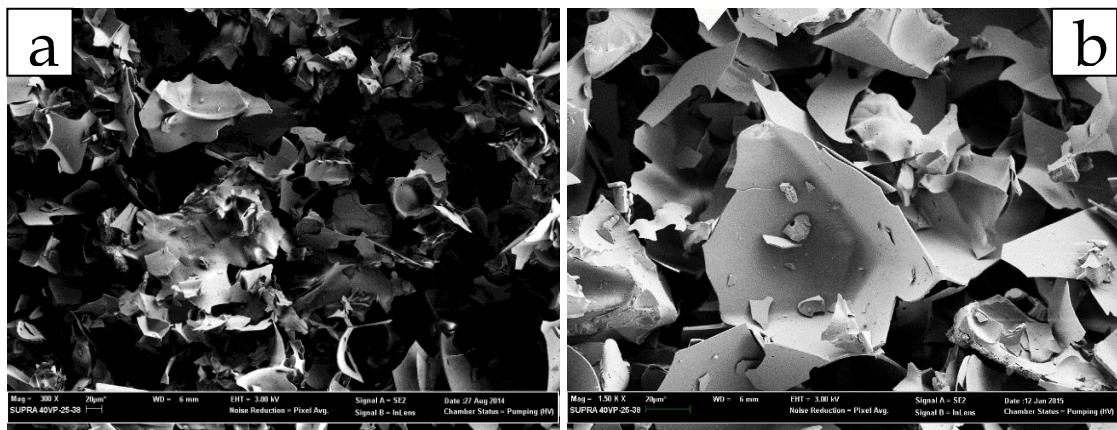


Fig. 3-10. SEM morphology of EPW

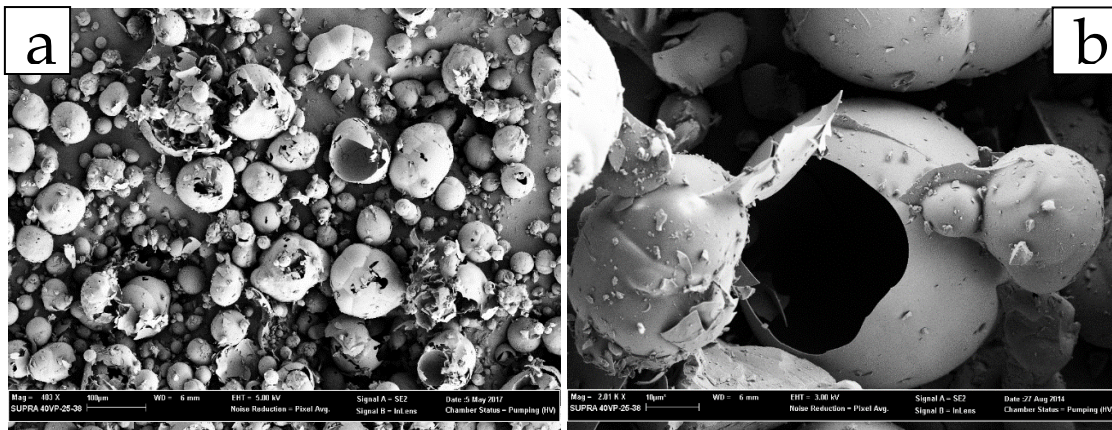


Fig. 3-11. SEM morphology of EPO (a) EPO granules (b) single spherical frustule

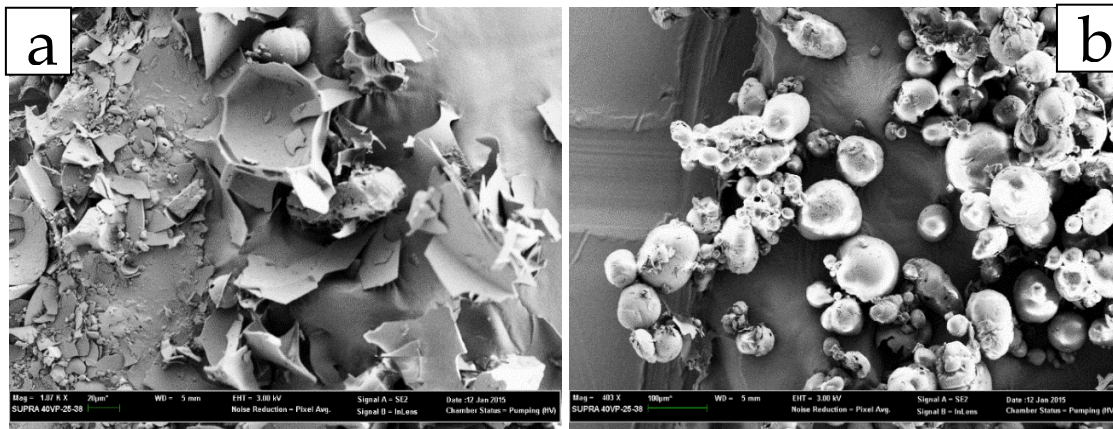


Fig. 3-12. SEM morphology of composite PCMs (a) EPWP (b) EPOP

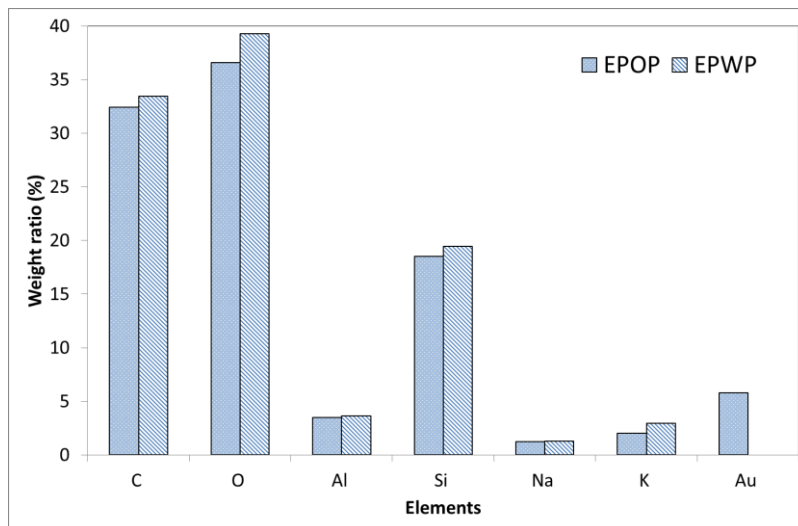


Fig. 3-13. Chemical composition of PCM composites

### 3.3.3. Thermophysical properties of PCM composites

The thermophysical properties such as phase transition temperature and latent heat capacity determined for paraffin, EPWP, and EPOP are depicted in Fig. 3-14. Table 3-4 also summarizes the calculated values of phase transition temperature and latent enthalpy determined from the heat flow measurement. In addition to the experimental values, theoretical latent heat capacity, based on the amount of PCM absorption into the porous granules, also determined for PCM composites using Eq. (3-2):

$$H_T = H_{paraffin} \times W_{paraffin} \quad (3-2)$$

Here  $H_{paraffin}$  and  $W_{paraffin}$  are the latent heat capacity of paraffin determined from DSC test and the weight percentage of paraffin used to fabricate PCM composite, respectively. The theoretical latent heat capacity values are compared with experimentally derived values to assess for any variation in latent heat capacity when PCM absorbed into micropores. Fig. 3-14 shows that the paraffin and fabricated PCM composites are showing two exothermic transitions during the cooling process and two endothermic transitions during the heating process. While the major exothermic and endothermic processes correspond to the phase transition of paraffin at approximately 27°C, the smaller peak occurring at nearly 0°C corresponds to the water impurities in the paraffin mixture, which melts and solidifies at 0°C.

On the other hand, Table 3-4 illustrates that the paraffin has onset phase transition temperatures of 25.07°C and 25.83°C for melting and freezing respectively, while the relevant peak melting and freezing temperatures were obtained as 27.15°C and 24.78°C respectively. The latent heat capacity of paraffin was determined as 164.8 J/g and 167.2 J/g respectively for melting and freezing processes. The PCM composites showed slightly lower melting phase transition temperatures of 26.71°C and 26.58°C for EPWP and EPOP respectively. Similar reductions were also observed for freezing phase transition temperatures. The slight reduction in phase transition temperature of PCMs is attributed to the physical interaction between the paraffin and inner surface of the porous materials and the confinement of paraffin in very small pores, as reported by previously [5]. On the other hand, the latent heat capacities of EPWP and EPOP were derived as 55.60 J/g and 81.21 J/g for melting and 55.01 J/g and 78.00 J/g for freezing

respectively, which are also quite close to the theoretical latent heat capacity calculated based on the PCM absorption ratio. This evident the uniform distribution of paraffin into the pores of EP materials.

Table 3-4 Phase change temperature and enthalpy of paraffin and form-stable PCMs

	Melting process				Freezing process			
	T <sub>Onset</sub> (°C)	T <sub>Peak</sub> (°C)	H <sub>M</sub> (J/g)	H <sub>T</sub> (J/g)	T <sub>Onset</sub> (°C)	T <sub>Peak</sub> (°C)	H <sub>F</sub> (J/g)	H <sub>T</sub> (J/g)
Paraffin	25.07	27.15	164.8	-	25.83	24.78	167.2	-
EPWP	24.78	26.71	55.60	57.68	24.74	23.30	55.01	58.52
EPOP	24.45	26.58	81.21	82.40	24.32	23.51	78.00	83.60

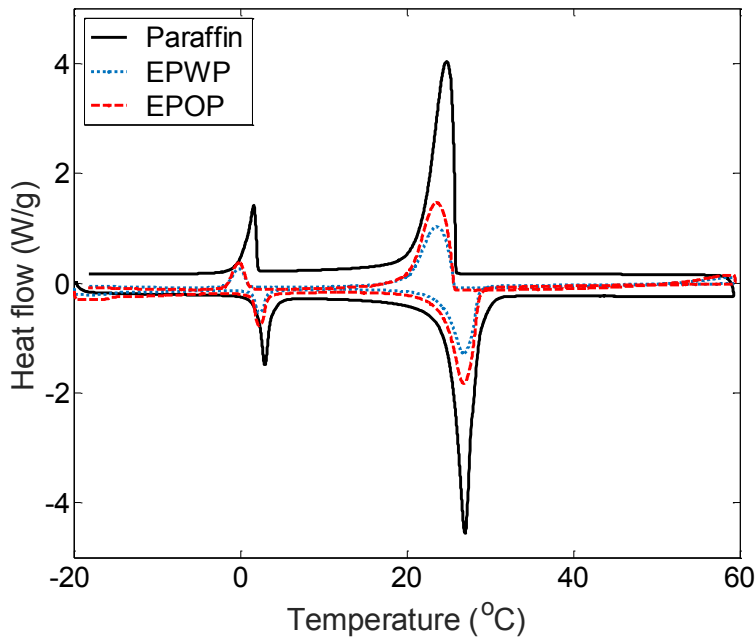


Fig. 3-14. DSC curves of paraffin and PCM composites

### 3.3.4. Stability of form-stable PCMs in cementitious composites

The stability of form-stable PCMs in cementitious composites was preliminarily evaluated by observing the paraffin leakage from the mix as proposed in Ref. [5, 6]. The Fig. 3-15 shows the liquid PCM leakage of different form-stable PCM composites when integrated into cement mortars. As shown in Fig. 3-15, the form-stable PCM composites showed different behaviour when integrated into cementitious composites. For EPWP composite in cementitious mixture, a significant amount of PCM leaked and segregated to the top of the mixture indicating the instability of EPWP in cementitious composites. This liquid was then transferred into another container and kept at 18°C for 24 hours for the evaluation of the purity of paraffin in this liquid. It was found this liquid had solidified completely and no trace of the liquid phase was observed. This evident that the leaked liquid contained paraffin and does not contain water. The leakage ratio was measured as 42%. On the other hand, the Fig. 3-15 also evident that the composite PCM fabricated on hydrophobic EP (EPOP) did not show any trace of liquid leakage when integrated into the cementitious composites. This reveals that the hydrophobic form-stable PCMs are highly stable and can be successfully integrated into cementitious composites without any leakage or instability issues. Furthermore, such high stability of PCM in cement mortars can prevent the interaction of PCM with cement matrix resulting in enhanced compatibility of composite PCM with cement matrix.

In order to further verify this phenomenon and to present accurate measurements of PCM leakage in cementitious composites, thermophysical properties of form-stable PCM integrated cementitious composites were determined using a differential scanning calorimetry. The DSC measurements were conducted to exuded liquid from EPWP, EPWP integrated cementitious composite and EPOP integrated cementitious composite. The corresponding DSC thermographs of exuded liquid and PCM integrated cementitious composites are illustrated in Fig. 3-16. Table 3-5 also summarizes the latent heat capacity of those materials determined from DSC thermographs coupled with the theoretical latent heat capacity values. It can be seen from Fig. 3-16 and Table 3-5 that the latent heat capacity of exuded liquid was very close to the paraffin used in the fabrication of EPWP. This indicates that the leaked liquid purely contain paraffin and no trace of water can be observed). Furthermore, the leakage ratio of EPWP in cement mortar was found as approximately 50%, which is slightly higher than the leakage ratio

measured from the weight measurements of leaked liquid. The higher leakage ratio derived from DSC analysis compared to weight measurements attributes to the evaporation of segregated liquid PCM during the curing period. This caused a reduced weight measurement in exuded liquid. Nevertheless, the leakage ratio of EPWP in cementitious composites is significant, thus presents a barrier for the construction applications of such form-stable PCM with cement based materials.

On the other hand, the latent heat capacity measured for EPOP integrated cementitious composite is approximately close to the theoretical latent heat capacity, indicating that there is no PCM leakage when integrating EPOP into cementitious composites. This further reinforces the conclusions drawn from the preliminary leakage tests, where form-stable PCM composites fabricated on EPO can successfully prevents the PCM leakage in cement-based materials.

The leakage behavior of form-stable PCM fabricated on hydrophilic supporting materials can be explained as follows. When a hydrophilic form-stable PCM (e.g. EPWP) is mixed with water, due to the hydrophilic nature of the EPW particles, water molecules quickly combine with it, causing separation of the paraffin from the EPW. This separation induces such liquid to segregate to the top surface due to their low density and flowability. Furthermore, compaction of such cementitious composites using mechanical vibration drives the segregated liquid to the surface. On the other hand, the form-stable PCM fabricated on hydrophobic supporting materials such as EPO, prevents the leakage of PCM in water environment due to their counter water affinity properties. In fact, hydrophobic surface coating (alkyl alkoxy silane coating) of EPO granules repels the water molecules in the cementitious mixture and prevents the contact of water to paraffin occupied in the pores of EPO, thus leading to highly stable composite in water environment. It is worth mentioning here that this thesis investigated the stability of PCM composites in cementitious composites and excludes the stability of such composites in concrete. The main reason for the prevention of PCM leakage was identified as counter water affinity of hydrophobic PCM composite, which prevents the contact between paraffin occupied in the pores and water. Therefore, a similar behaviour can also be expected in concrete containing this PCM composite as the only difference between the cementitious mixture and concrete is the absence of inert aggregates in cementitious mixture.

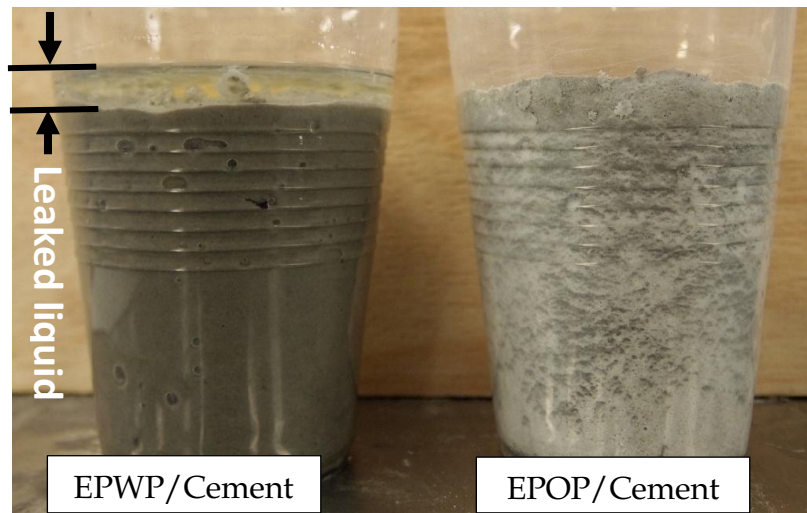


Fig. 3-15. Leakage of paraffin in cementitious mixtures

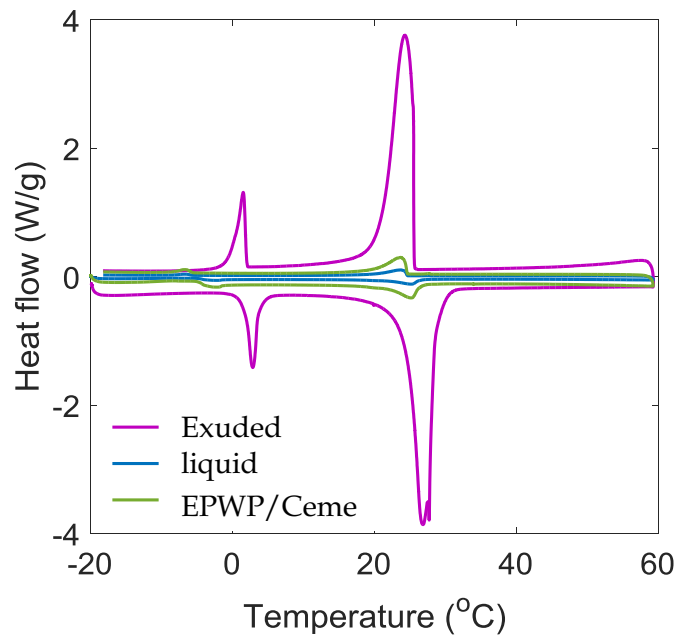


Fig. 3-16. DSC curve for exuded liquid and PCM integrated cementitious composites

Table 3-5 Leakage of form-stable PCMs in cementitious composites

	Melting process			Freezing process		
	$H_M$ (J/g)	$H_T$ (J/g)	Loss of paraffin	$H_F$ (J/g)	$H_T$ (J/g)	Loss of paraffin
Exuded liquid	158.82	-	-	163.40	-	-
EPWP/Cement	5.21	10.46	50.2%	5.32	10.31	48.4%
EPOP/Cement	14.11	14.33	negligible	14.32	14.75	negligible

### 3.3.5. Surface characteristics of PCM composites and PCM leakage

As discussed in Section 3.3.4, the stability of form-stable PCM in cementitious composite depends on the surface characteristics of supporting materials. More precisely, form-stable PCM fabricated on hydrophilic supporting material (i.e. EPW) resulted in the significant amount of PCM leakage, while hydrophobic form-stable PCM does not show any trace of liquid PCM leakage. Indeed, the capillary forces and surface tension are the main driving forces of the absorption of fluids (paraffin in this case) into the pores of granular materials. However, the leakage tests revealed that the PCM absorbed into the pores of EPW becomes exuded when it is mixed with the cementitious mixture. Thus, it is believed that the surface characteristics of form-stable PCMs such as wettability and contact angle can be correlated to the leakage phenomenon in such PCM integrated cementitious composites.

The wetting properties of form-stable PCMs with water, as measured by contact angle and wetting tension, are depicted in Fig. 3-17. The measured values of contact angle and wetting tension for three specimens with the average and standard deviation are also given in Table 3-6. Fig. 3-17 shows that the EPWP (a representation of hydrophilic PCM composite) has shown an acute contact angle (contact angle lesser than  $90^\circ$ ) and a positive wetting tension between PCM composite and water, which indicates that this composite PCM has high water affinity properties. Due to this high affinity, liquid PCM absorbed into the pores of EPW can be replaced by water in the cementitious environment. On the other hand, EPOP (a representation of hydrophobic PCM composite) has obtuse contact angle (contact angle higher than  $90^\circ$ ) and negative wetting tension properties. This indicates that this form-stable PCM has counter water affinity properties and hence repels the water molecules in cementitious composites. Due to the obtuse contact angle and negative wetting tension properties, EPOP can successfully prevent the PCM leakage in cementitious composites. It can be concluded, therefore, that the contact angle measurements of form-stable PCMs provides an accurate evaluation of the instability or PCM leakage in cementitious composites.

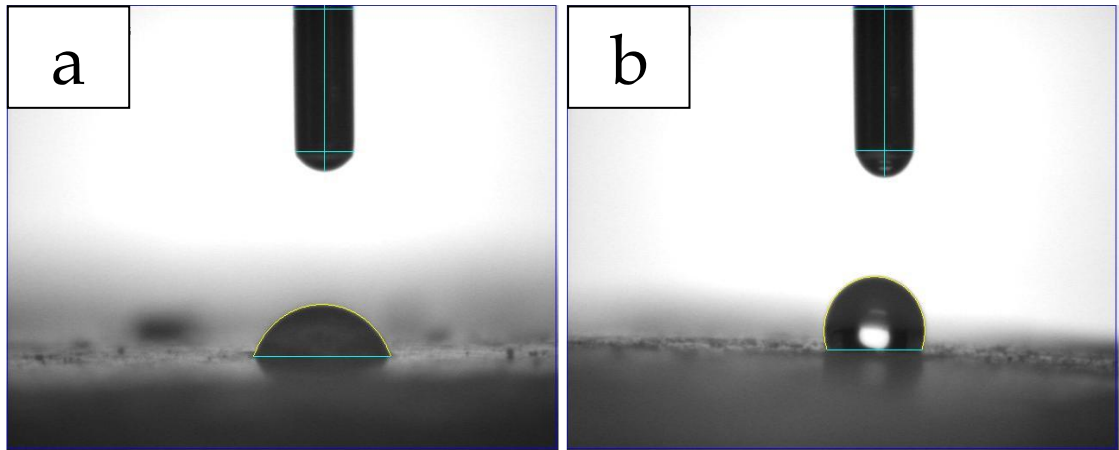


Fig. 3-17. Behavior of water droplet on the surface of composite PCMs (a) EPWP (b) EPOP

Table 3-6 Contact angle and wetting tension of PCM composites

Sample	Contact angle (Deg.)	Wetting tension (mN/m)	Average contact angle	Average wetting tension
EPWP	70.80	23.94	71.32 ( 1.04 )	23.31( 1.25 )
	70.64	24.13		
	72.52	21.87		
EPOP	110.88	-27.70	112.6( 1.85 )	-28.55( 1.48 )
	112.36	-27.70		
	114.56	-30.26		

### 3.4 Concluding remarks

This chapter addressed the first research question of this research by investigating the instability or PCM leakage of form-stable PCM composites when integrated into cement-based materials. Two different form-stable PCMs: one with expanded perlite (EPW) and another with hydrophobic expanded perlite (EPO), were fabricated and investigated for the integration into cementitious composites. Based on the experimental research, the following conclusions can be drawn:

1. The fabrication of form-stable PCMs using vacuum impregnation method resulted in the larger absorption capacity of paraffin compared to natural immersion method.
2. The form-stable PCMs fabricated on EPW and EPO had the PCM absorption ratio of 35wt% and 50wt% respectively of paraffin, in the composite. The SEM results showed that the paraffin was well incorporated in the pores of both EP granules.
3. The thermophysical properties of PCM composites showed that the EPWP and EPOP had the melting phase transition temperature of 26.71°C and 26.58°C respectively, while their relevant latent heat capacities of 55.60 J/g and 81.21 J/g.
4. The PCM composites showed a different behavior when integrated into cement mortars. The hydrophilic PCM composite (EPWP) showed a significant amount of paraffin leakage of approximately 50%, whereas no trace of paraffin leakage was observed for hydrophobic PCM composite (EPOP).
5. The instability of form-stable PCMs in the cementitious composite was correlated with surface characteristics of PCM composites such as contact angle and wetting tension measurements. It was revealed that the PCM composites having an obtuse contact angle and negative wetting tension properties with water could be integrated into cement-based materials without the PCM leakage issues.

Finally, the novel form-stable PCM composite fabricated on paraffin/hydrophobic expanded perlite can be further studied for the integration into cementitious composites without the PCM leakage issues.

# Chapter 4 Preparation, characterization, and properties of paraffin/ hydrophobic EP integrated cementitious composites

---

## 4.1. Introduction

As concluded in Chapter 3, the form-stable PCM composite fabricated on hydrophilic supporting materials such as expanded perlite cannot be directly integrated into cement-based materials due to a significant amount of PCM leakage. Furthermore, hydrophobic supporting materials prevents the PCM leakage in the cementitious composites due to their water repellent surface characteristics. In particular, the form-stable PCM composite fabricated with paraffin and hydrophobic EP (EPOP) showed high absorption capacity and negligible amount of PCM leakage when integrated into cementitious composites. However, before considering the application of this novel form-stable PCM in cementitious composites, it is necessary to study the characteristics of form-stable PCM such as chemical compatibility and thermal stability of the components in the composite. The chemical compatibility of composite PCM is necessary, since the paraffin was physically absorbed into the pores of EPO, and any chemical interaction between PCM and surface of the porous materials could significantly affect the thermophysical properties of form-stable PCM. Furthermore, the thermal stability of PCM should also be studied as most of the organic PCMs decompose or evaporates at medium-high operational temperatures of around 200-400°C [162]. Therefore, when such PCMs are absorbed into the pores, the decomposition temperature may decrease and the composite PCM becomes unsuitable for TES applications. The thermogravimetric analysis has been widely used to study the thermal stability of composite PCMs.

In addition, the integration of new form-stable PCM into cement matrix can cause variations in the mechanical properties and microstructural characteristics of resultant PCM integrated cementitious composites. It is reported that the PCM encapsulated in

polymer shells and porous materials can interact with the cement matrix, thus resulting in poor mechanical and durability properties [7, 73]. Furthermore, thermal properties and thermal performance of form-stable PCM integrated cementitious composites should also be evaluated to study the performance enhancement of novel form-stable PCM in increasing the TES capacity of cementitious composites.

This chapter initially investigates the chemical compatibility and thermal stability of EPOP composite PCM. Chemical compatibility between the components of composite PCM (i.e. paraffin and EPO) was investigated by Fourier transform infrared spectroscopy (FT-IR). The thermogravimetric analysis (TGA) was conducted to study the thermal stability of paraffin and composite PCM. The PCM composite was then integrated into cementitious composites to develop thermal energy storage cementitious composites (TESCs) and to study the microstructural characteristics and mechanical properties. Here, control cementitious composite and PCM integrated cementitious composite are denoted as NC and TESC respectively. Finally, thermal storage performance of TESC was studied with the aid of self-designed heat storage performance test. This study included the development of TESC panels containing approximately 2.7 kg/m<sup>2</sup> of PCM in 20 mm thick panels and comparison with similar sized NC panels. The thermal storage performance was studied by evaluating the thermal inertia and thermal energy storage rates of NC and TESC panels subjected to laboratory controlled climatic conditions.

## 4.2. Materials and Methods

### 4.2.1. Materials

The commercial grade paraffin (RT21) with the manufacturer rated phase transition temperature of 21°C and hydrophobic expanded perlite were purchased from Rubitherm® and Filchem Australia Pty Ltd respectively, for the fabrication of form-stable PCM. Ordinary Portland cement (OPC) complying with AS3972 was used for the preparation of NC and TESC. The chemical composition of OPC and EPO, determined by using the X-ray fluorescence method (XRF), is given in Table 1. Silica sand with maximum particle size of 1.18 mm was obtained by sieving the sand using No. 16 standard sieve (1.18 mm aperture). A commercial grade water reducing admixture (MasterPozzolith 370 from BASF) was used to improve the workability of TESC.

Table 4-1 Chemical composition of EPO and OPC

Series	SiO <sub>2</sub>	Al <sub>2</sub> O <sub>3</sub>	K <sub>2</sub> O	Fe <sub>2</sub> O <sub>3</sub>	Na <sub>2</sub> O	SO <sub>4</sub>	CaO	MgO
EPO	73.12	17.21	5.09	-	3.32	-	1.26	-
OPC cement	4.25	21.08	3.32	0.41	5.42	63.45	1.98	0.09

### 4.2.2. Fabrication of form-stable PCM and TESC

The EPOP form-stable PCM was fabricated by vacuum impregnation method as described in Chapter 3, where melted paraffin was absorbed into the open pores of EPO in vacuum conditions. The mix proportion of composite materials were considered as 50 wt% of paraffin in the composite, as determined from diffusion-oozing circle test in Chapter 3.

The NC and TESC were prepared by following the mix design of materials proposed in Table 4-2. The mixing method is as follows. First, dry materials were mixed at low speed (60 RPM) for one minute in a horizontal pan mixer (i.e. Hobart mixer). Once the dry materials had been uniformly mixed, water together with admixture was added and the low-speed mixing was followed for another three minutes. Finally, the mixing was completed by following the medium speed (120 RPM) mixing for one minute. The fresh

cementitious composite mixes were poured into 50 x 50 x 50 mm<sup>3</sup> steel cubic molds for the compressive strength test. For the thermal performance test, cementitious composite panels were cast at the dimensions of 300 x 300 x 20 mm using timber panel molds as shown in Fig. 4-1.

The cube and panel specimens were prepared as two layers and each layer was compacted using an external mechanical vibrator until the air bubbles cease to appear. Then they were kept in a moist environment for 24 hours. After 24 hours, specimens were demoulded and cured in water-bath at 23±0.5°C till the test date. It must be noted that, a higher W/C ratio was used in TESC to achieve adequate workability of mix. In fact, following a weight based mix design lead to larger volume contribution of PCM composite (compared to silica sand aggregates in NC) due to low density and this caused the requirement of higher water content. This dissimilarity in the mix design may lead to the reduction in the mechanical properties when compared with NC. Furthermore, TESC also completely replaces the fine aggregate with PCM composite and such TESC may not be appropriate for construction applications. However, the main purpose of this study was to investigate the microstructural characterization and the compatibility of composite PCM to cement matrix. Therefore, a complete replacement with adequate workability was considered to minimize the interference of fine aggregate with cement matrix and to clearly observe the cement-EPOP interfacial contact zone. The Chapter 5 of this thesis will study the construction applications of this form-stable PCM in cement mortars with the development of thermal energy storage cement mortars (TESCMs).

Table 4-2 Mix proportion of materials

Specimen type	Mixing proportion					20 mm thick panel
	Cement	EPOP	Sand	W/C ratio	WRA (% of cement)	PCM content (kg/m <sup>2</sup> )
TESC	0.6	0.4	-	0.6	-	2.7
NC	0.6	-	0.4	0.5	2.5	0



Fig. 4-1. TESC panels for thermal performance test (a) timber molds (b) compaction of TESC using mechanical vibration

### 4.2.3. Testing methods

#### 4.2.3.1. *Fourier transform infrared spectroscopy (FT-IR) test*

The chemical compatibility between the components in composite PCM (i.e. paraffin and EPO) was studied by acquiring the infrared spectra of paraffin, EPO and fabricated composite PCM using the FT-IR method. The procedure for obtaining the FT-IR spectra is as follows. First, powder sample and KBr were oven dried at 105°C for 24 hours to remove any moisture, and then mixed at 1:30 ratio in a controlled humidity environment (i.e. 23°C and 50% R.H). Next, the mixed sample was pressed using a hydraulic press at a controlled compression force of 10 kN and the holding duration of one minute. The obtained KBr pellet is then mounted in the sample compartment and the test was run in transmittance mode using Nicolet iS5 spectrometer from Thermo Scientific. To remove any instrumental characteristics from the spectrum, a background measurement was conducted before sample measurement was begun. This is done by running the experiment without the sample in the sample compartment. The sample measurements were performed at 32 scans per sample collected from 4000 to 525  $\text{cm}^{-1}$  at 4  $\text{cm}^{-1}$  resolution.



Fig. 4-2. Nicolet™ iS5 Spectrometer for FT-IR test

#### 4.2.3.2. *Thermo-gravimetric analysis*

The thermal stability of form-stable PCM was studied by thermogravimetric analysis (TGA) for EPOP and paraffin. TGA measurements were conducted using TGA Q500 from TA instruments. The temperature and weighing accuracy of Q500 are 1°C and 0.01% respectively. Approximately 25 mg of specimens were prepared in the ceramic sample pan and the sample pan was mounted in the pan holder of TGA instrument. During the heating process, sample pan resides in the furnace under the thermal environment controlled by a purge gas. The thermal stability or decomposition of paraffin in the composite was identified by measuring the weight loss during the heating process. The TGA measurements were conducted in the temperature range of 20-400°C at the constant heating rate of 10°C/min in nitrogen atmosphere.



Fig. 4-3. Thermo-gravimetric analysis (a) TGA apparatus (b) ceramic pan

#### 4.2.3.3. *Specific gravity and density test*

The specific gravity and density of PCM composite and silica sand were measured according to ASTM D854, where a pycnometric method was followed. The particle density of EPO and solid density of paraffin were derived as  $250 \text{ kg/m}^3$  and  $880 \text{ kg/m}^3$  from the manufacturer supplied data [163, 164]. In the pycnometric method, a water-pycnometer with glass stopper was used to determine the density and specific gravity of silica sand and PCM composite (Fig. 4-4). Initially, the empty pycnometer and glass stopper were cleansed with acetone and the empty bottle + glass stopper was weighed ( $W_1$ ) using a digital balance with the accuracy of 0.001 g. Then, a certain amount of sample was added into the pycnometer and the weight of the pycnometer was measured as  $W_2$ . This is followed by adding the water into pycnometer to the level between  $1/3$  and  $1/2$  of the depth of pycnometer and well agitated until a slurry is formed. The remaining volume of the pycnometer was filled with water and the new weight measurement was taken as  $W_3$ . Finally, the slurry in the pycnometer was removed and the pycnometer was thoroughly rinsed with water. The pycnometer was filled with water and the weight was measured as  $W_4$ . The temperature of the water was measured using a K-type thermocouple with the measurement accuracy of  $0.05^\circ\text{C}$ . The corresponding density of the water at the measured temperature ( $\rho_{w,t}$ ) was obtained from the table given in ASTM D854-14. The specific gravity ( $G_t$ ) and density ( $\rho_s$ ) of the granular materials are calculated using Eq. (4-1) and (4-2) respectively.

$$G_t = \frac{W_2 - W_1}{(W_2 - W_1) - (W_3 - W_4)} \quad (4-1)$$

$$\rho_s = G_t \times \rho_{w,t} \quad (4-2)$$



Fig. 4-4. Density bottle test (a) water pycnometer (b) sand slurry filled with water

#### 4.2.3.4. Mechanical properties and microstructural analysis of TESC

The mechanical properties of NC and TESC were studied by determining the compressive strength of cube specimens. The compressive strength test was carried out for 50 x 50 x 50 mm<sup>3</sup> cube specimens according to ASTM C109 using a Technotest automatic compression testing machine (Technotest C030/2T), as shown in Fig. 4-5. The accuracy of the compression machine is 0.1 kN. The cube specimens were first removed from water bath at the end of the testing period and allowed to drain for 30 minutes. The specimens were then subjected to compressive strength test at a loading rate of 0.5 MPa. Three samples from each mix were tested at 7 and 28 days of age and the average of three specimens was reported.

The micro-morphology characteristics of undisturbed TESC samples and compressive strength tested samples were studied using SEM. The undisturbed cement mortar samples were obtained by cutting thin slice specimen using a precision concrete cutter with diamond edge wheels as shown in Fig. 4-6. On the other hand, a small fragment of compressive strength tested specimen was utilized to study the fracture surface of the cement mortar specimens. To obtain proper positioning in SEM, the back side of the

fracture specimens were flattened by polishing the surfaces. The microstructure of the specimens was analyzed using Zeiss Supra 40VP SEM instrument under low vacuum mode at an accelerating voltage of 3 kV.



Fig. 4-5. Technotest C030/2T compressive strength testing machine

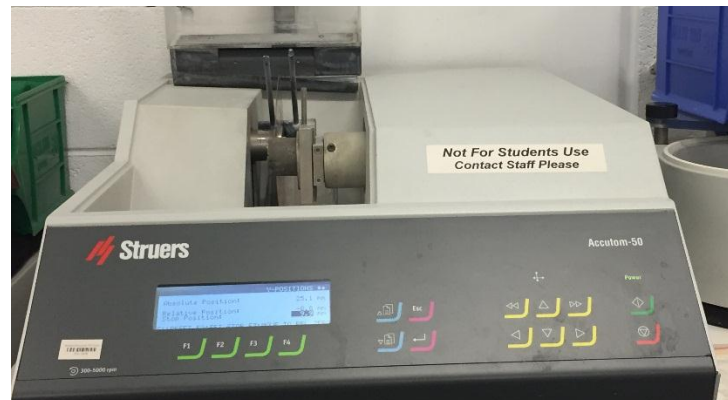


Fig. 4-6. Preparation of thin TESC specimen slice using precision diamond saw

#### 4.2.3.5. Pozzolanic reactivity analysis test

The chemical composition of EPO granules, as measured by XRF test, revealed approximately 73% of  $\text{SiO}_2$  in the EPO granules. The presence of such large  $\text{SiO}_2$  content could activate the pozzolanic reaction with portlandite in cementitious composites, thus, assisting in the bonding strength enhancement between the PCM composite and cement matrix. In order to study this phenomenon, the pozzolanic reactivity of EPO was evaluated through pH test as proposed by Yu et al. [165]. In this test, certain amount of saturated  $\text{Ca}(\text{OH})_2$  solution and EPO material were continuously stirred using a magnetic stirrer equipment and pH value of the solution was monitored during the reaction period. The ambient temperature of the solution was maintained at  $40 \pm 5$  °C using a water bath. The schematic diagram of the test setup is shown in Fig. 4-7. Initially, approximately 5.0 g of EPO material was added into a beaker containing 200 ml of  $\text{Ca}(\text{OH})_2$  solution at 40 °C and continuously agitated using a magnetic stirrer equipment. The opening of the beaker was tightly sealed to prevent carbonation induced by  $\text{CO}_2$  in air, which could cause the variation in pH measurement. The pH measurement was taken for 24 hours period using a digital pH meter.

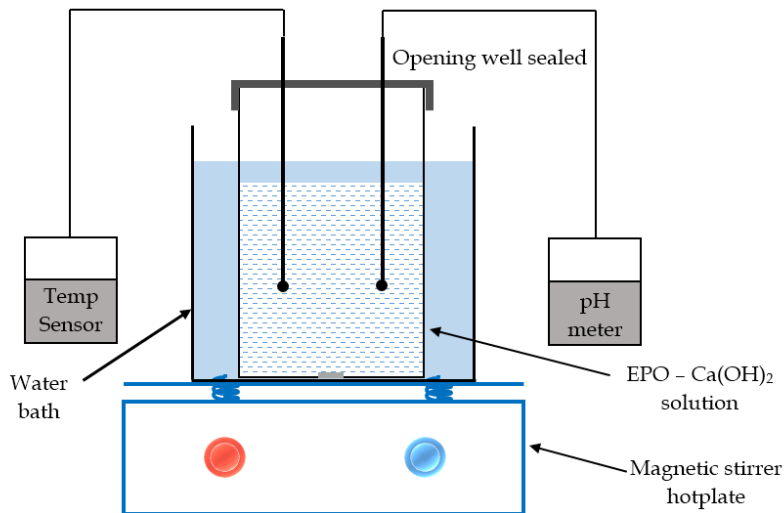


Fig. 4-7. Schematic diagram of pozzolanic reactivity test

#### 4.2.3.6. *Thermal energy storage performance assessment*

Thermal energy storage performance of TESC was evaluated by using a self-designed heat storage system. The setup consisted a small test room with the internal hollow volume of  $300 \times 300 \times 300 \text{ mm}^3$ , whose walls are made of 50 mm expanded polystyrene sheets for five surfaces and the testing panel at the top surface. The schematic diagram of the prototypes and physical arrangement of the test setup are shown in Fig. 4-8. This set up ensures that the test room is highly insulated on five surfaces and one-dimensional heat transfer would occur through the testing panel only. The test specimens having the size of  $300 \times 300 \times 20 \text{ mm}$  were fixed as the top surface of the test room. The heat flux sensors (Hukseflux, 5% accuracy) and K type temperature sensors (temperature accuracy of  $0.05^\circ\text{C}$ ) were attached on both sides of the testing panels to measure and record the temperature and heat fluxes at the interior and exterior surfaces. The test room was placed in a climate-controlled thermal chamber operated in the temperature cycles between  $15^\circ\text{C}$  and  $35^\circ\text{C}$  at a ramping rate of  $0.04^\circ\text{C}/\text{min}$ , which could also be assumed as a typical summer daily temperature variation in Australia. The temperature accuracy of the chamber was  $0.1^\circ\text{C}$ . The test room was initially kept at  $15^\circ\text{C}$  for 10 hours for the allowance of sufficient time to reach steady state conditions.

Regarding the thermal energy storage assessment, three indicators are chosen based on the heat transfer performance to indoor as shown below:

- (1) Thermal inertia ( $I$ ,  $^\circ\text{C}$ ) as measured by the temperature difference between the top ( $T_{out}$ ) and the bottom surface ( $T_{in}$ ) of the panel [Eq. (4-3)]. The larger temperature difference implies the higher thermal inertia.
- (2) Thermal energy storage rate ( $\Delta h_t$ ,  $\text{W}/\text{m}^2$ ) as measured by the difference between exterior and interior heat flux measurements as shown in Eq. (4-4)
- (3) Interior surface convective heat transfer rate ( $q_{in}$ ,  $\text{W}/\text{m}^2$ ) is the heat flow measurement from inner surface heat flux sensor. This indicator is used to study the heat transfer to indoor (inside the test room in this case), which indicates the heat addition or extraction to indoor air, thus influencing the indoor thermal comfort. The positive values of  $q_{in}$  indicates the heat is being added to the indoor air, while negative values reflect the heat is being extracted from indoor air.

$$I = T_{out} - T_{in} \quad (4-3)$$

$$\Delta h_t = \vec{Q}_{q,out} - \vec{Q}_{q,in} \quad (4-4)$$

It must be noted that the current self-designed heat storage setup investigates the thermal inertia and thermal energy storage performance as the performance indicators and would not consider the indoor temperature comparison study. This is because the current system uses PCM panel at only one surface and thus, this system would not represents the actual test room experiments. The Chapter 7 of this thesis is dedicated to study the performance of PCM panels in reducing the indoor temperature fluctuations with the aid of prototype test room and test hut experiments.

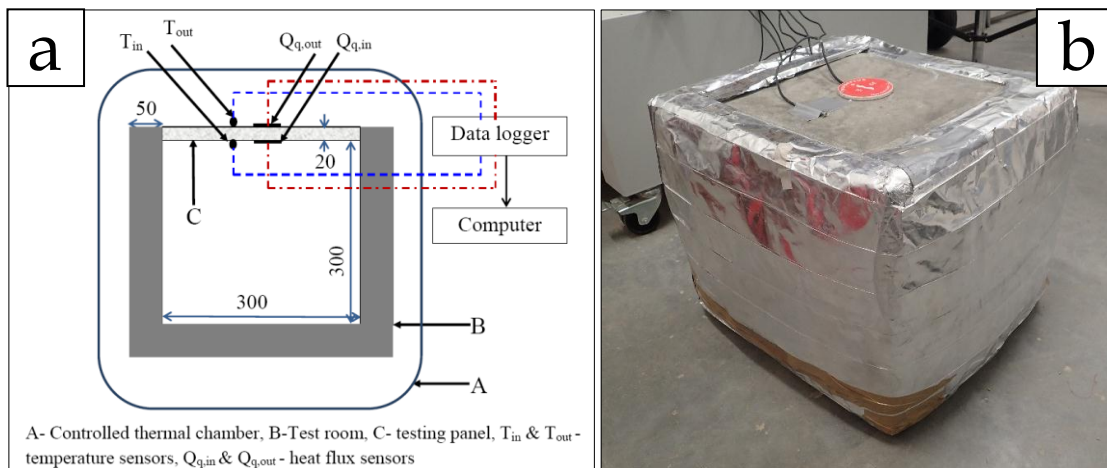


Fig. 4-8. Self-designed heat storage set up (a) schematic diagram of test setup (b) physical arrangement

### 4.3. Results and discussions

#### 4.3.1. Chemical compatibility analysis

The results of chemical compatibility between the components of PCM composite determined by FT-IR analysis are illustrated in Fig. 4-9. The corresponding absorption bands with relevant vibration mode are also summarized in Table 4-3. As shown in Fig. 4-9, paraffin has four characteristic absorption bands at 2915  $\text{cm}^{-1}$ , 2848  $\text{cm}^{-1}$ , 1466  $\text{cm}^{-1}$  and 720  $\text{cm}^{-1}$ , representing the stretching vibration of  $-\text{CH}_2$  and  $-\text{CH}_3$  (2915  $\text{cm}^{-1}$  and 2848  $\text{cm}^{-1}$ ), deformation vibration of  $-\text{CH}_2$  and  $-\text{CH}_3$  (1466  $\text{cm}^{-1}$ ) and rocking vibration of  $-\text{CH}_2$  (720  $\text{cm}^{-1}$ ) respectively. EPO has the characteristic absorption band at 791  $\text{cm}^{-1}$  and 1007  $\text{cm}^{-1}$ , which represents the bending vibration of SiO-H and asymmetry stretching vibration of Si-O-Si. Moreover, all the characteristic absorption bands observed in paraffin and EPO also appear in the composite PCM spectra without any additional peaks. This indicates that there is no chemical interaction between the EPO and paraffin during the absorption of paraffin into the pores of EPO, and the fabrication of composite PCM can be characterized as physical absorption. Therefore, the FT-IR results show good chemical compatibility between paraffin and EPO in the developed form-stable PCM composite.

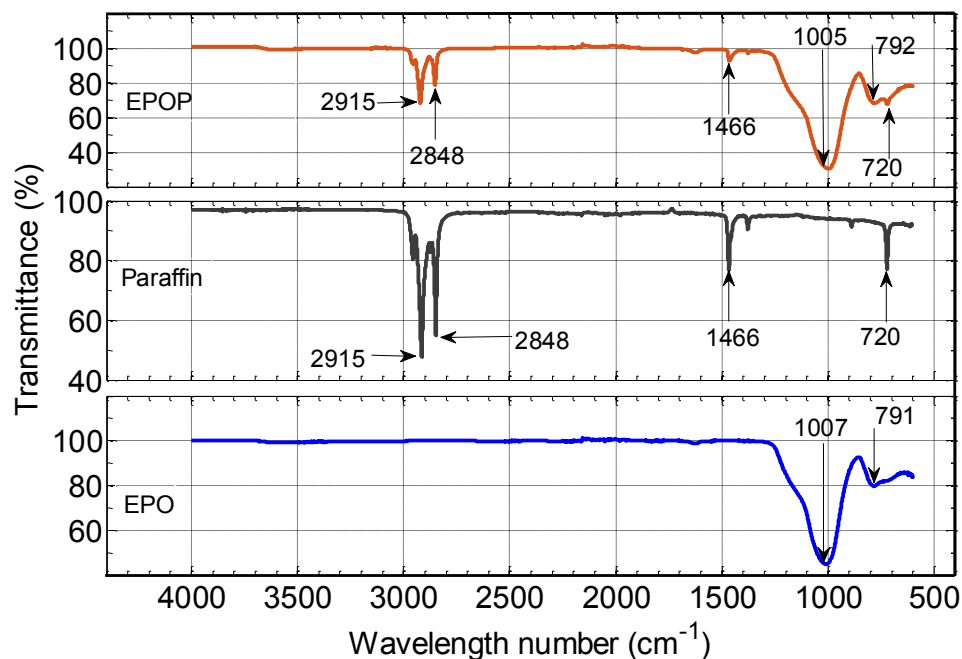


Fig. 4-9. FT-IR spectra of paraffin, EPO and EPOP

Table 4-3 FT-IR absorption bands and relevant assignments for EPO, paraffin, and  
EPOP

Specimen	-CH <sub>2</sub>	SiO-H	Si-O-Si	-CH <sub>2</sub> and -CH <sub>3</sub>		
EPO	-	791	1007	-	-	-
Paraffin	720			1466	2848	2915
EPOP	720	792	1005	1466	2848	2915

#### 4.3.2. Thermal stability of form-stable PCM

The thermal stability of EPOP form-stable PCM, as measured by the weight loss during the heating process, is shown in Fig. 4-10. As shown in the figure, the weight loss for both paraffin and EPOP form-stable PCM are beginning at approximately 150°C, indicating the absence of decomposition within 150°C. After that temperature, weight loss occurs in paraffin and EPOP until 271.5°C and 216.5°C respectively, and thereafter the sample weights remain constant. The observed clear weight losses are due to paraffin evaporation and the earlier occurrence of weight loss in EPOP can be attributed to the physical interaction between the paraffin and the inner surface of porous EPO, and the confinement of paraffin in very small pores [70]. Furthermore, the total weight loss of paraffin in the composite PCM was measured as 50.1%, which is quite close to the absorption amount of PCM in the composite. These results suggest the uniform distribution of paraffin in the form-stable PCM and this composite can be considered as thermally stable within its operative temperature range.

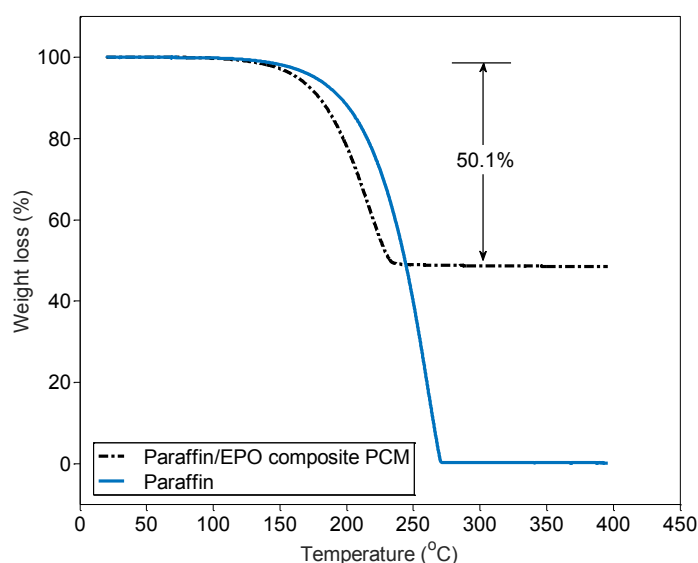


Fig. 4-10. TGA curves of paraffin and EPOP

### 4.3.3. Specific gravity and density of granular materials

The physical properties of PCM composite and silica sand, as measured by specific gravity and density are given in Table 4-4. The Table 4-4 shows that the composite PCM has very low density of 540 kg/m<sup>3</sup>, compared to the silica sand aggregate which has 2616 kg/m<sup>3</sup>. Such low density of PCM composite can be explained by the lightweight properties of EPO used to fabricate the composite PCM. Furthermore, paraffin also has the density of 880 kg/m<sup>3</sup>, which is also very low compared to silica sand. This has resulted in a low density of fabricated form-stable PCM.

Table 4-4 Specific gravity and density of fine aggregates

Specimen	Specific gravity	Density (kg/m <sup>3</sup> )
Silica sand	2.62	2616.07
Composite PCM	0.54	539.19

### 4.3.4. Mechanical properties and microstructural analysis of TESC

The summary of the compressive strength results at 7 and 28 days aged NC and TESC specimens are given in Table 4-5. The Table 4-5 indicates that the incorporation of form-stable PCM into cementitious composites significantly reduces the compressive strength of produced TESC. Considering 28-days compressive strength as an example, NC

achieved a compressive strength of 44.84 N/mm<sup>2</sup>, whereas TESC only achieved that of 8.24 N/mm<sup>2</sup>. This is approximately 81% reduction of compressive strength in TESC compared to the NC prepared for similar mix proportion. A similar mechanical behaviour was also reported for hydrophobic surface modified commercial form-stable PCM (PX25 from Rubitherm®) integrated cementitious composites with slightly different mix proportions by Li et al. [6] and their results are also presented in Table 4-5. It can be seen that the compressive strength values achieved in this study are quite close to the results from previous study, which suggests that this laboratory made form-stable PCM composite can well replaces commercial grade PCM with ease in fabrication.

The reduction in compressive strength with the replacement of PCM composite could be attributed to the soft and low strength EPOP aggregates compared to silica sand aggregates. It is also observed a large difference in the volume of NC and TESC when following a weight based mix design method. This is due to the low density of EPOP aggregates compared to silica sand and this resulted in reduced amount of binder content (cement binder in this case) for certain volume of mortar mix in TESC. Therefore, the weight based mix design would not be appropriate for the comparison of mechanical properties of PCM integrated cementitious composites due to the significant variation in density of materials. Furthermore, a volume based mix design could be considered as such mix design uses the same volume of PCM composite or fine aggregate, resulting in same binder content in produced cement mortars.

The microstructural analysis was conducted on the untested surface of TESC and fracture surface of compressive strength tested TESC. Fig. 4-11 and Fig. 4-12 show the SEM image of untested specimen surface and fracture surface of compressive strength tested specimen respectively. As can be seen from Fig. 4-11, the spherical composite PCMs are clearly visible in the SEM images indicating that the composite PCMs have neither been damaged nor destroyed when following the standard mixing procedure. It was also noted that the composite PCMs were effectively holding the PCM in the pores and they are evenly distributed in the cement matrix, indicating a good compatibility of composite PCM with cement matrix. Moreover, the SEM image of fracture surface in compressive strength tested specimen showed partially broken composites on the fracture surface of TESC. This indicates that the failure occurred due to very low shear strength and stiffness of PCM composites. Nevertheless, the form-stable PCM was well

bonded with cement matrix even after failure due to the irregular bubble-like structure of EPO granules. It can be concluded, therefore, the developed form-stable PCM can be considered as highly compatible with cement matrix and following appropriate mix design (i.e. volume based mix design) procedure would lead to the development of TESC with acceptable mechanical properties.

Table 4-5 Compressive strength of TESC at 7 and 28 days

Specimen	Compressive strength (N/mm <sup>2</sup> )		Average compressive strength (N/mm <sup>2</sup> )	
	7 day	28 day	7 day	28 day
NC	35.30	42.31		
	40.51	46.37	37.3	44.84
	36.09	45.84		
TESC	5.85	9.54		
	6.06	7.32	5.6	8.24
	4.89	7.85		
PX PCM /cement (Li et al. [6])			3.62	7.16

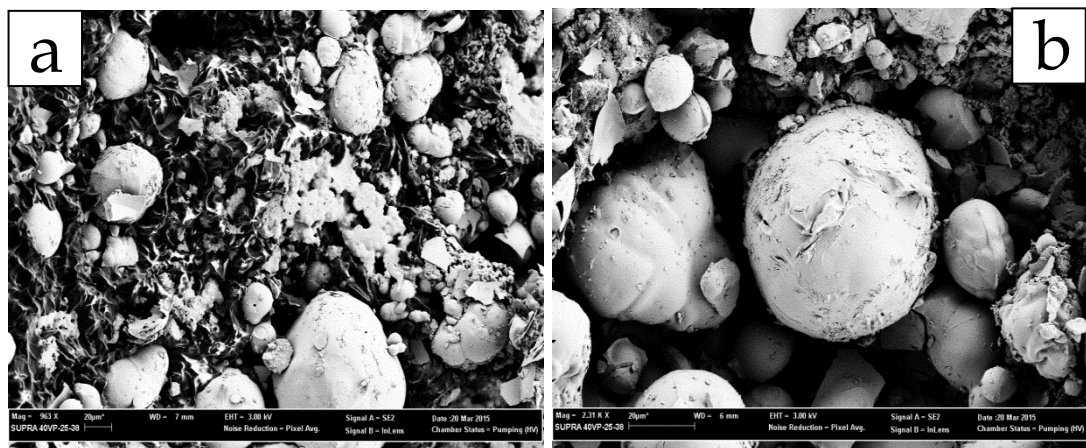


Fig. 4-11. SEM images of TESC (a) distribution of EPOP in cement matrix (b) a single EPOP composite

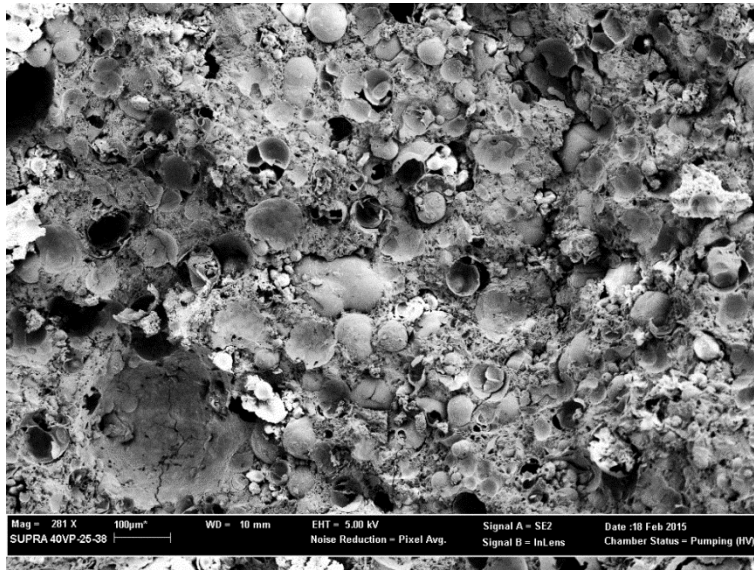


Fig. 4-12. SEM image of the fracture surface of cement/ EPOP paste

#### 4.3.5. Pozzolanic reactivity of EPO granules

The pozzolanic activity induced by EPO granules in the presence of saturated  $\text{Ca(OH)}_2$  solution, as measured by the pH value of the solution, is presented in Fig. 4-13. As shown in figure, the pH value of EPO- $\text{Ca(OH)}_2$  suspension solution remains approximately same throughout the test period. During the test period of 24 hours, the maximum reduction in the pH value was observed as 0.22 and such smaller reductions could be due to very slow reaction between EPO and  $\text{Ca(OH)}_2$  and the carbonation induced by air trapped in the beaker. Therefore, it can be concluded that the EPO granules have very low pozzolanic reactivity with  $\text{Ca(OH)}_2$  solution and they would not be able to stimulate a secondary hydration reaction in cement matrix. The primary reason for such low pozzolanic reactivity, even at the presence of high levels of  $\text{SiO}_2$ , could be due to the hydrophobic surface modification of the EPO granules, which again prevents the contact of amorphous  $\text{SiO}_2$  with  $\text{Ca(OH)}_2$  solution.

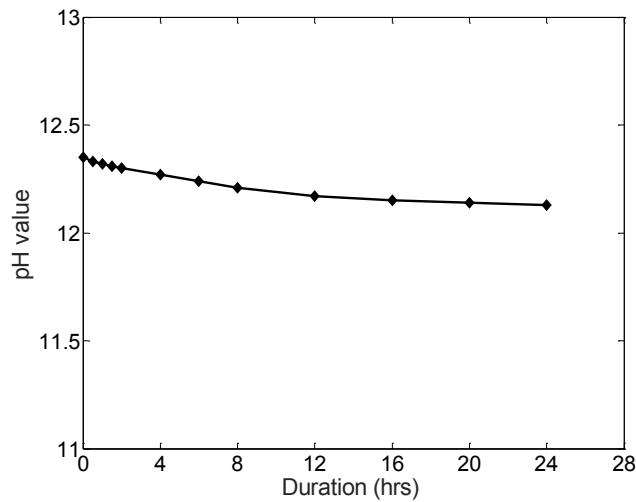


Fig. 4-13. pH variation trend of EPO- $\text{Ca(OH)}_2$  solution with time

#### 4.3.6. Thermal energy storage performance of TESC

The thermal storage performance of TESC as measured by thermal inertia, thermal energy storage rate and inner surface heat transfer rate are depicted in Fig. 4-14, Fig. 4-15 and Fig. 4-16 respectively. A significant enhancement in thermal inertia can be observed from the temperature difference between interior and exterior surfaces of the test panel as illustrated in Fig. 4-14. The maximum temperature difference between exterior and interior surface temperatures of the PCM panel were recorded as  $5.5^\circ\text{C}$  and  $4.5^\circ\text{C}$  during heating and cooling processes respectively, compared  $2.2^\circ\text{C}$  and  $2.1^\circ\text{C}$  in NC test room. The significant enhancement in thermal inertia attributed to the incorporation of PCM into cementitious composites, resulting in increased thermal energy storage and discharge. Besides, it should also be noted that the TESC panel has low thermal conductivity compared to ordinary cementitious composites, as EPO and paraffin have low thermal conductivities compared to other components in cementitious composites. Therefore, low thermal conductivity of TESC can be contributed to increasing the thermal resistance, leading to increased thermal inertia.

In order to clearly distinguish the thermal energy storage enhancement of form-stable PCM in TESC, thermal energy storage behavior of NC and TESC panels were plotted in Fig. 4-15. The comparison of heat storage behavior of NC and TESC panels evident a significant heat storage enhancement when EPOP integrated into cementitious composites. For instance, heat storage behavior of NC panel (Fig. 4-15) indicates that the

heat storage rate initially increases and reaches a constant value as per its specific heat capacity. The heat storage rate remained constant thereafter due to constant heat capacity and constant temperature ramp. Similar behavior can also be seen during the cooling process, where heat release rate follows a constant value as per its specific heat capacity. In the TESC panel, thermal energy storage rate showed approximately similar behavior to NC panel until the outdoor temperature reaches 21°C, due to the similar thermophysical behavior of both panels up to this temperature. However, the thermal energy storage behavior in this panel significantly increased when the temperature goes above 21°C. This reveals the latent heat storage of PCM in TESC, leading to very high heat storage rate compared to NC panel. As the temperature further increases, the thermal energy storage rate remained constant at peak value as part of the PCM content was still in operation. The maximum heat storage rate in TESC panel was recorded as 200 W/m<sup>2</sup> compared to 105 W/m<sup>2</sup> in NC panel, which is approximately 90% enhancement of thermal energy storage rate. Similar behavior was also observed during the heat release stage or cooling process.

The internal heat flux measurements were recorded to study the heat transfer to 'indoor' (i.e. inside the test room), which influences indoor thermal comfort. The convective heat transfer behaviour of inner surfaces, as depicted in Fig. 4-16, showed continuously increasing heat transfer rate in the NC panel until the outdoor air temperature reaches the maximum value. Afterward, the outdoor air temperature remained constant, leading to the reduction in internal heat transfer rate as the test panel reached its steady state conditions. The test room built with TESC panel, however, showed a different behavior in internal heat transfer rate by showing multiple peaks during the thermal energy storage process. In fact, there were two peaks observed during the heating process. As the outdoor temperature initially increases, internal heat flux has increased reaching the first peak and then began to decline. It can be assumed that the PCM in the TESC panel has begun to melt at this stage. The heat flux then increased as most of the PCM had melted completely, and reached the second peak internal heat flux and then reduces due to constant outdoor temperature. The ultimate peak internal heat flux recorded was about 52 W/m<sup>2</sup> (a 37% reduction compared to NC panel) with an attenuation of approximately 30 minutes.

On the other hand, the heat release process of test panels with the reduction in outdoor temperature can be explained as follows. As the outdoor temperature reduces, the NC panel showed continuously increasing negative heat flux measurement from the inner surface. This attributes to the thermal gradient from inner surface to the exterior surface of the panel (heat flow from indoor to outdoor). However, PCM panel showed a different behavior during the cooling process. Indeed, thermal gradient due to lower temperature of the exterior surface of TESC panel causes heat flow from interior surface to outdoor. At the same time, the discharge of stored latent heat energy of PCM induces heat flow from inner surface to indoor. This combined behavior can be identified from Fig. 4-16, where the heat flux measurements initially show increasing negative heat flow due to the thermal gradient from indoor to outdoor. When the outdoor temperature becomes 24°C, the negative heat flux reduces and reaches a peak value as the PCM begun to solidify at this stage. Thereafter, heat flux measurement starts to increase in negative heat flux as the PCM solidified completely. The identical heat flux behavior can be observed during the second thermal cycle as well. This shows that the fluctuations in inner surface heat flux measurements can be significantly reduced with the integration of form-stable PCM into cementitious composites, thus improving the indoor thermal comfort.

According to this study, the thermal inertia and thermal energy storage performance of the cementitious composites have been significantly improved with the incorporation of form-stable EPOP PCM composites. However, it should be stressed that the small sized test room experiments conducted in this study would not accurately reflect the thermal performance enhancement of buildings integrated with PCMs due to significantly high scaled-down. Following chapters will discuss the thermal performance of the PCM integrated cementitious composites in buildings with the aid of experimental and numerical analysis.

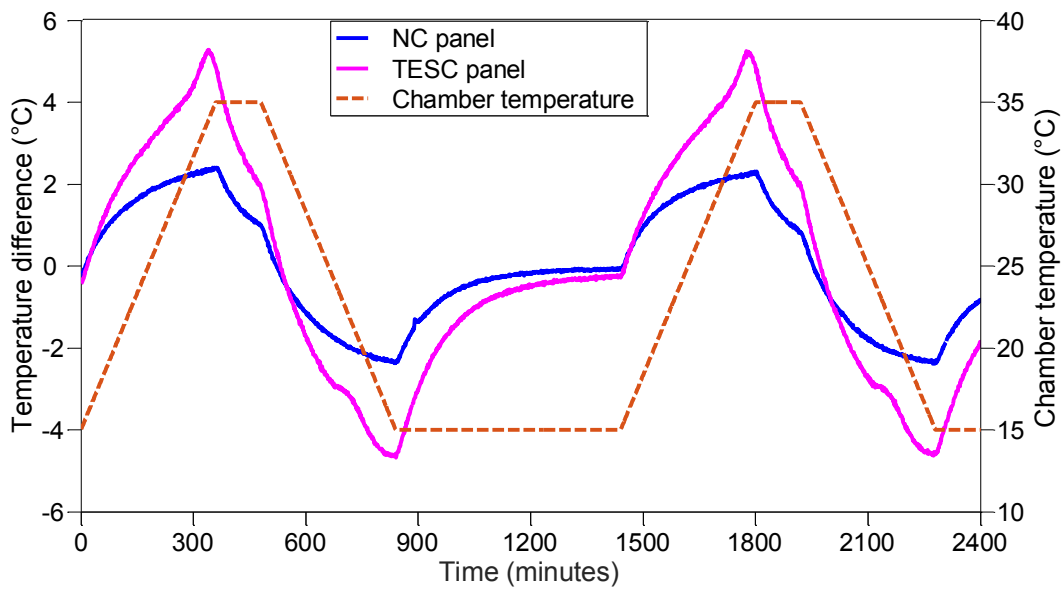


Fig. 4-14. Thermal inertia variation of NC and TESC

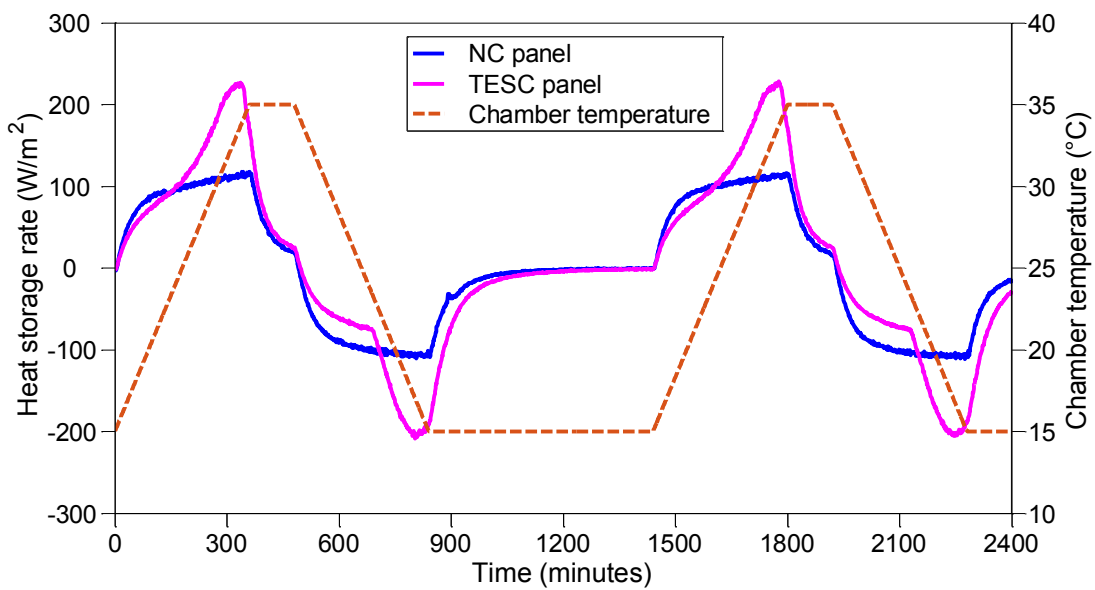


Fig. 4-15. Thermal energy storage rate of NC and TESC

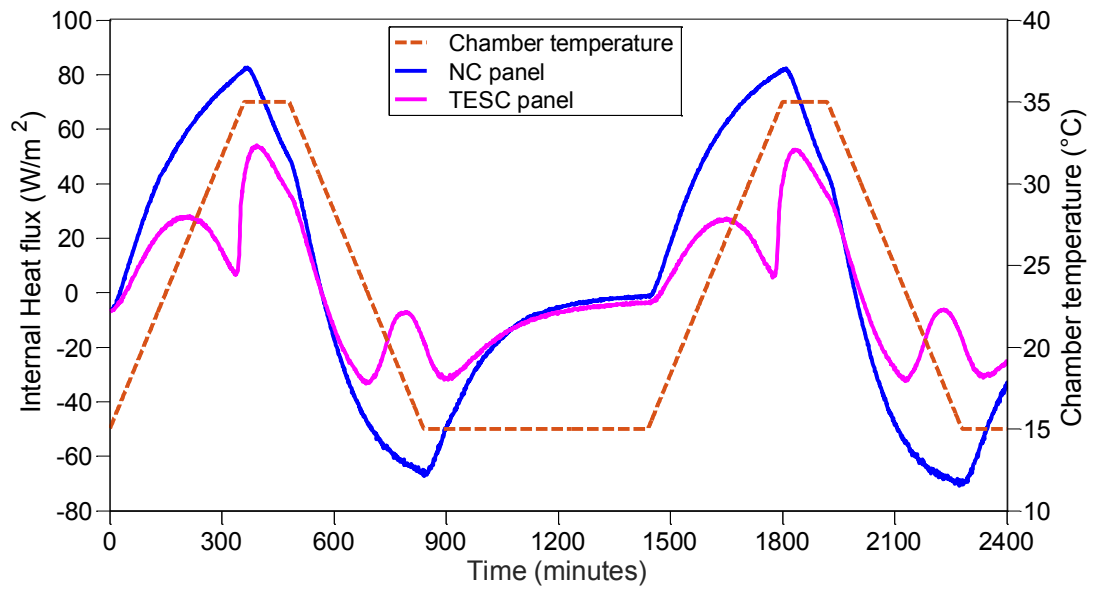


Fig. 4-16. Interior surface heat transfer behavior of NC and TESC

#### 4.4. Concluding remarks

This chapter reported the characterization of form-stable EPOP composite and the integration of such PCM composite into cementitious composites for the development of TESCs. The form-stable PCM composite was first characterized for chemical compatibility, thermal stability, and its physical properties. This was followed by the development of TESC and studying the mechanical properties, microstructural characterization, and thermal storage performance compared to control cementitious composites (NC). Based on the experimental works presented, the following conclusions can be drawn:

1. The chemical compatibility between the components of form-stable PCM analyzed by FT-IR test showed that the paraffin and EPO are chemically compatible and the absorption of paraffin into the pores of EPO would be characterized as physical absorption without any chemical interaction between the components of form-stable PCM.
2. The TGA analysis showed that this form-stable PCM is thermally stable within the operational temperature range and there are no signs of decomposition up to the temperature of 220°C.
3. The micromorphology characterization of TESC showed that the PCM composite is highly compatible with cement matrix and minimal destruction to composites was observed in the cement matrix. Furthermore, a good bonding characteristic between PCM composite and cement matrix was observed due to the irregular bubble structure of porous EPO.
4. The mechanical properties of TESC reduced significantly compared to NC, due to the soft and low strength of EPOP. Furthermore, following a weight based mix design lead to reduced binder content in TESC, which further exacerbates the loss of compressive strength. Therefore, a volume based mix design was recommended when developing TESCs.
5. The thermal performance assessment showed that the TESC significantly increases the thermal inertia and thermal energy storage rate of cementitious composites. At the same time, the interior surface heat transfer rates were largely reduced, indicating that the indoor thermal comfort would be improved with the application of such TESC in buildings.

# Chapter 5 Development of thermal energy storage cement mortars containing form-stable PCM composite

---

## 5.1 Introduction

In the previous chapter, the effect of paraffin/hydrophobic EP (EPOP) form-stable PCM in cementitious composites was discussed with the development of TESC. It was revealed that this novel form-stable PCM is highly compatible with cement matrix and shows very minimal destruction or damage to the composites when following a standard mixing method. Furthermore, the TESC showed significantly improved thermal inertia and thermal energy storage capacity, which will eventually lead to improving the indoor thermal comfort and energy efficiency when such TESCs are incorporated into buildings.

However, cementitious composites fabricated by mixing PCM composite with cement have limited applications in construction industry and they are commonly used with cement mortars and concrete in buildings. In particular, cement mortar prepared by mixing cement, sand, and water has great application in construction industry and incorporation of PCM into cement mortar would be regarded as an effective method for significant energy savings in buildings. The so-called thermal energy storage cement mortars (TESCMs), by integrating form-stable PCM into ordinary cement mortar, can be considered as an energy efficient cement mortar product for interior and exterior plastering mortar applications in buildings. Here, TESCM refers to conventional cement mortars containing form-stable EPOP and which differs from the TESC fabricated by mixing PCM composite with cement paste in the previous chapters.

An evaluation of the physical, mechanical and thermal properties of cement mortars containing EPOP is essential when developing TESCMs. Although the integration of form-stable PCM into cement mortars could lead to enhanced thermal performance due to large energy storage capacity, undesired adverse effects on the mechanical and durability properties have been reported. This is because of cement is being as the main strength gaining component in cement mortars and integration of soft and low strength form-stable PCMs lead to reduced mechanical properties. Furthermore, following a weight based mix design method also affects the strength development due to large volume contribution of composite PCM and subsequently causing reduced binder content. Hence, a detailed experimental program for the development of TESCMs with different replacement levels of PCM composite was carried out in this chapter. A volume based mix design method, by partially replacing the fine aggregate with form-stable PCM, was carried out to prevent the effect of significant variation in density of materials, as discussed in chapter 4.

TESCMs also need to be mechanically and thermally reliable over a long period of operation. That is, the TESCM should show little or no degradation in mechanical and thermal performance after exposed to multiple thermal cycles. The mechanical reliability of TESCM needed to be evaluated because the volume change of PCM during the phase transition process can generate internal stresses, which can degrade composites and hence reducing the mechanical properties over the long term. Similarly, the thermal reliability of TESCM also important as the PCM encapsulated in the porous supporting materials could be deteriorated and reducing the thermal capacity over time.

This chapter investigates the effects on physical, mechanical and thermal properties of TESCMs developed by integrating EPOP form-stable PCM into ordinary cement mortars at different replacement levels. This chapter also encompasses the evaluation TES performance of TESCMs with the aid of self-designed heat storage test. Finally, the mechanical and thermal reliability of TESCMs were studied by subjecting specimens to 3000 accelerated thermal cycles in a climate controlled thermal chamber and investigating the mechanical and thermophysical properties variation after 3000 thermal cycles. As a whole, this chapter contributes to the development of an appropriate and economical way of TES application in buildings with the characterization of its engineering properties necessary for building application of such form-stable PCMs.

## 5.2 Materials and Methods

### 5.2.1. Materials

The paraffin with the melting temperature of 27°C (RT27) and hydrophobic expanded perlite (EPO) were used to fabricate composite PCM. OPC complying with AS 3972 and silica sand with maximum particle size of 1.18 mm were used as aggregates in OCM and TESCM. A commercial grade water reducing admixture (MasterPozzolith 370 from BASF) was used to improve the workability of TESCMs.

### 5.2.2. Fabrication of TESCMs

In accordance with ASTM C109 [166], OCM was prepared by mixing OPC, silica sand and water in which the mass ratio of sand to the cement was 2.75, and the water to cement ratio was 0.485. TESCMs were prepared by partially substituting fine aggregate with form-stable PCM by a volume replacement method, with the replacement levels of 20%, 40%, 60% and 80% of the volume of fine aggregate. Here, the PCM composite contains 50wt% of paraffin and fabrication process of PCM composite was followed as described in Chapter 4. The mix design of materials is given in Table 2. The workability of mortar specimens was measured using a flow table method in accordance with ASTM C230/C230M [167]. The flow diameter of fresh mortars after 20 shakes of the table was measured as shown in Fig. 5-1, and kept at  $110 \pm 10$  mm by adjusting the water-reducing admixture (WRA) content.

The mixing procedure was as follows. First, cement, sand and PCM composite were dry mixed at low speed for 1 minute in a horizontal pan mixer (a Hobart mixer). After the dry materials had been uniformly mixed, water together with admixture was added and mixed for 3 minutes at low speed. The medium speed mixing was followed for one minute to complete the mixing procedure. Fresh mixes were cast in  $50 \times 50 \times 50$  mm<sup>3</sup> steel cubic molds, and  $300 \times 300 \times 20$  mm<sup>3</sup> timber panel molds and kept in a moist environment for about 24 hours. After 24 hours, specimens were demoulded and kept in a water-bath at  $23 \pm 0.5$ °C until the test date.

Table 5-1 Mix design of materials

Mix designation	Cement (kg/m <sup>3</sup> )	Water (kg/m <sup>3</sup> )	Silica sand (kg/m <sup>3</sup> )	PCM Composite (kg/m <sup>3</sup> )	WRA (kg/m <sup>3</sup> )	Flowability (mm)
OCM	525	255	1445	0	0	
TESCM-20	525	255	1156	61	0	
TESCM-40	525	255	867	122	2.6	110±10
TESCM-60	525	255	578	183	7.9	
TESCM-80	525	255	289	244	13.1	

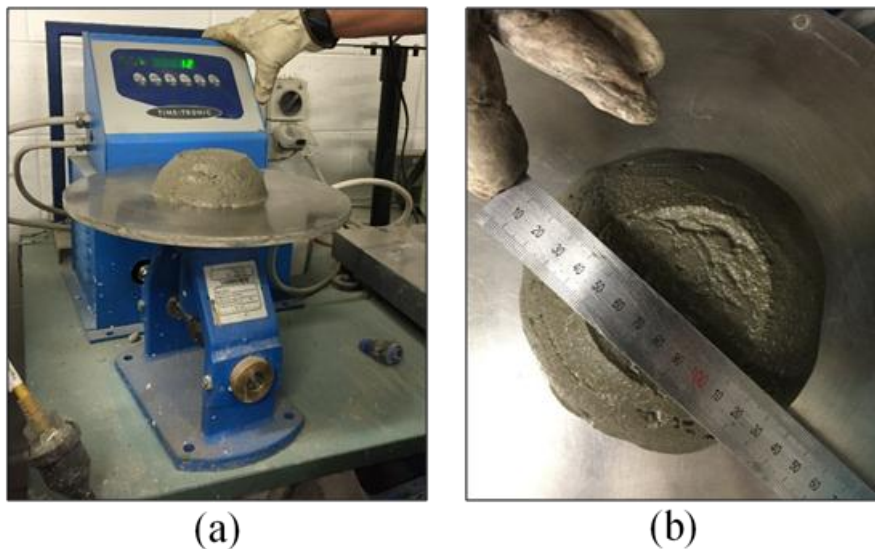


Fig. 5-1. Flow table test (a) flow table apparatus (b) flow measurement of TESCM-60

### 5.2.3. Testing methods

#### 5.2.3.1. Physical properties test

The physical properties of the OCM and TESCMs were evaluated by measuring the bulk density and apparent porosity of cube specimens in accordance with ASTM C830 [143]. The 28-days aged cube specimens were removed from the water bath and oven dried at 105°C until they reached a constant weight of D. Then the oven dried specimens were water saturated by means of a vacuum pressure vessel as shown in Fig. 5-2(a). In this process, specimens were initially placed in the vacuum chamber and vacuumed for

about 30 minutes to remove the air in the pores. Then water was supplied into the vacuum chamber and allowed to saturate the specimens at very low-pressure condition. Having kept for about one hour, the pressure in the vessel was gradually allowed to reach the atmospheric pressure and then saturated specimens were removed. Following the water saturation process, suspended weight (S) and saturated weight (W) were measured. All the measurements were conducted using a digital balance with the accuracy of 0.01 g. The bulk density (B) and apparent porosity (P) of the specimen was determined as follows:

$$B, \text{kg} / \text{m}^3 = \frac{D}{W - S} \quad (5-1)$$

$$P, \% = \left[ \frac{(W - D)}{(W - S)} \right] \times 100 \quad (5-2)$$

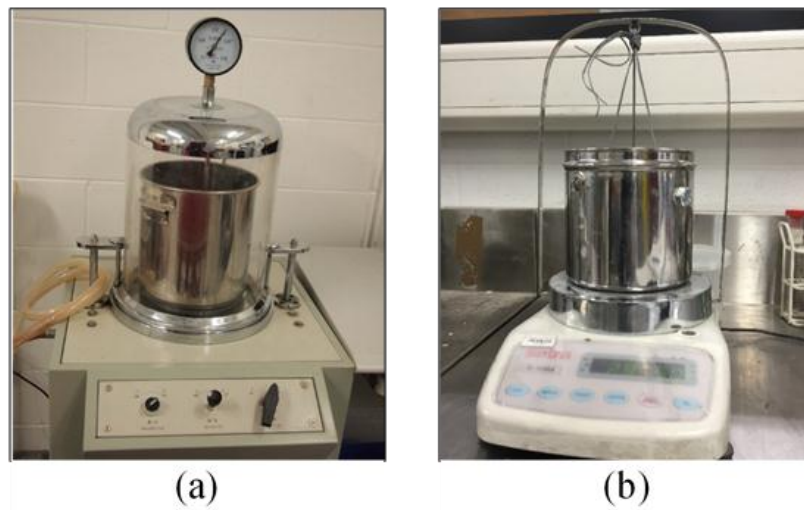


Fig. 5-2. Apparent porosity test (a) vacuum pressure vessel (b) digital balance

#### 5.2.3.2. *Drying shrinkage test*

In accordance with ASTM C596-09 [168], drying shrinkage of TESCM specimens was determined by measuring the length reduction of prismatic specimens caused by any factor other than externally applied forces under stated conditions of temperature and humidity environment. For this test, specimens with the dimensions of 25 x 25 x 285 mm were cast in steel molds and kept in a moist environment for 24 hours. After 24 hours, specimens were demoulded and initial length ( $l_0$ ) were measured. Then, the specimens were cured in a room with temperature and relative humidity of  $23 \pm 0.5^\circ\text{C}$  and  $50 \pm 5\%$  respectively for 55 days. Specimen lengths were periodically measured by a length

comparator with the accuracy of 0.001 mm. Specimen drying shrinkage strain at the  $i^{\text{th}}$  age ( $\varepsilon_i$ ) was then calculated as follows:

$$\varepsilon_i = \frac{l_i - l_o}{l_o} \quad (5-3)$$

where  $l_o$  is the initial specimen length in mm;  $l_i$  is the specimen length measured on the  $i^{\text{th}}$  testing day in mm.

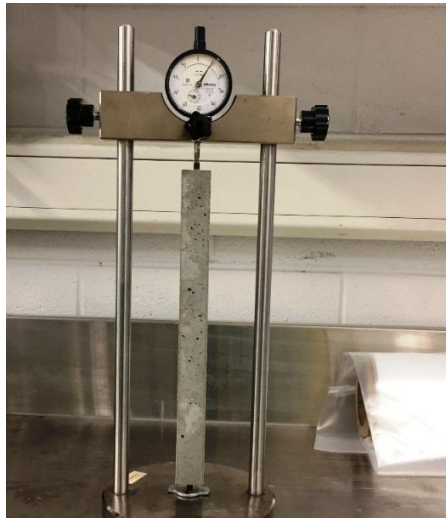


Fig. 5-3. Drying shrinkage measurement with length comparator

### 5.2.3.3. *Mechanical properties and microstructural analysis of TESCM*

The mechanical properties of TESCMs were evaluated by measuring the compressive strength of  $50 \times 50 \times 50 \text{ mm}^3$  prismatic specimens at 7 and 28 days. Compressive strength tests were performed using an automated compression-testing machine (Technotest C030/2T) at a loading rate of 0.5 MPa/s. The maximum capacity and accuracy of the compression machine is 300 kN and 0.01 kN respectively.

The microstructure characterization of TESCM was observed using a scanning electron microscopy (SEM, ZEISS Supra 40 VP). For this test, untested TESCM-60 specimen at the age of 28-days was used to observe the distribution and compatibility of composite PCM in cement mortar. The SEM test was performed under low vacuum mode at an accelerated voltage and working distance of 5kV and 6 mm respectively. Furthermore, to investigate the interfacial zone of EPOP form-stable PCM and cement matrix, the untested TESCM-60 specimen was cut into 5 mm thick slices using a precision diamond

saw. Then the samples were polished with #400 and #1200 fineness papers. Finally, polished specimens were subjected to vacuum drying and gold coating to clearly observe the interfacial zone of composite PCM to cement mortar.

#### 5.2.3.4. *Thermal conductivity of TESCMs*

The thermal conductivity of mortar specimens containing EPOP form-stable PCM composite was measured using a C-Therm TCi thermal conductivity analyzer. The TCi analyzer can measure the thermal conductivity and emissivity of small specimens based on modified transient plane heat source method. In this method, C-Therm TCi analyzer applies a unidirectional heat pulse on the specimen surface from the spiral heating element attached to the sensor. This results in an increase in the temperature of the interface between the sensor and specimen, which induces a voltage drop of the sensor element. The rate of sensor voltage drop is used to determine the thermal properties of the specimens. The results are displayed on the system's software interface by comparing the sensor response to the factory calibration.

The specimens for the thermal conductivity test were cast at 25 mm x 50 mm ( $\phi \times h$ ) cylindrical specimens and then cutting them to 10 mm thick slices using a precision diamond cutter as depicted in Fig. 5-4. The specimen surface was then polished with a sander to provide a good contact surface between sensor and specimen. A thin layer of Wakefield 120 thermal grease compound was applied on the surface of the specimen to improve the thermal contact resistance of the surface and to eliminate the impact of surface unevenness and pores. Specimens were then mounted on the TCi sensor and sample measurements were conducted. Before the sample measurements, thermal conductivity analyzer was calibrated using Pyrex block (for the calibration of thermal conductivity range of 0.13-1.2 W/(m.K)) and pyroceram block (for the calibration of thermal conductivity range of 1.1-29 W/(m.K)) that are supplied by the manufacturer. It must be noted that all sample measurements were conducted in the ambient environment of 10°C (using a thermal chamber) to eliminate the effects of latent thermal energy generated during phase transition process at room temperature.

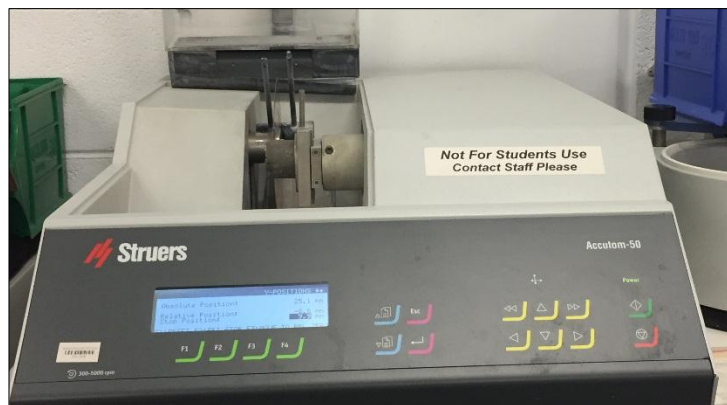


Fig. 5-4. Precision diamond cutting saw

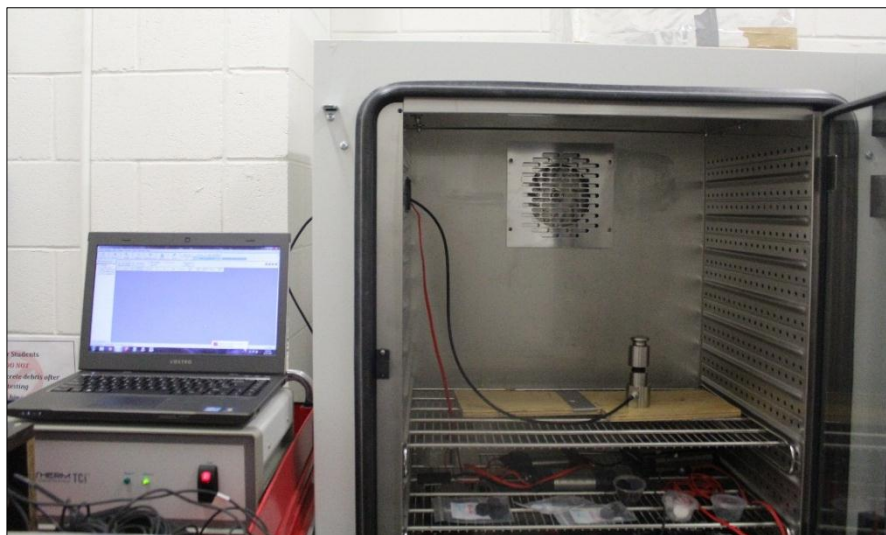


Fig. 5-5. Thermal conductivity test with the specimens kept at 10°C in thermal chamber

#### 5.2.3.5. *Thermal energy storage test*

The thermal energy storage performance of TESCMs was evaluated by using a self-designed heat storage set-up described in Chapter 4, in which the 300 x 300 x 300 mm sized test room mainly consists of 50 mm expanded polystyrene for five surfaces and the TESCM panel as the top surface was constructed. The heat flux sensors (Hukseflux, 5% accuracy) and K-type temperature sensors (temperature accuracy of 0.05°C) were also attached on both sides of the TESCM panel as shown in Fig. 4-8. The test room was subjected to summer design day temperature variation of 15 to 35 to 15°C at a ramping rate of 0.04°C/min. Thermal inertia, as demonstrated by the temperature difference between the top and bottom surfaces of the panel, and thermal energy storage capacity

of the TESC panels were monitored during the thermal cycles. Here, thermal inertia (I) and thermal energy storage capacity (H) were evaluated as follows:

$$I = T_{out} - T_{in} \quad (5-4)$$

$$\Delta h_t = \bar{Q}_{q,out} - \bar{Q}_{q,in} \quad (5-5)$$

$$H = \int_0^t \Delta h_t dt \quad (5-6)$$

where  $T_{in}$  and  $T_{out}$  are interior and exterior surface temperatures of the panel.  $Q_{q,in}$  and  $Q_{q,out}$  are heat flux measurements of the interior and exterior surfaces of the test panel.  $I$ ,  $\Delta h_t$  and  $H$  are thermal inertia, thermal energy storage rate and thermal energy storage capacity of the panel respectively.

#### 5.2.3.6. Mechanical and thermal reliability of TESCM under accelerated thermal cycles

The mechanical and thermal reliability of TESCMs were investigated by following the methodology suggested by Memon et al. [87] and Cui et al. [83], where the mechanical and thermal degradation of TESCM specimens were evaluated by subjecting them to accelerated thermal cycles. This was performed by keeping the TESCM specimens in the temperature and humidity controlled climate chamber and measuring the performance after multiple thermal cycles. The temperature program used for a single thermal cycle with the duration of 4 h was as follows:

Table 5-2 Temperature program for accelerated thermal cycles

Step 1	Temperature ramp from 10 °C to 40°C at the rate of 0.4°C/min
Step 2	Temperature kept at 40°C for 45 minutes
Step 3	Temperature ramp from 40 °C to 10°C at a rate of 0.4°C/min
Step 4	Temperature kept at 10°C for 45 minutes

The mechanical reliability of the TESCM specimens was evaluated by determining the variation in compressive strength between specimens subjected to accelerated thermal cycles and the specimens exposed to the ambient environment. Initially, 28-days aged cube specimens were removed from water bath and divided into two groups. One group of specimens was kept in the thermal chamber while the other group was kept in the ambient environment. After being kept in those conditions for 500 days (representing 3000 accelerated thermal cycles), the specimens were tested for compressive strength test using a similar testing configuration to that described in section 5.2.3.3.

The thermal reliability of TESCMs was evaluated with respect to the variation in thermophysical properties of TESCM specimens (i.e. phase transition temperature and latent heat capacity) before and after subjected to accelerated thermal cycles. This was performed by carrying out the DSC test for 28 days aged TESCM specimens (TESCM-60 and TESCM-80) and then keeping the samples in the climate controlled thermal chamber under the thermal cycle conditions described above. For this test, specimens were prepared by crushing cubes into a coarse powder and containing them in steel containers to facilitate high heat transfer rate to TESCMs. The DSC test was again carried out after 1000 and 3000 thermal cycles to evaluate the thermal degradation when subjected to accelerated thermal cycles. The test was conducted using a heat flux DSC (DSC Q1000 from TA Instruments) over the temperature range of 0 to 60°C at a temperature ramping rate of 5°C/min in Nitrogen (N<sub>2</sub>) atmosphere. The temperature and enthalpy accuracy of the DSC Q1000 were 0.1°C and 1% respectively.



Fig. 5-6. Specimens subjected to accelerated thermal cycles test

## 5.3 Results and Discussions

### 5.3.1. Physical properties of TESCMs

Fig. 5-7 demonstrates the physical properties of TESCMs with increasing amounts of PCM substitution, as measured by the bulk density and apparent porosity of cube specimens. The summary of densities and porosities with different PCM replacement level are also listed in Table 5-3. As shown in Fig. 5-7 and Table 5-3, the density of TESCMs reduces with the increasing PCM composite content. Essentially, the particle density of form-stable PCM ( $550 \text{ kg/m}^3$ ) is less compared to fine aggregate ( $2600 \text{ kg/m}^3$ ) causing the reduction in bulk density. Interestingly, TESCM-80, which contains the highest amount of PCM, has the bulk density of about  $1244 \text{ kg/m}^3$  and this indicates 39% reduction in the bulk density compared to that of OCM. The reduction in bulk density of TESCMs can be advantageous for increasing the thermal energy storage capacity of lightweight concrete, which is generally found to lack thermal capacity.

In regard to the apparent porosity of TESCMs, with increasing PCM replacement level, the apparent porosity increased from 5.7% to 16.65%. The reason for such dramatic increase would be the greater volume of the interfacial transition zone (ITZ) between form-stable PCM and cement matrix compared to the ITZ of silica sand and cement matrix, as also reported in previous studies [78, 169-171]. Furthermore, some EPO granules may also present as porous granules without absorbing the paraffin into their pores, further increasing the porosity of cement mortars.

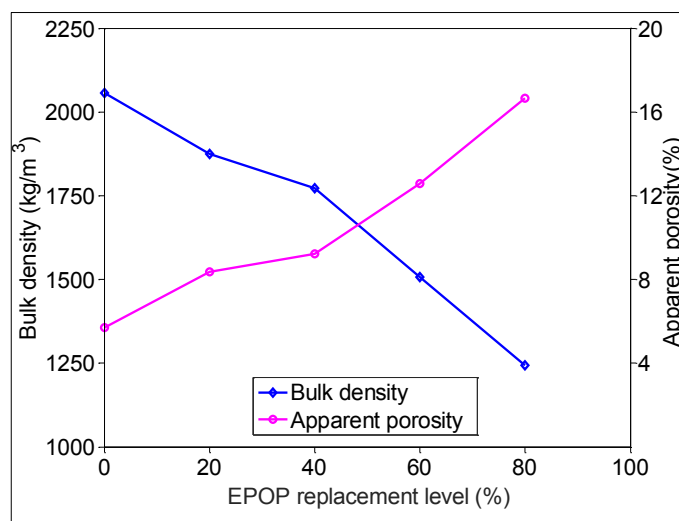


Fig. 5-7. Apparent porosity and density of OCM and TESCMs

Table 5-3 Bulk density and apparent porosity of TESCMs

Specimens	Bulk density (kg/m <sup>3</sup> )	Density decrease (%)	Apparent porosity (%)	Porosity increase (%)
OCM	2056.3	-	5.7	-
TESCM-20	1873.9	9%	8.35	46%
TESCM-40	1771.6	14%	9.21	62%
TESCM-60	1508.0	27%	12.57	121%
TESCM-80	1244.2	39%	16.65	192%

### 5.3.2. Drying shrinkage of TESCMs

The shrinkage strain in TESCMs due to the early age drying process or how resistant the PCM composite aggregates are to drying shrinkage in various TESCMs is shown in Fig. 5-8. The measured drying shrinkage trend shows that as the substitution level of composite PCM increases, the period of rapid drying shrinkage also increases. For instance, OCM underwent rapid drying shrinkage for 7 days, after which shrinkage developed more slowly, whereas, in TESCM-80, rapid shrinkage development occurred for about 21 days. More importantly, the TESCMs clearly show larger shrinkage deformations than OCM. The measured shrinkage strains at 56 days for OCM, TESCM-20, TESCM-40, TESCM-60 and TESCM-80 were found to be 0.065, 0.075%, 0.095%, 0.11% and 0.125% respectively. The increasing trend of shrinkage deformation with the increasing level of PCM composite could be due to the low stiffness of the form-stable PCM aggregates which had lower resistance to shrinkage than normal aggregates. Similar drying shrinkage behaviour have been reported by other authors for TESCMs produced with different types of PCM composites in cement mortars [76, 80, 172, 173].

In cementitious composites, drying shrinkage occurs when the capillary moisture evaporates from the cement paste. On the other hand, the potential for drying shrinkage is constrained by the inert rigid framework formed by the aggregates. Given the same amount of cement paste, the actual shrinkage depends upon the stiffness of the solid framework. The lower the stiffness of the aggregate framework, the higher will be the actual shrinkage of the cement mortar. In the TESCMs developed, cement content and water to cement ratio were fixed. Thus, with the increasing substitution level of

composite PCM, the stiffness of the aggregate framework reduced and hence, higher shrinkage levels were observed.

Assuming the shrinkage strain data of 56-day aged specimens as stable conditions, an empirical formula was developed for the relationship between the maximum drying shrinkage strains with the composite PCM substitution level (%) as shown in Fig. 5-9. The drying shrinkage strain at a stable state has a linear relationship with the substitution level of PCM composite. The regression relationship of maximum shrinkage strain with paraffin/EPO composite PCM substitution level can be expressed as follows:

$$Y = 0.077 X_{PCM} + 0.063 \quad (5-7)$$

where Y is maximum shrinkage strain;  $X_{PCM}$  is composite PCM substitution fraction. The goodness of fit ( $R^2$ ) is 0.9928.

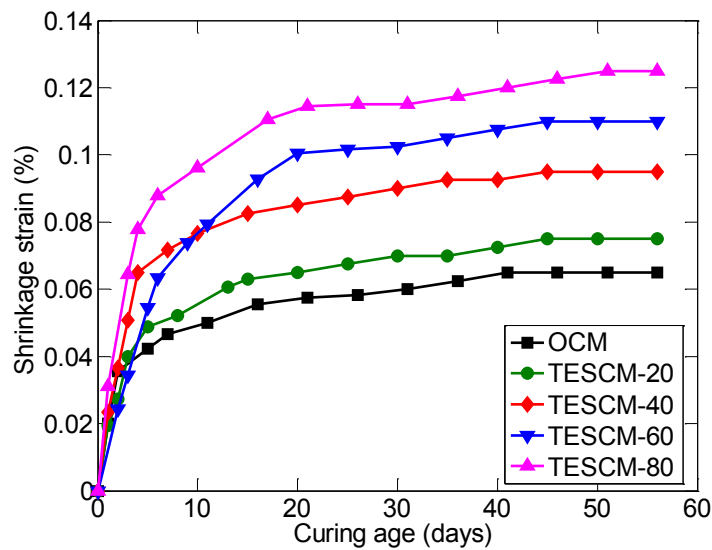


Fig. 5-8. Drying shrinkage development in OCM and various TESCMs

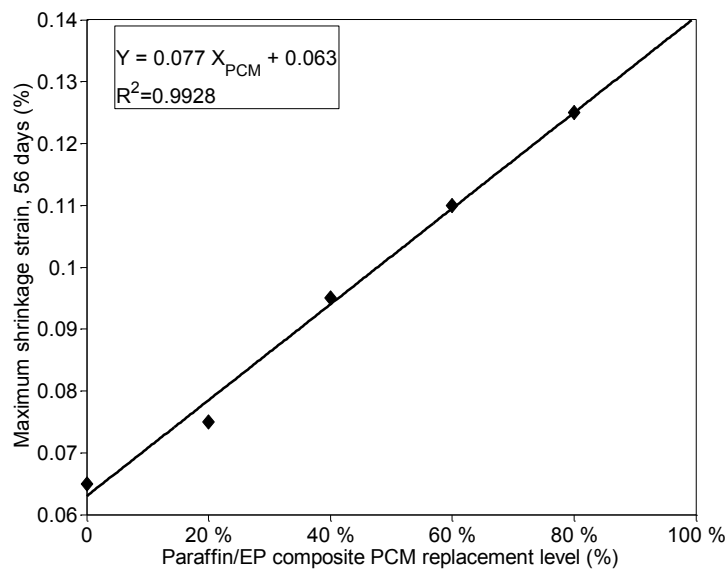


Fig. 5-9. Empirical relationship between shrinkage strain and PCM substitution level

### 5.3.3. Mechanical properties and microstructural analysis of TESCMs

The mechanical properties of TESCMs were evaluated by measuring the compressive strength of cube specimens at the age of 7 and 28 days. Fig. 5-10 demonstrates the compressive strength results of TESCMs with the PCM composite replacement levels of 0-80%. It is evident that the compressive strength of TESCM decreases with the increase in PCM substitution level. With replacement levels of 20%, 40% 60% and 80%, the corresponding strength reduction percentages at 7 days are 22%, 27%, 52%, 70% respectively, and at 28 days are 12%, 33%, 53%, 70% respectively. Although the compressive strength of the TESCMs is largely reduced in comparison with OCM (i.e. 53.8 N/mm<sup>2</sup> at 28 days), TESCM-60 with 60% replacement of composite PCM to fine aggregate had the compressive strength of 25 N/mm<sup>2</sup> at 28 days. This compressive strength would be sufficient for many construction applications, as reported in the literature [70, 88].

The SEM morphology of TESCM-60 is shown in Fig. 5-11. It can be seen that EPOP particles are well dispersed in the cement matrix and there is minimal or no destruction of composites when a standard mixing method is followed. Furthermore, Fig. 5-12 shows the interfacial zone between composite PCM and cement matrix. The figure shows that there is a good interfacial contact between EPOP and hardened cement paste, though there is a smaller gap at the interface. The visible gap at this interface could have been

formed during the sample grinding and polishing process. Furthermore, it can be seen that the depth of this gap is very shallow and hence, there is still a strong bond between EPO shell and cement paste. Therefore, it can be concluded that the interfacial contact between PCM composite and cement is good, ensuring good compatibility of EPOP and the cement matrix. Because of this good compatibility, with high substitution levels of composite PCM (i.e. 60% replacement), the TESCM still retains adequate mechanical properties.

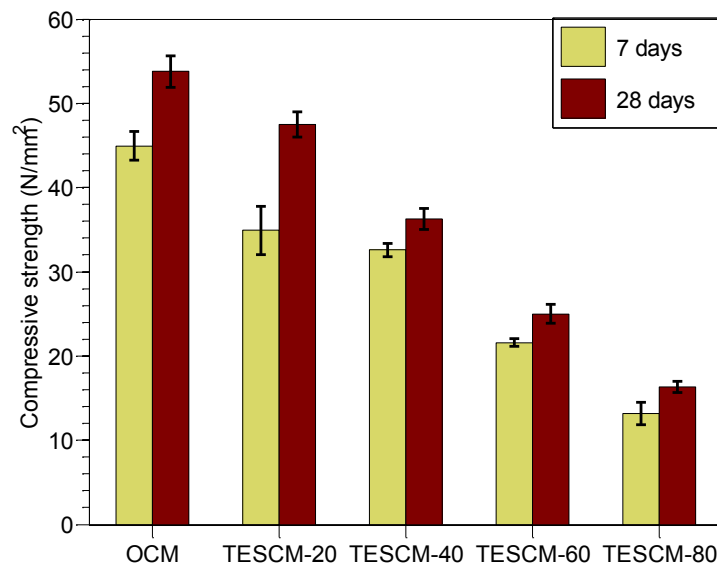


Fig. 5-10. Compressive strength of OCM and various TESCMs at 7 and 28 days

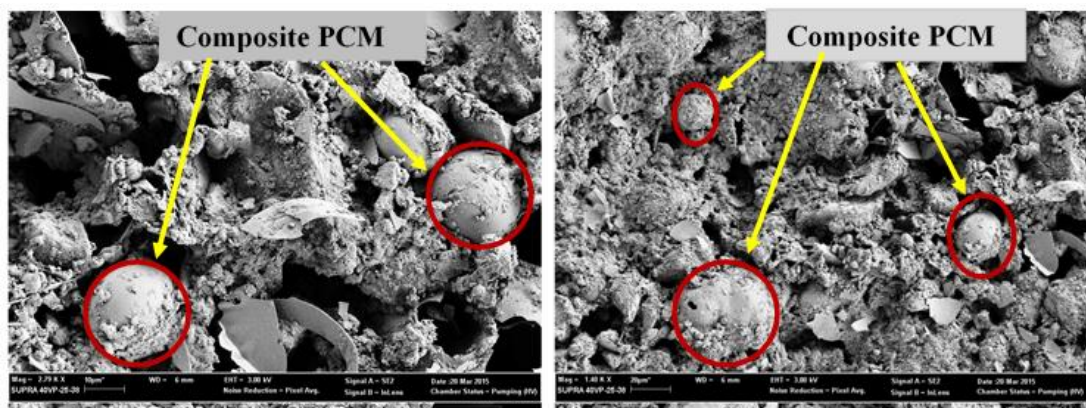


Fig. 5-11. SEM morphology of TESCM-60

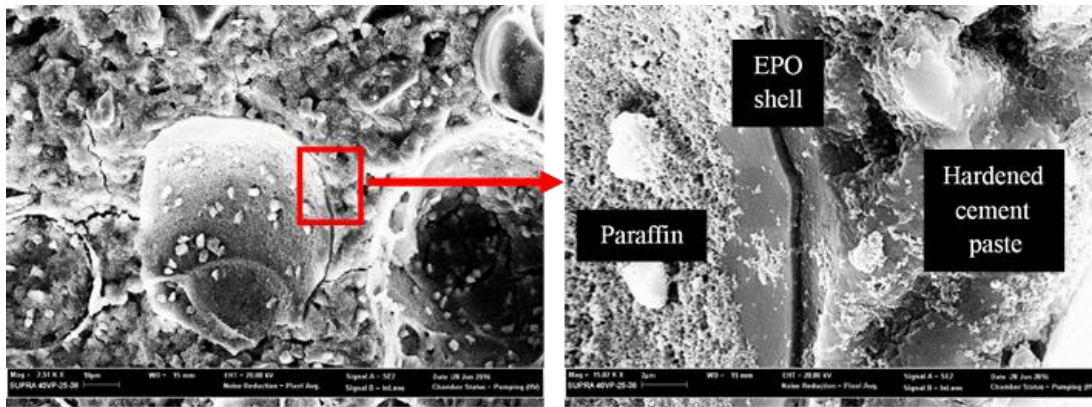


Fig. 5-12. SEM of interfacial contact zone of EPOP and cement matrix

#### 5.3.4. Thermal conductivity of TESCMs

The effect of integrating form-stable PCM into cement mortars in thermal conductivity was measured for 28-days aged specimens. Three specimens from each designated mix were used to measure the thermal conductivity and average measurement was plotted in Fig. 5-13. It can be seen from Fig. 5-13 that the thermal conductivity of TESCMs decreases with the increasing amount of PCM substitution. Compared to OCM, the reduction percentage of thermal conductivity for the composite PCM substitution levels of 20%, 40%, 60% and 80% were found as 15.8%, 31.6%, 52.6% and 65.8% respectively. The reducing trend of thermal conductivity with the increasing substitution level of PCM composite attributes to the low thermal conductivity of PCM composite (in the range of 0.2-0.4 W/m.K) compared to silica sand aggregate (1.74 W/m.K). The lower thermal conductivity of TESCMs would be advantageous to improve the thermal insulation performance of buildings when TESCMs is applied to building surfaces. However, the TESCMs are used for TES purpose in buildings and hence, low thermal conductivity of composite PCM present as a barrier for effective latent heat storage/discharge behavior of PCMs applied in buildings, as reported by many researchers [24, 103]. Therefore, the thermal conductivity of PCM composites should be improved to maximize the latent heat storage efficiency of PCM and following chapter will investigate the influence of adding heat transfer promoters into composite PCMs to increase the heat transfer performance of PCMs.

Furthermore, it has been found that there is a linear relationship exists between thermal conductivity and composite PCM substitution level as also displayed in Fig. 5-13. The regression relationship can be expressed as

$$Y = -1.356 X_{\text{PCM}} + 2.123 \quad (5-8)$$

where  $Y$  is the thermal conductivity of TESCM in  $W/(m.K)$  and  $X_{\text{PCM}}$  is the percentage substitution level of composite PCM. The goodness of fit of the linear relationship ( $R^2$ ) was found as 0.9916.

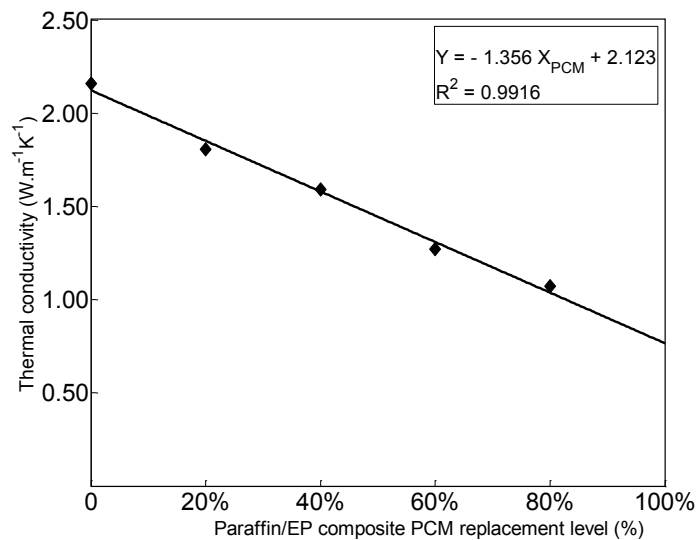


Fig. 5-13. Thermal conductivity of OCM and various TESCMs

### 5.3.5. Thermal energy storage performance of TESCMs

The comparison of thermal performance of OCM and various TESCMs were undertaken by the self-designed test room setup shown in Fig. 4-8. Here, thermal inertia and thermal energy storage capacity were used to evaluate the thermal performance and the results are charted in Fig. 5-14 and Fig. 5-15 respectively. It is worth mentioning here that this study excludes the use of TESCM-20 as the insignificant effect on thermal performance enhancement was observed.

As shown in Fig. 5-14, in comparison with OCM, the TESCMs demonstrate higher thermal inertia during the heating and cooling processes. Moreover, thermal inertia increases with the increasing level of EPOP in cement mortar (i.e. the maximum temperature difference in TESCM-60 is  $3.3^{\circ}C$ , compared to  $2.6^{\circ}C$  for OCM). This reveals the thermal mass enhancement of cement mortars. Besides, it should also be noted that the increased thermal resistance of TESCMs due to lower thermal conductivity could be another possible reason for the above observation. Therefore, to clearly understand the thermal storage enhancement, the TES capacity of cement mortar panels was studied as

charted in Fig. 5-15. It can be seen from Fig. 5-15 that the TES capacity of TESCMs is significantly greater than OCM. Maximum TES capacity of 126 kJ/kg can be observed in TESCM-80, in contrast with 47.31 kJ/kg in OCM, which is about 166% increment compared to ordinary cement mortar.

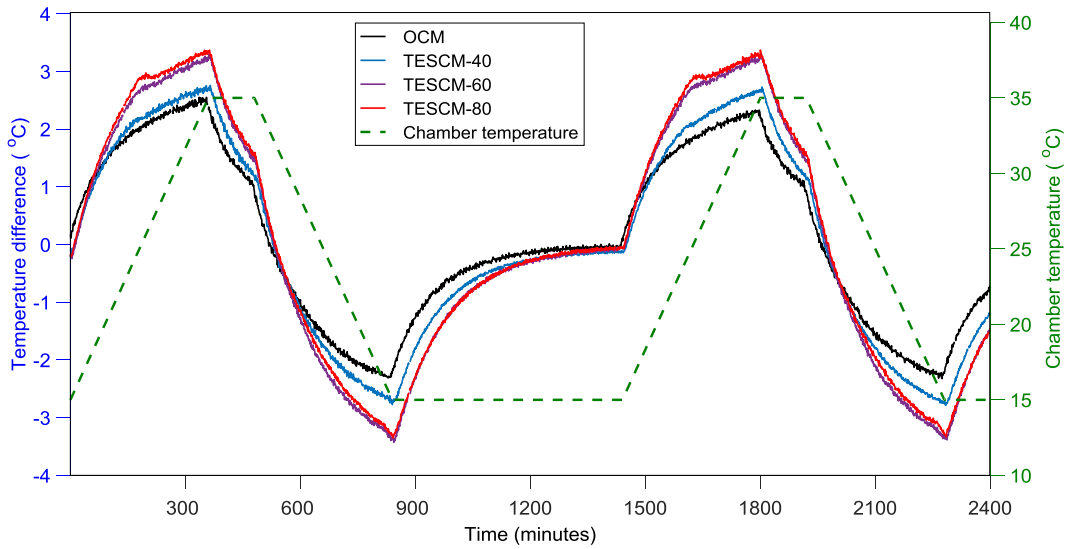


Fig. 5-14. Thermal inertia of OCM and various TESCMs

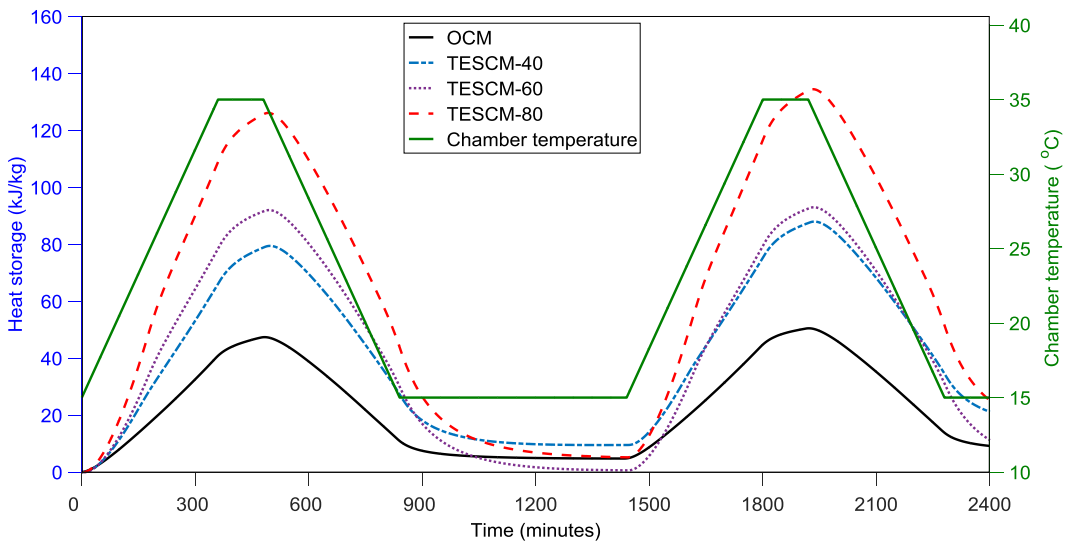


Fig. 5-15. TES capacity of OCM and various TESCMs

### 5.3.6. Mechanical and thermal reliability of TESCMs

The mechanical and thermal reliability of TESCMs were studied by subjecting the specimens to 3000 accelerated thermal cycles and studying the degradation in mechanical and thermophysical properties of thermally cycled specimens. The mechanical reliability of TESCMs was evaluated by measuring compressive strength of the thermally cycled specimens and comparing them with the same aged specimens that are exposed to the ambient environment for this period. The compressive strength results are charted in Fig. 5-16.

It can be seen that the compressive strength of thermally cycled OCM and TESCMs specimens is slightly lower than the ambient-exposed specimens. The reduction in compressive strength of PCM integrated specimens (i.e. TESCMs) can be explained by the following mechanism. During the accelerated thermal cycling, the PCM that filled in the open pores of EPO changes phase frequently and causes volume change during phase change processes. This volume change could induce internal stresses on the walls of the porous EPO granules and weaken the load transfer path in the cement matrix, giving rise to lower compressive strength compared to the ambient-exposed specimens. On the other hand, the compressive strength reduction in thermally cycled OCM specimens can be attributed to the excessive stresses generated at the interface between the fine aggregates and hardened cement paste as well as the continuous expansion/contraction process of moisture content in cement mortars, as reported in previous studies [174, 175]. Nevertheless, the compressive strength reduction of the TESCMs was very low and it is therefore considered that the internal stress generation due to phase transition had a limited influence on the mechanical properties of TESCMs. Thus, the TESCMs can be considered as mechanically reliable.

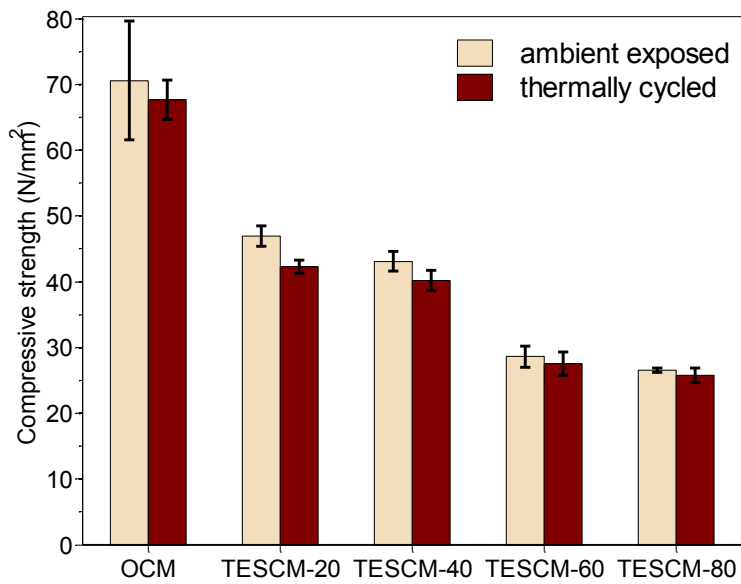


Fig. 5-16. Compressive strength of TESCMs after accelerated thermal cycles

The thermal reliability of the TESCM specimens was evaluated by subjecting the specimens to 3000 accelerated thermal cycles and then determining the changes in thermophysical properties such as phase transition temperature and latent heat capacity. The DSC curves of TESCM-60 and TESCM-80 before thermal cycles as well as after 1000 and 3000 thermal cycles are shown in Fig. 5-17. The theoretical value of latent heat capacity was also determined by Eq. (5-9) to study the changes in latent heat capacity during the accelerated thermal cycling process.

$$H_T = H_{EPOP} \times \frac{W_{EPOP}}{(W_{cement} + W_{sand} + W_{EPOP} + W_{Water})} \quad (5-9)$$

where  $H_T$  and  $H_{EPOP}$  are the theoretical values of the latent heat of TESCM and EPOP form-stable PCM respectively.  $W_{cement}$ ,  $W_{sand}$ ,  $W_{EPOP}$  and  $W_{Water}$  are the mass fraction of cement, sand, composite PCM (EPOP) and water in TESCM respectively as reported in Table 5-1.  $H_{EPOP}$  was determined as 81.21 J/g and 78.00 J/g for melting and freezing processes respectively in Chapter 3.

Table 5-4 summarizes the melting and freezing phase transition temperatures and relevant latent heat capacities for uncycled and thermally cycled TESCM specimens obtained from DSC curves and theoretical values. From Table 5-4, after 3000 thermal cycles, the peak melting temperature of TESCM-60 and TESCM-80 changed by +0.60°C

and +1.0°C respectively and the peak crystallization temperature value changes are +0.1°C and -0.3°C. On the other hand, the melting latent heat values changes by -5.3% and -10.3% respectively and the crystallization latent heat changes by -9.3% and -8.0% respectively. The small and irregular changes in phase transition temperature and heat capacities are in the negligible level and can be attributed to weight loss during thermal cycles. Furthermore, these values are very close to the theoretical values obtained from Eq. (5-9). It can be concluded, therefore, that TESCMs have good thermal reliability and can be used for building applications.

Table 5-4 Variation in thermophysical properties of TESCMs after 1000 and 3000 thermal cycles

Melting process		Calculated value	Uncycled		1000 cycles		3000 cycles	
		H <sub>M</sub> (J/g)	T <sub>Peak</sub> (°C)	H <sub>M</sub> (J/g)	T <sub>Peak</sub> (°C)	H <sub>M</sub> (J/g)	T <sub>Peak</sub> (°C)	H <sub>M</sub> (J/g)
	TESCM-60	9.59	26.1	9.38	25.6	9.14	26.7	8.88
	TESCM-80	14.94	25.3	14.55	25.2	13.91	26.3	13.05
Freezing process		Calculated value	Uncycled		1000 cycles		3000 cycles	
		H <sub>F</sub> (J/g)	T <sub>Peak</sub> (°C)	H <sub>F</sub> (J/g)	T <sub>Peak</sub> (°C)	H <sub>F</sub> (J/g)	T <sub>Peak</sub> (°C)	H <sub>F</sub> (J/g)
	TESCM-60	9.22	24.6	9.07	23.7	8.63	24.7	8.23
	TESCM-80	14.35	23.7	14.05	22.3	13.55	23.4	12.93

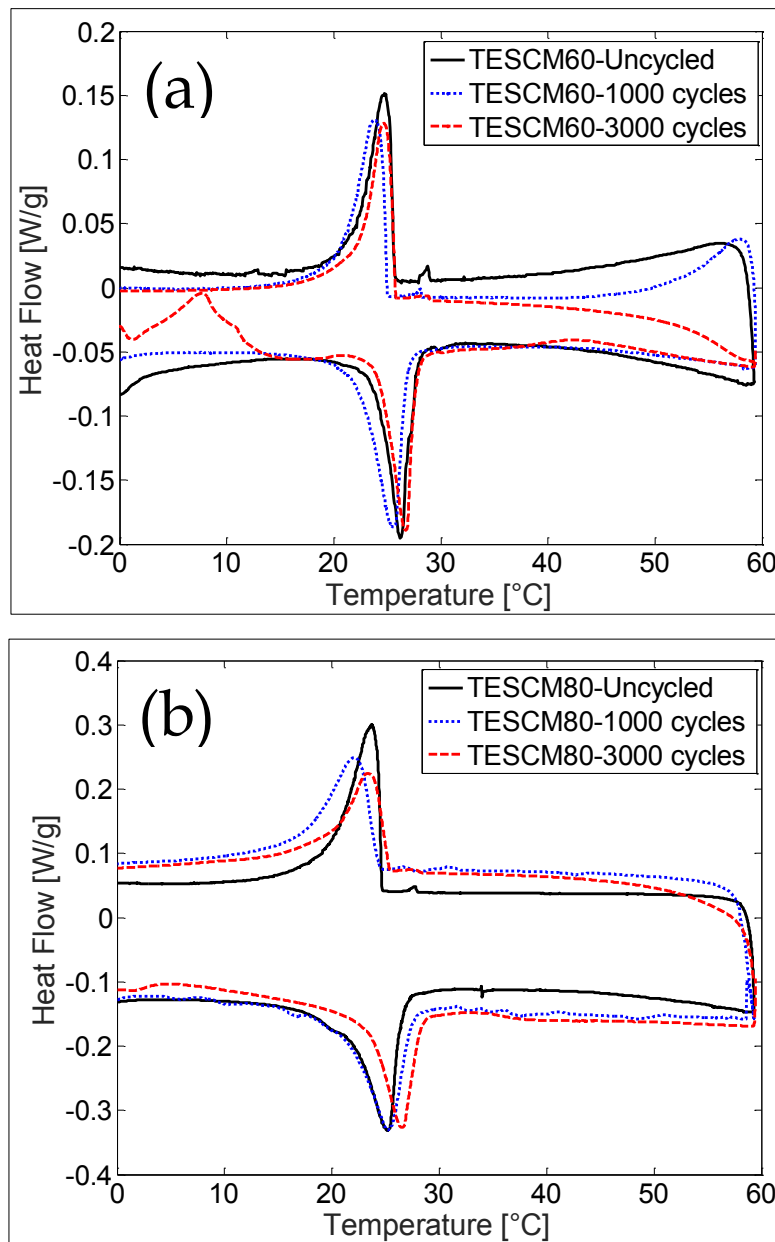


Fig. 5-17. DSC curves of TESCMs before and after accelerated thermal cycles (a) TESCM-60 (b) TESCM-80

## 5.4 Concluding remarks

This chapter investigated the effects on physical, mechanical and thermal properties of EPOP form-stable PCM integrated cement mortars as a potential application in buildings. Different amounts of PCM composite, starting from 0 to 80% volume replacement to fine aggregate, were mixed with ordinary cement mortar to develop thermal energy storage cement mortars (TESCMs) and their relevant properties were analyzed. Furthermore, thermal energy storage performance as well as mechanical and thermal reliability studies were also conducted with a self-designed heat storage set-up and accelerated thermal cycles test respectively. Based on the presented experimental works, following conclusions can be extracted:

- Incorporation of form-stable EPOP composite into cement mortar resulted in the reduction of mechanical properties, bulk density, and thermal conductivity. For example, 80% substitution of fine aggregate with composite PCM resulted in the reduction of 70%, 39% and 66% for 28-day compressive strength, bulk density, and thermal conductivity respectively.
- The TESCMs exhibited greater drying shrinkage strain than the OCM, largely due to the low stiffness of porous EPO.
- The thermal inertia and energy storage performance of TESCM can be significantly improved by increasing the composite PCM substitution level.
- The TESCM developed has very low mechanical degradation when subjected to accelerated thermal cycles by showing small changes in compressive strength. Therefore, it is mechanically reliable.
- TESCM specimens sustained 3000 thermal cycles of melting and freezing, and the changes observed in thermophysical properties such as phase transition temperature and latent heat after 3000 thermal cycles were small and negligible. Therefore, it is concluded that the TESCM developed has good thermal reliability and can be used for latent heat storage applications in buildings.

# Chapter 6 Heat transfer enhancement of form-stable PCM with the integration of carbon based additives

---

## 6.1 Introduction

The physical, mechanical and thermal properties of cementitious composites and cement mortars containing form-stable paraffin/hydrophobic EP (EPOP) composite PCM was experimentally studied in Chapter 4 and Chapter 5. It was shown that the TESCMs resulted in significant enhancement of TES performance with adequate mechanical properties, which makes their feasibility in construction applications. However, the thermal conductivity of TESCMs was found to be decreasing with the increasing amount of PCM content, mainly due to low thermal conductivity of paraffin. Although the lower thermal conductivity of TESCMs will help to improve the building thermal insulation performance, the main purpose of TESCMs are to use for thermal energy storage enhancement and thus, the heat transfer performance of TESCMs should be improved to enhance working efficiency of PCM [70].

In light of the heat transfer enhancement of PCM, a number of methods have been reviewed in the literature review and out of those, the integration of high conductive additives into form-stable PCMs is considered as an effective method to improve the heat storage/release performance. Amongst the different high conductive additives, carbon-based materials are considered as promising candidates due to their high thermal conductivity, large specific surface area, little or no corrosion effects and are inert compared to metallic additives. In this research, the heat transfer performance of EPOP form-stable PCM composite was increased with the integration of carbon-based additive. Different additives such as fine graphite (G), carbon nanotubes (CNTs) and graphene nanoplatelets (GNPs) were experimentally studied and compared to find the best appropriate heat transfer additive for the integration into form-stable PCMs.

The composite PCMs containing these additives are first fabricated and characterized for its micro-morphology, chemical compatibility and thermophysical properties with the aid of SEM, FT-IR, and DSC respectively. Afterward, the heat transfer performance enhancement was evaluated and compared. A thermal conductivity analyzer and infrared thermography were employed to evaluate the enhancement in thermal conductivity and heat storage/release rate. Moreover, a laboratory-made heat storage/release rate experiment, as reported in previous studies [108, 176, 177], was carried out to compare the heat transfer performance enhancement of composite PCM with different additives. Finally, the effect of heat transfer enhancement of form-stable PCM in TES applications was studied with the aid of laboratory scale prototype test cells. The TESCMs containing different heat transfer additives were prepared and tested for TES enhancement and improvement in indoor thermal conditions in the prototype test cells subjected to laboratory controlled climate conditions.

## **6.2 Materials and Methods**

### **6.2.1. Materials**

The commercial grade paraffin with the melting temperature of 27°C (RT27) and hydrophobic expanded perlite (EPO) were utilized for the fabrication of form-stable EPOP composite PCM. Heat transfer additives such as graphite (G), multi-walled carbon nanotubes (MWCNTs, L-MWNT-1020) and graphene nanoplatelets (GNP, C-750) were purchased from WestLab Pvt Ltd (Victoria, Australia), Shenzhen Nanotech Port Co. Ltd (NTP, Beijing China) and XG Sciences INC. respectively. The graphite used in this work had a particle size of 20-50  $\mu\text{m}$  with the thickness of 2-5  $\mu\text{m}$ . The purity of the graphite was > 95%. The MWCNTs had a diameter range of 10-20 nm, a length of 5-15  $\mu\text{m}$ , and a specific surface area of 100-160  $\text{m}^2/\text{g}$ . the purity of MWCNTs are > 97%, containing ash content of < 3 wt%. The GNP particles have been reported as the average particle size of < 2  $\mu\text{m}$ , particle thickness of 2-5 nm, and specific surface area of 750  $\text{m}^2/\text{g}$ . High purity acetone (Sigma-Aldrich, Sydney Australia) was used as the solution for the dispersion of additives.

### 6.2.2. Fabrication of paraffin/EPO/additives

The composite PCM containing heat transfer additives were fabricated by following a two-step method as proposed in Xu et al. [108], where step 1 involves the thermal conductivity enhancement of porous granules with the dispersion of additives and in step 2, the composite PCM was fabricated using thermal conductivity enhanced porous granules. The composite PCMs were designed with 49.75% paraffin, 49.75% EPO and 0.5% conductive additives. Hereafter, the new composite PCM containing heat transfer additives of G, CNT, and GNP are denoted as EPOP-G, EPOP-CNT, and EPOP-GNP respectively. The fabrication process of PCM composites containing heat transfer additive is as follows. First, carbon additive was dispersed in acetone using an ultrasonic bath till a homogenous suspension of the carbon material is derived as shown in Fig. 6-1. After the sonication for 20 minutes, EPO was added and EPO-additive-acetone mix was thoroughly mixed using a magnetic stirrer equipment for 2 hours. After a homogenous mixture of additive/EPO is achieved, the dry mixture was obtained by over-drying process at 70°C for 2 hours and then degassing in a vacuum oven for 4 hours.

The thermal conductivity enhanced porous granules were then mixed with paraffin to fabricate PCM composite by following the vacuum impregnation method explained in Chapter 3. Here, the EPO-additive composite was mixed with melted paraffin (at 60°C) at atmospheric pressure and immediately transferred to a vacuum chamber to enable vacuum impregnation process. The vacuuming process was held for about 30 minutes and then the pressure was gradually released to reach the atmospheric pressure. Finally, paraffin-EPO-additive composite PCM was obtained after cooling down to below phase transition temperature.



Fig. 6-1. Dispersion of CNT in acetone using ultrasonic bath (a) before dispersion (b) after dispersion

### 6.2.3. Preparation of TESCMs containing high conductive additives

The TESCMs containing high conductive additives were developed following the mix design of materials and mixing method described in Chapter 5. Only the TESCM-80 consisting of 80% substitution level of fine aggregate with PCM composite was prepared, due to the highest amount of PCM constitution. OCM and TESCM-80 without additives were also prepared to compare the performance enhancement of different additives. The mix proportion materials of cement mortars are given in Table 6-1. The mixing procedure was carried out as described in Chapter 5, where dry materials were first mixed at low speed for 1 minute in a Hobart mixer. After a homogenous mixture of dry materials was achieved, water together with admixture was added and mixed at low speed for 3 minutes and medium speed for one minute. Fresh mortar mixes were cast in 300 x 300 x 16 mm timber molds and kept in a moist environment for about 24 hours. After 24 hours, specimens were demolded and cured in a water bath at  $23\pm 0.5^{\circ}\text{C}$  for 28 days.

Table 6-1 Mix design of materials

Mix designation	Cement (kg/m <sup>3</sup> )	Water (kg/m <sup>3</sup> )	Silica sand (kg/m <sup>3</sup> )	PCM composite (kg/m <sup>3</sup> )					WRA (kg/m <sup>3</sup> )
				EPOP	EPOP-G	CNT	EPOP-GNP	GNP	
OCM	525	255	1445	-	-	-	-	-	0
TESCM-80	525	255	289	244	-	-	-	-	13.1
TESCM-80/G	525	255	289	-	244	-	-	-	13.1
TESCM-80/CNT	525	255	289	-	-	244	-	-	13.1
TESCM-80/GNP	525	255	289	-	-	-	244	-	13.1

## 6.2.4. Testing methods

### 6.2.4.1. *Micro-morphology characterization of composite PCMs containing high conductive additives*

The micro-morphology characteristics of carbon additives and form-stable PCM composites containing those additives were studied using a scanning electron microscopy (SEM, ZEISS Supra 40 VP). The powder samples of EPO-additive and EPOP-additive were prepared on the SEM sample mounting plate to observe the morphologies of carbon additives integrated porous granules and form-stable PCMs respectively. The sample preparation of carbon additives, particularly with CNT and GNP, was conducted differently to minimize the agglomeration of nanoparticles. Initially, the homogenous suspension of CNT/acetone and GNP/acetone were directly transferred onto the SEM sample mounting plate and then kept at 60°C for 2 hours to evaporate acetone. In this way, dispersion of CNT and GNP was ensured during the SEM imaging process. The mounted specimens were first gold coated at a thickness of ~2 nm and analyzed under low vacuum mode at a working distance of 6 mm using backscattered electron imaging (BSE) method.

#### **6.2.4.2. *Chemical compatibility of composite PCMs containing carbon additives***

The chemical compatibility between the components of form-stable EPOP containing carbon additives should be evaluated to study the interaction of -micro and -nano-sized carbon-based additives with the paraffin occupied in the pores. It has been shown in Chapter 4 that the paraffin and EPO are chemically compatible as there was no chemical interaction between these components. However, the fabrication process of thermally enhanced form-stable PCM resulted in paraffin and carbon additives are occupied together in the pores of EPO, which can potentially cause interaction between these two components. Therefore, it must be ensured that there will not be any chemical interaction between the components of PCM composite containing carbon additives.

The chemical compatibility between the components of form-stable PCM composites was studied by using FT-IR spectra analysis. In this test, the infrared spectra of thermally enhanced form-stable PCMs were recorded to identify the absorption bands and corresponding vibration modes within the infrared spectra of those materials. This was then compared with the infrared spectra of the PCM composite without carbon additives to identify the occurrence of any additional peaks when new additives are introduced into form-stable PCM. The FT-IR spectra were acquired using a Thermo Scientific Nicolet iS5 spectrometer using the KBr pellet method described in Chapter 4 of this thesis.

#### **6.2.4.3. *Thermophysical properties of composite PCMs containing carbon-based additives***

The fabrication of thermally enhanced form-stable PCM by dispersing high conductive additives into the PCMs can also affect the thermophysical properties of developed PCM composites, as these additives are in direct contact with PCM (paraffin in this case). Furthermore, integration of additional materials into PCM composites can reduce the resultant latent heat capacity as these additives are not involving in the phase change process. Thus, it is necessary to study the thermophysical properties of PCM composites containing carbon-based additives. The thermophysical properties such as phase transition temperatures and latent heat capacity of EPOP, EPOP-G, EPOP-CNT and EPOP-GNP were determined using a differential scanning calorimetry (DSC) method. The DSC measurements were conducted using a heat flux DSC (DSC Q1000, TA Instruments) for the temperature range of -20°C to 60°C in Nitrogen (N<sub>2</sub>) atmosphere.

The theoretical latent heat capacity of these PCM composites with the designed portion of paraffin in the composite of 49.5% was also determined as follows:

$$H_T = H_{paraffin} \times W_{paraffin} \% \quad (6-1)$$

where  $H_{paraffin}$  and  $W_{paraffin}$  are the measured latent heat capacity of paraffin (J/g) and design portion of paraffin in the PCM composite (%) respectively.

#### 6.2.4.4. Thermal conductivity measurement

The thermal conductivity of form-stable EPOP containing different carbon additives was measured using a TCi thermal conductivity analyzer. The TCi, developed by C-Therm Technologies Ltd., is a device that measures the thermal conductivity of small samples by the modified transient plane source (MTPS) method. The composite PCMs were pressed into solid disc samples at the specimen diameter of 25.4 mm and a thickness of 10 mm with a manually controlled hydraulic press as shown in Fig. 6-2. All specimens were prepared at the same specimen mass of 10 g and a constant compression force and holding time of 10 kN and one minute respectively. During the pressing process, sample holder was connected to a vacuum pump to minimize the presence of air pores in the solid disc specimens.



Fig. 6-2. Pelletizing of PCM composite discs containing carbon additives

The specimens were then mounted on the sensor of the TCi thermal conductivity analyzer with the application of water droplets as contact agent to improve the contact thermal resistance. All measurements were conducted in the ambient environment of 10°C to eliminate the transient latent heat energy storage of PCM occurring during the temperature range of 20-30°C. The thermal conductivity analyzer was calibrated using the Pyrex block (for the calibration of thermal conductivity range of 0.13-1.2 W/m.K) before conducting sample measurements. Three specimens from each composite PCMs were used to measure the thermal conductivity and average thermal conductivity value of three reading for each specimen were taken into account.

#### **6.2.4.5. Heat storage/release test**

The heat transfer performance enhancement of PCM composites with the integration of high conductive additives were evaluated by using a laboratory made heat storage/release rate test setup as shown in Fig. 6-3. In this test, approximately 20.0 g of PCM composite powder was placed into the glass tube and gently pressed to form solid cylindrical specimens. Temperature sensors (K-type thermocouples with the measurement accuracy of 0.05°C) were placed at the mid-point of the cylindrical specimen to measure and record the mid-point temperature variation when subjected to heating and cooling processes. The opening of the glass tubes was sealed with a cork stopper. The thermocouples were connected to a measurement system consisting a data-logger and a computer, and continuously recorded the temperature at the frequency of 1 minute. Two water baths at the temperatures of 10°C and 40°C were adopted for heating and cooling processes respectively. Initially, the glass tubes containing specimens and thermocouples were kept at 10°C until they reach steady state conditions. This was ensured by monitoring the mid-point temperature and steady-state conditions were considered when the midpoint temperature varies between  $\pm 0.1^\circ\text{C}$ . After the specimens had reached steady state conditions, they were immediately transferred to a water bath at 40°C to study the transient heat storage behavior of PCM composites containing various additives. Once the specimens reached steady state conditions at 40°C, they were immediately transferred to the water bath at 10°C to study the transient heat discharge behavior of those specimens.

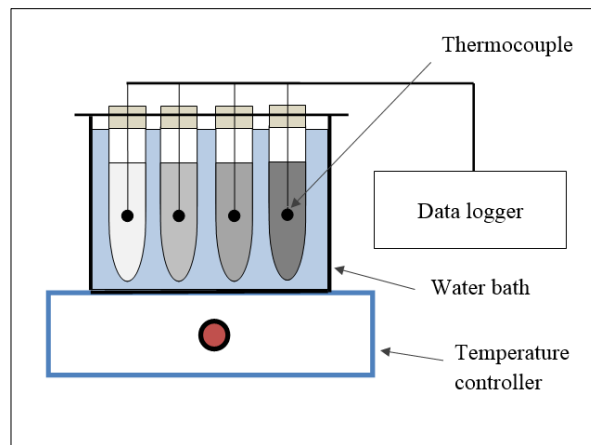


Fig. 6-3. Schematic diagram of heat storage/release performance test

#### 6.2.4.6. *Infrared thermography test*

The heat transfer performance of PCM composites with the integration of high conductive additives was also assessed by observing the top surface temperature variation of cylindrical specimens subjected to conductive heat transfer from the bottom surface. Thermal imaging technology was employed to capture the surface temperature variation of the top surface using an infrared (IR) thermal imaging camera (Testo 885-2 Set, Testo Australia). The cylindrical specimens ( $\Phi$  25.4 mm  $\times$  6 mm) prepared for the thermal conductivity test were utilized for IR image capturing test. The cylindrical specimens were initially kept at 20°C for 2 hours (to allow all samples to achieve the same initial temperature of 20°C) and immediately transferred to a heated plate surface at 45°C. The IR images were captured periodically to observe the top surface temperature behavior with time.

The heat transfer mechanism and corresponding surface temperature variation profile of this test is as follows. Firstly, when the specimens were transferred to high-temperature surface, the temperature of the specimen linearly increases and reaches the onset melting temperature of PCM due to heat conduction. At this point, the paraffin in the composites began to absorb thermal energy as latent heat until completely melted. Once the PCM had been completely melted, the surface temperature of the specimens again linearly increases and stabilizes at hotplate surface temperature. The temperature increment rate of the specimens are significantly affected by the heat transfer rate to PCM occupied in the pores of EPO, and hence, the surface temperature variation of specimens containing heat transfer additives would be different.

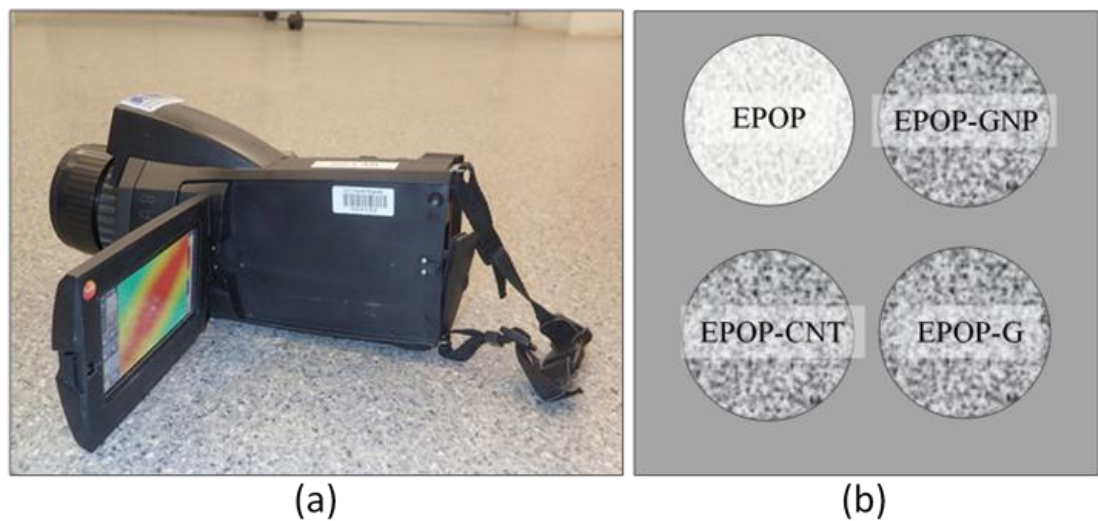


Fig. 6-4. Thermal imaging test (a) Testo thermal imaging camera (b) schematic diagram of specimen arrangement

#### 6.2.4.7. *Thermal energy storage performance measurement of TESCMs*

The thermal storage performance of thermally enhanced form-stable PCM in cement mortars was assessed by using a laboratory scale prototype test room experiment. In this experiment, a prototype test cell consisting hollow cubes, with an internal hollow volume of  $300 \times 300 \times 300 \text{ mm}^3$  was built, whose walls are composed of (from outside to the inside of the cube): a 13-mm thick timber layer and a 16-mm thick layer of the test panel. One face of the cube was functioned as a removable lid to facilitate access to the room. The schematic diagram of the prototype and physical arrangement of the test setup are shown in Fig. 6-5.

It must be underlined that the current prototype experiment is different from the self-designed heat storage set up used in Chapter 4 and Chapter 5, which evaluated the thermal energy storage performance of TESC and TESCMs. In the self-designed heat storage set up, the heat transfer occurred through the designated test panel located at the top surface of the test room, as the other surfaces were highly insulated. This experiment, on the other hand, ensures the heat transfer from all surfaces and also represents the scaled down prototype of typical test room experiments. Furthermore, as opposed to the self-designed heat storage set up, this prototype experiment uses different performance indicators to directly measure the impact of heat transfer enhancement with high conductive additives as explained below.

The heat flux sensors (Hukseflux, 5% accuracy) and K type temperature sensors (temperature accuracy of 0.05°C) were attached on the interior and exterior surface of one wall of the test cell to measure and record the temperature and heat fluxes. The prototype test cell was placed in a climate-controlled thermal chamber operated in the temperature cycles between 15°C and 35°C at a ramping rate of 0.04°C/min. The temperature accuracy of the thermal chamber is 0.1°C. The prototype test cell was initially kept at 15°C for 10 hours for the allowance of sufficient time to reach steady state conditions. The thermal chamber also allowed the control of internal relative humidity, which was set to the value of 50% throughout the experiments. The temperature and heat flux sensors were connected to an automatic data acquisition system (data-logger), with the data acquiring frequency of one minute.

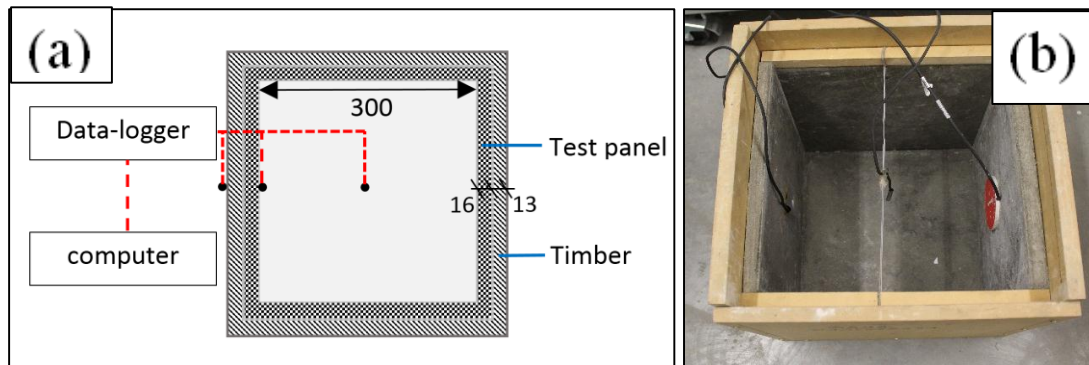


Fig. 6-5. Prototype experiment set up (a) schematic diagram of test cell (b) physical set up

Regarding the thermal performance assessment, two performance indicators are chosen based on the heat transfer performance enhancement to indoor as shown below:

1. Inner surface convection heat gain rate ( $q_{in}$ , W/m<sup>2</sup>) is the heat gain from indoor to the inner surface of the test cell, which can be directly measured from inner surface heat flux sensor. This indicator can be used to study the heat transfer rate to indoor (inside the test room in this case), which indicates the heat addition or extraction to indoor air, thus influencing the indoor thermal comfort. The positive values of  $q_{in}$  indicates the heat is being extracted from indoor air, while negative values reflect the heat is being added to the indoor air.

2. Inner surface convection heat gain energy ( $Q_{in}$ , kJ/m<sup>2</sup>) is determined from the internal heat gain rate to describe the cumulative heat energy transferred from indoor air to inside surface of the test panel for a given time-period.  $Q_{in}$  in a surface can be calculated from the convection heat gain rate ( $q_{in}$ ) as follows:

$$(Q_{in})_{t=T} = \int_{t=0}^{t=T} q_{in} \cdot dt \quad (6-2)$$

## 6.3 Results and discussions

### 6.3.1. Morphology characterization of paraffin/EPO/additives

The micro-morphology characteristics of carbon additives and corresponding form-stable PCM composites are illustrated in Fig. 6-6, Fig. 6-7 and Fig. 6-8 for graphite, CNT and GNP additives respectively. Fig. 6-6 shows the morphology characteristics of form-stable PCM composite integrated with graphite additive in terms of graphite, EPO-graphite, and EPOP-graphite. Fig. 6-6(a) shows that the graphite particles have a 2-dimensional sheet-like structure with the particle size of approximately 10-20  $\mu\text{m}$ . Due to the sheet-shaped structure of graphite, they can develop a high conductive interconnecting network in the porous media of EPO. However, Fig. 6-6(b) reveals that the graphite based additives cannot develop such high conductive network inside the pores of EPO, due to the larger size of graphite particles compared to the pore diameter of EPO and hence, they cannot be accommodated into the pores. This causes the graphite particles are just surrounding the EPO granules and they would not be able to enhance the heat transfer to paraffin occupied in the pores of EPO. This can be further verified by observing the SEM images of EPOP-G as depicted in Fig. 6-6(e) and Fig. 6-6(f), where graphite sheets are surrounding the composite PCMs and hence they are not connected to paraffin.

The SEM images corresponding to the composite PCM fabricated by having CNTs as heat transfer promoters is presented in Fig. 6-7. The dispersed CNTs as shown in Fig. 6-7(a) and Fig. 6-7 (b) reveals that the CNTs are a one-dimensional material with the approximate diameter of 20 nm. Furthermore, Fig. 6-7 (c) shows the SEM images of EPO-CNT, where CNTs are forming an interconnecting network in the pores of EPO. The enlarged image of the open pore of EPO in Fig. 6-7 (d) clearly evident that the CNTs are partially connected to the pores of EPO, which can improve the heat transfer to paraffin when absorbed into these pores. Furthermore, from Fig. 6-7 (e), one can observe that the PCM composites are containing a paraffin-CNT network in the pores of EPO with the CNT particles are partially exposed to the surrounding. The enlarged SEM image of the pore opening area in Fig. 6-7 (f) further verifies this concept as CNTs are connecting paraffin to the surrounding of the composite PCMs. Such high conductive heat transfer network connecting the PCM (i.e. paraffin) occupied in the pores of EPO can

significantly improve the heat storage and discharge performance of EPOP. However, CNTs can only assist in one-dimensional heat transfer enhancement and hence, the thermal energy storage enhancement could be limited.

On the other hand, the heat transfer performance enhancement of PCM composites with the dispersion of GNPs are depicted in Fig. 6-8. The dispersed GNP particles as illustrated in Fig. 6-8(a) and Fig. 6-8(b) shows that each platelet is having approximately  $5\mu\text{m}$  of linear dimension and the thickness of few nanometers. Due to the two-dimensional structure and very thin nature of these nanoplatelets, it can have very high surface area and hence, they can improve the heat transfer rates significantly. The SEM morphology corresponding to the porous EPO granules containing GNP is shown in Fig. 6-8(c). The enlarged image of the EPO-GNP connecting network is also shown in Fig. 6-8(d). As can be seen from Fig. 6-8(c) and Fig. 6-8(d), the GNPs can be well integrated into the pores of EPO and they are randomly oriented in the pores of EPO. Furthermore, Fig. 6-8(e) & (f) evident that the GNP particles are partially immersed into the paraffin occupied in the pores of EPO in order to form a high conductive heat transfer media to surroundings.

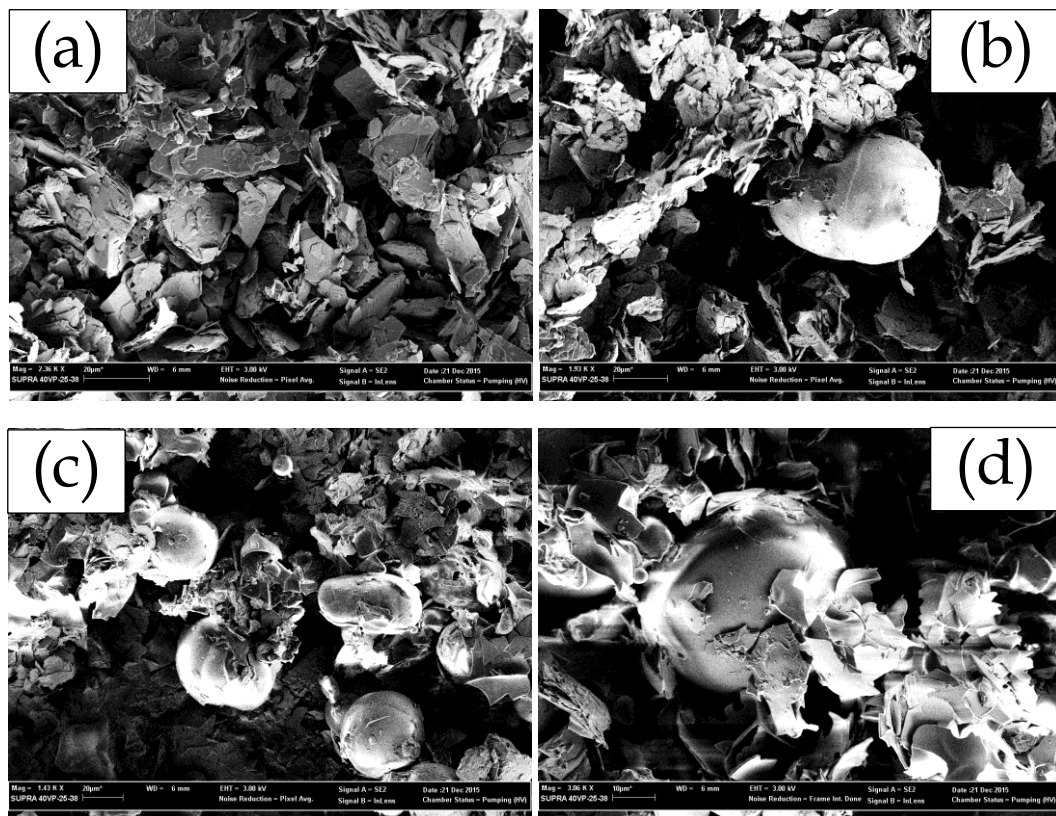


Fig. 6-6. SEM images of EPOP-G (a) graphite (b) EPO/graphite (c) & (d) EPOP-G

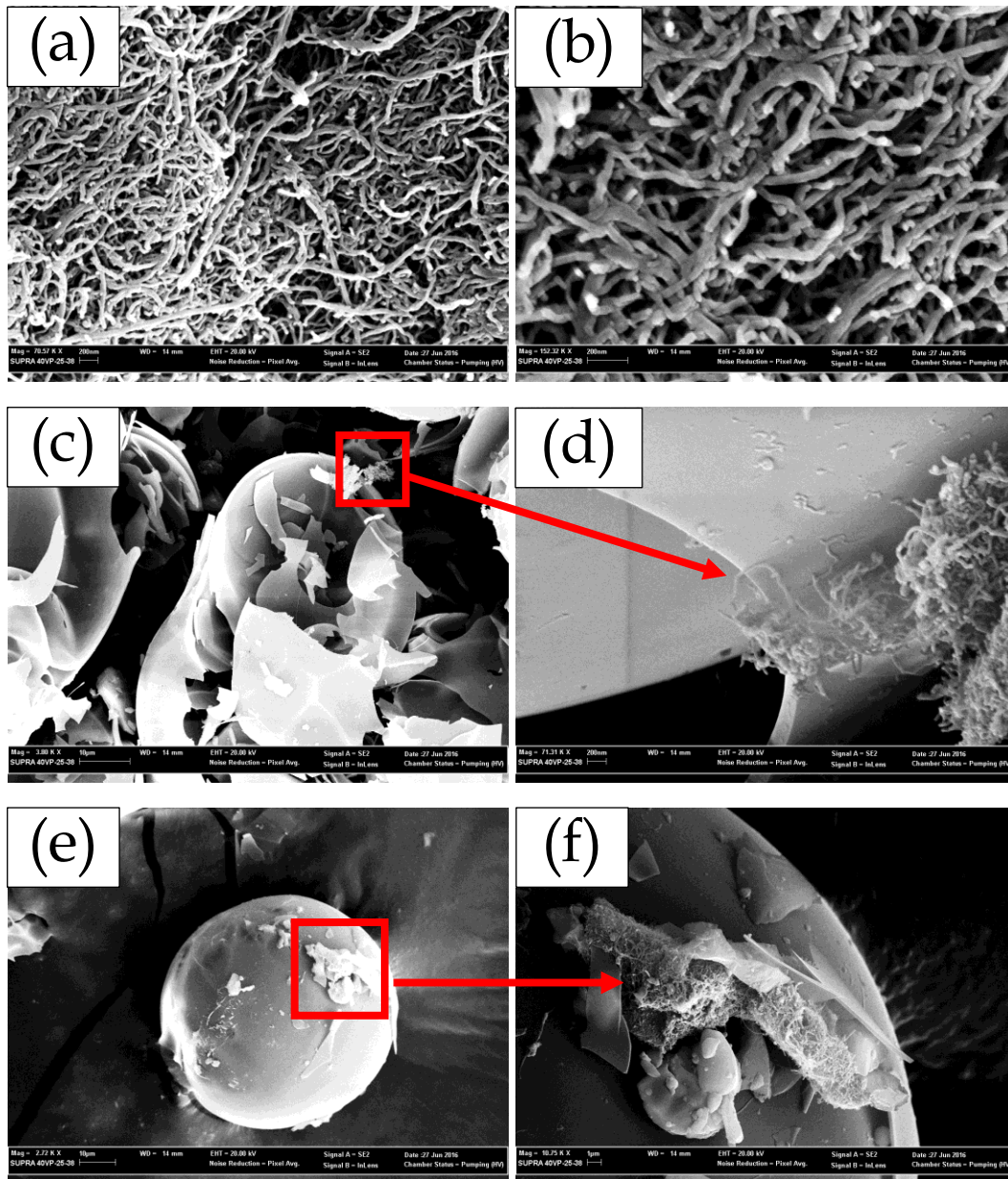


Fig. 6-7. SEM images of EPOP-CNT (a) & (b) MWCNTs, (c) & (d) EPO-CNT, (e) & (f) EPOP-CNT

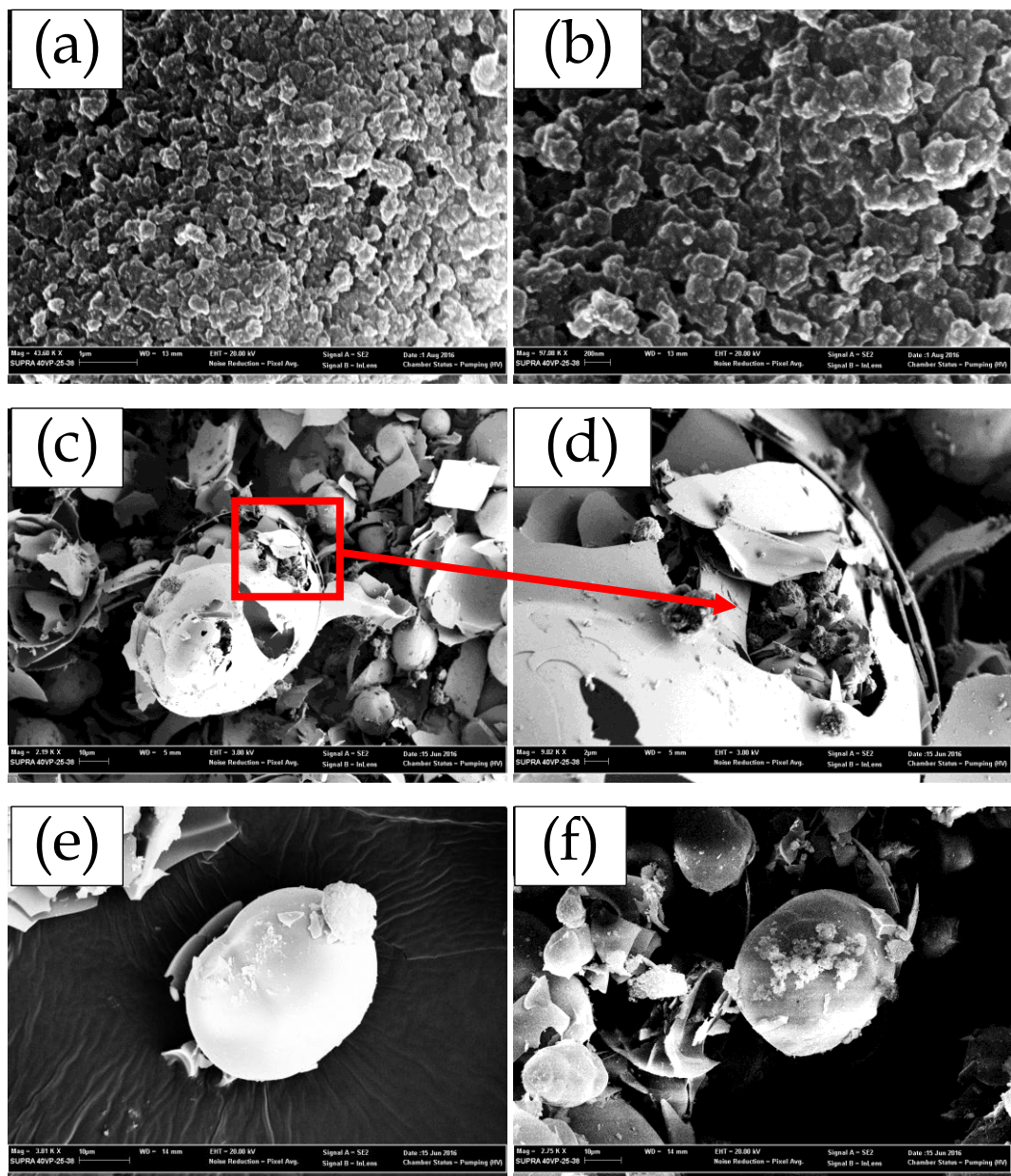


Fig. 6-8. SEM images of EPOP-GNP (a) & (b) GNP, (c) & (d) EPO-GNP, (e) & (f) EPOP-GNP

### 6.3.2. Chemical compatibility of PCM composite/additive

The chemical compatibility between the components of EPOP and different heat transfer additives, as measured by FT-IR spectra, are presented in Fig. 6-9. As can be seen from Fig. 6-9, EPOP has its characteristic absorption bands at  $720\text{ cm}^{-1}$ ,  $792\text{ cm}^{-1}$ ,  $1005\text{ cm}^{-1}$ ,  $1466\text{ cm}^{-1}$ ,  $2848\text{ cm}^{-1}$  and  $2915\text{ cm}^{-1}$ . They respectively reveal the rocking vibration of  $\text{CH}_2$  at  $720\text{ cm}^{-1}$ , bending vibration of  $\text{SiO-H}$  at  $792\text{ cm}^{-1}$ ,  $\text{Si-O-Si}$  asymmetry stretching vibration at  $1005\text{ cm}^{-1}$ , deformation vibration of  $-\text{CH}_2$  and  $-\text{CH}_3$  at  $1466\text{ cm}^{-1}$  and stretching vibration of  $-\text{CH}_2$  and  $-\text{CH}_3$  (at  $2848\text{ cm}^{-1}$  and  $2915\text{ cm}^{-1}$ ). Furthermore, it can be clearly seen that the above-mentioned absorption peaks are also present in the PCM composites containing carbon-based additives without showing any additional peaks, indicating that there is no chemical interaction between the components of EPOP and carbon-based additives. Thus, FT-IR analysis shows that the integration of carbon-based additives into EPOP composite PCM imply good chemical compatibility between the components and these composites can be further studied for their thermal energy storage performance.

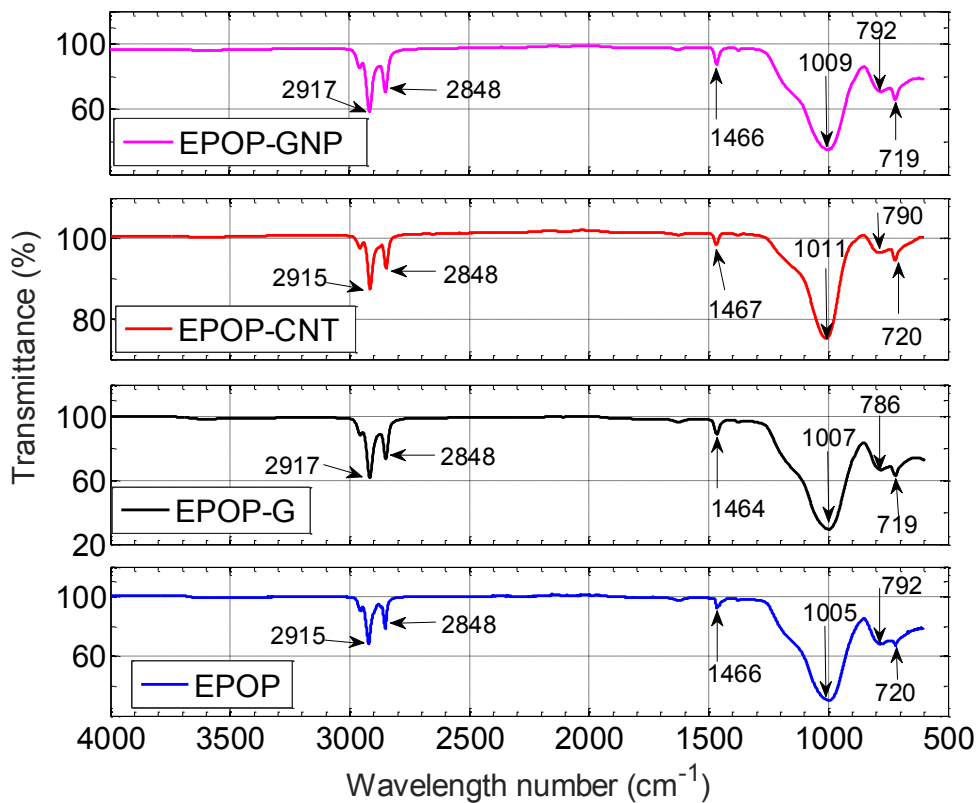


Fig. 6-9. FT-IR spectra of EPOP, EPOP-G, EPOP-CNT and EPOP-GNP

### 6.3.3. Thermophysical properties of PCM composite/additive

The thermophysical properties of EPOP form-stable PCM composite with different heat transfer additives are presented in Fig. 6-10, Fig. 6-11 and Fig. 6-12 for the additives of G, CNT, and GNP respectively. Table 6-2 also summarizes phase transition temperature and latent heat capacity of these composites. As can be seen from figures and table, the integration of high conductive additives into the form-stable EPOP PCM does not have a significant impact on the phase transition properties. This can be explained by the absence of any chemical interaction between these heat transfer additives and paraffin as revealed from FT-IR analysis, and a smaller amount (0.5wt%) of heat transfer additives are integrated into the composite PCM. Furthermore, composite PCMs containing different heat transfer additives showed the latent heat capacity of 78-80 J/g for melting and 81.5-82.2 J/g for freezing processes respectively, which is also quite close to the theoretical latent heat capacity determined for form-stable EPOP composite. This indicates that the carbon-based additives into form-stable PCM leads to trivial changes in phase transition properties and latent heat capacity.

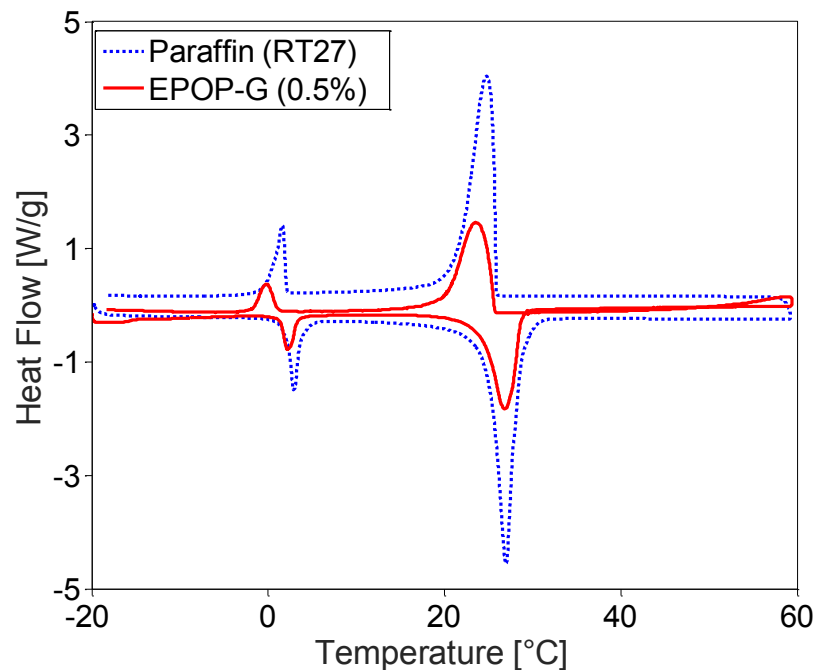


Fig. 6-10. DSC curves of paraffin and EPOP-G

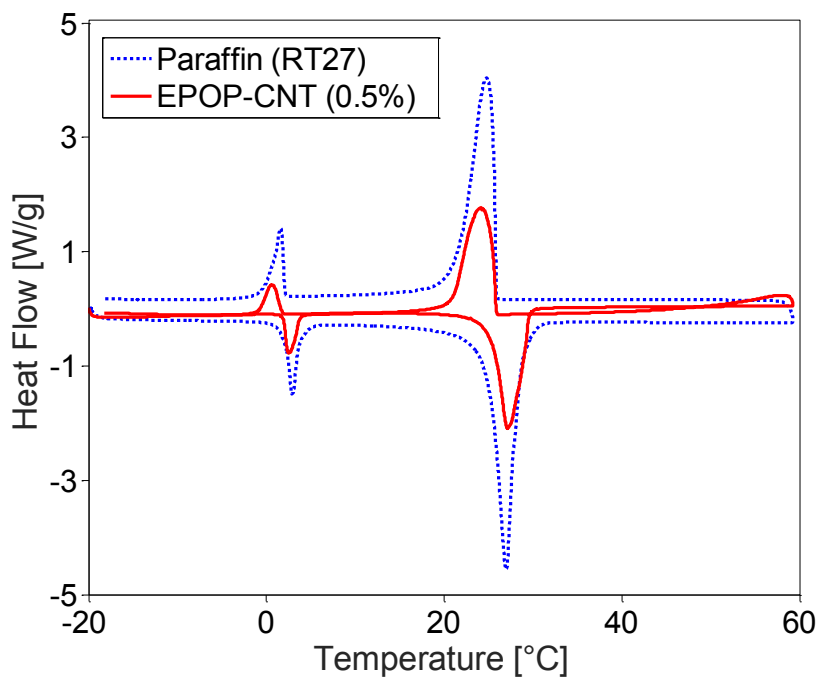


Fig. 6-11. DSC curves of paraffin and EPOP-CNT

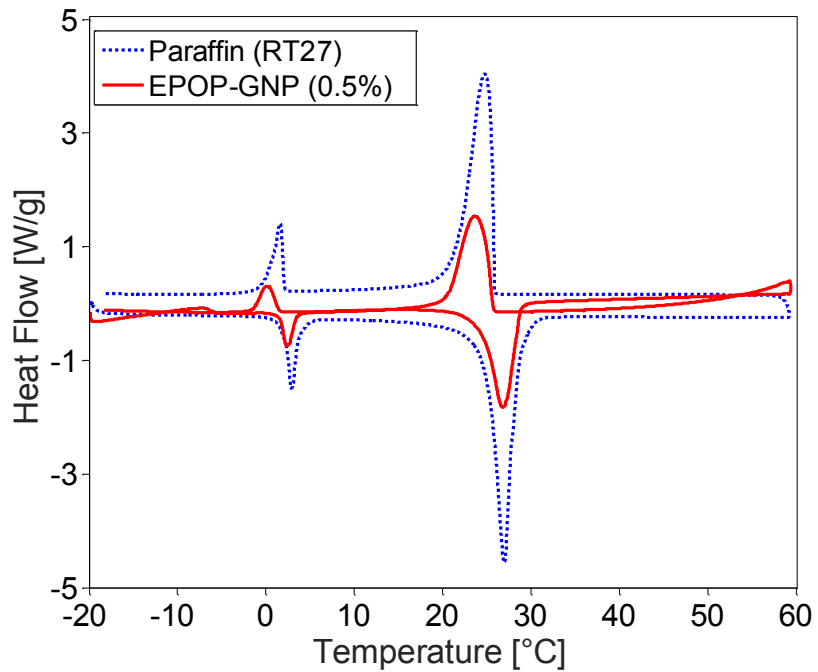


Fig. 6-12. DSC curves of paraffin and EPOP-GNP

Table 6-2 Thermophysical properties of EPOP with different heat transfer additives

	Melting process				Freezing process			
	T <sub>Onset</sub>	T <sub>Peak</sub>	H <sub>M</sub>	H <sub>T</sub>	T <sub>Onset</sub>	T <sub>Peak</sub>	H <sub>F</sub>	H <sub>T</sub>
	(°C)	(°C)	(J/g)	(J/g)	(°C)	(°C)	(J/g)	(J/g)
Paraffin	25.07	27.15	164.8	-	25.83	24.78	167.2	-
EPOP	24.45	26.58	81.21	82.40	24.32	23.51	78.00	83.60
EPOP - G	24.28	26.90	79.00	81.58	24.28	23.52	81.93	82.76
EPOP - CNT	25.38	27.16	78.61	81.58	25.88	24.14	81.59	82.76
EPOP - GNP	24.50	26.94	79.35	81.58	25.71	23.74	82.22	82.76

### 6.3.4. Thermal conductivity of PCM composite/additive

The thermal conductivity can be an indicator to measure the heat transfer performance enhancement of PCM composites containing high conductive additives. The measured thermal conductivity of EPOP with carbon additives, as measured by TCi thermal conductivity analyzer, is charted in Fig. 6-13, where a relative increase in thermal conductivity was also reported. As can be seen from Fig. 6-13, the EPOP composite PCM has the thermal conductivity of 0.35 W/(m.K) as a result of low thermal conductivity of paraffin and porous EPO granules. The integration of additives into PCM composite significantly boosted the thermal conductivity with the relative increment of 45%, 30% and 49% for G, MWCNT, and GNP respectively.

Out of those three additives, CNT was resulted in the lowest enhancement of thermal conductivity due to the one-dimensional heat transfer enhancement of CNT compared to other two additives. On the other hand, graphite addition showed a 45% increase in thermal conductivity, even though there was not an effective heat transfer network observed in SEM analysis between paraffin and graphite. This can be attributed to the fact that heat transfer occurs through the high conductive graphite sheets that are surrounding the PCM composites and heat pulse would not penetrate through paraffin occupied in the pores of EPO. Thus, TCi thermal conductivity analyzer detects a high thermal conductivity, regardless of the effect of paraffin occupied in the pores of EPO.

It can be said, therefore, the thermal conductivity enhancement does not accurately reflect the heat storage/release performance of fabricated PCM composite and the beneficial effects of heat transfer additives should be studied by measuring the heat storage/release performance of such PCM composites. Nevertheless, the dispersion of GNP additives into the EPOP composite resulted in largest thermal conductivity enhancement level of 49%, which was also seen to have an excellent interconnecting high conductive network into porous granules as observed from SEM analysis.

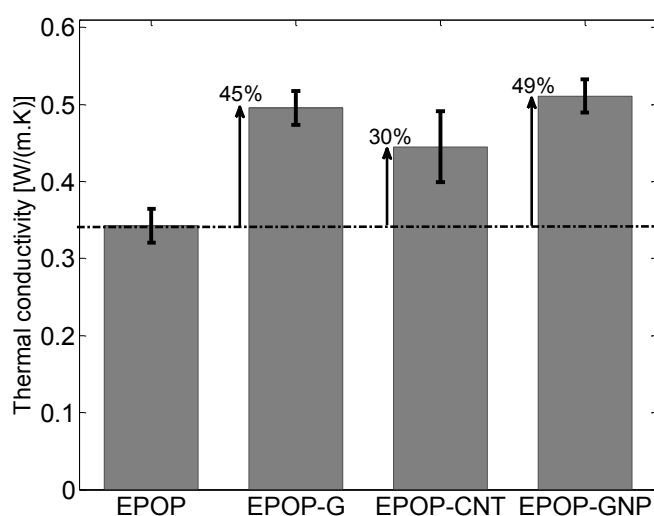


Fig. 6-13. Thermal conductivity of composite PCMs containing heat transfer additives

### 6.3.5. Heat storage/release performance

The beneficial effect of integrating heat transfer additives into form-stable EPOP composite to improve TES performance can be seen from the measured temperature development trends during heat storage and release processes as depicted in Fig. 6-14 and Fig. 6-15 respectively. The time span of the heat charge and discharge processes during the phase transition temperature range are also given in Table 6-3. As shown in Fig. 6-14 and Fig. 6-15, all PCM composites showed obvious temperature plateaus in the heating and cooling processes due to phase change. Nevertheless, the composite PCMs containing high conductive additives showed faster heat storage and release rates than EPOP. For example, during the heat storage process, the required time for heating the specimens from 25-30°C decreased by 12.2%, 14.6% and 15.5% for EPOP-G, EPOP-CNT, and EPOP-GNP respectively, compared to EPOP. Similarly, during the heat discharge process, the time duration for cooling from 27°C to 22°C of EPOP-G, EPOP-CNT, and

EPOP-GNP was decreased by 14.6%, 17%, and 19.9%, respectively. While the amount of PCM in composites was same in all specimens, the faster heat charge and discharge rates were achieved when high conductive additives are integrated. This evident that the heat transfer rates to PCM is accelerated with the use of high conductive additives and hence, the energy storage efficiency of TES applications can be enhanced. Amongst the different heat transfer additives, GNP can be considered as the best candidate to enhance the heat storage performance as the dispersion of GNP particles resulted in lowest duration for phase change charge and discharge processes.

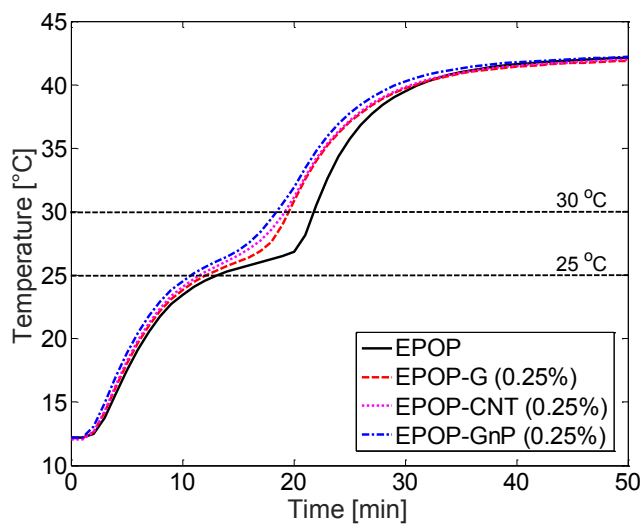


Fig. 6-14. Heat storage behavior of EPOP containing heat transfer additives

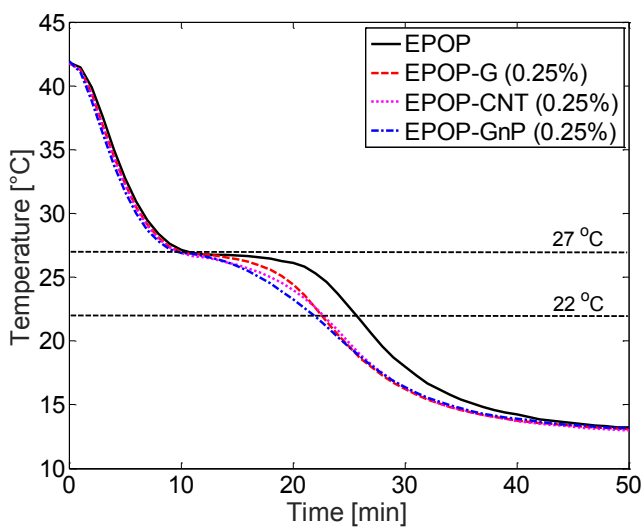


Fig. 6-15. Heat discharge behavior of EPOP containing heat transfer additives

Table 6-3 Heat charge/ discharge durations of EPOP containing heat transfer additives

Specimen and sample composition	Time required for heat charge from 25-30°C (s)	Time required for heat discharge from 27-22°C (s)
EPOP	521.4	909.6
EPOP-G	457.8	776.4
EPOP-CNT	445.2	755.4
EPOP-GNP	440.8	728.4

### 6.3.6. Heat transfer performance using IR thermography

The heat transfer performance of EPOP form-stable PCM composite integrated with carbon-based additives, as measured by infrared thermography, are depicted in Fig. 6-16. The surface temperature distributions of the PCM composites were captured by infrared thermal imaging camera when the specimens heated at 45°C using a heated hotplate. As illustrated in Fig. 6-16, at a given instance, the surface temperature variations of specimens containing different heat transfer additives were found to be different. Indeed, the PCM composites containing high conductive additives (specimens b, c, and d) showed rapid temperature rise compared to composite PCM without any additive (specimen a). In particular, the PCM composites containing GNP showed very rapid temperature rise due to excellent heat transfer performance of GNP.

For example, at 4 minutes, the paraffin occupied in EPOP-GNP had been almost completely melted, and surface temperature exceeded 33°C compared to other composite PCMs which were still in the melting temperature range of 26-30°C. On the other hand, EPOP-G and EPOP-CNT had also showed improved heat transfer rate compared to just EPOP, as observed from surface temperature distributions at 4 and 5 minutes. The observations of inhomogeneity in the specimen surface temperature variations could be due to the fact that the hotplate generates more heat at the central area of the plate compared to surrounding areas. Nevertheless, the specimens are located at the same distance from the central area and hence the heat penetration to the specimens can be assumed as same. Furthermore, the thermal images also evident that the hot plate surface temperature variation was very small at all times.

These results reveal that the composite PCMs containing high conductive additives possesses excellent thermal storage performance as it can lead to more rapid heat storage process during phase transition stage. Furthermore, temperature increase and heat penetration are occurring more quickly in composite PCM with GNP than other PCM composites, thus inducing a higher heat transfer rate essentially during phase change process. Therefore, to put these into perspective, the PCM composite integrated with GNP is a promising route to improve energy storage efficiency in TES applications due to the inherent merits of two-dimensional heat transfer additives of GNP such as very high thermal conductivity and large specific surface area.

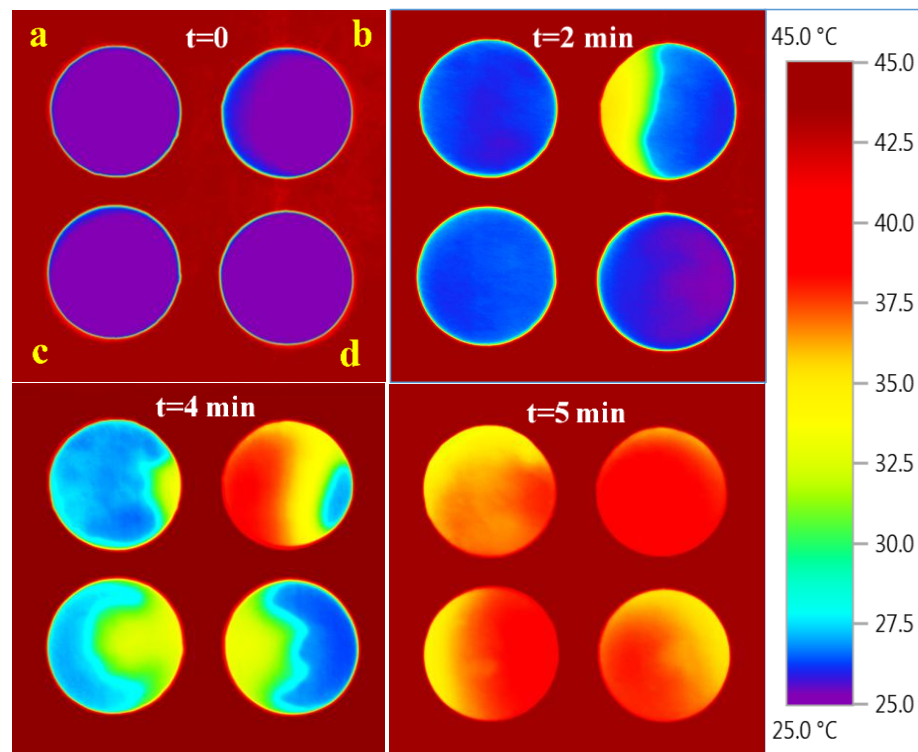


Fig. 6-16. IR thermography of EPOP integrated with carbon additives, (a) EPOP, (b) EPOP-GNP, (c) EPOP-CNT and (d) EPOP-G

### 6.3.7. Thermal energy storage performance of prototypes

The effect of integrating high conductive additives into form-stable PCM in increasing the heat storage performance of cement mortars was studied with the aid of a laboratory scaled prototype test cell. The TES behavior of TESCM panels integrated with different carbon additives is observed when the test cell is subjected to typical summer design day temperature variations. Fig. 6-17 and Fig. 6-18 illustrates the TES behavior of test panels in terms of inner surface convective heat gain rate ( $q_{in}$ , W/m<sup>2</sup>) and inner surface convection heat gain energy ( $Q_{in}$ , kJ/m<sup>2</sup>) respectively.

As can be seen from Fig. 6-17, the integration of high conductive additives into EPOP form-stable PCM brings obvious benefits in improving the surface heat gain rates, though the enhancement levels were found to vary for different additives. Taking the peak convective heat gain rate as an example, the TESCM-80 panels incorporated with graphite (G) and GNP improved the heat storage rate by 38% and 78% respectively, while the incorporation of CNT reduced the peak storage rate by 19%. On the other hand, the relevant increase in peak heat discharge rate was determined as 39%, 93% and 125% for G, CNT, and GNP respectively. The increased thermal energy storage and discharge rate indicate that the application of such additives in TESCM can potentially improve diurnal energy storage efficiency when such TESCMs are incorporated into buildings. On the other hand, the reduced peak heat storage rate with the addition of CNT can be explained as the heat storage process started very early so that most of PCM heat storage occurred before reaching the peak heat storage rate, resulting in lower peak energy storage rate.

The potentiality of improving energy storage efficiency with high conductive additives is more evident if convective heat gain energy behavior of TESCM panels are considered, as presented in Fig. 6-18. It can be observed that the integration of carbon-based additives enabled higher convective heat gain energy in cement mortar panels, leading to more effective energy storage efficiency. This is particularly reflected by the increased total heat gain energy with the integration of carbon additives, for which the increment of 78%, 122%, and 200% was obtained for the integration of G, CNT, and GNP respectively.

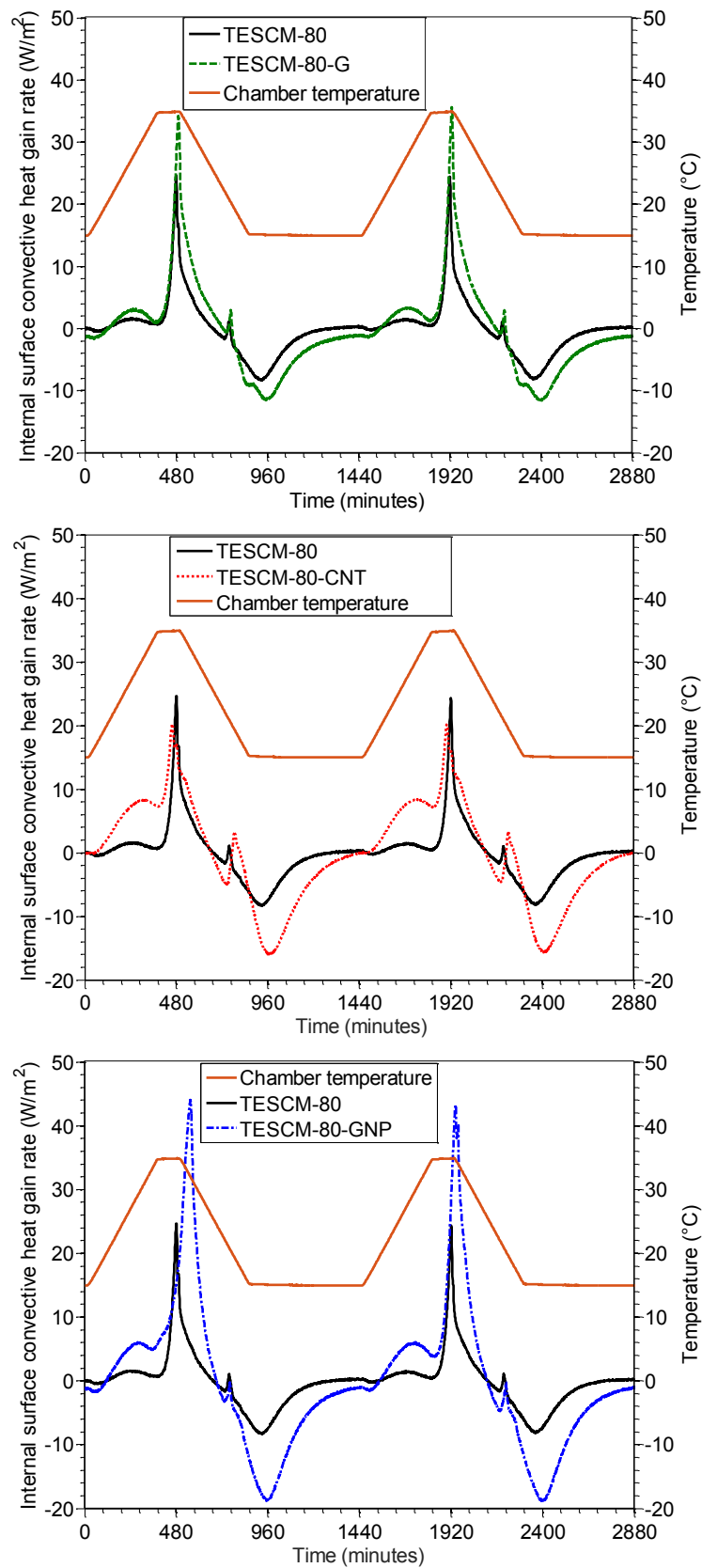


Fig. 6-17. Comparison of inner surface heat gain rate of TESCM-80 with additives

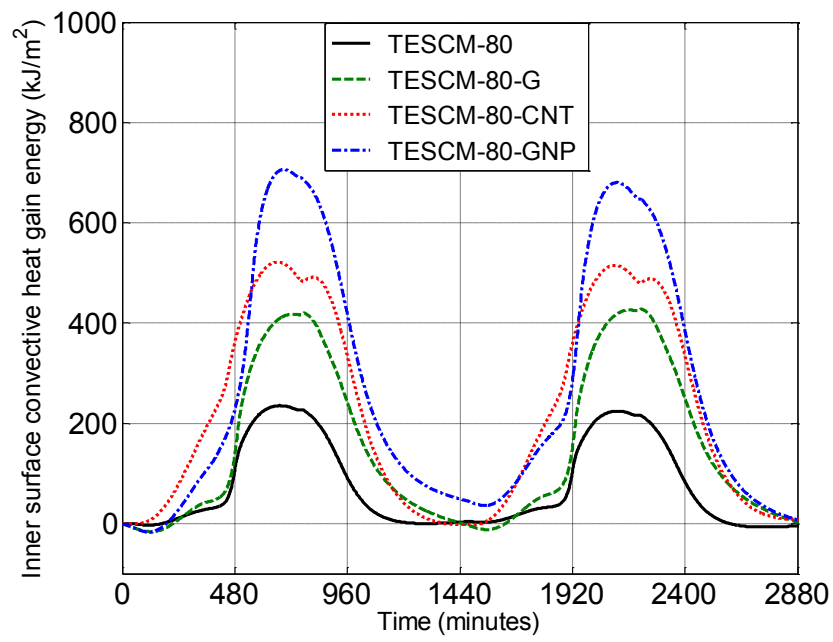


Fig. 6-18. Convective heat gain energy variation of TESCM-80 with additives

## 6.4 Concluding remarks

This chapter investigated the contrasting enhancement in heat transfer performance of paraffin/hydrophobic expanded perlite (EPOP) form-stable PCM composites seeded with various carbon-based additives. Graphite (G), carbon nanotubes (CNTs) and graphene nanoplatelets (GNPs) were considered as the heat transfer additives. The PCM composites containing carbon-based additives were fabricated by following a two-step fabrication process, where step 1 developed an effective heat transfer network in the pores of EPO by dispersing carbon-based additives into porous EPO granules and step 2 involved the vacuum impregnation of paraffin into porous network. The PCM composites containing high conductive additives were then characterized and studied for heat transfer performance enhancement using various techniques. Based on the experimental works presented, the following conclusions can be drawn:

1. The micro-morphology characteristics conducted by SEM analysis showed that the carbon-based additives of CNTs and GNPs could formulate a good high conductive network into the porous EPO granules due to their nano-sized particle dimensions and very high specific surface area. On the other hand, graphite particles would not be able to develop an interconnecting network and they were just surrounding the EPO granules, due to their larger particle size compared to pore diameter of EPO.
2. The chemical compatibility analysis using FT-IR spectra study showed that all carbon-based additives are chemically compatible with form-stable EPOP composites.
3. The thermophysical properties of PCM composites with carbon additives, as measured by DSC analysis, showed that the dispersion of 0.5wt% of carbon additives has negligible variation in the thermophysical properties of fabricated composite PCMs.
4. Compared to EPOP composite PCM, the dispersion of 0.5wt% of carbon-based additives resulted in significant enhancement of thermal conductivity and the increment levels of 45%, 30% and 49% were achieved for the addition of G, CNT, and GNP respectively.
5. The heat transfer performance of PCM composites measured from heat storage/release test and infrared thermography analyses revealed that the

dispersion of carbon-based additives brings beneficial effects in enhancing the heat transfer rate to PCM occupied in the pores of EPO. Integration of GNP showed highest performance enhancement and graphite addition resulted in lowest performance enhancement.

6. The TES performance of TESCM panels (i.e. TESCM-80) integrated with carbon-based additives was studied by prototype test cell experiments. It was found that the integration of heat transfer enhanced form-stable PCM into cement mortars improves the inner surface convective heat gain rates and total convective heat gain energy. In comparison to TESCM-80, the addition of G, CNT, and GNP enhanced the total heat gain energy by 78%, 122%, and 200% respectively.

Finally, it is concluded that the integration of high conductive carbon-based additives into form-stable EPOP composite PCM would have potentiality in enhancing the energy storage rates. The performance enhancement levels of different additives were found to be different. Out of the three additives studied, GNP showed highest performance enhancement while graphite (G) showed least.

# Chapter 7 Thermal performance assessment of form-stable PCM integrated cement mortars in buildings

---

## 7.1 Introduction

The incorporation of PCM into building materials and components for the purpose of indoor climate control have been extensively studied with the aid of experimental, analytical and numerical approaches. PCM Incorporated building components such as wallboards [178, 179], tiles [180], bricks [181], cement mortars and concrete [73, 155] were widely investigated as they offer large heat transfer surface area within the building, enabling a high heat transfer rate. Out of those different methods, PCM integrated cement mortars for the application of interior and exterior surface coatings in buildings can be considered as a versatile method because it has high heat exchange surface to depth ratio, large amount of PCM can be accommodated as they are non-structural elements and they can be used in existing buildings as an energy refurbishment approach.

Although several studies identified the PCM integrated cement mortars as a potential technology to improve indoor thermal comfort, most of the studies were based on commercially available microencapsulated PCM and cement mortars containing form-stable PCMs have been scarcely reported in the literature. Furthermore, the previous chapter of this thesis showed that the TESCM developed by integrating EPOP form-stable PCM into cement mortars could be used for building applications as it has very high thermal energy storage capacity with adequate mechanical properties.

The main objective of this chapter is to assess the thermal performance enhancement of TESCM incorporated into buildings for the improvement in indoor thermal comfort. A comprehensive experimental and numerical work is carried out to study the reduction

in peak indoor temperature, diurnal temperature fluctuations and improvement in indoor thermal comfort conditions.

The experimental study includes laboratory scaled prototype test cells subjected to controlled climatic conditions and test huts exposed to the outdoor environment. The PCM incorporated cement mortar boards (PCM CB) and ordinary cement mortar boards (OCB) with the mix proportions of materials identified as TESCM-80 and OCM respectively in Chapter 5, were cast at the thickness of 16 mm and utilized as interior surface elements in prototype test cells and test huts. A commercially available gypsum plasterboard (GPB) was also considered for this thermal performance study as they are widely used as an interior surface element in modern buildings. It must be noted that the current thermal performance study does not consider the use of high conductive additives due to the limited resource availability and fabricating nano sized additives integrated PCM composites in large scale would be difficult at this stage.

The prototype test cells were subjected to the climatic conditions similar to summer daily variation and summer design day variation to study and compare the thermal performance enhancement of PCM CB with OCB and GPB. On the other hand, two test huts, built on timber framework with the test panels as an interior surface element, were exposed to the outdoor climatic conditions in Croydon campus of Swinburne University of Technology, Melbourne, Australia. The experiment has been conducted for a period of five months (01/10/2016 to 01/03/2017) to study the performance enhancement of PCM CB during spring and summer climatic conditions. While one test hut was tested with PCM CB as an interior surface element throughout the entire period of the experiment, another test hut was tested with GPB and OCB for two months and three months periods respectively.

Furthermore, numerical simulations were carried out for the thermal enhancement of building refurbished with PCM CB as interior surface plastering mortars of building walls. A multi-storey office building without active air-conditioning system was refurbished by applying the PCM CB as an interior surface plastering mortar of brick walls. A case of building refurbishment with OCB was also considered to compare the performance enhancement of PCM CB with OCB. Dynamic thermal simulations were performed to investigate the thermal performance enhancement of PCM CB, compared to the cases of no refurbishment and building refurbishment with OCB. Furthermore,

studies were also conducted to further enhance the thermal performance of PCMCB in buildings, by improving the solidification of PCM with the activation of mechanical night ventilation.

## 7.2 Materials and Methods

### 7.2.1. Materials and mix design

The raw materials used for the synthesis of EPOP form-stable PCM are paraffin (RT27) with the phase transition temperature of 27°C and hydrophobic expanded perlite (EPO). Ordinary Portland cement (OPC) complying with AS3972 and silica sand (maximum particle size of 1.18 mm) were used for the development of cement mortars. A commercial grade water reducing admixture (MasterPozzolith 370 from BASF) was used to improve the workability of TESCM.

The cement mortar panels with the dimensions of 300 x 300 x 16 mm were cast as described in Chapter 5 of this thesis. The mix proportion of materials for the development of OCB and PCMCB were chosen as similar to OCM and TESCM-80, and are also given in Table 7-1. The physical, mechanical and thermal properties of OCM and TESCM-80 were studied and reported in Chapter 5 of this thesis. The gypsum plasterboards utilized in this study were purchased from Gyprock Pvt Ltd with the dimensions of 3000 x 1200 x 16 mm and then cut into smaller pieces at required sizes.

Table 7-1 Mix proportion of materials

Mix designation	Cement (kg/m <sup>3</sup> )	Water (kg/m <sup>3</sup> )	Silica sand (kg/m <sup>3</sup> )	PCM Composite (kg/m <sup>3</sup> )	WRA (kg/m <sup>3</sup> )
OCB	525	255	1445	0	0
PCMCB	525	255	289	244	13.1

## 7.2.2. Prototype experiments under controlled climate conditions

### 7.2.2.1. *Design of prototypes*

The performance assessment of PCMCB as interior surface plastering mortars for buildings was carried out with laboratory scale prototype experiments under controlled climatic conditions. Three identical sized prototype test cells were built: one with GPB, one with OCB and another with PCMCB. The prototype cells were hollow cubes, with an internal hollow volume of  $300 \times 300 \times 300 \text{ mm}^3$ , whose walls are composed of (from outside to inside of the cube) 13-mm thick timber layer and 16-mm thick layer of the test panel. One face of the cube functioned as a removable lid to facilitate access to the room. The schematic diagram of the prototype test cell and physical arrangement of the test setup are shown in Fig. 6-5. It must be noted that the composition of the walls of the test cell is not typical in building construction. In fact, the aim of this laboratory scale study was to have a preliminary assessment of thermal performance by constructing a small sized prototype, accommodating into the laboratory climate chamber so that the outdoor environment conditions could be controlled and precisely monitored. Although the results of this laboratory thermal performance tests cannot be directly extrapolated to real buildings, such tests can assist in prior assessment of significance of TESCMs before large scale experiments. Furthermore, a relatively thin wall construction in this prototype enables the contribution of test panels to the thermal responses received by outdoor temperature variations.

The prototypes were placed inside a climate controlled thermal chamber with the allowance of sufficient clearance for the air circulation inside the chamber. The climate chamber was operated for typical summer daily temperature variations and summer design day temperature variations as described in the following sections. In regard to temperature monitoring, k-type thermocouples (with an accuracy of  $0.05^\circ\text{C}$ ) were positioned at the inner and outer surface of the test room and in the geometric center of the room, with the final intention to compare the internal temperature variations and improvement in indoor thermal comfort conditions. The thermal chamber also allowed the control of internal relative humidity, which was set to 50% throughout the experiments. All temperature sensors were connected to an automated data acquisition system (data-logger), with a data recording frequency of one minute.

### 7.2.2.2. Experiments under summer climatic conditions

The thermal performance study under summer climatic conditions was assessed by subjecting the prototypes to typical summer daily temperature variations similar to the weather conditions during seven consecutive days (22-26, January), as derived from representative meteorological year (RMY) weather files for Melbourne, Australia. The outdoor air dry-bulb temperature variation during this period is depicted in Fig. 7-1. The corresponding temperature variation was programmed in the climate controlled thermal chamber for the thermal performance assessment of prototypes under such climatic conditions.

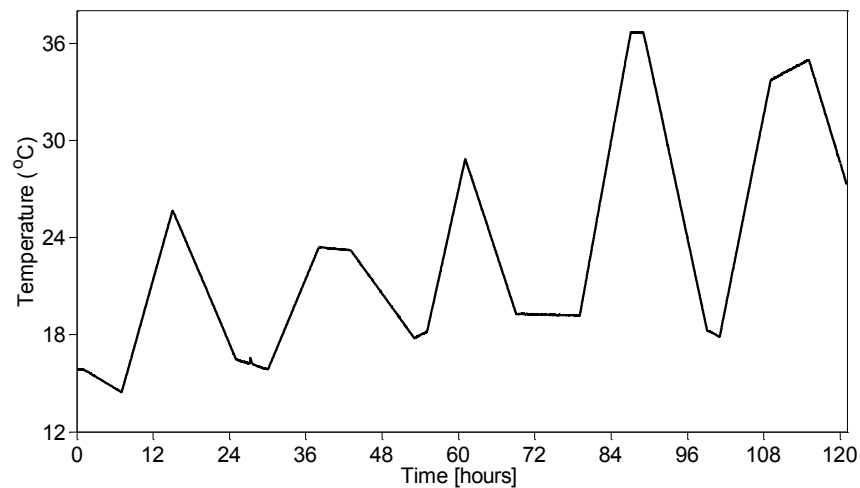


Fig. 7-1. Summer daily temperature variation during seven consecutive days (22-26, January) in Melbourne, Australia

### 7.2.2.3. Experiments under summer design day conditions

The summer design days for the prototype experiments were assumed as having a diurnal temperature variation of 15-35°C with the temperature ramp rate of 0.04°C/min. The purpose of introducing summer design days temperature variation was to enable full exploitation of latent heat capacity and also to have complete solidification of melted PCM at night (as of low night temperatures 15°C). The chamber temperature variation considered for a period of 48 hours is plotted in Fig. 7-2.

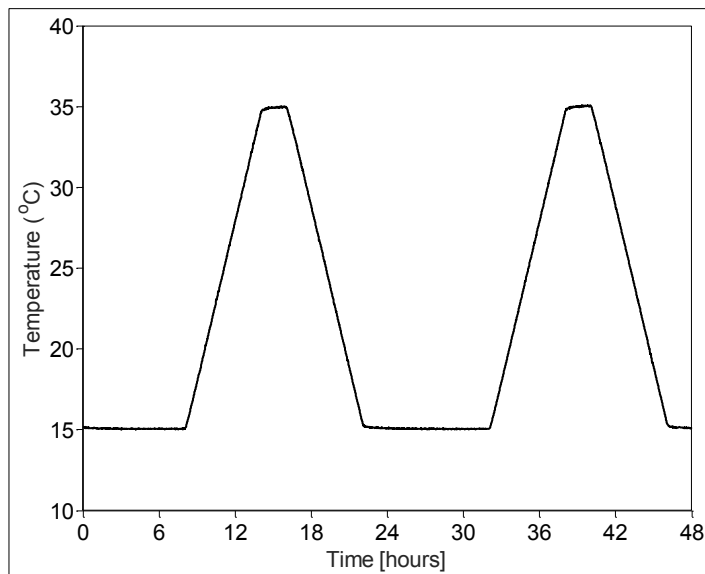


Fig. 7-2. Summer design day outdoor air temperature variation in the climate chamber

### 7.2.3. Test huts exposed to outdoor climatic conditions

#### 7.2.3.1. Description of modular test rooms

The major limitations of the above-described prototype experiments are their scaled down sizes and their exposure to laboratory controlled climatic conditions. To assess the thermal performance of PCM CB as the interior surface element in buildings, the test cells must be chosen in a reasonable size and they should be exposed to outdoor climatic conditions. On this basis, two identically sized test huts were built on the timber framed structure with an inner volume of  $1130 \times 725 \times 690 \text{ mm}^3$ . The floor and walls of the test rooms were constructed on timber and fully insulated at the interior with 90 mm thick (R 2.0) glass wool insulation material. The interior surface of the walls and floor were made of test panels. A double-glazing window was located on the east wall of the test huts through which solar radiation can enter. The roof is made of R 1.8 insulation layer prefabricated by manufacturer in between 2 mm corrugated iron sheets (outside layer) and 10 mm thick timber panels (inside layer). Fig. 7-3 shows the construction of test huts with the installation of insulation to timber walls followed by the PCM CB test panels as interior wall and floor elements. The detailed construction elements of the test huts are given in Table 7-2.



Fig. 7-3. Test hut set up (a) installation of insulation to the interior walls (b) PCMCB installed to the interior surfaces

The test huts were exposed to the outdoor environment during the period of 01/10/2016 to 01/03/2017. While the PCM incorporated test hut consisted PCMCB as the interior surface element throughout the entire test period (01/10/2016 to 01/03/2017), the reference test hut was constructed by incorporating GPB for the period of two months (01/10/2016 to 30/11/2016) and OCB for the period of three months (01/12/2016 to 01/03/2017). This is to study the performance enhancement of PCMCB compared to different construction materials of GPB and OCB. The test huts were placed in Croydon campus of the Swinburne University of Technology in Melbourne Australia, where the window of the test huts were facing east without much shading of trees and neighboring buildings. The view of the test huts is displayed in Fig. 7-4.

Table 7-2 Construction materials/elements of test huts

Surface	Construction materials (outside to inside)
External walls	12mm timber, 90mm thick (R 2.0) insulation with reflective foil on one side, test panels.
Roof	2mm corrugated iron sheet, R 1.8 insulation, 10 mm thick timber.
Floor	10mm timber, 90mm thick (R 2.0) insulation with reflective foil on one side, test panels
Window	Double glazing window.



Fig. 7-4. View of the test huts at site

#### 7.2.3.2. Measurements

The test huts were equipped with a set of thermocouples, which are connected to a data acquisition system and continuously monitored and recorded the temperature variation during the test period. The temperature measurements were collected at an interval of 3 minutes. The temperature accuracy of the thermocouples was rated as  $\pm 0.05^{\circ}\text{C}$ , according to the specifications of the manufacturer. The temperature sensors were attached at the interior surface of the west wall, east wall and floor to measure the surface temperatures as well as at the geometric center of the test hut to measure the indoor temperature.

The weather conditions of the site location were measured by using a Wireless Vintage Pro 2 weather station from Davis Instruments. The weather station was mounted on a pole at an elevation of approximately 10 m from the ground. It was ensured that the weather station is free from any shading effects by trees and buildings. The weather station encompasses a digital thermometer for the measurement of site outdoor dry bulb temperature, humidity meter and a solar sensor for the measurement of relative humidity and horizontal global irradiance, anemometer measuring the wind speed and a wind vane for the detection of wind direction. The sensors of the weather station with the relevant accuracy of the sensors are summarized in Table 7-3. All these parameters are detected by relevant sensors and wirelessly transferred to a console unit at a regular time interval of one hour. The console unit can be located within 300m range of the weather station and should be located in a place where it is free from vandalism or theft. In this research, the console unit has been located in a nearby room at a distance of 90 m from the weather station. This unit also includes two sensors to measure the indoor thermal conditions such as dry bulb temperature and relative humidity.

The thermal performance enhancement of PCMCB compared to GPB and OCB was studied by comparing the indoor temperature and inner surface temperature variations during the test period. The reductions in peak indoor temperature and diurnal temperature fluctuations were considered as the indicators to measure the thermal performance enhancement with PCMCB in buildings.



Fig. 7-5. Meteorological station at the test site (a) weather station (b) console unit

Table 7-3 The measurement system and accuracy of Vantage Pro 2 weather station

Parameter	Unit	Measurement accuracy
Dry-bulb temperature	°C	±0.05°C
Humidity	%	±5%
Solar irradiance	W/m <sup>2</sup>	±5%
Wind speed	m/s	±5%
Rain rate	mm/h	±1 mm/h

## 7.2.4. Thermal performance of PCMCB in buildings

### 7.2.4.1. *Building description*

The experimental studies conducted with the laboratory scaled prototypes and test huts are to assess the thermal performance of TESCMs compared to typical construction materials such as cement mortars and gypsum plasterboards. However, direct extrapolation of the results of experimental prototypes and test huts to real scale buildings are not feasible due to the scaled down experiments and non-consideration of internal heat gains or occupancy. As such, thermal performance enhancement of PCMCB in real scale buildings was investigated with the aid of a numerical approach.

A multi-storey office building, as shown in Fig. 7-6, was considered for the refurbishment with PCMCB. It is considered to be a typical office building construction, consisting of a concrete structure frame enclosed by large glazed facades with brick-veneer partition walls separating the offices. Movable blinds are also operated when the incident solar radiation on the glazing exceeds  $200 \text{ W/m}^2$ . The main façade of the building is due west and each room is 4 m by 4 m, with a floor to floor height of 3 m. The detailed construction elements and relevant thermophysical properties of the building materials are given in Table 7-4 and Table 7-5, respectively. The thermophysical properties of typical construction materials were derived from previous studies conducted on Australian buildings [100, 141].

With reference to our numerical approach, three different case studies were simulated for the weather scenario similar to Melbourne, Australia during the period of 22-26 January:

- Case 1: the building without refurbishment
- Case 2: the building refurbished by means of OCB as interior surface plastering mortar of brick walls
- Case 3: the building refurbishment by PCMCB as interior surface plastering mortar of brick walls

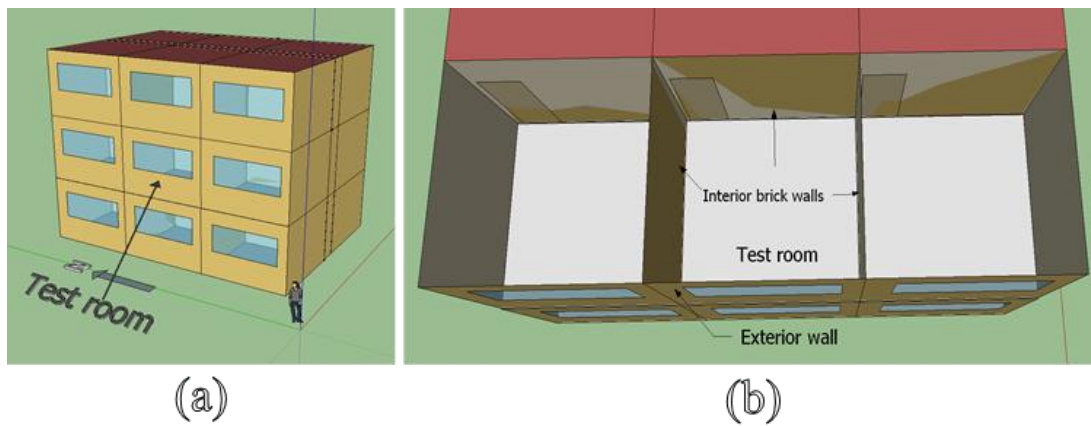


Fig. 7-6. Simulated building model (a) thermal zones of the house (b) test room details

Table 7-4 Construction materials/elements of multi-storey office building

Surface	Description
Exterior walls	110-mm thick brick veneer construction internally finished with OCB/PCMCB
Floors and ceilings	200 mm thick non-insulated concrete, rendered by 10 mm cement mortar and surface finished with floor carpets
Roof	Flat roof with concrete roof tiles
Windows and shadings	4 mm thick double glazing windows with an aluminum frame. Internal venetian blinds are operated when the incident solar radiation exceeds 200 W/m <sup>2</sup>
Doors	Timber doors (50mm thickness)

Table 7-5 Thermophysical properties of building materials

Building materials	Thermophysical properties			
	Thickness (m)	Conductivity (W/(m.K))	Density (kg/m <sup>3</sup> )	Specific heat (J/(kg.K))
Concrete	0.100	1.42	2400	880
Bricks	0.110	0.61	1690	878
Roof tiles	0.02	1.42	2400	880
Carpet	0.02	0.0465	104	1420
Timber doors	0.05	0.16	1122	1260
OCB	0.016	2.16	2056.3	890
PCMCB	0.016	1.07	1244.2	1790

#### 7.2.4.2. Numerical approach

The thermal performance assessment was carried out with the aid of numerical simulation method since the experimental analysis in large scale buildings is difficult to achieve due to limited resource availability. Furthermore, with the recent developments in advanced energy simulation tools, thermal performance assessments in buildings incorporated with PCM have become a reality with a wide variety of application methods in the buildings. In this regard, dynamic thermal simulations were performed by using building energy and thermal load simulation software EnergyPlus v8.5. EnergyPlus is chosen for the numerical approach because it is highly accredited thermal simulation tool and has been successfully used for the evaluation of energy efficiency and thermal performance of buildings incorporated with PCMs [13].

EnergyPlus uses one-dimensional conduction finite difference (CondFD) algorithm for building materials having variable thermophysical properties, such as PCMs. The CondFD algorithm can be chosen in between two different schemes such as the Crank-Nicholson scheme or a fully implicit scheme as described in Literature review of this thesis. In this research, a fully implicit CondFD scheme, as illustrated in Eq. (7-1), was adopted. It is first order in time and uses a user-defined enthalpy-temperature function

to account for phase change process [Eq. (7-1)]. The EnergyPlus assures that the temperature dependent specific heat capacity (C) is updated at every iteration according to effective heat capacity calculated from the enthalpy-temperature function as depicted in Eq.(7-2).

$$C\rho\Delta x \frac{T_i^{j+1} - T_i^j}{\Delta t} = \left( k_W \frac{(T_{i+1}^{j+1} - T_i^{j+1})}{\Delta x} + k_E \frac{(T_{i-1}^{j+1} - T_i^{j+1})}{\Delta x} \right) \quad (7-1)$$

$$C = \frac{h_i^j - h_i^{j-1}}{T_i^j - T_i^{j-1}} \quad (7-2)$$

With reference to Eq. (7-1) and (7-2), “C” and “ρ” are the temperature dependent specific heat capacity and density of the material, respectively. “T” and “h” are node temperature and user defined specific enthalpy as a function of node temperature, respectively, “i” is the node being modelled, where “i+1” and “i-1” are referred to the adjacent nodes in the directions of inner and outer sides of the building structure, respectively. “k<sub>E</sub>” and “k<sub>W</sub>” are thermal conductivities of interfaces between nodes of “i-1” and “i” and between nodes “i” and “i+1”, respectively. “j” and “j-1” are the simulation time step and previous time step, respectively.

It should be highlighted that extensive verification and validation studies have been performed by many researchers [133-136, 141] as well as the EnergyPlus developer team [117, 118], to create robust and reliable numerical models with PCMs. For example, Tabares-Velasco et al. [117] calibrated the EnergyPlus v7.2 model with experimental results and proposed the following guidelines for accurate prediction of PCM module in EnergyPlus:

- Time step should be equal to or shorter than three minutes
- Finer refinement (node spacing of 1/3 of default value is recommended) should be used for the accurate prediction of hourly results
- PCMs with strong hysteresis could lead to inaccurate results when modeled.

To model the phase change process of PCM in EnergyPlus software, the temperature dependent thermophysical properties such as the enthalpy-temperature function of PCM is required. In this study, enthalpy of PCMCB was derived from the DSC

thermograph and defined as a set of enthalpy-temperature pairs. Fig. 7-7 shows the enthalpy-temperature curve of PCMCB.

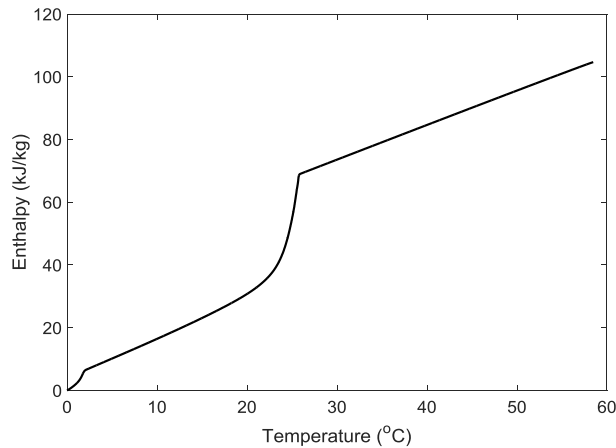


Fig. 7-7. Enthalpy temperature curve of PCMCB

Building simulations were conducted for the climate zone of Melbourne using the representative meteorological year (RMY) weather files generated by EnergyPlus. The interior and exterior surface convective heat transfer algorithms selected were TARP and DOE-2 respectively, from EnergyPlus [182]. TARP was developed by Walton with a comprehensive model for exterior convection by combining the correlations reported in ASHRAE and flat plate experiments reported from sparrow et al.[183] with the consideration of variable natural convection from the surface to indoor air based on the temperature difference. The heat transfer process between the floor and ground was modeled through the “GroundHeatTransfer: Slab” model given in EnergyPlus. An infiltration rate of 0.5 ACH was considered through an effective leakage area model. The ventilation models were developed by introducing a scheduled night ventilation profile operated between 22:00 to 07:00 at the air circulation rate of 8 ACH.

As far as the boundary conditions of the test room are concerned, the exterior wall of the test room (i.e. west wall) is exposed to outdoor. The north and south walls connect to a series of identical rooms facing west. Furthermore, the space behind the rooms is occupied by a corridor area connecting another series of identical rooms facing east. It is assumed that all rooms generate equal internal heat gains with the same occupancy rate. The main properties of the test room are reported in Table 7-6. The building thermal simulations were conducted for the run period of 22-26, January to represent the typical summer days and to compare with the prototype experimental study.

Table 7-6 Test room properties

Parameter	Value
Test room dimensions	4 x 4 x 3 m
Floor area	16 m <sup>2</sup>
Window size	3 x 1.2 m
Door size	0.8 x 2 m
Occupancy time	From 07:00 to 19:00
Occupancy rate	0.14 people/m <sup>2</sup>
Lights	2.5 W/m <sup>2</sup>
Electrical appliances	50 W/m <sup>2</sup>
Blinds operation	Open when incident solar radiation on the glazing exceeds 200 W/m <sup>2</sup>

#### 7.2.4.3. Analysis method

The analysis method was defined to measure the thermal performance enhancement of PCM application as interior surface plastering mortars in buildings in improving the indoor thermal comfort conditions. Two indicators, based on the indoor thermal conditions, were chosen to evaluate the thermal performance of PCM incorporated building envelopes.

- (1) Indoor operative temperature ( $T_{OPE}$ , °C): As defined by the weighted average of indoor air dry bulb temperature and mean radiant temperature of the enclosing surfaces as depicted in Eq. (7-3)

The indoor operative temperature measurements provide an accurate evaluation of improvement in indoor thermal comfort conditions as previously shown [12, 13]. For example, ASHRAE adaptive thermal comfort model [122] has the mean comfort zone band of 5°C for 90% acceptability and 7°C for 80% acceptability, both centered around the optimum comfort temperature ( $T_{conf}$ ) as determined from Eq.(7-4). In other words, thermal comfort conditions with 80% acceptability are met when  $T_{OPE}$  falls in the bandwidth of  $T_{conf} \pm 3.5^{\circ}C$ .

$$T_{OPE} = \gamma T_{MRT} + (1 - \gamma) T_{drybulb} \quad (7-3)$$

$$T_{comf} = 0.31 T_{a,out} + 17.8 \quad (7-4)$$

where  $T_{OPE}$ : Indoor operative temperature (°C),  $T_{MRT}$ : Mean radiant temperature (°C),  $T_{drybulb}$ : Indoor air temperature (°C),  $T_{comf}$ : Optimum comfort temperature (°C) and  $T_{a,out}$ : Mean monthly outdoor air temperature (°C). In this equation, the radiative factor  $\gamma$  depends on the air velocity and for low air movement conditions (air velocity lesser than 0.2 m/s), the typical value of 0.5 will apply as recommended in ISO 77300 [184].

- (2) Inner surface convective heat gain rate ( $q$ , W/m<sup>2</sup>) is the heat energy transferred by the indoor air to the interior surfaces by means of convection. The convective heat transfer energy is determined based on the classic convection model as shown in Eq. (7-5):

$$q = h_c \times A \times (T_{surf} - T_{air}) \quad (7-5)$$

where  $h_c$  is the inner surface convective heat transfer coefficient and it is calculated from the inside surface heat transfer algorithm (TARP) defined in EnergyPlus.  $T_{surf}$  and  $T_{air}$  are inner surface temperature and indoor air temperature respectively.  $A$  is the opaque surface area.

The positive values of  $q$  indicate that the heat is being added to the surface whereas negative values indicate that the heat is being extracted from the surface. The application of PCMCB as internal surface plastering mortar of the building walls will lead to increased TES capacity such that the heat energy transferred to the indoor air will be reduced during the daytime. Therefore, inner surface convective heat gain rate offers the evaluation of thermal performance enhancement in terms of reduced heat transfer rate to indoor air, thus improving the thermal comfort sensations experienced by indoor occupants.

## 7.3 Results and discussions

### 7.3.1. Thermal performance assessment of prototypes

#### 7.3.1.1. *Under summer day climatic conditions*

The monitored indoor temperature variations in the prototypes along with the outdoor air temperature for summer climatic conditions similar to Melbourne, Australia is shown in Fig. 7-1. It can be observed that, throughout the test period, the peak indoor temperature in the PCMCB test cell was lower than OCB and GPB test cells. For the first day, the PCMCB test cell showed a reduction of 1.3°C in peak indoor temperature, compared to the GPB test cell. However, the OCB test cell showed similar behavior to PCMCB on the same day. In fact, the maximum outdoor temperature registered on the first day was about 26°C, which was not sufficient to activate the fully exploit the latent heat capacity. It is likely for this reason that we observed similar indoor temperature behavior between PCMCB and OCB test cells on this day.

Nevertheless, a significant reduction in peak indoor temperatures was observed when the outdoor air temperature exceeded the melting phase transition temperature of PCM. For instance, a maximum reduction in peak indoor temperature of 2.8°C and 1.5°C was observed on the 5<sup>th</sup> day of the experiment, compared to GPB and OCB test cells respectively. The minimum indoor temperature in the PCMCB test cell was also increased by 1.2°C on the same day, due to the latent heat discharge at night. Furthermore, it is interesting to note that the daily temperature amplitude inside the GPB prototype cell was 17.5°C (between 36°C and 18.5°C) on the 5<sup>th</sup> day of experiment, whereas the PCMCB test cell showed a significantly lower internal temperature amplitude of 12.5°C (between 33.25°C and 20.75°C), revealing the isothermal energy storage of PCM.

The delay between peak outdoor temperature and peak indoor temperature, as defined by time lag, registered as approximately 3 hours and 4.5 hours for the GPB test cell and PCMCB test cell respectively. Hence, there were approximately 1.5 hours higher time lag in the PCMCB test cell throughout the testing period. This increased time lag in the PCMCB test cell suggests that the application of such interior surface coatings in buildings can help to shift the peak cooling energy demands to off-peak periods.

However, the current comparison study does not provide the complete benefits of PCM integrated cementitious composites as the maximum outdoor temperatures were close to the melting temperature of PCM on most days and, hence, a full exploitation of PCM was not evident.

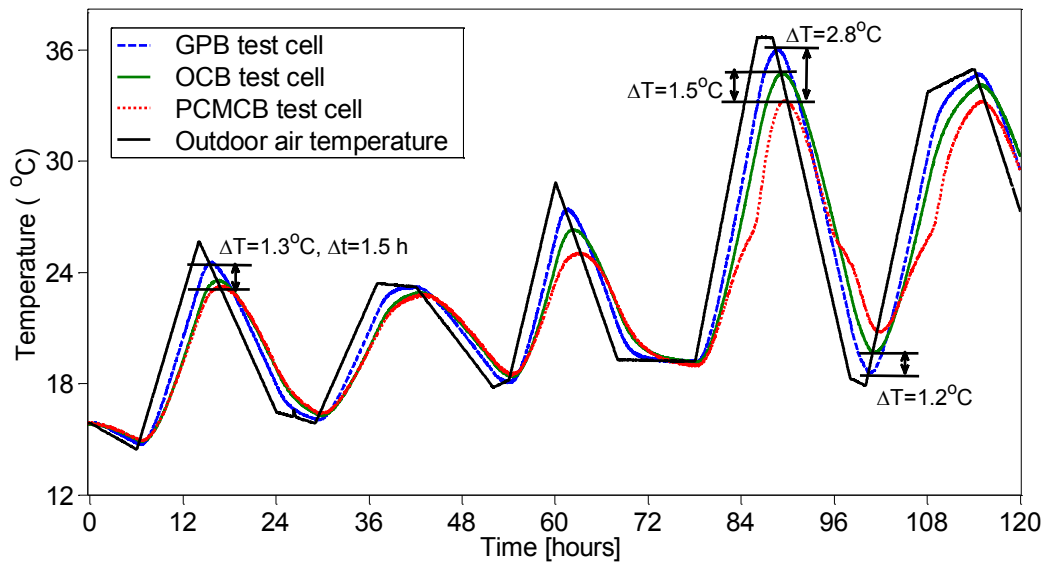


Fig. 7-8. Indoor temperature variation during typical summer days

### 7.3.1.2. Under summer design day climatic conditions

To operate a complete exploitation of PCM in the prototypes and to allow adequate time to solidify the PCM at night, two consecutive summer design days were assumed, having the diurnal temperature variation between 15°C and 35°C. Fig. 7-9 shows the indoor temperatures registered for the summer design days scenario in the prototype cells along with the outdoor air temperature. Again, we observed that the peak indoor temperature in the PCMCB test cell was lower than OCB and GPB test cells. However, a significant reduction in peak indoor temperature was now evident, as the higher outdoor temperature activates a full exploitation of PCM with the provision of sufficient time for the operation. This is particularly demonstrated by the peak temperature reduction of 4.43°C in the PCMCB test cell compared to the GPB test cell over two consecutive days. Moreover, the melting heat transfer behavior of PCM is clearly seen in this experiment. The temperature evolution in the PCMCB test cell indicates a temperature plateau when the internal temperature exceeds 26°C, which is the melting onset temperature of RT-27 paraffin used in this study.

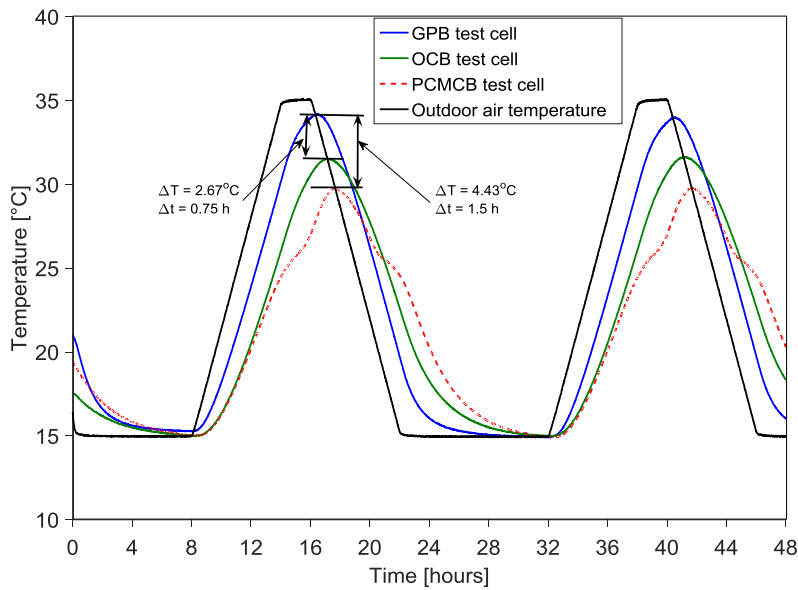


Fig. 7-9. Indoor temperature variation during summer design days

### 7.3.2. Thermal performance assessment of test huts

#### 7.3.2.1. Overview

The temperature monitoring of the test huts during five months period (01/10/2016 to 01/03/2017) resulted in a large amount of data collection that provides the insights of the influence of PCM integrated cement mortars (known as PCMCB in this case) over typical building materials such as GPB and OCB. However, reporting such large amounts of data would be difficult. Thus, the comparison of PCMCB with GPB and OCB is analyzed and reported for eight (08) consecutive days. It must be noted that, in all cases, the behavior of PCMCB can be distinguished into three situations based on the melting heat transfer behavior of PCM (i.e. 25-27°C) as described below:

1. The PCM was not thermally activated throughout the day, as the outdoor temperature or solar irradiance was not sufficient to increase the PCM surface temperature above 25°C.
2. The PCM was thermally activated during the day and returned back to the solid phase during the night, as of high daytime temperature/ solar irradiance and low night temperature.
3. The PCM was thermally charged during the day and stayed in the melted phase during the night, because of sufficient daytime temperature/ solar irradiance and high night temperature.

The analysis period was chosen to show some or all of these above-mentioned PCM behaviors and to compare with GPB and OCB. In this regard, thermal performance assessment of PCMCB with GPB and OCB were analyzed for the period of 08-15, November 2016 and 14-22, January 2017 respectively.

### 7.3.2.2. *Thermal performance assessment of PCMCB with GPB*

During the time period of 08-15 November 2016, the measured temperatures of the west wall, floor and indoor air for GPB and PCMCB test huts are shown in Fig. 7-10, Fig. 7-11 and Fig. 7-12 respectively. Table 7-7 summarizes the diurnal temperature amplitude of these temperatures. Inspection of the figures reveals that, throughout the eight consecutive days, the wall and floor surface temperatures as well as indoor air temperature in PCMCB incorporated test hut was lower than the GPB test hut. Considering the west wall surface temperature as an example, the GPB test hut reached the peak inner wall surface temperature above 30°C for four days, although outdoor air temperature rarely reached 22°C. This attributes to high solar irradiance during the daytime that enters through the window. The PCMCB test hut, however, achieved a lower peak wall surface temperature throughout the test period. For example, the reduction in peak wall surface temperatures of up to 2.1°C and 2.4°C were observed on the first and second day, respectively. However, the PCM was completely charged only on the first and fourth day of the test period as the surface temperature exceeded 27°C. The surface temperature reduction on other days attributed to partial latent heat storage, high sensible heat storage and high thermal resistance of PCMCB, compared to GPB. Moreover, Table 7-7 reveals that the PCMCB not only reduced the peak temperature but increased the daily minimum temperatures due to the discharge of stored latent heat. This ultimately reduces the diurnal temperature fluctuations in indoor, thus improving the indoor thermal comfort.

Although a significant reduction in surface temperatures was achieved in first five days of the test period, the effect of PCM was not evident on following three days. This attributes to the first situation of PCM behavior explained above, where outdoor air temperature or solar irradiance was not sufficient to thermally activate PCM. Thus, the reduction in peak indoor temperature and diurnal temperature fluctuations were not significant during these days. A minor improvement was evident as high sensible heat

capacity and high thermal resistance (low thermal conductivity) of PCMCB assisted in reducing the peak temperatures.

On the other hand, the floor temperature variation, as displayed in Fig. 7-11, indicates that the day time temperatures of the floor made of GPB can exceed 40°C due to direct solar radiation falls on the floor through the window. However, PCMCB incorporated test hut reveals that the floor surface temperatures can be limited within the melting temperature range due to the exploitation of latent heat capacity. Moreover, peak temperature attained by floor was lower the wall surface temperature in PCMCB incorporated test hut. This can be explained by that the floor surface was exposed to solar irradiance for a shorter duration, compared to the walls. Thus, the temperature rise in the floor would be lesser than the temperature increment of wall surfaces.

The comparison of indoor air temperature variation as depicted in Fig. 7-12 shows that the indoor air temperature behavior was quite similar to the wall surface temperatures within the test huts, due to the smaller volume of test huts and hence, heat balance between surfaces and indoor air can be attained quickly. The peak indoor temperature in the PCMCB test hut was found to be significantly lower than the GPB test hut. This attributes to the LHTES of PCM incorporated into cement mortars, thus significantly improving the indoor thermal conditions. However, both test huts had reached very high peak indoor temperatures of up to 30-35°C, though the peak outdoor air temperature was about 18-25°C. Such high indoor temperatures are due to inadequate ventilation and infiltration (i.e. air leakage) into these test huts, leading to overheating of indoor. Such overheating issues are not present in real buildings as buildings have adequate ventilation and infiltration mechanisms with the use of windows, doors and mechanical ventilation systems. In any case, the main purpose of this test hut experiment was to compare the thermal performance enhancement of PCMCB with traditional construction materials and not to assess the performance enhancement in real buildings.

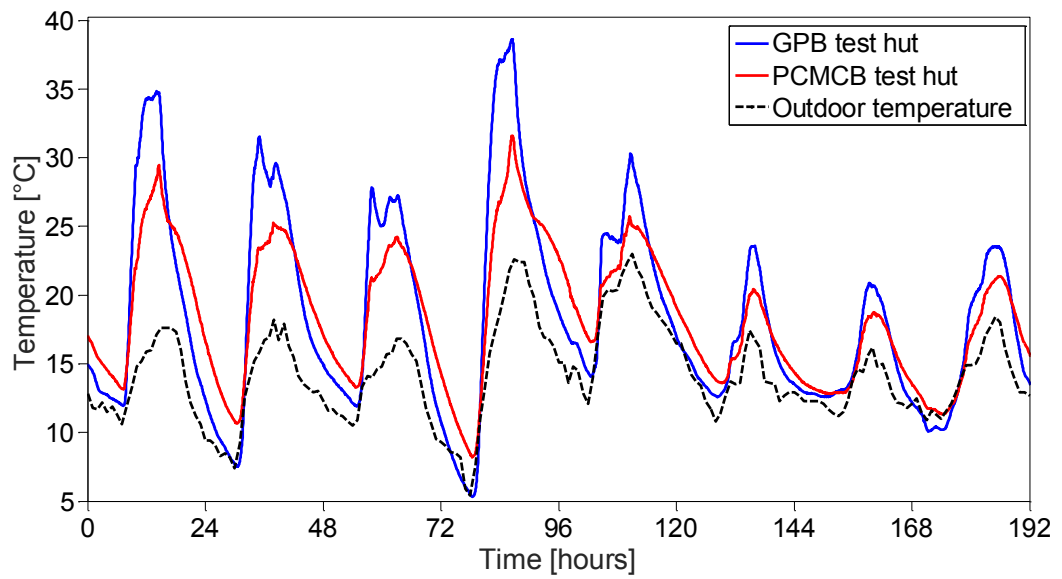


Fig. 7-10. West-wall surface temperature in GPB and PCMCB test huts

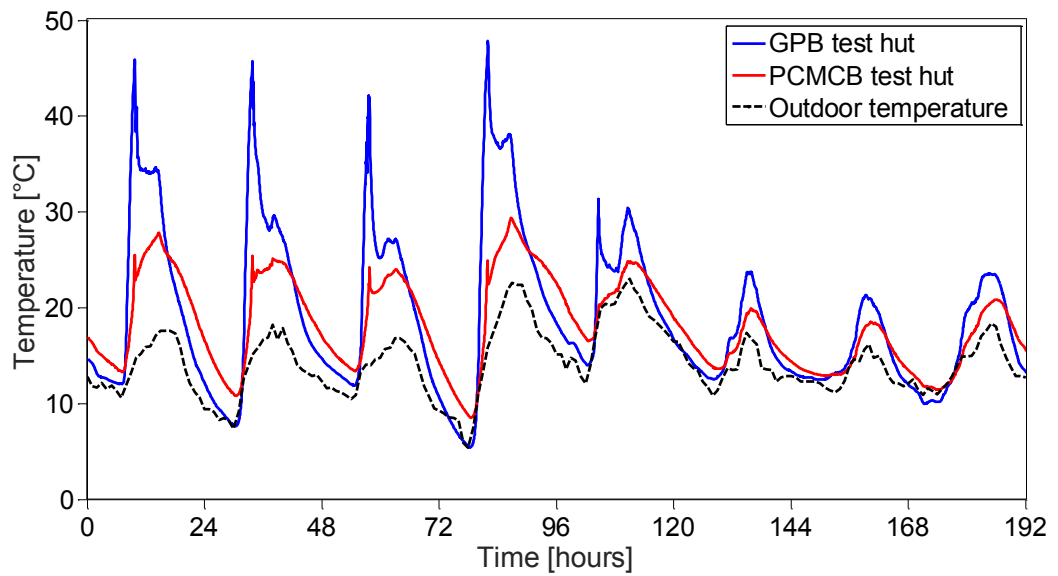


Fig. 7-11. Floor surface temperature in GPB and PCMCB test huts

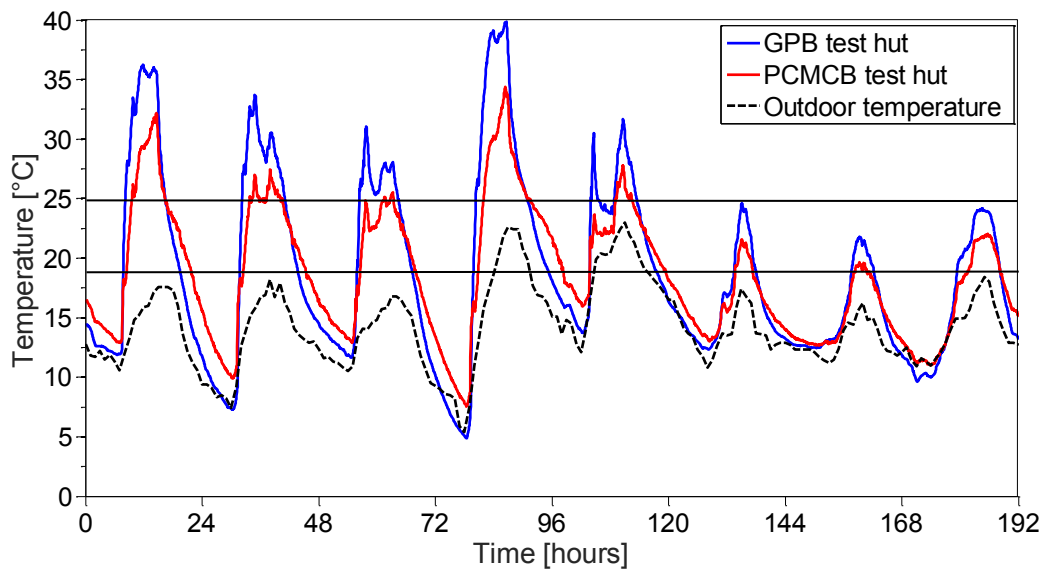


Fig. 7-12. Indoor air temperature in GPB and PCMCB test huts

Table 7-7 Diurnal temperature amplitudes in GPB and PCMCB test huts

Date	Test hut: GPB			Test hut: PCMCB		
	Min-Max (°C)			Min-Max (°C)		
	West-wall	Floor	Indoor	West-wall	Floor	Indoor
8-Nov	22.9	33.8	24.4	18.3	16.3	14.5
9-Nov	24.0	38.0	26.5	15.2	14.6	14.6
10-Nov	16.8	31.3	20.7	11.4	11.0	10.9
11-Nov	33.3	42.4	35.0	25.1	23.4	20.9
12-Nov	16.3	17.4	18.0	9.2	9.1	8.3
13-Nov	11.0	11.2	12.3	7.0	6.8	6.3
14-Nov	8.5	9.1	9.8	6.3	6.0	5.6
15-Nov	13.5	13.6	14.6	10.3	10.0	9.4

### 7.3.2.3. *Thermal performance assessment of PCMCB with OCB*

In the former comparison study of PCMCB with GPB, the peak temperatures and diurnal temperatures fluctuations were showing large differences between two test huts, indicating that the PCMCB works very well compared to GPB. In this section, a comparison between the test huts made of OCB and PCMCB are compared. During the period of 14-21 January 2017, the measured temperatures of the west wall, floor, and indoor air are displayed in Fig. 7-13, Fig. 7-14 and Fig. 7-15 respectively. Table 7-8 summarizes the diurnal temperature amplitudes on wall and floor surfaces as well as indoor air temperatures for both test huts. From figures, it can once more be noticed that the PCMCB test hut assures the reduction in peak indoor and surface temperatures compared to the OCB test hut.

When comparing the temperature measurements of the west wall and floor surfaces as shown in Fig. 7-13 and Fig. 7-14 respectively, the reduction in peak surface temperature was only significant on first, second and eighth days. In these days, the maximum surface temperature reached in the OCB test hut was approximately 30°C which is adequate to thermally activate the PCM in the PCMCB test hut. Thus, the surface temperatures in the PCMCB test hut were significantly lower than OCB test hut. During the other days, the peak surface temperature measurements were higher than 30°C and hence, the PCM was completely melted during a shorter period and becomes ineffective. Moreover, it was also observed that the minimum surface temperature of the PCMCB test hut was higher than the OCB test hut due to latent heat discharge of PCM. For instance, the minimum wall and floor surface temperatures were increased by up to  $2.2\pm 0.3^{\circ}\text{C}$  during this period.

On the other hand, the inspection of indoor air temperature as illustrated in Fig. 7-15 reveals that the PCM was found to be effective when the maximum indoor temperature reached around 30°C. The PCM becomes ineffective when the maximum indoor temperature reached higher than 30°C. This is demonstrated by comparing second (02<sup>nd</sup>) and eighth (08<sup>th</sup>) days of the test period with third (03<sup>rd</sup>) and fourth (04<sup>th</sup>) days, where the days with maximum indoor temperature around 30°C [second (02<sup>nd</sup>) and eighth (08<sup>th</sup>) days] were resulted in the reduction of peak indoor temperature by approximately 2.2°C, compared to just about 0.5°C on other days. It can be concluded, therefore, the PCM incorporation into interior surface element can be very effective when the maximum

indoor temperature exceeds 2-3°C above PCM melting temperature. Furthermore, significantly higher peak indoor temperature above PCM operating temperature will result in rapid melting process and completely melted within a shorter period, thus become ineffective in reducing the peak indoor temperature and diurnal temperature fluctuations. In this regard, future studies are required to consider the incorporation of multiple PCMs with different melting points into cementitious materials, so that the particular PCM becomes thermally active when the indoor thermal conditions are favorable to it.

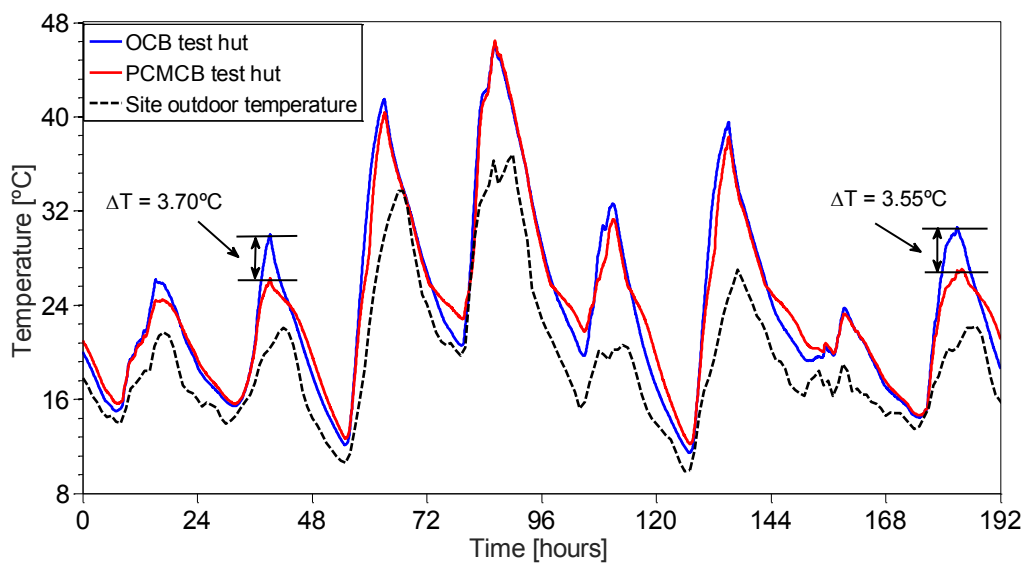


Fig. 7-13. West-wall surface temperature variation in OCB and PCMCB test huts

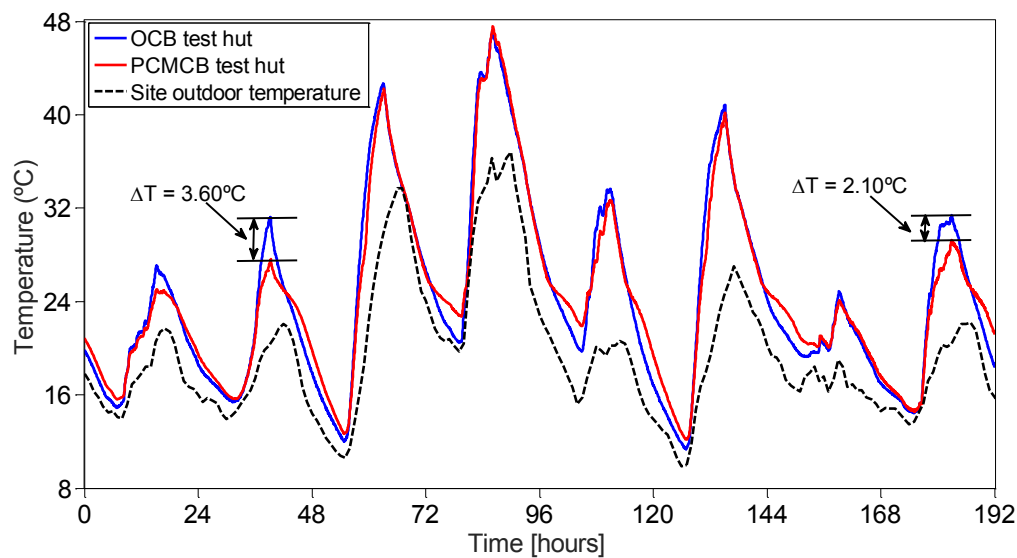


Fig. 7-14. Floor surface temperature variation in OCB and PCMCB test huts

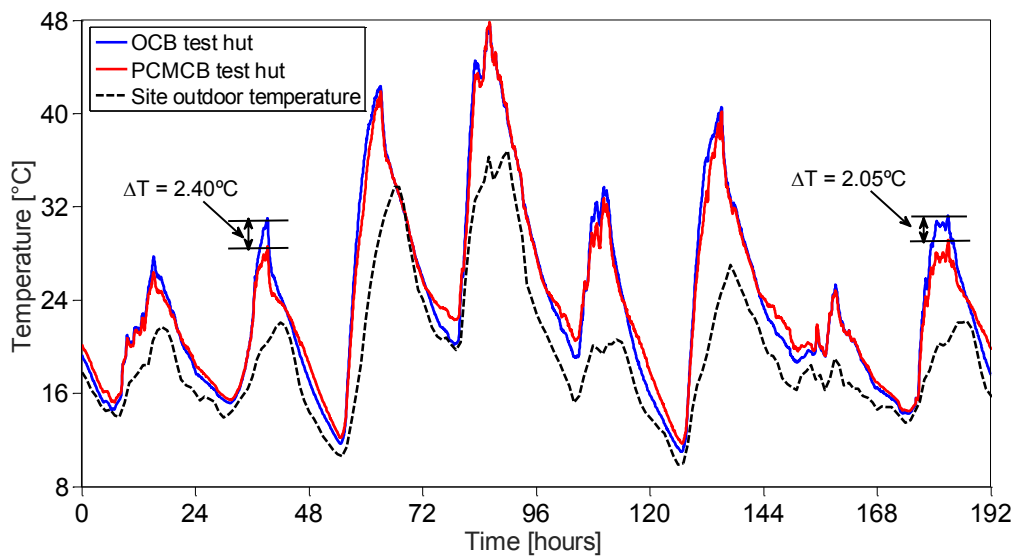


Fig. 7-15. Indoor air temperature variation in OCB and PCMCB test huts

Table 7-8 Diurnal temperature amplitudes in OCB and PCMCB test huts

Date	Test hut: OCB			Test hut: PCMCB		
	Min-Max (°C)			Min-Max (°C)		
	West-wall	Floor	Indoor	West-wall	Floor	Indoor
14-Jan	11.2	12.2	13.2	8.9	9.5	11.2
15-Jan	14.6	15.9	15.8	10.7	12.0	13.2
16-Jan	29.4	30.6	30.7	27.7	29.6	29.7
17-Jan	25.6	26.8	27.3	23.6	24.9	25.5
18-Jan	15.4	16.6	17.7	11.5	12.9	14.7
19-Jan	28.1	29.5	29.5	26.1	28.0	28.5
20-Jan	7.4	7.7	8.8	7.5	7.3	7.9
21-Jan	16.2	16.9	16.9	12.4	14.7	14.7

### 7.3.3. Thermal performance assessment of PCMCB in buildings

#### 7.3.3.1. *Under summer climatic conditions*

The prototype test cells and test hut experiments showed that the application of PCMCB as interior surface coatings of building walls could potentially reduce the indoor temperatures, resulting in increased thermal comfort. However, direct extrapolation of prototype experimental results to real scale buildings is not feasible due to the significantly scaled-down experiments used in prototype test cells as well as the inadequate ventilation in test huts. As such, thermal performance enhancement of PCMCB in real scale buildings was investigated with the aid of a numerical approach.

The thermal performance enhancement was assessed for the climatic conditions similar to Melbourne, Australia during five consecutive days of 22-26, January. Fig. 7-16 and Fig. 7-17 shows the performance enhancement of PCMCB refurbishment in the test room in terms of indoor operative temperature and inner surface convective heat gain rate respectively. Inspection of Fig. 7-16 reveals that the effect of PCM refurbishment in reducing the indoor operative temperature was significant on some days whereas PCMCB had an insignificant effect on other days. For example, the effect of PCM refurbishment was not evident on the second and third day of the run period due to the lower outdoor air temperature and/or solar radiation on these specific days, such that the thermal energy transferred to PCM layer was not sufficient to exploit the latent heat capacity. This is further verified by reporting the internal wall surface temperatures, as shown in Fig. 7-18. Fig. 7-18 shows that the maximum PCM layer temperature was close to the melting temperature of PCM during this period, which is not sufficient to activate the PCM latent heat storage. Similar behavior was also observed in the laboratory made prototype experimental study for the same period.

A significant reduction in indoor operative temperatures was observed on the next two days. The building refurbishment with PCMCB reduced the peak indoor operative temperature by up to 1.25°C and 2.1°C on 25<sup>th</sup> and 26<sup>th</sup> of January, respectively. Furthermore, the significant contribution of latent heat storage of PCMCB was revealed during these two days, as the building refurbishment with OCB resulted in approximately 0.45°C and 0.7°C respectively. In addition, the diurnal temperature fluctuation was reduced for building refurbishment with PCMCB during these two days,

indicating the reduced thermal discomfort sensations observed by occupants. This confirms the importance of latent heat storage in improving the indoor thermal comfort in buildings.

The effect of PCM refurbishment in reducing the peak indoor operative temperature was not reflected on the first day (22 January), although the peak indoor temperature was above the PCM melting temperature. By contrast, the PCM CB refurbishment reduced the indoor operative temperature after reaching the peak temperature, as observed in Fig. 7-16. This is because of the significant deviation between indoor air temperature and wall surface temperatures, leading to lower wall surface temperatures even when the indoor air temperature is very high. More information can be gathered by comparing the indoor air temperature and inner surface temperature depicted in Fig. 7-16 and Fig. 7-18 respectively. The comparison of these two temperature profiles reveals that the wall surface temperature was below the PCM melting temperature (i.e. 26°C) when the indoor temperature reached its peak and hence, PCM was not activated until this time. Furthermore, the wall surface temperature exceeds 26°C once the indoor passed its peak temperature, resulting in a reduction in the indoor temperature after this time.

These results suggest that, even if the indoor operative temperature exceeds the PCM melting temperature, the PCM CB would be less effective due to a large deviation in indoor and wall surface temperatures. This is particularly true in passive buildings where no mechanical ventilation systems are utilized and the convective heat transfer between indoor air and inner surfaces is very low, leading to significant variations in indoor and inner surface temperatures. Furthermore, large façade surfaces in office buildings also lead to increased heat transfer through windows, which cause a higher indoor air temperature compared to surface temperatures. It can be said, therefore, the effectiveness of PCM as interior surface elements in passive buildings require adequate ventilation to improve the convective heat exchange between surfaces and indoor air.

On the other hand, the effect of PCM refurbishment on the heat transfer through the walls was demonstrated with the inner surface convective heat gain rate measurements as shown in Fig. 7-17. The  $q$  values showed positive heat gain during the daytime, indicating that the interior surface element receives thermal energy from the indoor air. In fact, during the mid-day, the indoor air heats up more quickly than surfaces due to the direct solar radiation coming through the windows. Once the indoor air heated up,

the TES of building walls gradually absorbs thermal energy from the indoor air which, in turn, prevents the further increment in indoor temperature. Compared to an ordinary building (building without refurbishment) and a building refurbished with OCB, PCMCB refurbishment showed significantly larger amounts of convective heat gain rates during the warmest days (first and fourth day). The maximum heat gain rate on the first and fourth day was 120W and 90W respectively for PCM refurbishment, compared to 50W and 5W for the ordinary building.

In contrast, the performance of PCMCB refurbishment in enhancing the convective heat gains was not evident on the fifth day, despite the interior surface temperature reached above PCM melting temperature. This is due to a high indoor temperature on the previous night (i.e. fourth day), that resulted in poor cold storage or solidification of the PCM layer. The minimum indoor temperature on the fourth day was 26.1°C, which is not sufficient to completely solidify the PCM, and therefore, the LHTES availability on the next day was significantly low. It should also be noted that the outdoor air temperature on the fourth night was reported to be as low as 18°C. This is a major limitation of the PCM application as an interior surface element in buildings, since the high night indoor temperature limits heat discharge of PCM and prevents solidification. To overcome this limitation, cool outdoor air should be circulated to the indoors at night to improve the discharge process of PCM. This method is called night ventilation and has been widely investigated as an effective mechanism to improve cold storage of PCM [185-187].

The PCMCB refurbishment also showed an insignificant improvement in convective heat gain rates during the second and third day. The PCM has not been thermally activated on these days, due to inadequate solar thermal energy solicited by low outdoor air temperature and/or solar irradiance.

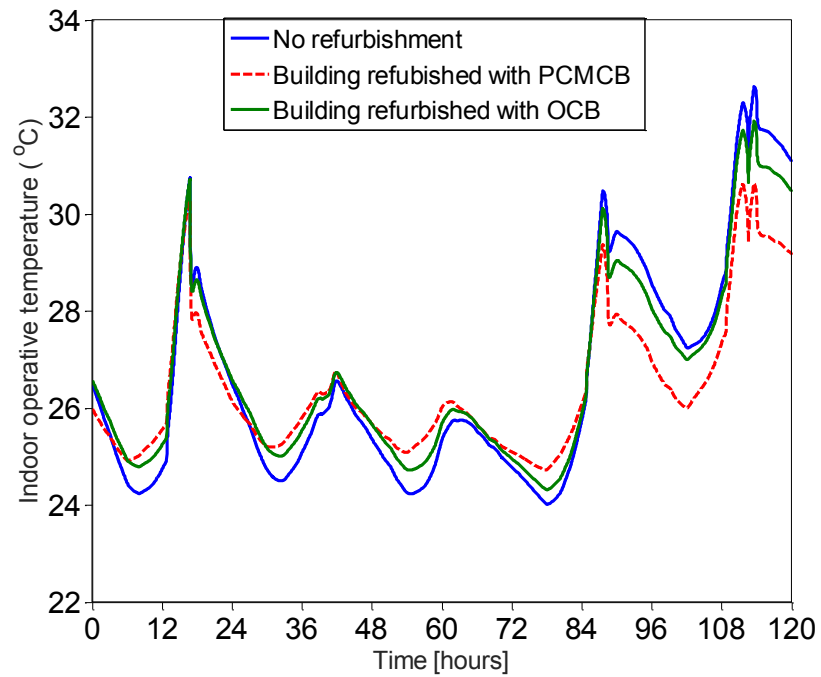


Fig. 7-16. Indoor operative temperature variation in the test room

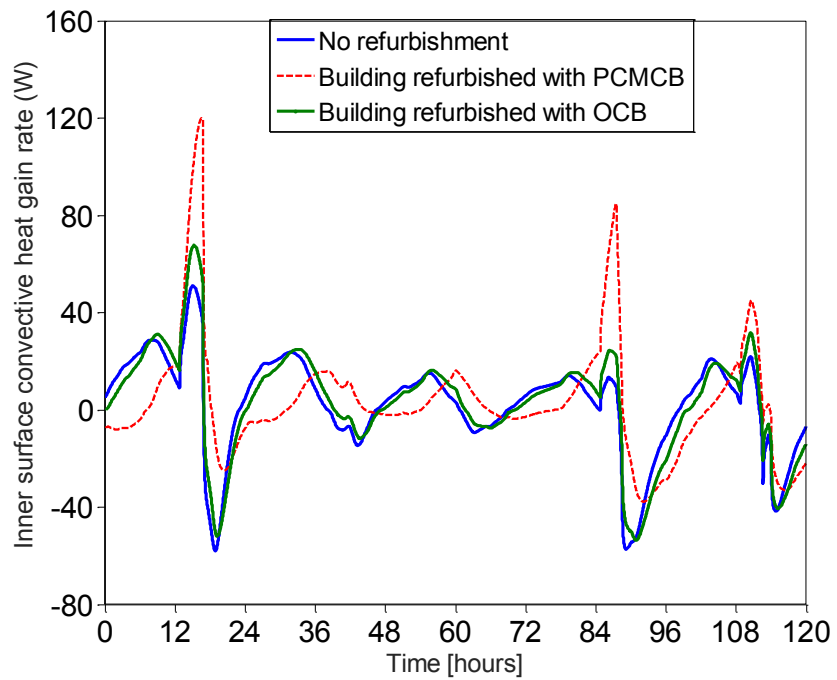


Fig. 7-17. Variation of inner surface convective heat gain rates

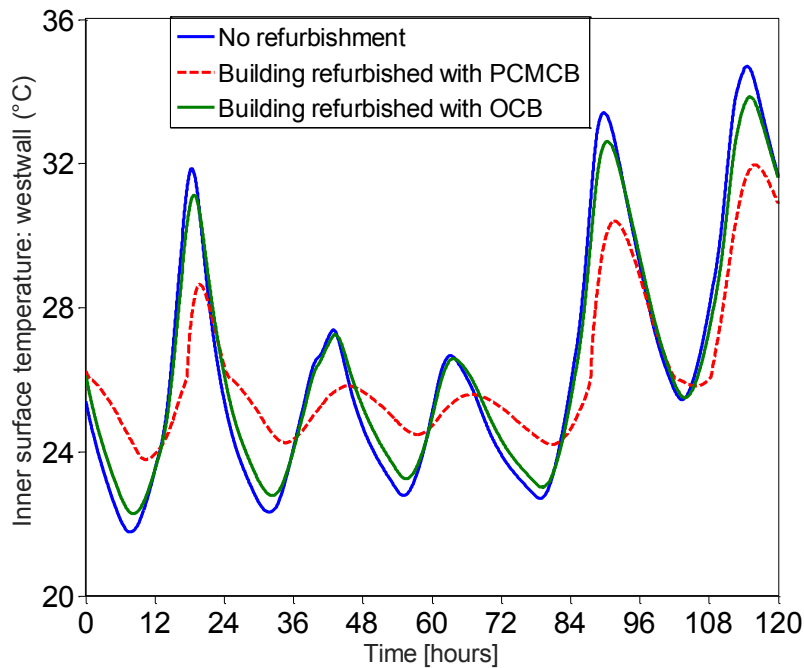


Fig. 7-18. Inner surface temperature variation of the exterior wall (west wall)

### 7.3.3.2. Thermal performance enhancement of PCMCB combined with night ventilation

In attempting to maximize the diurnal heat storage and to improve latent heat discharge at night, PCM incorporated building was operated with night ventilation. A mechanical night ventilation of 8 air circulation per hour (ACH) during the time interval of 22:00-07:00 was operated. A building without refurbishment was also studied for the activation of night ventilation to distinguish the effect of night ventilation in improving the latent heat storage of PCM. The results pertaining the indoor operative temperature variation for combined application of PCMCB refurbishment with night ventilation are illustrated in Fig. 7-19.

The figure shows that the cooling potential of PCM was significantly improved with the operation of night ventilation, as it further reduced the peak indoor operative temperature. In particular, the effect of night ventilation can be clearly seen on the fourth and fifth day where the peak indoor operative temperatures were reduced by up to 1.8°C and 3.4°C, compared to the building without refurbishment. Furthermore, such reductions were not reflected for the operation of night ventilation without PCM refurbishment, indicating that the night ventilation had a significant influence on latent

heat storage. It is also evident that the operation of night ventilation has resulted in lower indoor operative temperatures throughout the second and third day, compared to building refurbished with PCMCB only. Therefore, the incorporation of PCM as interior surface coatings in passive buildings has limited thermal performance enhancement due to poor heat discharge/solidification at night. However, such poor heat discharge issues can be reduced by introducing night ventilation, which can improve the solidification process of PCM.

The inner surface temperature variation of the exterior wall (west wall) of the test room was also plotted for different cases in Fig. 7-20. The surface temperature measurements showed that, for the studied period, the application of night ventilation further reduced the PCM surface temperature throughout the simulation period. Particularly, the activation of night ventilation limited the PCM operation within the melting range of PCM on the first day as the maximum surface temperature was lower than the end-set melting temperature of the PCM. This is explained by the adequate heat discharge on the previous night, therefore, a large amount of latent heat storage can be operated. However, the surface temperature measurements differed significantly from the indoor operative temperature during daytime. Again, this can be attributed to inadequate ventilation during the daytime, which results in reduced heat transfer performance from PCM surfaces to indoor air. Further research studies are required to focus on effective natural ventilation mechanisms in passive buildings to provide higher heat transfer performance between PCM surfaces and indoor air to improve the heat transfer performance of PCM. Nonetheless, the issues related to poor cold storage or solidification process of PCM can be successfully eliminated with the application of natural night ventilation.

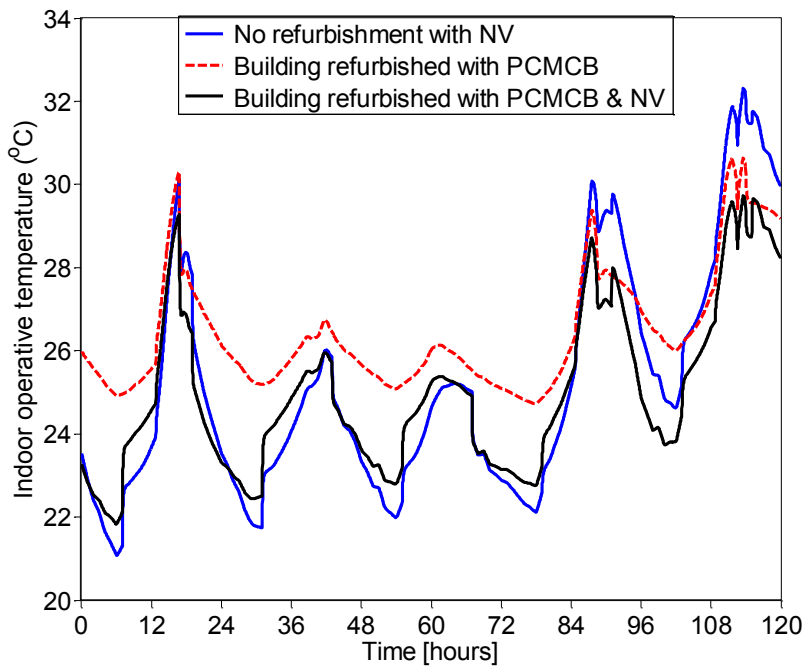


Fig. 7-19. Effect of night ventilation on indoor operative temperature variation

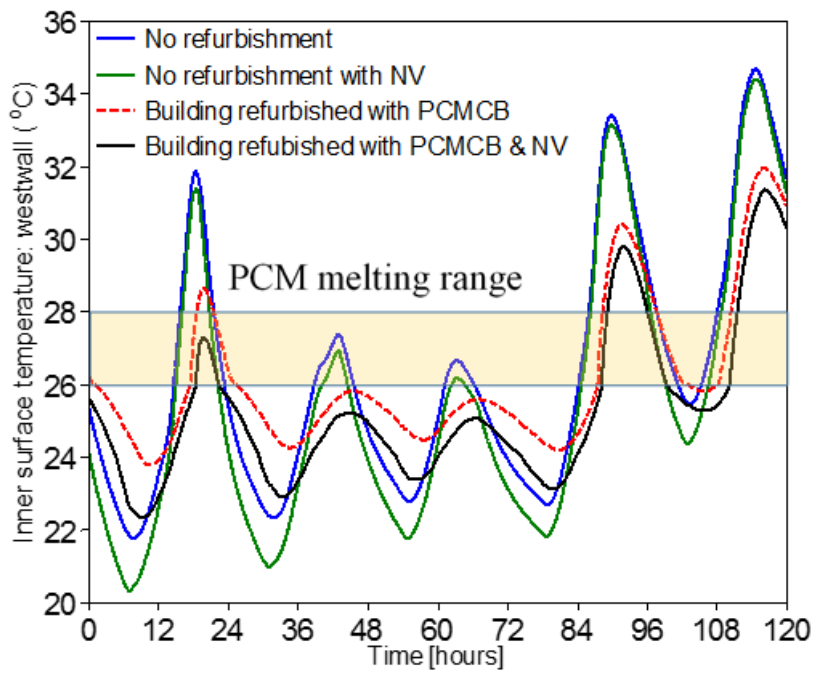


Fig. 7-20. Effect of night ventilation on inner surface temperature of exterior wall (west wall)

## 7.4 Concluding remarks

This chapter presented a comprehensive experimental and numerical investigation of the thermal performance enhancement of cement mortars containing EPOP form-stable PCM composite. The investigations were conducted on PCM integrated cement boards (PCM CB) containing 80% substitution level of fine aggregate with PCM composite. A series of experiments and numerical simulations were performed to demonstrate the thermal performance enhancement of PCM CB, as compared to the behavior of ordinary cement mortar boards (OCB) or those commercially available gypsum plasterboards (GPB). The experimental study utilized prototype test cells subjected to controlled climate conditions and test huts exposed to the outdoor environment. The numerical simulations were performed to evaluate the potential application of PCM CB as interior surface coatings in buildings. Based on the presented experimental and numerical study, following conclusions can be drawn:

1. The prototype test cell made with PCM CB as interior surface element showed the highest reduction in peak indoor temperature and the largest attenuation of the external thermal amplitudes on its indoor, compared to the prototypes made with GPB and OCB. For example, a maximum reduction of 2.8°C and 4.43°C was observed during the summer days and summer design days respectively, compared to the GPB test room.
2. Test huts exposed to outdoor climatic conditions showed that the PCM CB test hut resulted in significant reduction in peak indoor temperature and diurnal temperature fluctuations compared to GPB test hut. The comparison study of PCM CB with OCB revealed that the significance of PCM CB could be observed when the peak indoor temperature reached 2-3°C above the phase transition temperature of PCM. Very high peak indoor temperature resulted in rapid melting of PCM and its effectiveness in reducing the indoor temperature became insignificant.
3. Numerical simulations performed on a multi-storey office building refurbished with PCM CB and OCB revealed that the application of PCM CB in passive buildings could reduce the peak indoor operative temperature by up to 2.5°C. Indeed, such PCM performance is largely affected by poor latent heat discharge at night, due to high night indoor temperature

4. The heat discharge of PCM can be significantly improved by introducing night ventilation, where the outdoor air is circulated into the indoor during cooler nights. It was found that the combined application of PCM CB and night ventilation can further reduce the peak indoor operative temperature, resulting in increased thermal comfort sensations experienced by occupants. This is particularly demonstrated by the indoor operative temperature reduction of up to 3.4°C for the combined application of PCM CB and night ventilation, as opposed to 2.5°C with PCM CB alone.

# Chapter 8 Parametric analysis for performance optimization of buildings incorporated with phase change materials

---

## 8.1 Introduction

The thermal performance optimization of LHTEs with PCM is vital to provide maximum beneficial effects of PCM in buildings in order for improving the indoor thermal comfort and energy efficiency. Particularly, with the increasing interest in various PCM application methods in passive buildings, the thermal performance optimization of such buildings become very important. However, although passive buildings enable a wide variety of PCM incorporation methods, its thermal performance evaluation would be very difficult as they do not consist active heating/cooling system to provide direct measurements.

As a consequence, studies that are evaluating the performance of PCM in passive buildings were mainly relied on the indoor temperature variation and hence indirectly measuring the improvement in indoor thermal comfort conditions. Furthermore, many studies used thermal comfort theories to evaluate the performance enhancement of PCM incorporated buildings, by measuring the improvement in indoor thermal comfort conditions compared to a building without PCM. In addition to thermal comfort assessment, new performance indicators were also proposed in few research as described in Literature review of this thesis.

However, as also pointed out by several researchers [12, 16], even if several criteria are identified to measure the thermal performance of passive buildings, there is still a lack of proper indicators to carry out an optimized PCM design in buildings. Moreover, previous research studies have primarily focused on the performance enhancement of PCM in improving indoor thermal comfort conditions, whilst the storage efficiency of

PCMs has not been adequately addressed. Here, storage efficiency is defined as the diurnal latent charging and discharging capability of PCM compared to its latent heat capacity. It must be stressed at this point that the thermal performance of PCM should be evaluated considering the combined effects of latent heat storage efficiency of PCM and enhancement in indoor thermal comfort conditions.

In this regard, we introduce latent heat storage efficiency of PCM as a thermal performance criterion that should be studied in terms of the diurnal latent charge and discharge operation of PCM. More precisely, a PCM storage system that stores a smaller fraction of its latent capacity or that discharges partially is not useful. Therefore, amounts of diurnal energy storage and discharge become as important factors of PCM efficiency. In addition to the energy storage and discharge, the operational period of a PCM thermal storage system in daily cycles also becomes another important factor that influences the storage efficiency. Indeed, a PCM layer that reaches its capacity in a relatively shorter period is not suitable, as it is not utilized for the entire day. Furthermore, a PCM system that stays in the solidified state or completely melted state is also not preferred. A PCM layer that transits from one phase to another for a long duration means that it operates efficiently in daily cycles. Therefore, operational periods of charge and discharge become another set of factors of PCM efficiency. Although these factors were addressed by Evola et al. in his study [12], separate consideration of their effect would not reflect the efficiency of PCM. It is necessary to develop an indicator by combining these factors together to propose an optimized storage efficiency of PCM.

On the other hand, optimal storage efficiency of PCM does not necessarily meet the optimum indoor thermal comfort conditions. Thus, the effectiveness of PCM in improving indoor thermal comfort becomes another performance criterion.

From these performance criteria, it emerges that the thermal performance of PCM in buildings should be evaluated considering both the latent energy storage efficiency of PCM and improvement in indoor thermal comfort conditions. On this basis, this chapter presents a design optimization method of PCM incorporation in passive buildings. The development of performance indicators coupled with the formulation of such indicators in numerical simulation method is discussed in methodology. The design optimization study was conducted on a single-storey residential house with the incorporation of a commercially available macro-encapsulated PCM, the so-called Bio-PCM™, in between

the ceiling insulation and plasterboard of the living zone. A parametric case study was also conducted to identify the influence of thermophysical properties of PCM and night ventilation performance on the PCM storage efficiency and effectiveness. The case study considers four major climate zones in Australia: Melbourne, Sydney, Perth, and Brisbane.

## 8.2 Methodology

### 8.2.1. Building description

The performance optimization of PCM was carried out with the systematic parametric analysis by installing PCM into a standard Australian single storey residential house shown in Fig. 8-1 and Fig. 8-2. This house model was chosen for the case study because it is one of the eight sample house models used to evaluate the building energy efficiency rating in Australia [188-190]. The residential house mainly consists of four bedrooms, a living room, a kitchen/dining area, a laundry and a bathroom. The gross floor area of the house is 232 m<sup>2</sup> and it is reported to have 5-star energy rating according to the Australian standard energy rating scheme developed by NatHERS (Nationwide house energy rating system). NatHERS determines the energy rating according to the annual operative energy consumption according to local climatic conditions and compares with the energy bandwidth assigned to the number of stars in the scale of 0 to 10. The star rating achieved by each house mainly depends on the building geometry and orientation, construction materials and components, and local climatic conditions. The detailed building materials and construction elements are given in Table 8-1 and the thermophysical properties of these materials are reported in Table 8-2.

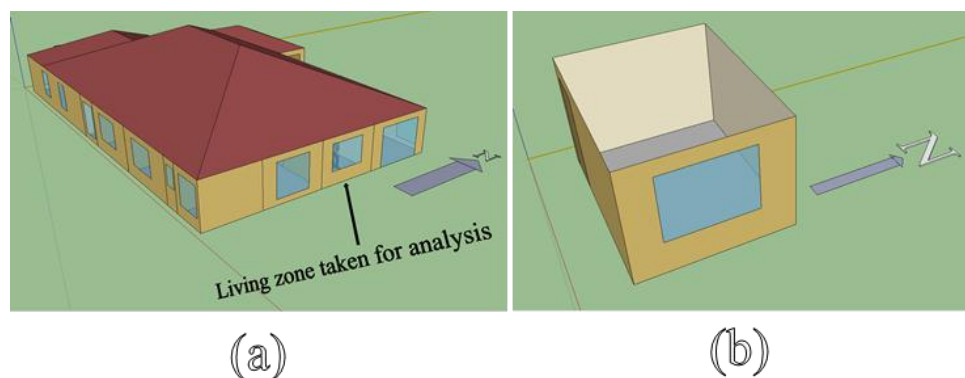


Fig. 8-1. (a) Residential house for case study (b) living zone taken for analysis

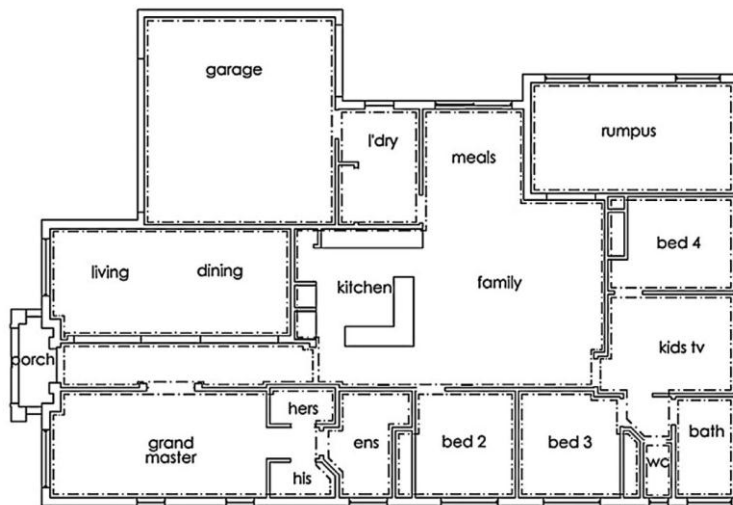


Fig. 8-2. Floor plan of the residential house

Table 8-1 Construction materials/elements of residential house

Surface	Description
Exterior Wall	Brick veneer construction, R1.0 insulation to the cavity and 10 mm wall plasterboard to the internal surface.
	Garage walls: Brick veneer, no insulation (air gap) to the cavity and 10 mm plasterboard to internal surface
Floor	Concrete slabs on ground carpeted directly to the floor
Roof	Pitched roof with concrete roof tiles
Ceiling	Flat ceiling having 13 mm ceiling plasterboard and R3.5 insulation; PCM installed between insulation and plasterboard
Window	Single glazed aluminum framed windows
Door	Timber doors (50mm thickness)

Table 8-2 Thermophysical properties of building materials

Building materials	Thermophysical properties			
	Thickness (m)	Conductivity (W/(m.K))	Density (kg/m <sup>3</sup> )	Specific heat (J/(kg.K))
Concrete	0.100	1.42	2400	880
Brick veneer	0.110	0.61	1690	878
Roof insulation	0.044	0.044	12	883
Roof tiles	0.02	1.42	2400	880
plasterboard	0.013	0.17	847	1090
Carpet	0.02	0.0465	104	1420
Timber doors	0.05	0.16	1122	1260
Bio-PCM	0.0125	0.2	235	2400

The parametric case study was defined as installing a macro-encapsulated PCM (Bio-PCM™) in the ceiling of the living room in between ceiling insulation and plasterboard. The Bio-PCM™ consists of refined fatty acids in square pouches and produced as mat-form. The parametric analysis considers the commercially available Bio-PCM™ with three different standard melting temperatures of 23°C, 25°C and 27°C with the corresponding melting range of 22-25°C, 24-27°C and 26-29°C respectively. However, with the purpose of exploring the optimum phase transition temperature for TES applications, two additional melting temperatures were assumed as 29°C and 31°C with the melting temperature ranges of 28-31°C and 30-33°C respectively. Regarding the quantity of PCM application, it is available in three different sizes of 1.5, 2.7 and 4.9 kg/m<sup>2</sup> with the corresponding equivalent thickness of 7.5, 12.5 and 21 mm respectively.

The size of the living room is 4 m x 4 m x 3 m (floor area of 16 m<sup>2</sup>) and it consists one south facing door and a window on the east wall. The dimensions of the window are 2.5 m x 1 m and consists of a 3-mm single glazing window with an aluminum frame. The internal venetian blinds are also operated whenever the incident solar radiation exceeds 200 W/m<sup>2</sup> and kept open all other time. The effect of night ventilation in the efficiency and effectiveness of PCM was studied by introducing natural ventilation into the living

zone during the period of 22:00 to 07:00. The main properties of the test room are reported in Table 8-3. The building simulations were mainly focused on the living room with PCM incorporation, but living room without PCM layer was also simulated to compare the performance enhancement of PCM application in terms of improvement in indoor thermal comfort.

Table 8-3 Test room properties

Parameter	Value
Test room size	4 x 4 x 3 m
Floor area	16 m <sup>2</sup>
Window size	2.5 x 1 m
Door size	0.8 x 2 m
PCM surface area	16 m <sup>2</sup>
Occupancy time	From 07:00 to 22:00
Occupancy rate	0.0625 people/m <sup>2</sup>
Lights	2.5 W/m <sup>2</sup>
Electrical appliances	1.875 W/m <sup>2</sup>
Window opening	Open when indoor temperature exceeds 26°C
NV rate	From 0 to 8 ACH
NV operation period	From 22:00 to 07:00, unless outdoor temperature exceeds 26 °C

### 8.2.2. Development of performance indicators

As described in the Introduction of this chapter, the factors that are influencing the efficiency of PCM during its operational stage are identified as the diurnal latent storage and the duration of operation. Therefore, the efficiency of PCM during the diurnal charging and discharging operations, as defined by *cooling efficiency coefficient (CE)* and *heating efficiency coefficient (HE)*, were formulated with respect to these factors as shown in Table 8-4. In addition to efficiency, the effectiveness of PCM in improving the indoor thermal comfort is measured by the ASHRAE Adaptive thermal comfort model, a well-defined thermal comfort theory used throughout the world.

Table 8-4 Factors influencing the performance indicators

Performance Indicators	Variables	
	Diurnal storage capacity	Diurnal activation period
Cooling efficiency coefficient ( <i>CE</i> )	Latent charge fraction ( $L_C$ ): Effective diurnal latent energy storage based on latent capacity	Charging duration ( $T_C$ ): Latent energy storage duration based on daytime
Heating efficiency coefficient ( <i>HE</i> )	Latent discharge fraction ( $L_{DC}$ ): Effective diurnal latent energy discharge based on latent capacity	Discharging duration ( $T_{DC}$ ): Latent energy discharge duration based on night-time
Effectiveness coefficient ( <i>e</i> )	ASHRAE Adaptive thermal comfort model status based on occupancy period	

Here, parameters  $L_C$  and  $L_{DC}$  reports the fraction of diurnal latent heat charge and discharge of the PCM thermal storage system as a result of melting and freezing processes respectively. It is well known that a TES system that stores a smaller portion of its capacity would not be effective or economical as the cost associated with the development of a TES system would be very high. Therefore, the larger value of  $L_C$  represents that the TES system operates more efficiently. On the other hand, a LHTES system is expected to solidify a greater amount from the melted stage so that there is a large amount of TES available for next day. In this regard, a higher value of  $L_{DC}$  is

favorable in a LHTES system. The quantified value of  $L_C$  and  $L_{DC}$  can be determined as follows:

$$L_C = \frac{\text{diurnal latent charge}}{\text{latent heat capacity}} \quad (8-1)$$

$$L_{DC} = \frac{\text{diurnal latent discharge}}{\text{latent heat capacity}} \quad (8-2)$$

While the effective storage capacity of PCM is prime important in a LHTES system, its operation period should not be ignored. A PCM storage system that is operated for a longer period in a day provides isothermal energy storage for a longer time. In this case, parameters that are corresponding to charging and discharging durations are introduced and quantified by following equations:

$$T_C = \frac{\text{charging duration (minutes)}}{\text{Day time (= 720 minutes)}} \quad (8-3)$$

$$T_{DC} = \frac{\text{discharging duration (minutes)}}{\text{Night time (= 720 minutes)}} \quad (8-4)$$

It is assumed that the TES system required to be charged and discharged during the day- and night time and hence, the respective time frames for these variables are assigned as 720 minutes (i.e. 12 hours in a day).

It is worth noting here that the charging/ discharging behavior of a PCM storage system largely depends on the outdoor thermal conditions and thus, the exploitation of latent heat may not occur for 12 hours every day. Nevertheless, an ideal LHTES system is assumed to store the thermal energy during the day and discharges completely at night to provide diurnal energy storage behavior in buildings. Here,  $T_C$  and  $T_{DC}$  determines how closely real PCMs behave to idealized conditions which will eventually bring maximum benefits to buildings and its occupants.

By combining the factors influencing the *cooling efficiency coefficient (CE)* and *heating efficiency coefficient (HE)*, the formulas for these parameters can be assigned as follows:

$$CE = \sqrt{L_C \times T_C} \quad (8-5)$$

$$HE = \sqrt{L_{DC} \times T_{DC}} \quad (8-6)$$

While the efficiency coefficients represent how efficiently PCM storage systems are operated diurnally, their effectiveness in improving the indoor thermal comfort should also be assessed. In this regard, another parameter which influences the effectiveness of PCM, as measured by the fraction of time in which the indoor operative temperature falls within the mean comfort zone, is defined as *effectiveness coefficient (e)*. Here, the mean comfort zone is defined as the 80% acceptability limits defined by ASHRAE adaptive thermal comfort models and the effectiveness of PCM was measured during the occupancy period of the living zone. As specified in ASHRAE 55-2010[122]:

$$T_{comf} = 0.31xT_{a,out} + 17.8 \quad (8-7)$$

$$T_{Ind} = 0.5 \times (T_a + T_r) \quad (8-8)$$

$$e = \frac{\sum_{t=1}^P TC_t}{P} \quad (8-9)$$

$$\text{where } TC_t = \begin{cases} 1 & \text{if } |T_{comf} - T_{Ind}| < 3.5 \\ 0 & \text{if } |T_{comf} - T_{Ind}| \geq 3.5 \end{cases}$$

With respect to Eq. (8-8) and (8-9),  $T_{comf}$  is the optimum comfort temperature (°C),  $T_{a,out}$  is the mean monthly outdoor air temperature (°C),  $T_{Ind}$  is the indoor operative temperature (°C),  $T_a$  is the indoor air temperature (°C) and  $T_r$  is the mean radiant temperature (°C)

### 8.2.3. Simulation procedure

The dynamic thermal simulations were performed by using building energy and thermal load simulation software EnergyPlus as explained in Section 7.2.4. The simulations were run over the summer period (December 1 to February 28) for four major climatic zones in Australia: Melbourne, Sydney, Perth, and Brisbane. The relevant weather files were obtained from Representative Meteorological Year (RMY) weather files given in EnergyPlus.

The infiltration and ventilation models were developed through the airflow network module provided in EnergyPlus. The airflow network module has the ability to accurately model forced airflow systems and wind driven airflow caused by the pressure difference. The schematic diagram of the airflow network is given in Fig. 8-3. The airflow network model excludes heating and cooling coils as this study assumes a non-air-conditioned building and the ventilation model is used solely for natural ventilation purposes. It is worthwhile to mention here that the Airflow network provided in EnergyPlus has been validated by Lixing Gu [191].

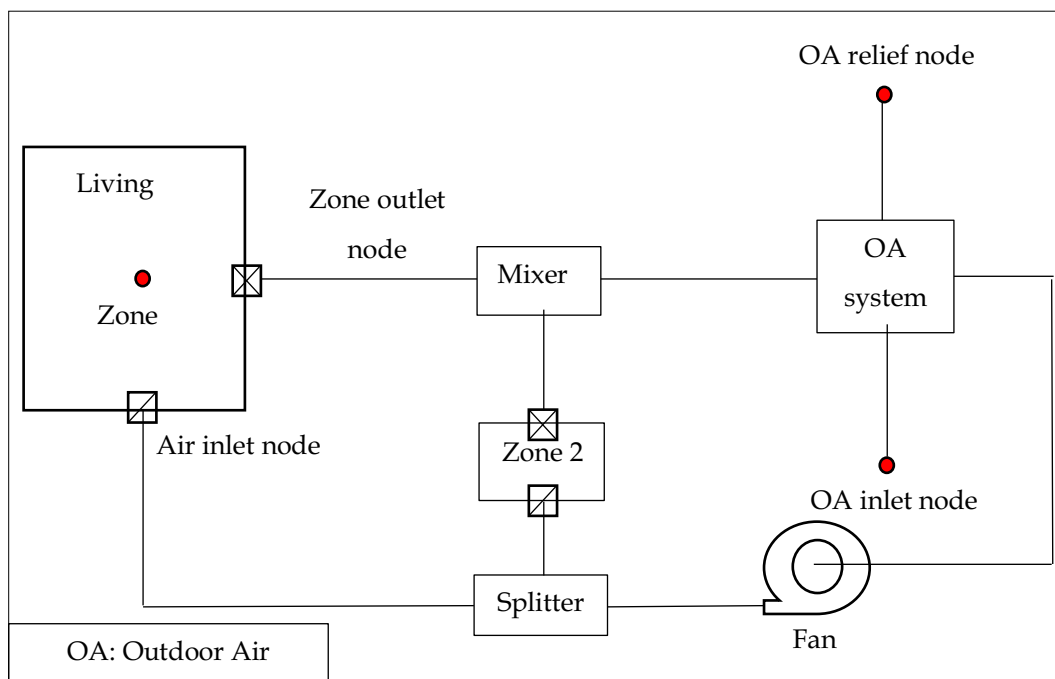


Fig. 8-3. Airflow network for night ventilation in living zone

#### 8.2.4. Derivation of performance indicators

The derivation of performance indicators defined in Section 8.2.2 requires the information about the latent heat storage behavior of PCM layer. However, EnergyPlus can only generate the output of surface energy storage and it is hard to differentiate the latent heat storage of PCM layer from the total energy storage of the ceiling surface. Thus, a new algorithm was developed to determine the latent energy storage of PCM layer in building surfaces as explained below.

As EnergyPlus can report the node temperature variation in building surfaces assigned with CondFD heat transfer algorithm, the relevant node temperature at any instant can

be correlated with the node enthalpy from the enthalpy-temperature variation (Fig. 8-4).

The latent storage of  $i^{th}$  node  $[\Delta H(i)]$  can be written as follows:

$$\Delta H(i) = \begin{cases} 0 & \text{if } T \leq T_0 \\ H(T_i) - H(T_0) & \text{if } T_0 < T \leq T_e \\ \Delta H & \text{if } T \geq T_e \end{cases}$$

The effective latent storage of PCM layer ( $\eta$ ) at any instant can be found by integrating the latent heat storage of all nodes in the PCM layer, as also shown in Eq. (8-10).

$$\eta = \sum_{i=1}^N \left\{ \frac{\Delta H(i)}{\Delta H} \right\} \quad (8-10)$$

where  $H(T_i)$  and  $H(T_0)$  are the specific enthalpy at  $i^{th}$  node and specific enthalpy at lower transition temperature ( $T_0$ ) of Bio-PCM respectively.  $\Delta H$  is the latent enthalpy of PCM layer and  $N$  is the total number of nodes in PCM layer.  $T_0$  and  $T_e$  are the onset melting temperature and end-set melting temperature respectively.  $H(T_i)$  is determined from the node temperature result reported by EnergyPlus.

In Eq. (8-10),  $\eta=0$  represents a completely solidified state and  $\eta=1$  represents a completely melted state of PCM layer. The partially charged/discharged status of PCM layer can be identified as when  $0 < \eta < 1$  as also shown in Fig. 8-5. Therefore, diurnal latent charge ( $L_C$ ) and diurnal latent discharge ( $L_{DC}$ ) can be derived from the variation of  $\eta$  in a day and can be written as,

$$L_C = \eta_{max:day} - \eta_{min:day} \quad (8-11)$$

$$L_{DC} = \eta_{max:night} - \eta_{min:night} \quad (8-12)$$

The corresponding  $T_C$  and  $T_{DC}$  can also be determined from the time interval between the  $\eta_{max}$  and  $\eta_{min}$  during the day and night respectively. These indicators were calculated from the building simulation results and then integrated for the entire summer period to represent the efficiency of PCM layer for the entire season. Similarly, effectiveness coefficient was also assessed for the whole summer period and the average value of effectiveness coefficient was considered for the performance comparison of PCM layer.

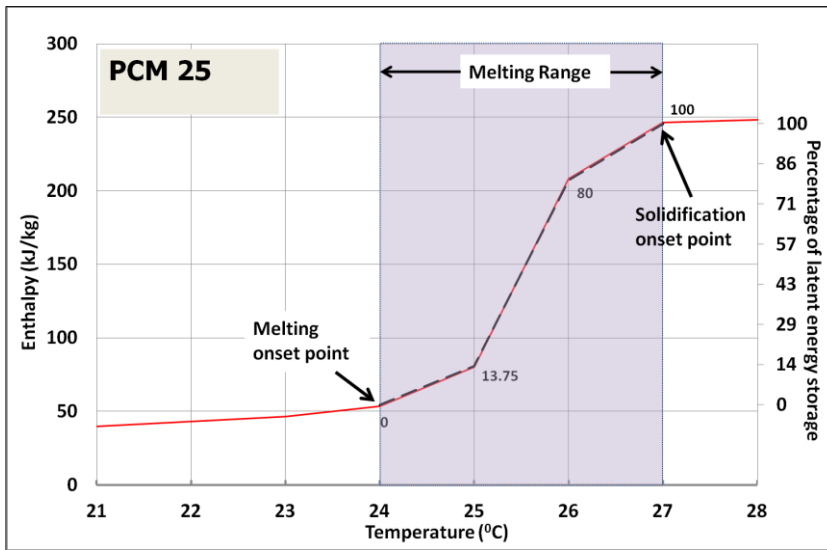


Fig. 8-4. Enthalpy temperature relationship for Bio-PCM™-25

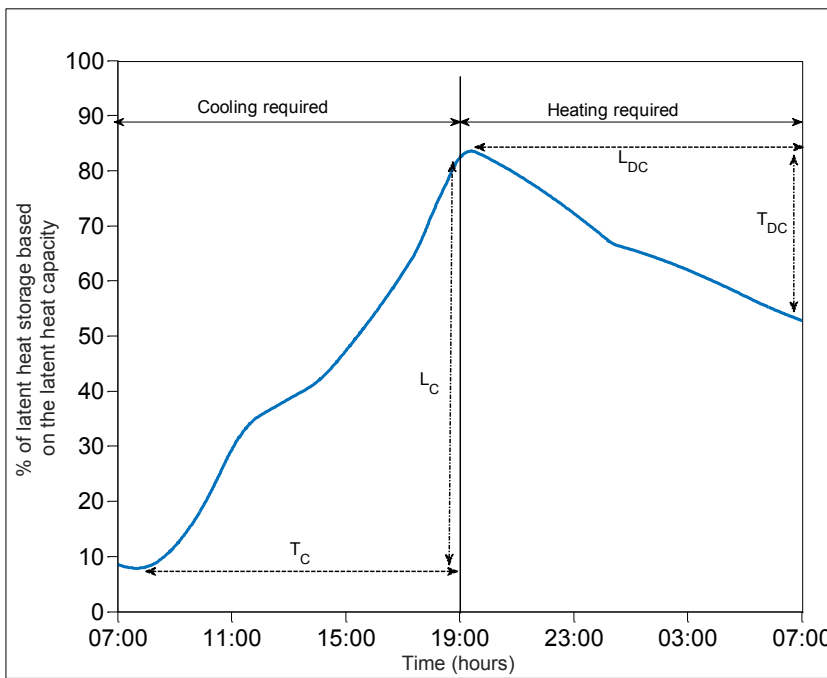


Fig. 8-5. Effective latent energy storage variation for a typical daily cycle

## 8.3 Results and discussions

### 8.3.1. Efficiency and effectiveness of PCM

A preliminary study on the diurnal efficiency and effectiveness of PCM was conducted before detailing the case study, by considering two consecutive summer days of 1-2 December in Melbourne, Australia. The Bio-PCM™ with the melting temperature and quantity of 25°C and 2.7 kg/m<sup>2</sup> were chosen for this analysis. The results pertaining the indoor operative temperature and latent energy storage behaviour of PCM layer are depicted in Fig. 8-6. As can be seen from Fig. 8-6, the incorporation of PCM yields a reduction in the peak indoor operative temperature of 1°C and 2.5°C on first and second day respectively, indicating the improvement in indoor thermal conditions. Moreover, a significant reduction in the indoor operative temperature fluctuation was also evident. For instance, the daily operative temperature fluctuation was reduced from 8.9°C and 13.9°C to 7.5°C and 11.1°C on two consecutive days respectively. This confirms the importance of latent heat storage in improving the indoor thermal comfort in buildings.

Furthermore, one can also observe that the latent energy storage behavior of PCM has a strong influence on indoor operative temperature. More precisely, the indoor operative temperature variation was similar in both cases up to the point where PCM began to store energy ( $\eta=0$ ). As the PCM starts to store the energy in the form of latent heat ( $\eta>0$ ), the rate of indoor temperature increment reduces in PCM incorporated building and the peak indoor operative temperature attained was found to lower than the case of building without PCM. Similarly, the indoor operative temperature in PCM incorporated building was slightly higher than the building without PCM when the PCM starts to discharge the latent energy. It is evident, therefore, the latent energy storage behavior can be a good indicator to measure the performance of PCM in buildings.

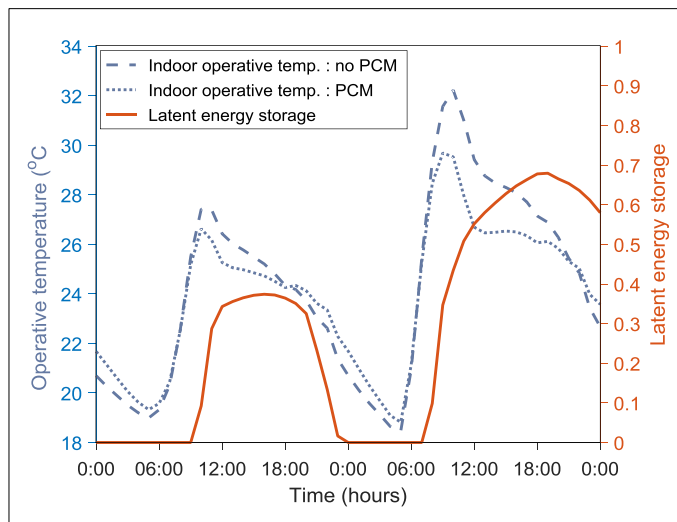


Fig. 8-6. Effect of PCM application on two consecutive days (1-2 December)

However, before reaching stable conclusions, more detailed information regarding the efficiency coefficient and effectiveness coefficient should be studied. In this regard, Table 8-5 summarizes the relevant parameters for these days. From Table 8-5, it is possible to conclude that the PCM incorporation into the building components improved the indoor thermal comfort significantly, as effectiveness coefficient ( $e$ ) increased from 0.89 to 1 and 0.23 to 0.71 during two consecutive days. However, it is also evident that the storage efficiency of PCM was very low. Diurnal latent energy storage fractions ( $L_C$ ) of 0.37 and 0.68 can be observed for those two days, and their respective operational periods ( $T_C$ ) were 0.64 and 0.76 of the daytime respectively. Thus, the cooling energy coefficient ( $CE$ ) obtained were 0.49 and 0.72 on two consecutive days, indicating the partial storage efficiency of PCM in buildings.

Table 8-5 Efficiency and effectiveness of PCM on two consecutive days (1-2 December)

Melbourne: PCM_25 (1-2, December)								
Cooling efficiency coefficient ( $CE$ )			Heating efficiency coefficient ( $HE$ )			Effectiveness coefficient ( $e$ )		
$L_C$	$T_C$	$CE$	$L_{DC}$	$T_{DC}$	$HE$	No PCM	PCM	
Day 1	0.37	0.64	0.49	0.35	0.28	0.31	0.89	1
Day 2	0.68	0.76	0.72	0.34	1	0.58	0.22	0.71

Therefore, it is clear that the incorporation of PCM into buildings had a significant enhancement in indoor thermal comfort, however, its storage efficiency should be improved. To optimize the performance of PCM in terms of its efficiency and effectiveness, it is necessary to choose optimized thermophysical properties according to local climatic conditions. To this end, a case study was undertaken by considering the thermophysical properties of PCM such as phase transition temperature, quantity and activation of a night ventilation system. Furthermore, with the consideration of optimized design during the entire summer season, the analysis was carried out over the summer period (December to February) in Australian climatic conditions, measuring the integrated average performance of efficiency and effectiveness.

### **8.3.2. Optimized phase transition temperature for local climatic conditions**

The selection of optimum phase transition temperature in a LHTES system strongly depends on local climatic conditions and can be determined with the aid of the performance indicators developed in this study. On this basis, the PCM incorporated building was simulated for the major climate zones of Australia (Melbourne, Sydney, Brisbane and Perth) for different phase transition temperatures and the optimum phase transition temperature was determined by analyzing the efficiency and effectiveness.

Fig. 8-7 shows the effect of phase transition temperature on thermal performance enhancement of PCM incorporated buildings in terms of efficiency and effectiveness. The phase transition temperature of PCM was varied between 23-31°C while assuming a constant quantity of PCM as 2.7 kg/m<sup>2</sup>. From Fig. 8-7, it is evident that the choice of phase transition temperature has significant impact on the efficiency and effectiveness of PCM for a particular climatic condition. Considering the effectiveness coefficient ( $e$ ) as a performance indicator, with the increasing phase transition temperature,  $e$  increases and reaches a maximum value. However, as the phase transition temperature further increases, the value of  $e$  reduces making such PCM as ineffective. This can be explained by the fact that increasing the phase transition temperature of PCM will result in the solidification process of that PCM at occupant comfort temperature, leading to an increased indoor operative temperature at night and thus, causing increased discomfort. This reveals that the choice of phase transition temperature should be carefully made, as

very low or very high phase transition temperature PCM results in increased thermal discomfort levels.

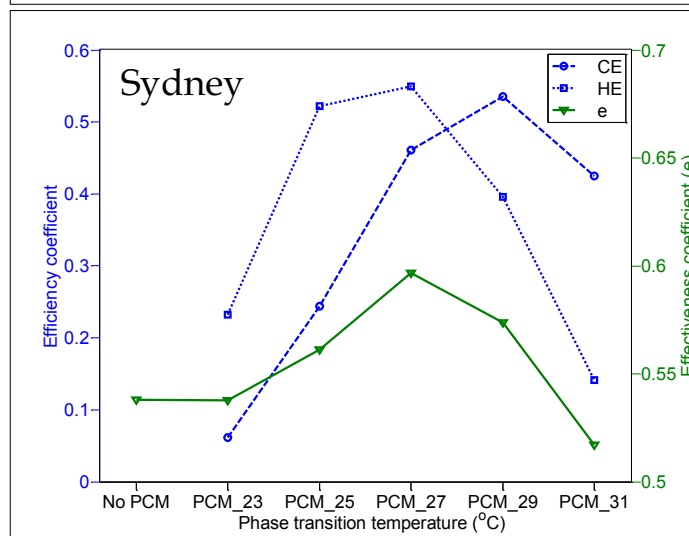
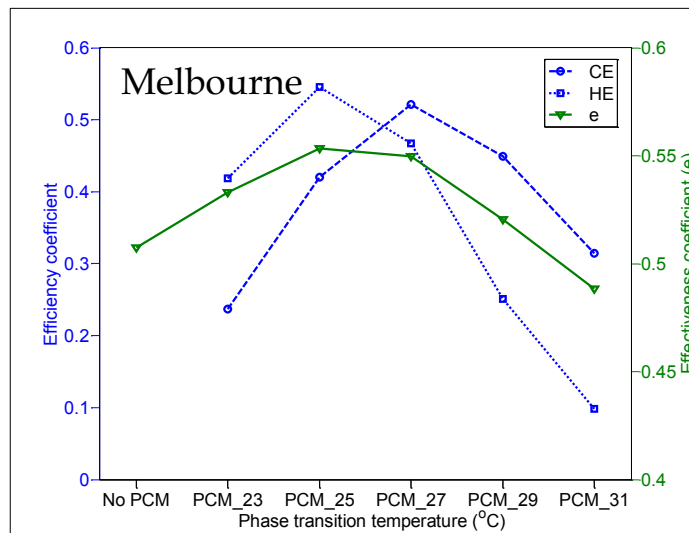
Besides, a significant variation in efficiency of PCM can also be observed with different phase transition temperature of PCM. For instance, the optimum cooling efficiency ( $CE$ ) of PCM for the climate zone of Sydney was derived as 0.54 with PCM\_27, which is much higher than the  $CE$  obtained for PCM\_23 ( $CE=0.06$ ). A similar trend of variation can be seen for all climatic conditions. In fact,  $CE$  and  $HE$  increase with increasing phase transition temperature and reaches a maximum value. Afterward, it decreases with further increase in phase change temperature.

To reveal the reasons behind such variation in efficiency, the factors that are influencing the efficiency of PCM, as identified by diurnal charge and discharge ( $L_C$  and  $L_{DC}$ ) as well as diurnal activation periods ( $T_C$  and  $T_{DC}$ ), were plotted against the phase transitions temperature of PCM and results are shown in Fig. 8-8. As can be seen from Fig. 8-8, low melting temperature PCMs are not efficient due to the shorter periods of operation ( $T_C$  and  $T_{DC}$  were low). On the other hand, high melting temperature PCMs can be operated for a longer duration, but the latent storage and discharge were very low and hence the efficiency reduces. Thus, the optimum efficiency of PCM can be seen as when both factors are at maximum, which can be clearly identified from the developed performance indicators.

Results pertaining the optimum efficiency and effectiveness of PCM together with the average summer outdoor temperature for different climate zones are summarized in Table 8-6. It is interesting to note that the highest efficiency and effectiveness occur at different phase transition temperatures. Moreover, the optimum effectiveness of PCM can be seen at 3-5°C higher than the average outdoor temperature, but optimum efficiency requires further augmenting the melting temperature. Therefore, the choice of phase transition temperature can be made on the highest effectiveness of PCM, in which case optimal efficiency may not eventuate.

Table 8-6 Summary of results for highest efficiency and effectiveness

Location	$T_{out}$ (°C)	Optimum PCM melting temperature	
		High $e$	High $CE$
Melbourne	19.82	25 (24-27)	27 (26-29)
Sydney	22.89	27 (26-29)	29 (28-31)
Brisbane	24.36	27 (26-29)	29 (28-31)
Perth	23.34	27 (26-29)	27 (28-31)



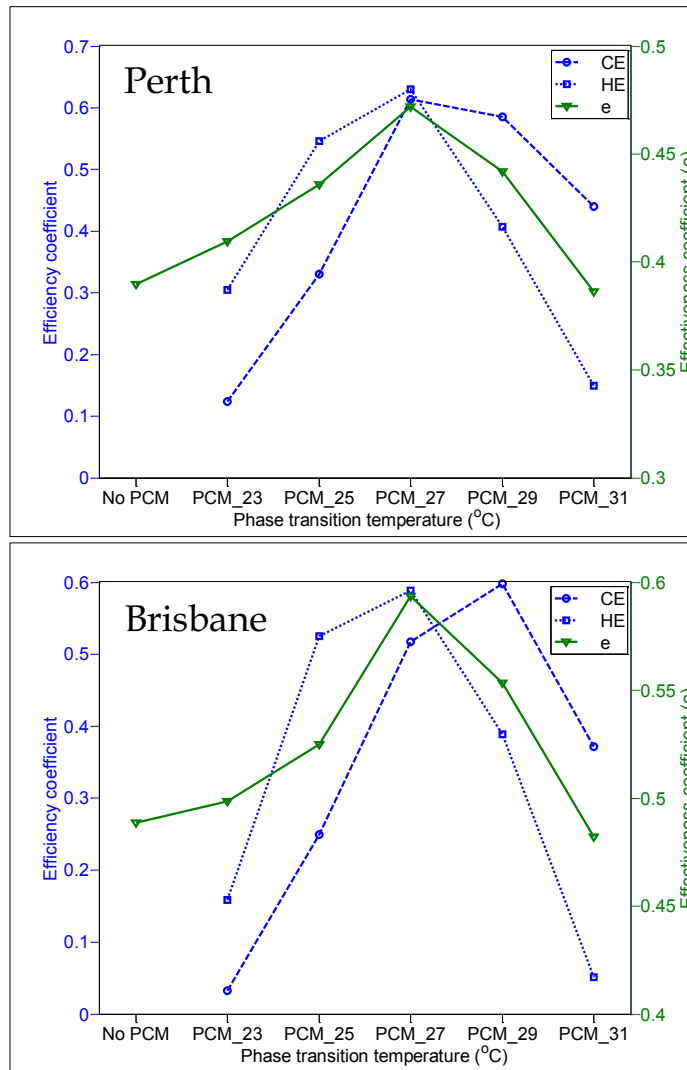
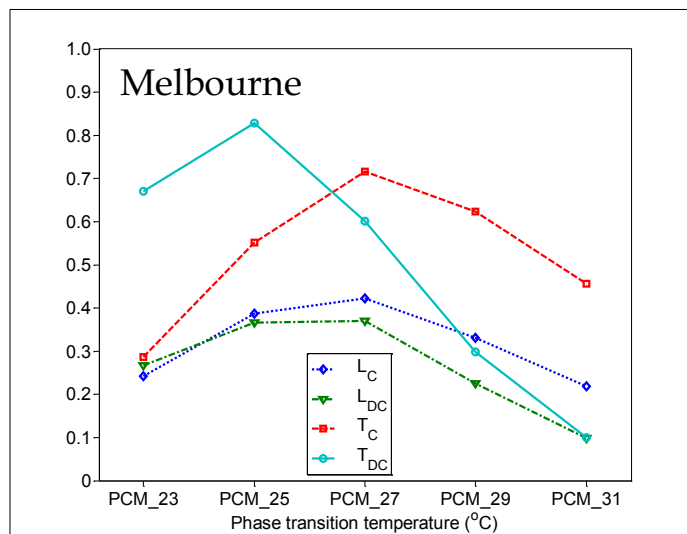


Fig. 8-7. Effect of phase transition temperature on PCM performance



factors

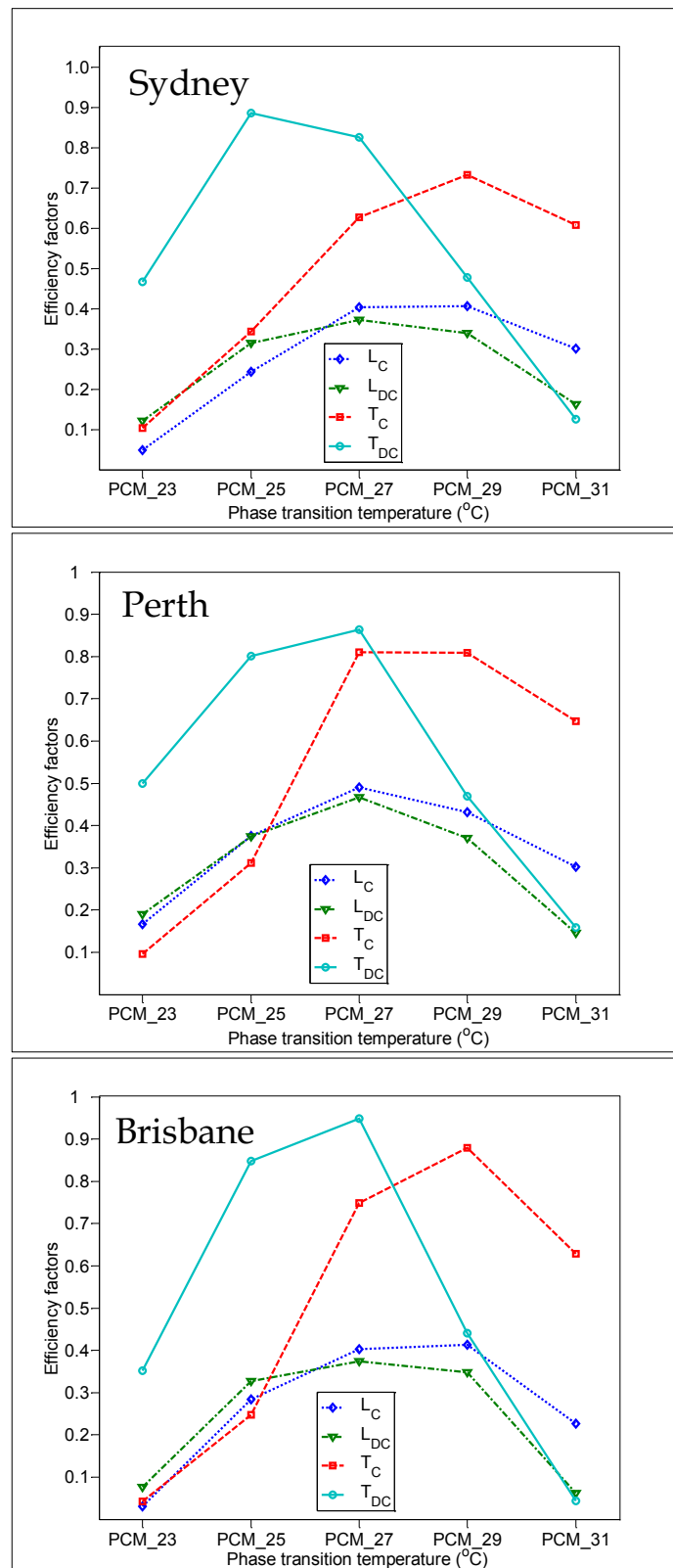


Fig. 8-8. Variation of efficiency factors for different phase transition temperatures

### 8.3.3. Effect of PCM quantity on the thermal performance enhancement

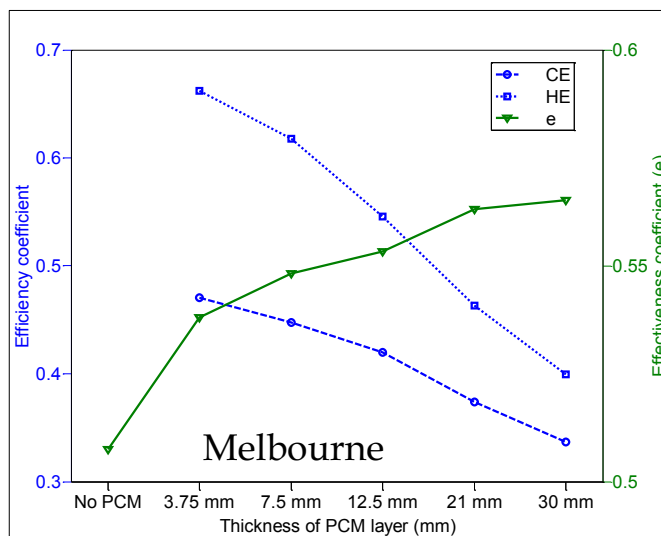
Increasing the quantity of PCM would result in increased latent heat capacity as well as longer periods of operation. However, as a consequence of the increased amount or equivalent thickness, charging and discharging fraction may be reduced due to the poor heat transfer rate of organic PCMs. Furthermore, increasing the quantity of PCM will incur a high cost and subsequently leads to the uneconomical design of PCM in buildings. Therefore, with the aim of exploring the optimal quantity of PCM (as represented by equivalent thickness), the simulated case study was repeated for different PCM layer thicknesses and the results are shown in Fig. 8-9. It is worth noting here that the simulations were performed for the optimal PCM phase transition temperature of the respective climate zones derived from previous analysis. The results regarding the climate zones of Melbourne and Perth are reported here, as other two cities have similar behavior to Perth.

As can be seen from Fig. 8-9, the effectiveness coefficient ( $e$ ) or improvement in indoor thermal comfort conditions increases with the increasing amount of PCM or its equivalent thickness. This can be explained by that the increase in PCM quantity will result in more latent heat storage availability. Besides, the increase in PCM layer thickness will also improve the thermal resistance as Bio-PCM has a very low thermal conductivity of  $0.2 \text{ W}/(\text{m.K})$ . Thus, to distinguish the effect of latent heat storage with the PCM layer thickness, efficiency coefficient of PCM with increasing layer thickness must be studied.

The efficiency coefficients ( $CE$  &  $HE$ ) of PCM incorporation with increasing PCM layer thickness is also plotted in Fig. 8-9. As can be seen from Fig. 8-9, the trend of  $CE$  and  $HE$  behaves differently for different climate zones. For the cool temperate climate zone of Melbourne, the  $CE$  and  $HE$  steadily decreases with increasing PCM quantity, while the warm temperate climate zone of Perth shows an increasing trend initially and then decreases. However, for both climate zones, high  $CE$  and  $HE$  can be achieved up to the thickness of 12.5 mm. The further increment in PCM layer thickness resulted in significantly low efficiency. Considering the climate zone of Perth as an example, 7.5 mm thick PCM layer results in the cooling efficiency of 0.68, however, the  $CE$  reduced to 0.50 for the equivalent thickness of 21mm.

This indicates that the consideration of PCM layer thickness up to 12.5 mm would be economical to incorporate into buildings. Moreover, the trend of  $e$  also shows that, up to the PCM layer thickness of 12.5 mm, the enhancement in indoor thermal comfort steeply increases. As the thickness further increase, a mild increase in effectiveness can be observed. It can be concluded, therefore, the optimum PCM layer thickness of PCM incorporation in buildings can be considered as 12.5 mm for all major climate zones in Australia.

More detailed results can be drawn by reporting the variation of factors that are influencing the efficiency and effectiveness of PCM performance as shown in Fig. 8-10. Inspection of Fig. 8-10 reveals that the large amount of PCM incorporation (high equivalent layer thickness) will result in poor PCM charge/discharge, though the diurnal activation periods ( $T_C$ ) increases. As the significant reduction in  $L_C$  and  $L_{DC}$  dominates the increase in  $T_C$  and  $T_{DC}$ , the efficiency of PCM reduces with increasing PCM layer thickness.



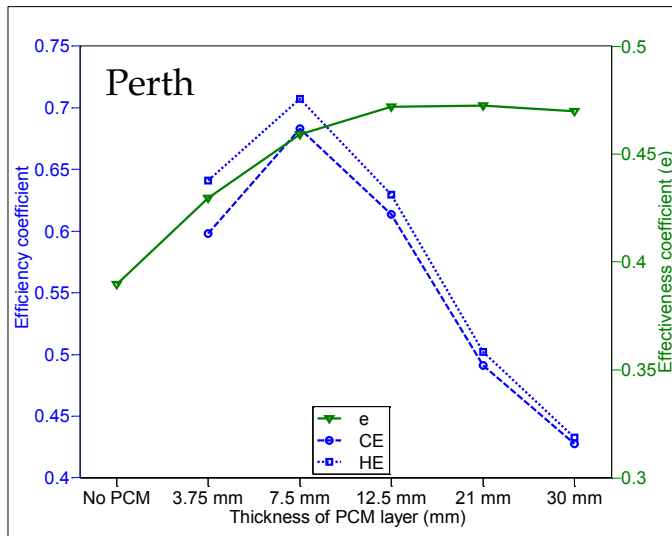


Fig. 8-9. Effect of PCM layer thickness on efficiency

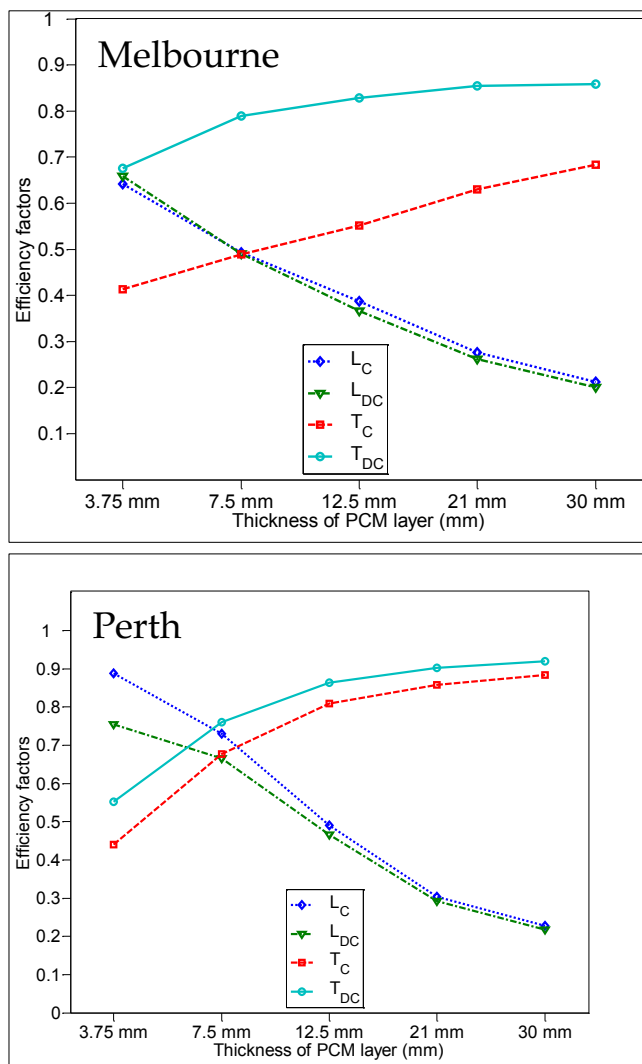


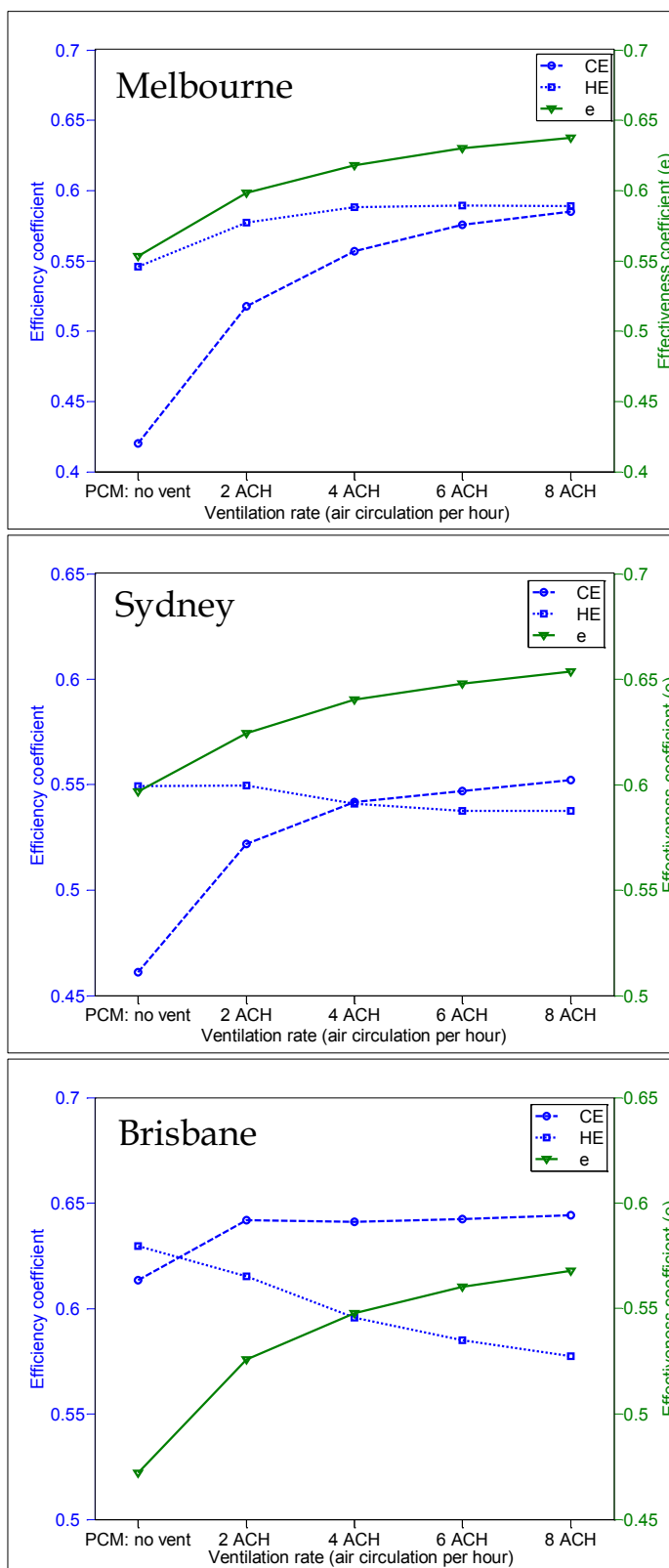
Fig. 8-10. Variation of efficiency factors for different PCM layer thicknesses

#### 8.3.4. Impact of night ventilation on PCM performance

One of the major limitation for the efficient operation of PCM in buildings has been identified as inadequate heat discharge of PCM at night, thus preventing the melted PCM from solidification. Due to the poor night solidification, the PCM remains partially melted state on the next day and contributes to lower latent energy storage availability. This problem continues to occur until the PCM layer fully discharges stored latent heat and solidify completely. The activation of night ventilation has been reported as a potential solution to improve the discharge process of PCM and, hence to mitigates the poor efficiency. In order to quantify the effect of night ventilation in improving the PCM heat discharge and to find optimum night ventilation rate in buildings, the currently developed performance indicators would be key parameters. In this regard, the simulations were conducted for PCM incorporated building with the activation of natural night ventilation by drawing outdoor air into the thermal zone. The efficiency and effectiveness of PCM were evaluated for different night ventilations rates of 0 to 8 air circulations per hour (ACH) operated for the period of 22:00 to 07:00. Fig. 8-11 shows the effect of increasing night ventilation rates in improving the PCM storage efficiency and indoor thermal comfort (as measured by efficiency coefficients and effectiveness coefficient respectively).

From Fig. 8-11, one can observe a remarkable improvement in  $CE$  and  $e$  for all major climate zones in Australia. Considering Melbourne as an example, the introduction of NV at a rate of 2 ACH improves the cooling efficiency by 24%, compared to the efficiency achieved without NV. As the night ventilation further increases up to 4 ACH, the cooling efficiency steadily increases. However, a further increase in NV resulted in negligible improvement in  $CE$ . At the NV rate of 4 ACH,  $CE$  was improved by 33%, 17%, 5% and 19% for the climate zones of Melbourne, Sydney, Perth and Brisbane respectively. Therefore, it can be said that the NV rate of 4 ACH is adequate to improve the latent heat discharge of PCM layer.

Furthermore, it can also be seen that the ASHRAE Adaptive thermal comfort period is guaranteed for more than 60% of the occupancy period (measured  $e$  value is greater than 0.6) in the climate zone of Melbourne with the activation of natural night ventilation, which is 13% more than in the building without PCM and 8% more than the case of PCM without night ventilation.



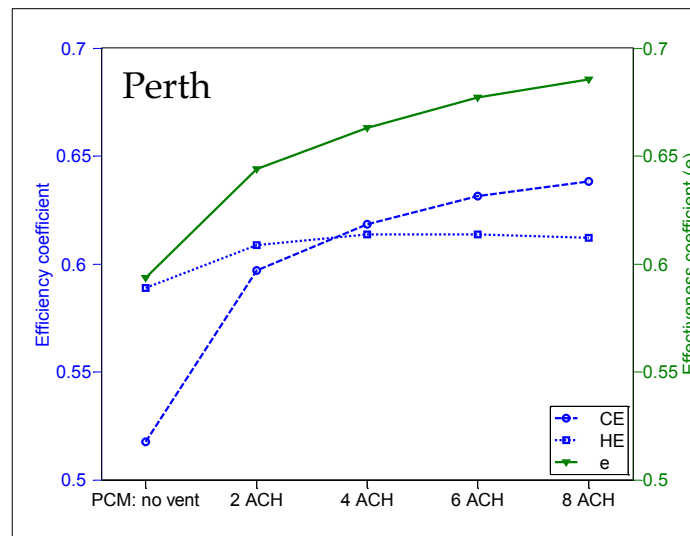


Fig. 8-11. Effect of night ventilation on PCM performance

### 8.3.5. Discussion of optimization process

According to abovementioned studies, it is clear that the developed performance indicators allowed the selection of PCM with optimum phase transition temperature and quantity (per m<sup>2</sup>) so that the resultant PCM storage efficiency and indoor thermal comfort are optimized. After the selection of phase transition temperature and quantity of PCM, night ventilation is introduced to further enhance the performance of PCM. The main results concerning the efficiency and effectiveness of PCM achieved for the optimized conditions in all climate zones are summarized in Table 8-7, where a comparison with the results obtained for no PCM and non-optimized PCM refurbishment are also proposed. It is worth mentioning here that the non-optimized PCM conditions are assumed as Bio-PCM™ with the melting temperature and layer thickness of 23°C and 12.5 mm respectively.

From Table 8-7, it can be seen that at optimum configuration, there is a significant enhancement in the effectiveness of PCM in improving the indoor thermal comfort, as observed by the effectiveness coefficient (e). It is also evident that the storage efficiency of PCM was significantly increased at optimized conditions. For instance, cooling efficiency (CE) of PCM was observed in the range of 0.54-0.64 for all climatic conditions, which is significantly high compared to the non-optimized PCM refurbishment, where the cooling efficiency falls in the range of 0.10-0.25.

Table 8-7 Optimized results of PCM refurbishment for various climate zones

Location	Refurbishment method	$e$	$CE$	$HE$	Optimized conditions
Melbourne	No PCM	0.51	-	-	PCM_25 with the thickness of 12.5 mm; night ventilation of 4 ACH.
	Non-optimized PCM	0.53	0.24	0.42	
	Optimized PCM	0.62	0.56	0.59	
Sydney	No PCM	0.54	-	-	PCM_27 with the thickness of 12.5 mm (equivalent quantity of 2.7 kg/m <sup>2</sup> ); night ventilation of 4 ACH.
	Non-optimized PCM	0.54	0.06	0.23	
	Optimized PCM	0.64	0.54	0.54	
Perth	No PCM	0.39	-	-	(equivalent quantity of 2.7 kg/m <sup>2</sup> ); night ventilation of 4 ACH.
	Non-optimized PCM	0.41	0.12	0.30	
	Optimized PCM	0.55	0.64	0.60	
Brisbane	No PCM	0.49	-	-	
	Non-optimized PCM	0.50	0.03	0.16	
	Optimized PCM	0.66	0.62	0.61	

## 8.4 Concluding remarks

This chapter presented a design optimization related to the application of passive latent energy storage with PCM in buildings, which aims to maximize the utilization of latent energy storage and improvement in indoor thermal comfort throughout the entire summer season of the year. Two performance indicators were developed to measure the degree of latent heat capacity and improvement in indoor thermal comfort. The corresponding indicators were termed as efficiency coefficient and effectiveness coefficient respectively. A simulated case study was carried out on a typical Australian residential building by incorporating Bio-PCM™ mats on the ceiling of the living thermal zone. The optimization study considered various parameters such as phase transition temperature of PCM, quantity, and the activation of night ventilation.

From the simulated case study, it was revealed that the quantitative evaluation of thermal performance indicators could provide more accurate assessment of PCM behavior in terms of efficiency and effectiveness. The most important findings from this chapter are as follows:

1. Quantitative assessment of the efficiency of PCM incorporation in buildings, as measured by the degree of utilization of latent heat capacity and operational period enabled the identification of how efficiently PCM is operated for particular climatic conditions.
2. Evaluation of the effectiveness coefficient ( $e$ ) of PCM through the ASHRAE adaptive thermal comfort model allows the identification of how effectively PCM enhances the indoor thermal comfort perceived by occupants.
3. The design optimization process proposed by optimizing the efficiency and effectiveness of PCM application in buildings is most appropriate approach to maximize the improvement in indoor thermal comfort while optimizing the storage efficiency of PCM.
4. For each major climate zones in Australia (i.e. Melbourne, Sydney, Perth, and Brisbane), the maximum improvement in indoor thermal comfort was achieved when the phase transition temperature is about 3-5°C higher than summer average outdoor air temperature. But, optimal efficiency would not occur at this phase transition temperature.

5. Increasing the quantity of PCM would steadily increase the indoor thermal comfort, but reduces the efficiency drastically. Thus, the choice of appropriate quantity of PCM should be carefully made to achieve high effectiveness and substantial efficiency, which would lead to an economical design.
6. The introduction of night ventilation up to a ventilation rate of 4 ACH has a significant improvement in efficiency and effectiveness of PCM application in buildings. Further increase in the night ventilation rate would have insignificant improvement.

Finally, the proposed design optimization methodology can be applicable as a preliminary design tool in a new building construction for appropriate selection of PCM or can be considered for the performance assessment in existing PCM incorporated buildings.

# Chapter 9 Conclusions and Recommendations

---

## 9.1 Summary

The use of PCM to increase TES capacity in buildings has gradually grown in the last few decades due to the fact that PCM has large volumetric heat capacity and undergo little temperature variation during the energy storage process. In particular, the integration of PCM into cementitious materials have been considered as great potential in energy management due to their broad use in the construction industry as forms of cement mortars and concrete. The main aim of this research was to overcome major issues associated with the integration of PCM into cementitious composites, including PCM instability or leakage and poor heat transfer performance. Hence, a novel form-stable PCM was developed to address these issues and consequently to improve the performance of PCM integrated cementitious composites. The outcomes of this research study would thus be useful to construction industries as well as research institutes, assisting in their search for new ways to integrate PCM into cementitious composites leading to the innovation for the next generation of building envelope designs.

The feasibility of integrating form-stable PCM into cementitious composites was assessed by investigating the leakage or instability of PCM. Two different form-stable PCM composites were fabricated by impregnating paraffin into normal expanded perlite (EPW) and hydrophobic coated expanded perlite (EPO) granules. The composite PCMs behaved differently when they were mixed with cement mortars. The hydrophilic composite PCM that was fabricated using EPW had shown paraffin leakage of up to 50%, whereas traces of leakage were not observed for the newly developed EPOP composite PCM. The surface characteristics of PCM composites such as contact angle and wetting tension were also studied and correlated with the instability phenomenon of form-stable PCM composites. It was found that the PCM composites with an obtuse contact angle and negative wetting tension to water can be successfully integrated into cement-based materials without any associated leakage issues.

Since EPOP was identified as the most promising candidate for integration into cementitious composites without any associated leakage issues, it was then considered for further experimental studies. The FT-IR and TGA analyses showed that the fabricated composite PCM has good chemical compatibility and thermal stability. The micro-morphology characteristics of TESC indicated a good compatibility between EPOP and cement matrix. The mechanical properties of the TESC, determined by 7 and 28-day compressive strength test results, were found to be relatively low and this is likely due to the low stiffness of EPOP that has replaced fine aggregates. Furthermore, a weight based mix design also lead to further loss in compressive strength. The thermal performance study revealed that the TESC panels have larger thermal inertia and thermal energy storage rates than the control cement mortar panels.

The experimental studies were extended to incorporate EPOP into cement mortars for the development of thermal energy storage cement mortars (TESCMs). The TESCMs were developed by following a volume based mixed design method where the partial substitution of fine aggregates by PCM composites was undertaken for substitution levels of 20%, 40% 60% and 80%. It was found that the maximum observed reduction in 28-day compressive strength, bulk density and thermal conductivity in comparison with ordinary cement mortar (OCM) were 70%, 48%, and 66% respectively. The developed TESCMs also exhibited greater drying shrinkage strain than OCM, suspected to be largely due to the low stiffness of porous EPO. Nevertheless, the thermal energy storage performance of TESCMs was significantly enhanced with the increasing substitution levels of PCM composites. Furthermore, the mechanical and thermal reliability of TESCMs were shown to be satisfactory when subjected to 3000 accelerated thermal cycles.

Apart from the heat capacity enhancement of cementitious composites and cement mortars with PCM, its heat transfer rate and energy storage efficiency were improved by integrating high conductive additives into form-stable PCM. Three different heat transfer additives including G, CNT, and GNP were integrated into EPOP composites and their heat transfer performance enhancements were assessed. The use of 0.5wt% of carbon-based additives led to significant improvements in thermal conductivity, heat storage/release rates and TES performance. It was further determined that among the considered heat transfer additives, GNP performed the best and graphite the least.

The next stage of investigation included an experimental and numerical study on the thermal performance of PCM integrated cement boards (PCM CB) compared to ordinary cement mortar boards (OCB) and gypsum plasterboards (GPB). The prototype test room experiments showed that the PCM CB could reduce the maximum peak indoor temperature by up to 2.8°C and 4.43°C than GPB test rooms for typical summer days and summer design days, respectively. In addition, test huts exposed to outdoor climatic conditions revealed that PCM CB was more effective than OCB, especially when peak indoor temperature reached approximately 2-3°C above the phase transition temperature of PCM. Numerical simulations performed on buildings refurbished with PCM CB showed that the interior surface application of PCM suffers from inadequate cold storage at night leading to incomplete solidification of PCM. To improve the solidification of PCM, night ventilation is proposed and promising results were achieved. The combined application of PCM CB and night ventilation reduced the indoor operative temperature by up to 3.4°C, as opposed to the 2.5°C achieved for the building refurbished with PCM CB only.

Finally, a parametric study was conducted for the application of PCM in residential buildings. Two performance indicators, termed as efficiency coefficient and the effectiveness coefficient, were developed to evaluate the PCM storage efficiency and indoor thermal comfort. A simulated case study was carried out for the incorporation of Bio-PCM™ mats on the ceiling of the residential building. By evaluating the efficiency and effectiveness of PCM in buildings, it was revealed that the improvements in indoor thermal comfort could be maximized while optimizing corresponding storage efficiency of PCM. All climate zones showed maximum effectiveness when the phase transition temperature of PCM was about 3-5°C higher than the summer average outdoor air temperature. Increasing the PCM quantity continuously increases the effectiveness of PCM, but drastically reduces the efficiency. Moreover, the activation of night ventilation for up to 4 ACH can significantly improve the efficiency and effectiveness of PCM.

## 9.2 Conclusions

1. The cementitious composites integrated with form-stable PCM can be considered as suitable method for the passive latent heat storage applications in buildings. Cementitious composites and cement mortars containing form-stable PCM was developed in this study and was shown that the TES capacity and thermal performance were significantly enhanced with adequate mechanical properties.
2. The major issue associated with the integration of form-stable PCM into cementitious composites was found as PCM leakage or instability and this problem has been successfully overcome by developing a novel form-stable PCM based on paraffin and hydrophobic EP (EPOP) granular material.
3. Heat transfer performance of form-stable PCM and corresponding latent heat storage efficiency in TES applications were also improved by integrating high conductive carbon based additives into EPOP composite. Among the different additives studied, GNP performed the best and graphite additive showed the least.
4. The integration of form-stable EPOP into cementitious composites has resulted in significant reduction of peak indoor temperature and diurnal temperature fluctuations as revealed from the thermal performance tests conducted on prototype test cells and test huts.
5. The application of form-stable PCM integrated cement mortars as interior surface plastering mortars in passive buildings was affected by incomplete solidification at night, leading to reduced diurnal energy storage efficiency. The use of mechanical night ventilation improved the solidification of PCM and further enhanced the indoor thermal performance.
6. Integration of form-stable PCM into cement mortars led to a reduction in the mechanical properties and increase in early age shrinkage strain developments, primarily due to low strength and stiffness of PCM composites. However, substantial level of PCM replacement of up to 60% in cement mortars can be considered for structural uses.
7. The parametric case study performed with the development of new performance indicators revealed that the developed performance indicators assisted in maximizing the improvements in indoor thermal comfort, while optimizing corresponding storage efficiency of PCM.

### 9.3 Recommendations for future works

A large number of research has already been conducted on the state-of-the-art technology using PCM for thermal performance enhancement in buildings. The present research work has extended previous studies to experimentally and numerically investigate the utilization of a novel form-stable PCM as well as its integration into cementitious composites such as cement mortar for application in buildings. Our research revealed that this novel form-stable PCM can be successfully integrated into cementitious materials to significantly improve TES capacity and thermal performance of buildings. However, prior to the large-scale application of TES in buildings, the following are explorative suggestions should be considered for future study:

1. While the integration of this novel form-stable EPOP PCM into cementitious materials such as cement mortar was investigated, it would be beneficial to study the effects of integrating EPOP into concrete.
2. The integration of EPOP into cementitious materials has led to reduced mechanical properties (i.e. compressive strength) due to the low strength and stiffness of porous EPO granules. The addition of pozzolanic materials such as silica fume or nanosilica into the cement matrix could be considered as viable options to reduce this strength loss. Such additives could improve compressive strength and durability due to the nature of pozzolanic reactivity and the presence of large surface areas. Furthermore, the strengthening of composite PCMs by introducing a stronger outer shell through methods such as epoxy coating or hydrated cement coatings could also be studied.
3. The TESCMs exhibited high early age shrinkage strain compared to ordinary cement mortars. Methods to mitigate high levels of drying shrinkage and the impact of early age shrinkage cracks should be further investigated.
4. The use of carbon-based additives such as CNT and GNP in form-stable PCM enhanced thermal properties and TES performance. However, these additives are very expensive and can be hazardous to the environment. Therefore, alternative additives should be investigated for safety and economic viability of such developments.
5. Though TESCMs perform well for summer climatic conditions due to the availability of adequate solar energy, they remain dormant for the climatic

conditions of winter. Therefore, the use of TESCMs during winter must be investigated to effectively use its large TES capacity and reduce heating energy demands throughout the year.

6. The experimental studies of this research utilized test huts to evaluate the thermal performance of TESCMs. However, it would be preferential to use real scale experimental tests on actual buildings/test rooms in future studies on the behavior of TESCM for real-world applications. Furthermore, the thermal performance enhancement of high conductive additives integrated cement mortars should also be studied in large scale experiments. Simulation studies can further assist in choosing the optimized thermophysical properties of PCMs as tailored to local climatic conditions.

# References

---

- [1] Lucon, O., et al., *Buildings*, in *Climate Change 2014: Mitigation of Climate Change. Contribution of Working Group III to the Fifth Assessment Report of the Intergovernmental Panel on Climate Change*, O. Edenhofer, R. Pichs-Madruga, Y. Sokona, E. Farahani, S. Kadner, K. Seyboth, A. Adler, I. Baum, S. Brunner, P. Eickemeier, B. Kriemann, J. Savolainen, S. Schlömer, C. von Stechow, T. Zwickel and J.C. Minx, Editor. 2014, Cambridge University Press: Cambridge, United Kingdom and New York, NY, USA.
- [2] Soares, N., et al., *Review of passive PCM latent heat thermal energy storage systems towards buildings' energy efficiency*. *Energy and Buildings*, 2013. **59**(0): p. 82-103.
- [3] Zhou, D., C.Y. Zhao, and Y. Tian, *Review on thermal energy storage with phase change materials (PCMs) in building applications*. *Applied Energy*, 2012. **92**(0): p. 593-605.
- [4] Tyagi, V.V. and D. Buddhi, *PCM thermal storage in buildings: A state of art*. *Renewable and Sustainable Energy Reviews*, 2007. **11**(6): p. 1146-1166.
- [5] Li, X., J.G. Sanjayan, and J.L. Wilson, *Fabrication and stability of form-stable diatomite/paraffin phase change material composites*. *Energy and Buildings*, 2014. **76**(0): p. 284-294.
- [6] Li, H., et al., *Development of thermal energy storage composites and prevention of PCM leakage*. *Applied Energy*, 2014. **135**(0): p. 225-233.
- [7] Liu, L., et al., *Thermal conductivity enhancement of phase change materials for thermal energy storage: A review*. *Renewable and Sustainable Energy Reviews*, 2016. **62**: p. 305-317.
- [8] Kheradmand, M., et al., *Assessing the feasibility of impregnating phase change materials in lightweight aggregate for development of thermal energy storage systems*. *Construction and Building Materials*, 2015. **89**(0): p. 48-59.
- [9] Zalba, B., et al., *Review on thermal energy storage with phase change: materials, heat transfer analysis and applications*. *Applied Thermal Engineering*, 2003. **23**(3): p. 251-283.
- [10] Regin, A.F., S.C. Solanki, and J.S. Saini, *Heat transfer characteristics of thermal energy storage system using PCM capsules: A review*. *Renewable and Sustainable Energy Reviews*, 2008. **12**(9): p. 2438-2458.
- [11] Cabeza, L.F., et al., *Heat transfer enhancement in water when used as PCM in thermal energy storage*. *Applied Thermal Engineering*, 2002. **22**(10): p. 1141-1151.
- [12] Evola, G., L. Marletta, and F. Sicurella, *A methodology for investigating the effectiveness of PCM wallboards for summer thermal comfort in buildings*. *Building and Environment*, 2013. **59**(0): p. 517-527.
- [13] Ascione, F., et al., *Energy refurbishment of existing buildings through the use of phase change materials: Energy savings and indoor comfort in the cooling season*. *Applied Energy*, 2014. **113**(0): p. 990-1007.
- [14] Sharma, A., et al., *Review on thermal energy storage with phase change materials and applications*. *Renewable and Sustainable Energy Reviews*, 2009. **13**(2): p. 318-345.
- [15] Khudhair, A.M. and M.M. Farid, *A review on energy conservation in building applications with thermal storage by latent heat using phase change materials*. *Energy Conversion and Management*, 2004. **45**(2): p. 263-275.

- [16] Kuznik, F., et al., *A review on phase change materials integrated in building walls*. Renewable and Sustainable Energy Reviews, 2011. **15**(1): p. 379-391.
- [17] Hawes, D.W., *Latent heat storage in concrete*. 1991, Concordia University.
- [18] Memon, S.A., *Phase change materials integrated in building walls: A state of the art review*. Renewable and Sustainable Energy Reviews, 2014. **31**(0): p. 870-906.
- [19] Pereira da Cunha, J. and P. Eames, *Thermal energy storage for low and medium temperature applications using phase change materials – A review*. Applied Energy, 2016. **177**: p. 227-238.
- [20] Baetens, R., B.P. Jelle, and A. Gustavsen, *Phase change materials for building applications: A state-of-the-art review*. Energy and Buildings, 2010. **42**(9): p. 1361-1368.
- [21] Kenisarin, M. and K. Mahkamov, *Solar energy storage using phase change materials*. Renewable and Sustainable Energy Reviews, 2007. **11**(9): p. 1913-1965.
- [22] Kenisarin, M.M. and K.M. Kenisarina, *Form-stable phase change materials for thermal energy storage*. Renewable and Sustainable Energy Reviews, 2012. **16**(4): p. 1999-2040.
- [23] Jegadheeswaran, S. and S.D. Pohekar, *Performance enhancement in latent heat thermal storage system: A review*. Renewable and Sustainable Energy Reviews, 2009. **13**(9): p. 2225-2244.
- [24] Velraj, R., et al., *Heat transfer enhancement in a latent heat storage system*. Solar Energy, 1999. **65**(3): p. 171-180.
- [25] Feldman, D., et al., *Obtaining an energy storing building material by direct incorporation of an organic phase change material in gypsum wallboard*. Solar Energy Materials, 1991. **22**(2-3): p. 231-242.
- [26] Feldman, D., D. Banu, and D.W. Hawes, *Development and application of organic phase change mixtures in thermal storage gypsum wallboard*. Solar Energy Materials and Solar Cells, 1995. **36**(2): p. 147-157.
- [27] Waqas, A. and Z. Ud Din, *Phase change material (PCM) storage for free cooling of buildings – A review*. Renewable and Sustainable Energy Reviews, 2013. **18**(0): p. 607-625.
- [28] Raj, V.A.A. and R. Velraj, *Review on free cooling of buildings using phase change materials*. Renewable and Sustainable Energy Reviews, 2010. **14**(9): p. 2819-2829.
- [29] Cabeza, L., et al., *Materials used as PCM in thermal energy storage in buildings: a review*. Renewable and Sustainable Energy Reviews, 2011. **15**(3): p. 1675-1695.
- [30] Schossig, P., et al., *Micro-encapsulated phase-change materials integrated into construction materials*. Solar Energy Materials and Solar Cells, 2005. **89**(2-3): p. 297-306.
- [31] Hawlader, M.N.A., M.S. Uddin, and M.M. Khin, *Microencapsulated PCM thermal-energy storage system*. Applied Energy, 2003. **74**(1-2): p. 195-202.
- [32] Tyagi, V.V., et al., *Development of phase change materials based microencapsulated technology for buildings: A review*. Renewable and Sustainable Energy Reviews, 2011. **15**(2): p. 1373-1391.
- [33] Zhao, C.Y. and G.H. Zhang, *Review on microencapsulated phase change materials (MEPCMs): Fabrication, characterization and applications*. Renewable and Sustainable Energy Reviews, 2011. **15**(8): p. 3813-3832.
- [34] Konuklu, Y., et al., *Review on using microencapsulated phase change materials (PCM) in building applications*. Energy and Buildings, 2015. **106**: p. 134-155.
- [35] Zhang, Y.P., et al., *Preparation, thermal performance and application of shape-stabilized PCM in energy efficient buildings*. Energy and Buildings, 2006. **38**(10): p. 1262-1269.

- [36] Sari, A., *Form-stable paraffin/high density polyethylene composites as solid-liquid phase change material for thermal energy storage: preparation and thermal properties*. Energy Conversion and Management, 2004. **45**(13-14): p. 2033-2042.
- [37] Mu, M., et al., *Shape stabilised phase change materials based on a high melt viscosity HDPE and paraffin waxes*. Applied Energy, 2016. **162**: p. 68-82.
- [38] Cheng, W.-l., et al., *Heat conduction enhanced shape-stabilized paraffin/HDPE composite PCMs by graphite addition: Preparation and thermal properties*. Solar Energy Materials and Solar Cells, 2010. **94**(10): p. 1636-1642.
- [39] Jeong, S.-G., et al., *Thermal performance evaluation of Bio-based shape stabilized PCM with boron nitride for energy saving*. International Journal of Heat and Mass Transfer, 2014. **71**(0): p. 245-250.
- [40] Mehrali, M., et al., *Shape-stabilized phase change materials with high thermal conductivity based on paraffin/graphene oxide composite*. Energy Conversion and Management, 2013. **67**(0): p. 275-282.
- [41] Zhang, D., et al., *Granular phase changing composites for thermal energy storage*. Solar Energy, 2005. **78**(3): p. 471-480.
- [42] Zhang, D., et al., *Development of thermal energy storage concrete*. Cement and Concrete Research, 2004. **34**(6): p. 927-934.
- [43] Memon, S.A., et al., *Development of form-stable composite phase change material by incorporation of dodecyl alcohol into ground granulated blast furnace slag*. Energy and Buildings, 2013. **62**(0): p. 360-367.
- [44] Zhang, D., S. Tian, and D. Xiao, *Experimental study on the phase change behavior of phase change material confined in pores*. Solar Energy, 2007. **81**(5): p. 653-660.
- [45] Li, W., *Shape-stablized EP/paraffin composite for latent heat storage*. Journal of Wuhan University of Technology. Materials science edition, 2013. **28**(4): p. 682.
- [46] Wang, C., et al., *Shape-stabilized phase change materials based on polyethylene glycol/porous carbon composite: The influence of the pore structure of the carbon materials*. Solar Energy Materials and Solar Cells, 2012. **105**(0): p. 21-26.
- [47] Li, X. and Z. Li, *Development of thermal insulation and storage materials using extrusion technique*. ACI Special Publication, 2009. **260**.
- [48] Jiang, Y., E. Ding, and G. Li, *Study on transition characteristics of PEG/CDA solid-solid phase change materials*. Polymer, 2002. **43**(1): p. 117-122.
- [49] Kenisarin, M.M., *Form-stable phase change materials for thermal energy storage*. Renewable & sustainable energy reviews, 2012. **16**(4): p. 1999-2040.
- [50] Xiao, M., B. Feng, and K. Gong, *Preparation and performance of shape stabilized phase change thermal storage materials with high thermal conductivity*. Energy Conversion and Management, 2002. **43**(1): p. 103-108.
- [51] Biçer, A. and A. Sarı, *New kinds of energy-storing building composite PCMs for thermal energy storage*. Energy Conversion and Management, 2013. **69**(0): p. 148-156.
- [52] Karaipekli, A. and A. Sarı, *Preparation, thermal properties and thermal reliability of eutectic mixtures of fatty acids/expanded vermiculite as novel form-stable composites for energy storage*. Journal of Industrial and Engineering Chemistry, 2010. **16**(5): p. 767-773.
- [53] Karaman, S., et al., *Polyethylene glycol (PEG)/diatomite composite as a novel form-stable phase change material for thermal energy storage*. Solar Energy Materials and Solar Cells, 2011. **95**(7): p. 1647-1653.
- [54] Li, M., et al., *Study on preparation and thermal property of binary fatty acid and the binary fatty acids/diatomite composite phase change materials*. Applied Energy, 2011. **88**(5): p. 1606-1612.

- [55] Sun, Z., *Preparation and thermal energy storage properties of paraffin/calcined diatomite composites as form-stable phase change materials*. *Thermochimica acta*, 2013. **558**: p. 16-21.
- [56] Sari, A., A. Karaipekli, and C. Alkan, *Preparation, characterization and thermal properties of lauric acid/expanded perlite as novel form-stable composite phase change material*. *Chemical Engineering Journal*, 2009. **155**(3): p. 899-904.
- [57] Sari, A. and A. Karaipekli, *Preparation, thermal properties and thermal reliability of capric acid/expanded perlite composite for thermal energy storage*. *Materials Chemistry and Physics*, 2008. **109**(2-3): p. 459-464.
- [58] Lu, Z., et al., *Preparation and characterization of expanded perlite/paraffin composite as form-stable phase change material*. *Solar Energy*, 2014. **108**(0): p. 460-466.
- [59] Karaipekli, A. and A. Sari, *Capric-myristic acid/vermiculite composite as form-stable phase change material for thermal energy storage*. *Solar Energy*, 2009. **83**(3): p. 323-332.
- [60] Xu, B., et al., *Paraffin/expanded vermiculite composite phase change material as aggregate for developing lightweight thermal energy storage cement-based composites*. *Applied Energy*, 2015. **160**: p. 358-367.
- [61] Wang, W., et al., *Preparation and thermal properties of polyethylene glycol/expanded graphite blends for energy storage*. *Applied Energy*, 2009. **86**(9): p. 1479-1483.
- [62] Wang, S., et al., *A novel sebacic acid/expanded graphite composite phase change material for solar thermal medium-temperature applications*. *Solar Energy*, 2014. **99**(0): p. 283-290.
- [63] Zhang, Z. and X. Fang, *Study on paraffin/expanded graphite composite phase change thermal energy storage material*. *Energy Conversion and Management*, 2006. **47**(3): p. 303-310.
- [64] Hawes, D.W., D. Feldman, and D. Banu, *Latent heat storage in building materials*. *Energy and Buildings*, 1993. **20**(1): p. 77-86.
- [65] Ahmad, M., et al., *Experimental investigation and computer simulation of thermal behaviour of wallboards containing a phase change material*. *Energy and Buildings*, 2006. **38**(4): p. 357-366.
- [66] Shilei, L., Z. Neng, and F. Guohui, *Impact of phase change wall room on indoor thermal environment in winter*. *Energy and Buildings*, 2006. **38**(1): p. 18-24.
- [67] Sari, A., A. Karaipekli, and K. Kaygusuz, *Capric acid and stearic acid mixture impregnated with gypsum wallboard for low-temperature latent heat thermal energy storage*. *International Journal of Energy Research*, 2008. **32**(2): p. 154-160.
- [68] Oliver, A., *Thermal characterization of gypsum boards with PCM included: Thermal energy storage in buildings through latent heat*. *Energy and Buildings*, 2012. **48**(0): p. 1-7.
- [69] Bentz, D.P. and R. Turpin, *Potential applications of phase change materials in concrete technology*. *Cement and Concrete Composites*, 2007. **29**(7): p. 527-532.
- [70] Xu, B. and Z. Li, *Paraffin/diatomite composite phase change material incorporated cement-based composite for thermal energy storage*. *Applied Energy*, 2013. **105**(0): p. 229-237.
- [71] Hawes, D.W. and D. Feldman, *Absorption of phase change materials in concrete*. *Solar Energy Materials and Solar Cells*, 1992. **27**(2): p. 91-101.
- [72] Hawes, D.W., D. Banu, and D. Feldman, *The stability of phase change materials in concrete*. *Solar Energy Materials and Solar Cells*, 1992. **27**(2): p. 103-118.
- [73] Hunger, M., et al., *The behavior of self-compacting concrete containing micro-encapsulated Phase Change Materials*. *Cement and Concrete Composites*, 2009. **31**(10): p. 731-743.

- [74] Gschwander, S., P. Schossig, and H.M. Henning, *Micro-encapsulated paraffin in phase-change slurries*. *Solar Energy Materials and Solar Cells*, 2005. **89**(2-3): p. 307-315.
- [75] Cabeza, L.F., et al., *Use of microencapsulated PCM in concrete walls for energy savings*. *Energy and Buildings*, 2007. **39**(2): p. 113-119.
- [76] Meshgin, P. and Y. Xi, *Effect of phase-change materials on properties of concrete*. *ACI Materials Journal*, 2012. **109**(1).
- [77] Cui, H., et al., *Thermophysical and mechanical properties of hardened cement paste with microencapsulated phase change materials for energy storage*. *Materials*, 2014. **7**(12): p. 8070-8087.
- [78] Dehdezi, P.K., et al., *Thermal, mechanical and microstructural analysis of concrete containing microencapsulated phase change materials*. *International Journal of Pavement Engineering*, 2013. **14**(5): p. 449-462.
- [79] Eddhahak-Ouni, A., et al., *Experimental and multi-scale analysis of the thermal properties of Portland cement concretes embedded with microencapsulated Phase Change Materials (PCMs)*. *Applied Thermal Engineering*, 2014. **64**(1-2): p. 32-39.
- [80] Fernandes, F., et al., *On the feasibility of using phase change materials (PCMs) to mitigate thermal cracking in cementitious materials*. *Cement and Concrete Composites*, 2014. **51**: p. 14-26.
- [81] Jayalath, A., et al., *Properties of cementitious mortar and concrete containing micro-encapsulated phase change materials*. *Construction and Building Materials*, 2016. **120**: p. 408-417.
- [82] Cui, H., et al., *Development of structural-functional integrated energy storage concrete with innovative macro-encapsulated PCM by hollow steel ball*. *Applied Energy*, 2017. **185, Part 1**: p. 107-118.
- [83] Cui, H., S.A. Memon, and R. Liu, *Development, mechanical properties and numerical simulation of macro encapsulated thermal energy storage concrete*. *Energy and Buildings*, 2015. **96**(0): p. 162-174.
- [84] Memon, S.A., et al., *Utilization of macro encapsulated phase change materials for the development of thermal energy storage and structural lightweight aggregate concrete*. *Applied Energy*, 2015. **139**(0): p. 43-55.
- [85] Alam, T.E., et al., *Macroencapsulation and characterization of phase change materials for latent heat thermal energy storage systems*. *Applied Energy*, 2015. **154**: p. 92-101.
- [86] Dong, Z., et al., *Development of hollow steel ball macro-encapsulated PCM for thermal energy storage concrete*. *Materials*, 2016. **9**(1): p. 59.
- [87] Memon, S.A., et al., *Development of structural-functional integrated concrete with macro-encapsulated PCM for thermal energy storage*. *Applied Energy*, 2015. **150**(0): p. 245-257.
- [88] Zhang, Z., et al., *Thermal energy storage cement mortar containing n-octadecane/expanded graphite composite phase change material*. *Renewable Energy*, 2013. **50**(0): p. 670-675.
- [89] Ye, R., et al., *Preparation, Mechanical and Thermal Properties of Cement Board with Expanded Perlite Based Composite Phase Change Material for Improving Buildings Thermal Behavior*. *Materials*, 2015. **8**(11): p. 7702-7713.
- [90] Nepomuceno, M.C.S. and P.D. Silva, *Experimental evaluation of cement mortars with phase change material incorporated via lightweight expanded clay aggregate*. *Construction and Building Materials*, 2014. **63**(0): p. 89-96.
- [91] Li, M., Z. Wu, and J. Tan, *Heat storage properties of the cement mortar incorporated with composite phase change material*. *Applied Energy*, 2013. **103**: p. 393-399.

- [92] He, Y., X. Zhang, and Y. Zhang, *Preparation technology of phase change perlite and performance research of phase change and temperature control mortar*. Energy and Buildings, 2014. **85**(0): p. 506-514.
- [93] Fang, G., S. Wu, and X. Liu, *Experimental study on cool storage air-conditioning system with spherical capsules packed bed*. Energy and Buildings, 2010. **42**(7): p. 1056-1062.
- [94] Wang, X. and J. Niu, *Performance of cooled-ceiling operating with MPCM slurry*. Energy Conversion and Management, 2009. **50**(3): p. 583-591.
- [95] Mazo, J., et al., *Modeling a radiant floor system with Phase Change Material (PCM) integrated into a building simulation tool: Analysis of a case study of a floor heating system coupled to a heat pump*. Energy and Buildings, 2012. **47**(0): p. 458-466.
- [96] Farid, M. and W.J. Kong, *Underfloor heating with latent heat storage*. Proceedings of the Institution of Mechanical Engineers, Part A: Journal of Power and Energy, 2001. **215**(5): p. 601-609.
- [97] Moreno, P., et al., *The use of phase change materials in domestic heat pump and air-conditioning systems for short term storage: A review*. Renewable and Sustainable Energy Reviews, 2014. **39**: p. 1-13.
- [98] Waqas, A. and Z. Ud Din, *Phase change material (PCM) storage for free cooling of buildings – A review*. Renewable and Sustainable Energy Reviews, 2013. **18**: p. 607-625.
- [99] Sage-Lauck, J.S. and D.J. Sailor, *Evaluation of phase change materials for improving thermal comfort in a super-insulated residential building*. Energy and Buildings, 2014. **79**(0): p. 32-40.
- [100] Alam, M., et al., *Energy saving potential of phase change materials in major Australian cities*. Energy and Buildings, 2014. **78**(0): p. 192-201.
- [101] Shi, X., et al., *Experimental assessment of position of macro encapsulated phase change material in concrete walls on indoor temperatures and humidity levels*. Energy and Buildings, 2014. **71**: p. 80-87.
- [102] Bio-PCM. *Phase Change Energy Solutions*. 2016 [cited 2016 08-04]; Available from: <http://phasechange.com.au>.
- [103] Zhang, P., X. Xiao, and Z.W. Ma, *A review of the composite phase change materials: Fabrication, characterization, mathematical modeling and application to performance enhancement*. Applied Energy, 2016. **165**: p. 472-510.
- [104] Bose, P. and V.A. Amirtham, *A review on thermal conductivity enhancement of paraffinwax as latent heat energy storage material*. Renewable and Sustainable Energy Reviews, 2016. **65**: p. 81-100.
- [105] Wang, H., et al., *Experimental investigation on the thermal performance of a heat sink filled with porous metal fiber sintered felt/paraffin composite phase change material*. Applied Energy, 2016. **176**: p. 221-232.
- [106] Xiao, X., P. Zhang, and M. Li, *Preparation and thermal characterization of paraffin/metal foam composite phase change material*. Applied Energy, 2013. **112**: p. 1357-1366.
- [107] Nourani, M., et al., *Thermal behavior of paraffin-nano-Al<sub>2</sub>O<sub>3</sub> stabilized by sodium stearoyl lactylate as a stable phase change material with high thermal conductivity*. Renewable Energy, 2016. **88**: p. 474-482.
- [108] Xu, B. and Z. Li, *Paraffin/diatomite/multi-wall carbon nanotubes composite phase change material tailor-made for thermal energy storage cement-based composites*. Energy, 2014. **72**(0): p. 371-380.

- [109] Lu, Z., et al., *Preparation and characterization of an expanded perlite/paraffin/graphene oxide composite with enhanced thermal conductivity and leakage-bearing properties*. RSC Advances, 2015. **5**(130): p. 107514-107521.
- [110] Fethi, A., et al., *Investigation of a graphite/paraffin phase change composite*. International Journal of Thermal Sciences, 2015. **88**: p. 128-135.
- [111] Mantilla Gilart, P., et al., *Development of PCM/carbon-based composite materials*. Solar Energy Materials and Solar Cells, 2012. **107**: p. 205-211.
- [112] Elgafy, A. and K. Lafdi, *Effect of carbon nanofiber additives on thermal behavior of phase change materials*. Carbon, 2005. **43**(15): p. 3067-3074.
- [113] Kim, S. and L.T. Drzal, *High latent heat storage and high thermal conductive phase change materials using exfoliated graphite nanoplatelets*. Solar Energy Materials and Solar Cells, 2009. **93**(1): p. 136-142.
- [114] Jeong, S.-G., et al., *Improvement of the thermal properties of Bio-based PCM using exfoliated graphite nanoplatelets*. Solar Energy Materials and Solar Cells, 2013. **117**: p. 87-92.
- [115] Warzoha, R.J., R.M. Weigand, and A.S. Fleischer, *Temperature-dependent thermal properties of a paraffin phase change material embedded with herringbone style graphite nanofibers*. Applied Energy, 2015. **137**: p. 716-725.
- [116] Karaipekli, A., A. Sari, and K. Kaygusuz, *Thermal Characteristics of Paraffin/Expanded Perlite Composite for Latent Heat Thermal Energy Storage*. Energy Sources, Part A: Recovery, Utilization, and Environmental Effects, 2009. **31**(10): p. 814-823.
- [117] Tabares-Velasco, P.C., C. Christensen, and M. Bianchi, *Verification and validation of EnergyPlus phase change material model for opaque wall assemblies*. Building and Environment, 2012. **54**(0): p. 186-196.
- [118] Tabares-Velasco, P.C., C. Christensen, and M. Bianchi, *Validation methodology to allow simulated peak reduction and energy performance analysis of residential building envelope with phase change materials*. ASHRAE Transactions, 2012. **118**(2).
- [119] Sá, A.V., et al., *Thermal enhancement of plastering mortars with Phase Change Materials: Experimental and numerical approach*. Energy and Buildings, 2012. **49**(0): p. 16-27.
- [120] Kheradmand, M., et al., *Experimental and numerical studies of hybrid PCM embedded in plastering mortar for enhanced thermal behaviour of buildings*. Energy, 2016. **94**: p. 250-261.
- [121] Kheradmand, M., et al., *Thermal behavior of cement based plastering mortar containing hybrid microencapsulated phase change materials*. Energy and Buildings, 2014. **84**(0): p. 526-536.
- [122] ASHRAE, A., *Standard 55-2013: "Thermal Environmental Conditions for Human Occupancy"*; ASHRAE, in Atlanta USA. 2013.
- [123] Thiele, A.M., G. Sant, and L. Pilon, *Diurnal thermal analysis of microencapsulated PCM-concrete composite walls*. Energy Conversion and Management, 2015. **93**(0): p. 215-227.
- [124] Zhu, N., Z. Ma, and S. Wang, *Dynamic characteristics and energy performance of buildings using phase change materials: A review*. Energy Conversion and Management, 2009. **50**(12): p. 3169-3181.
- [125] Lamberg, P., R. Lehtiniemi, and A.-M. Henell, *Numerical and experimental investigation of melting and freezing processes in phase change material storage*. International Journal of Thermal Sciences, 2004. **43**(3): p. 277-287.
- [126] Joulin, A., et al., *Experimental and numerical investigation of a phase change material: Thermal-energy storage and release*. Applied Energy, 2011. **88**(7): p. 2454-2462.

- [127] Al-Saadi, S.N. and Z. Zhai, *Modeling phase change materials embedded in building enclosure: A review*. Renewable and Sustainable Energy Reviews, 2013. **21**(0): p. 659-673.
- [128] Al-Saadi, S.N. and Z. Zhai, *Modeling phase change materials embedded in building enclosure: A review*. Renewable and Sustainable Energy Reviews, 2013. **21**: p. 659-673.
- [129] Sajjadian, S.M., J. Lewis, and S. Sharples, *The potential of phase change materials to reduce domestic cooling energy loads for current and future UK climates*. Energy and Buildings, 2015. **93**(0): p. 83-89.
- [130] Muruganantham, K., *Application of Phase Change Material in Buildings: Field Data vs. EnergyPlus Simulation*. 2010, Arizona State University.
- [131] Chernousov, A.A. and B.Y.B. Chan, *Numerical simulation of thermal mass enhanced envelopes for office buildings in subtropical climate zones*. Energy and Buildings, 2016. **118**: p. 214-225.
- [132] EnergyPlus, *Engineering Reference Handbook*. 2012.
- [133] Mateus, N.M., A. Pinto, and G.C.d. Graça, *Validation of EnergyPlus thermal simulation of a double skin naturally and mechanically ventilated test cell*. Energy and Buildings, 2014. **75**(0): p. 511-522.
- [134] Chan, A.L.S., *Energy and environmental performance of building façades integrated with phase change material in subtropical Hong Kong*. Energy and Buildings, 2011. **43**(10): p. 2947-2955.
- [135] Zhuang, C.-l., et al., *Validation of Veracity on Simulating the Indoor Temperature in PCM Light Weight Building by EnergyPlus*, in *Life System Modeling and Intelligent Computing*, K. Li, et al., Editors. 2010, Springer Berlin Heidelberg. p. 486-496.
- [136] Shrestha, S., et al. *Modeling PCM-enhanced insulation system and benchmarking EnergyPlus against controlled field data*. in *Building Simulation 2011: 12th Conference of International Building Performance Simulation Association, Sydney, Australia*. 2011.
- [137] Zhuang, C.-l., et al., *Validation of Veracity on Simulating the Indoor Temperature in PCM Light Weight Building by EnergyPlus*, in *Life System Modeling and Intelligent Computing: International Conference on Life System Modeling and Simulation, LSMS 2010, and International Conference on Intelligent Computing for Sustainable Energy and Environment, ICSEE 2010, Wuxi, China, September 17-20, 2010, Proceedings, Part I*, K. Li, et al., Editors. 2010, Springer Berlin Heidelberg: Berlin, Heidelberg. p. 486-496.
- [138] Campbell, K.R., *Phase Change Materials as a Thermal Storage Device for Passive Houses*. 2011.
- [139] Chan, A., *Energy and environmental performance of building façades integrated with phase change material in subtropical Hong Kong*. Energy and Buildings, 2011. **43**(10): p. 2947-2955.
- [140] Kuznik, F., J. Virgone, and J.-J. Roux, *Energetic efficiency of room wall containing PCM wallboard: A full-scale experimental investigation*. Energy and Buildings, 2008. **40**(2): p. 148-156.
- [141] Jamil, H., et al., *Investigation of PCM as retrofitting option to enhance occupant thermal comfort in a modern residential building*. Energy and Buildings, 2016. **133**: p. 217-229.
- [142] Tabares-Velasco, P.C. and B. Griffith, *Diagnostic test cases for verifying surface heat transfer algorithms and boundary conditions in building energy simulation programs*. Journal of Building Performance Simulation, 2012. **5**(5): p. 329-346.
- [143] Cen, E., 15251, *Indoor environmental input parameters for design and assessment of energy performance of buildings addressing indoor air quality, thermal environment,*

- lighting and acoustics*. European Committee for Standardization, Brussels, Belgium, 2007.
- [144] Ye, H., et al., *The performance evaluation of shape-stabilized phase change materials in building applications using energy saving index*. *Applied Energy*, 2014. **113**(0): p. 1118-1126.
- [145] Pisello, A.L., M. Goretti, and F. Cotana, *A method for assessing buildings' energy efficiency by dynamic simulation and experimental activity*. *Applied Energy*, 2012. **97**(0): p. 419-429.
- [146] Zhou, G., Y. Yang, and H. Xu, *Performance of shape-stabilized phase change material wallboard with periodical outside heat flux waves*. *Applied Energy*, 2011. **88**(6): p. 2113-2121.
- [147] Zhang, Y., et al., *Ideal thermal conductivity of a passive building wall: Determination method and understanding*. *Applied Energy*, 2013. **112**: p. 967-974.
- [148] Zeng, R., et al., *New concepts and approach for developing energy efficient buildings: Ideal specific heat for building internal thermal mass*. *Energy and Buildings*, 2011. **43**(5): p. 1081-1090.
- [149] Scalat, S., et al., *Full scale thermal testing of latent heat storage in wallboard*. *Solar Energy Materials and Solar Cells*, 1996. **44**(1): p. 49-61.
- [150] Athienitis, A.K., et al., *Investigation of the thermal performance of a passive solar test-room with wall latent heat storage*. *Building and Environment*, 1997. **32**(5): p. 405-410.
- [151] Neeper, D.A., *Thermal dynamics of wallboard with latent heat storage*. *Solar Energy*, 2000. **68**(5): p. 393-403.
- [152] Kuznik, F. and J. Virgone, *Experimental assessment of a phase change material for wall building use*. *Applied Energy*, 2009. **86**(10): p. 2038-2046.
- [153] Kuznik, F., J. Virgone, and K. Johannes, *In-situ study of thermal comfort enhancement in a renovated building equipped with phase change material wallboard*. *Renewable Energy*, 2011. **36**(5): p. 1458-1462.
- [154] Borreguero, A.M., et al., *Improvement of the thermal behaviour of gypsum blocks by the incorporation of microcapsules containing PCMS obtained by suspension polymerization with an optimal core/coating mass ratio*. *Applied Thermal Engineering*, 2010. **30**(10): p. 1164-1169.
- [155] Entrop, A.G., H.J.H. Brouwers, and A.H.M.E. Reinders, *Experimental research on the use of micro-encapsulated Phase Change Materials to store solar energy in concrete floors and to save energy in Dutch houses*. *Solar Energy*, 2011. **85**(5): p. 1007-1020.
- [156] Voelker, C., O. Kornadt, and M. Ostry, *Temperature reduction due to the application of phase change materials*. *Energy and Buildings*, 2008. **40**(5): p. 937-944.
- [157] Lv, P., C. Liu, and Z. Rao, *Review on clay mineral-based form-stable phase change materials: Preparation, characterization and applications*. *Renewable and Sustainable Energy Reviews*, 2017. **68**, **Part 1**: p. 707-726.
- [158] Alkan, M. and M. Doğan, *Adsorption of Copper(II) onto Perlite*. *Journal of Colloid and Interface Science*, 2001. **243**(2): p. 280-291.
- [159] Tekin, N., et al., *Surface properties of poly(vinylimidazole)-adsorbed expanded perlite*. *Microporous and Mesoporous Materials*, 2006. **93**(1-3): p. 125-133.
- [160] Dubey, A., *Lightweight cementitious compositions and building products and methods for making same*. 2011, Google Patents.
- [161] Ma, B., et al., *Preparation of composite shape-stabilized phase change materials for highway pavements*. *Construction and Building Materials*, 2013. **42**: p. 114-121.

- [162] Rathod, M.K. and J. Banerjee, *Thermal stability of phase change materials used in latent heat energy storage systems: A review*. Renewable and Sustainable Energy Reviews, 2013. **18**(0): p. 246-258.
- [163] Silbrico. *Sil-Cell Technica Data*. 2014 [cited 2014 24 09]; Available from: <http://www.silbrico.com/sil-cellTechData.html>.
- [164] Rubitherm. *Technical Datasheet RT21*. [cited 2014 25 09]; Available from: [https://www.rubitherm.eu/media/products/datasheets/Techdata\\_RT21\\_EN\\_05112015.PDF](https://www.rubitherm.eu/media/products/datasheets/Techdata_RT21_EN_05112015.PDF).
- [165] Yu, Q., et al., *The reaction between rice husk ash and Ca(OH)<sub>2</sub> solution and the nature of its product*. Cement and Concrete Research, 1999. **29**(1): p. 37-43.
- [166] ASTM C109 / C109M-16a, in *Standard Test Method for Compressive Strength of Hydraulic Cement Mortars (Using 2-in. or [50-mm] Cube Specimens)*. 2000, ASTM International: West Conshohocken, PA, 2016, [www.astm.org](http://www.astm.org).
- [167] Duan, Z.-j., et al., *CaCl<sub>2</sub>·6H<sub>2</sub>O/Expanded graphite composite as form-stable phase change materials for thermal energy storage*. Journal of Thermal Analysis and Calorimetry, 2014. **115**(1): p. 111-117.
- [168] ASTM C596-09, in *Standard Test Method for Drying Shrinkage of Mortar Containing Hydraulic Cement*. 2009, ASTM International: West Conshohocken, PA, 2009, [www.astm.org](http://www.astm.org).
- [169] Zhang, H., et al., *A novel phase-change cement composite for thermal energy storage: Fabrication, thermal and mechanical properties*. Applied Energy, 2016. **170**: p. 130-139.
- [170] Xu, W., et al., *Strategy for interfacial overlapping degree in multiphase materials with complex convex particles*. Powder Technology, 2015. **283**: p. 455-461.
- [171] Sicat, E., et al., *Experimental investigation of the deformational behavior of the interfacial transition zone (ITZ) in concrete during freezing and thawing cycles*. Construction and Building Materials, 2014. **65**: p. 122-131.
- [172] Shin, K.-J., B. Bucher, and J. Weiss, *Role of lightweight synthetic particles on the restrained shrinkage cracking behavior of mortar*. Journal of Materials in Civil Engineering, 2010. **23**(5): p. 597-605.
- [173] Xu, B. and Z. Li, *Performance of novel thermal energy storage engineered cementitious composites incorporating a paraffin/diatomite composite phase change material*. Applied Energy, 2014. **121**(0): p. 114-122.
- [174] Al-Tayyib, A.J., et al., *The effect of thermal cycling on the durability of concrete made from local materials in the Arabian Gulf countries*. Cement and Concrete Research, 1989. **19**(1): p. 131-142.
- [175] Kanellopoulos, A., et al., *Mechanical and fracture properties of cement-based bi-materials after thermal cycling*. Cement and Concrete Research, 2009. **39**(11): p. 1087-1094.
- [176] Wang, T., et al., *Enhancement on thermal properties of paraffin/calcium carbonate phase change microcapsules with carbon network*. Applied Energy, 2016. **179**: p. 601-608.
- [177] Yuan, Y., et al., *Thermal performance enhancement of palmitic-stearic acid by adding graphene nanoplatelets and expanded graphite for thermal energy storage: A comparative study*. Energy, 2016. **97**: p. 488-497.
- [178] Zhou, G., et al., *Thermal characteristics of shape-stabilized phase change material wallboard with periodical outside temperature waves*. Applied Energy, 2010. **87**(8): p. 2666-2672.
- [179] Zhou, D., G.S.F. Shire, and Y. Tian, *Parametric analysis of influencing factors in Phase Change Material Wallboard (PCMW)*. Applied Energy, 2014. **119**(0): p. 33-42.

- [180] Novais, R.M., et al., *Lightweight dense/porous PCM-ceramic tiles for indoor temperature control*. Energy and Buildings.
- [181] Castell, A., et al., *Experimental study of using PCM in brick constructive solutions for passive cooling*. Energy and Buildings, 2010. **42**(4): p. 534-540.
- [182] DOE, U., *Energyplus engineering reference*. The Reference to EnergyPlus Calculations, 2010.
- [183] Sparrow, E., *Effect of Finite Width on Heat Transfer and Fluid Flow about an Inclined Rectangular Plate~ fc*. Journal of Heat Transfer, 1979. **101**: p. 199.
- [184] Niu, J. and J. Burnett, *Integrating radiant/operative temperature controls into building energy simulations*. ASHRAE Transactions, 1998. **104**: p. 210.
- [185] Zhou, G., et al., *Numerical analysis of effect of shape-stabilized phase change material plates in a building combined with night ventilation*. Applied Energy, 2009. **86**(1): p. 52-59.
- [186] Faheem, A., et al., *A numerical study on the thermal performance of night ventilated hollow core slabs cast with micro-encapsulated PCM concrete*. Energy and Buildings, 2016. **127**: p. 892-906.
- [187] Diaconu, B.M., *Thermal energy savings in buildings with PCM-enhanced envelope: Influence of occupancy pattern and ventilation*. Energy and Buildings, 2011. **43**(1): p. 101-107.
- [188] Ren, Z., X. Wang, and D. Chen, *Heat stress within energy efficient dwellings in Australia*. Architectural Science Review, 2014(ahead-of-print): p. 1-10.
- [189] Wang, X., D. Chen, and Z. Ren, *Global warming and its implication to emission reduction strategies for residential buildings*. Building and Environment, 2011. **46**(4): p. 871-883.
- [190] Ren, Z., Z. Chen, and X. Wang, *Climate change adaptation pathways for Australian residential buildings*. Building and Environment, 2011. **46**(11): p. 2398-2412.
- [191] Gu, L. *Airflow network modeling in EnergyPlus*. in *Building Simulation*. 2007.